University of Strathclyde
Department of Pure and Applied Chemistry

Monitoring of fermentation processes using novel on-line techniques

Melissa Black

A thesis submitted to the Department of Pure and Applied Chemistry, University of Strathclyde, Glasgow, in part fulfilment of the regulations for the degree of Doctor of Philosophy.

December 2017

Copyright

This thesis is the result of the author's original research. It has been composed by the author and has not been previously submitted for examination which has led to the award of a degree.

The copyright of this thesis belongs to the author under the terms of the United Kingdom Copyright Acts as qualified by University of Strathclyde Regulation 3.50. Due acknowledgement must always be made of the use of any material contained in, or derived from, this thesis.

Signed:
Date:

For my family

Omnia accipit fides et fiducia…

Acknowledgements

Firstly, I would like to thank my supervisor Dr Alison Nordon for her support and guidance throughout my PhD. When things were difficult, she was there to provide advice and help from broken thermometers to microorganisms that just wouldn't grow!

To my second supervisor Professor Brian McNeil, I thank you for all the knowledge you passed on and support you gave to a chemist attempting to become a fermentation scientist.

I was lucky enough to work on three separate studies working with two very interesting companies and I thank Greg Emmerson from Stratophase for the help with the refractive index system and I also thank Bioinnovel for providing the acoustic probe to begin to tackle the acoustic monitoring.

I would like to acknowledge EPSRC for providing the funding through an Industrial Case awards, which led me to be able to participate in this opportunity.

I had the pleasure of working with two excellent research groups at Strathclyde. The analytical group was there from the first day to always provide tea, support and quite a few laughs along the way. Who knew on my first day I would meet the other half of the 'terrible two' and I have certainly made friends for life with people in this group. The fermentation center group were amazing in the two years I worked in SIPBS from the lab move to heavy lifting and the occasional flood. Special thanks go to Walter McEwan for his technical help throughout my time in SIPBS and Dr Peter Gardner for his muscles in lifting the fermenter in and out of the autoclave and dealing with the nitrogen cylinders.

The outside support I received throughout my PhD has been amazing. I am grateful to my friends at dancing that patiently listened to me complain and explain what I was doing especially my 'sister' Sharon. To my friends at the Royal Society of Chemistry, I thank you for your support and encouragement while I was writing up and a special mention to Dr Fiona McMillan who proof read chapters and offered advice on so many occasions.

Finally, and most importantly, I will be forever grateful for the support my family have given me throughout my education, to my big sister Heather thanks go to putting up with me and providing financial support whilst I was studying. To mum and dad thank you for sacrificing everything that you did to provide Heather and I with the best education we could have ever hoped for and for the support you always have and continue to provide.

Abstract

Biotechnology processes are crucial to the pharmaceutical and many other industries including the oil industry. These processes are often complex and poorly understood and hence frequently developed and operated sub-optimally. There are many techniques that could be used to monitor and improve these processes including infrared spectroscopy, acoustic monitoring and refractive index measurements. Novel probes have been designed by Bioinnovel and Stratophase that have the potential to monitor these processes using these techniques. This work investigates these new probes to monitor *Xanthomonas campestris* and *Escherichia coli* fermentations and the use of infrared to monitor a *X. campestris* fermentation which has not previously been studied.

From the work investigating the use of infrared monitoring of a *X. campestris* fermentation it was shown to be possible to model the fermentation using a combination of off-line reference analyses. Mid-infrared off-line monitoring produced a PLS model which could monitor the glucose consumption within the fermenter using the 980 -1200 cm^{-1} region. The root mean squared error of calibration (RMSEC) of this model was 2.78 g/L over a measured glucose concentration range of 0-35 g/L. A model was also built to monitor the xanthan production of these fermentations using the same region. The RMSEC of this model was 2.78 g/L over a measured glucose concentration range of 0-25 g/L. The error associated with these models are higher than desired because of poor reference analysis as well as difficulties of the overlapping peaks of xanthan and glucose in this region.

The Bioinnovel acoustic monitoring probe was first characterised to identify the optimal experimental conditions. Model analyte solutions of agar, starch, glycerol and xanthan were analysed and a relationship between the concentration of the solution and the velocity of the acoustic wave was identified. These velocities were in good agreement with the literature for example pure glycerol's measured velocity was 1914 ms^{-1} (Std. dev 2.19 ms^{-1}) in comparison to the literature value of 1904 ms^{-1}. To explore potential combination of acoustic and rheological properties, the rheological characterisation of model xanthan was carried out including viscosity measurements of 0-2% wt./v xanthan solutions. The viscosity of the solutions increases as the

concentration increases therefore it may be possible in the future to combine velocity measurements with the viscosity measurements with further experiments. Throughout the experiments with the Bioinnovel probe potential improvements for the probe design were noted.

The refractive index probe designed by Stratophase was used to monitor an *E. coli* fermentation. First the probe was characterised and off-line analysis demonstrated the potential to monitor certain analytes within the fermentation broth such as glucose and biomass. These experiments found the Bragg wavelength shift increased as the concentration of the analytes increased for example the wavelength shift of 2.5 g/L was measured as 5.50 pm and of 15 g/L was measured as 73.41 pm. When the probe was used to analyse the fermentation samples off-line the combination of the changes in the Bragg wavelength (decrease of 66 pm over 12 hours) were as expected after the model solution analysis, the decrease of the glucose concentration playing the largest part in the change in Bragg wavelength. However, on-line analysis proved difficult as the probe fouled due to biomass on the sensor window and the probe itself did not always survive the autoclaving process due to the high temperature and pressure conditions.

1 Introduction

1.1 Bioprocesses & monitoring

A bioprocess is a process that uses living cells or their components to obtain the desired products or to treat a waste stream, these products include biopharmaceuticals and flavourings for food. The bioprocess industry is changing rapidly as the focus switches from natural products to recombinant proteins and naturally occurring production strains to genetically reconstructed strains.[1]

Biopharmaceuticals are having an important impact in the fight against diseases such as cancer, Alzheimer's, diabetes and asthma, which are rising rapidly in incidence in the western world. The biotechnology processes used to develop these products are complex, poorly understood, and are often developed and operated sub-optimally. Biopharmaceutical development can take up to 12 years and a typical drug costs $1.8bn to take it from initial research to market. Biopharmaceuticals are costly compared to earlier generation drugs such as penicillin resulting in a need to develop and apply measurement systems capable of providing both chemical and physical information at all stages, from discovery to full scale production. This is challenging as these processes involve solids (e.g. cells), liquids (e.g. oil and water) and gases. On-line and real-time monitoring may reduce cost and the time taken for development of biopharmaceuticals.[2]

A fermentation process is a multi-step process and there are many factors that must be considered when it is carried out including the medium design, the inoculum and the type of reactor. These factors will also affect the type of monitoring that can be carried out within the fermenter. For example fermentation vessels have essential variables that must be monitored off-line and on-line.[3] The monitoring of fermentation reactions poses problems that may not be present in other chemical processes such as maintaining sterility potentially having to with stand high temperatures and pressures during sterilisation.[4] Instrument stability and re-calibration are important factors to consider due to the length of time fermentation reactions can take. The fermentation broth will consist of multiple phases and the rheological properties will change over the course of the reaction so this must also be taken into consideration. The sensors

used must also not contaminate the bioprocess and the components of the sensor must not leak into the culture.[5]

1.2 Current measurement techniques

At present there are many control systems used with the fermenter vessel and there are a number of process variables that need to be monitored on-line during fermentation. Sensors can be used to monitor these process variables and one way of classifying these sensors is by their location in regard to the fermenter and the contact they have with the fermentation broth. Using this classification system there are three classes of sensor used within fermentation monitoring and control.[6] These three classes of sensors are:

- Those which penetrate the interior of the vessel (pH, dissolved Oxygen)
- Those which continuously draw samples from the vessel (gas analyser for off-gas)
- Sensors which do not come into contact with the fermentation fluid (temperature)

1.2.1 Fermenter conditions monitoring

There are many well-established measurement techniques for monitoring the conditions in the fermenter including electrical resistance thermometers and thermistors for monitoring temperature.[7, 8] Rotameters are used for measuring the gas flow within the fermenter [9, 6] and dissolved oxygen can be measured by are galvanic or polarographic probes. Both measure the partial pressure of the dissolved oxygen in comparison of saturation of air.[6] pH can also be monitored using a combined glass electrode within the fermenter.[5, 6, 8, 10] Assays are also used for testing and measuring the activity of an organism or an organic sample. Chromatographic assays, bioassays and immunoassays are used for biochemical analysis. Immunoassays take advantage of the binding properties of antibodies and antigens.[11]

1.2.2 Optical techniques

Optical techniques can also be used to monitor the fermentation reaction. The level of information content provided by these techniques, the robustness and the cost of these monitoring systems must be considered when implementing as monitoring systems.

1.2.2.1 Infrared

Near infrared spectroscopy (NIR) can be used for analysis and control of fermentation processes both small and large scale. In most fermentation processes, there are multiple substrates present which can cause problems with designing a NIR method for analysis.[12] For in-line analysis, the NIR probe is interfaced with a specific fermenter and is inserted into a standard fermenter port. The probes are designed to be resistant to multiple sterilisation cycles. The NIR spectra is collected in either reflectance or transmittance mode. For transmittance, the narrow optical path lengths in conjunction with the fluid dynamics of the broth media can make this difficult to implement. NIRS has yet to be fully exploited due to regulatory problems although NIR has been shown to be useful in both aerobic and anaerobic fermentation processes.

Typical fed-batch bioprocesses involve very close control of one or more nutrients at very low levels. Mid infrared (MIR) spectra provide more useful information than corresponding weaker NIR absorbances. NIR spectroscopy has difficulties generating useful information for analytes at sub g L^{-1} levels. MIR spectroscopy can distinguish microbes at the strain level and two very closely related chemical species in a biotransformation process. MIR spectroscopy can also determine the concentration of individual sugars in complex mixtures. Roychoudhury *et al.* (2006) found that MIR is a significant technique in bioprocess monitoring but it has some limitations.[13] It is often used as a secondary technique so accuracy is determined by the reference assay and it also has limited multiplexing advantages. The advantages of MIR spectroscopy include rapidity of measurement, flexibility in application and there is potential to include process variations through chemometrics. MIR has advantages over competing techniques such as NIR spectroscopy, for example the ability to quantify analytes present at limiting levels and potentially to identify aspects of product quality (e.g. folding patterns).[13] Advantages of infrared spectroscopy are its wide range of process

information available, high speed and sensitivity. Multivariate data processing is required for evaluation.[14]

1.2.2.2 Fluorescence spectroscopy

Fluorescent analytical methods make up the majority of the ultrasensitive assays carried out by light emission spectroscopy in the pharmaceutical sciences.[15] Some molecules within the fermentation broth can be excited by ultraviolet and visible radiation and the emitted radiation measured.[11] It is a selective detection method and can be used to monitor changes in complex molecules such as proteins. A wide range of process information can be accessed on-line.[14] However, for evaluation of the system multivariate data processing is required. There can also be interference by temperature and UV-absorbing species e.g. heavy ions. This technique can be used to determine nitrate or succinate levels and also for monitoring of downstream.[15]

1.2.2.3 Ultraviolet and visible spectrophotometry

High resolution UV spectrophotometers are used for on-line monitoring of fermentation processes.[14] It is used to determine active ingredients in formulations.[11] Recent developments in light detectors and electronics have led to the development of new UV spectrometers. These detectors are used for monitoring bioprocesses due to their sensitivity, robustness and low cost. Multivariate data processing is again required for evaluation of data.

1.2.2.4 Raman spectroscopy

Raman spectroscopy has been used to monitor bioprocess reactions. It can be deployed on-line to monitor multiple analytes in complex industrial bioprocesses. It can also be used for monitoring of a specific parameter such as the glucose-ethanol biotransformation by yeast.[16] There are some problems as the strong fluorescence activity of many biological molecules often overlay the Raman scattering bonds.[17] Lee *et al.* (2003) have used Raman to estimate the concentration of glucose in *E. coli* bioprocesses.[18] Attenuation caused by light scattering by the air bubbles and biomass was corrected for by using internal referencing. The physical model of the system

rather than noise was found to be the limiting factor in the estimation of the accuracy. For Raman to be used to monitor *E. coli* bioprocess adjustments must be made to the physical model to improve the detection limits and the sensitivity of the technique. There are also problems with sterilisation and the robustness of Raman spectroscopy that would require more investigation.

1.2.3 Biosensors

Optical biosensors use fluorescent dyes that are often immobilised on the tip of an optical fibre. On-line measurement of pH, CO_2 and O_2 can be carried out depending on the fluorophore. These sensors are used for control of micro bioreactors in high throughput systems and for these small bioreactors it is not possible to use standard size probes.[17] An optical biosensor has been developed by NASA to determine the pH within a space bioreactor.[19] There are many drawbacks to this method as pre-treatment is often required for the sample and the samples have to be removed for the fermenter. However, biosensors can be used to monitor this process and they have the advantage of automation and the speed of results. These biosensors monitor the pH variation within the fermenter which is proportional to the glucose concentration as the determination of glucose is based on the enzymatic reaction using glucose-oxidase.[4, 20]

1.2.4 Rheology

The rheological properties of the fermentation broth allow for better understanding of the fluid characterisation of the process. The changes in the rheology of a fermentation broth through the process are due to the modification of the media by the growing culture and the concentration of biomass within. An example of this is the presence of starch within the media; fermentation media often contain starch as a source of carbon. The starch makes the medium non-Newtonian and relatively viscous. However, the starch will be degraded as the organism within the culture grows which will alter the rheology of the medium and its viscosity.[21]

1.2.5 Acoustic

Ultrasound measurement maybe a novel way of monitoring the fermentation process as it is currently being carried out on food processes. Ultrasound can provide information on the fundamental physical and chemical properties of the material. The main advantages of ultrasound are that it is rapid, non-destructive and can be applied to systems that are concentrated and optically opaque. These advantages are similar to those of nuclear magnetic resonance (NMR) spectroscopy with the additional advantage of being low-cost and the adaptable for on-line measurements. There are various methods of ultrasound measurement including pulse-echo, through transmission and continuous wave which all have different advantages and disadvantages depending on the sample being measured.[22, 23]

1.3 Current on-line monitoring sensor design

In-situ probes are available for fermentation processes to measure many different types of experimental conditions. pH and dissolved oxygen probes have been used for many years and the probe design of these has been well established. A pH probe as discussed in 1.21 is usually a glass electrode which is inserted in to the vessel and remains in the vessel throughout the fermentation. These probes are designed to withstand the sterilisation process and can continue to work to temperatures of 140 ºC. The probe has no crevices where biomass may become trapped and these probes can easily be cleaned after the fermentation and re-used. The pH probe has a connection to the control unit and can monitor pH continually which allows the fermenter in an automatic control setting to regulate its own pH. The probes can be calibrated using pH standards before autoclaving and thus allows accurate measurements during the process. During the course of the fermentations discussed, a Mettler Toledo InPro 3250 probe was used which has been specifically designed for biotechnology, pharmaceutical and chemical process applications. (Figure 1) The electrode contains a liquid-electrolyte pH sensor which can measure a pH range of 0-14 and up to a pressure of 4 bars. Care has been taken when designing the probe so that fouling is not a problem with an internal overpressure to ensure an electrolyte flow that is gradual and so that the process medium does not enter the reference electrode.

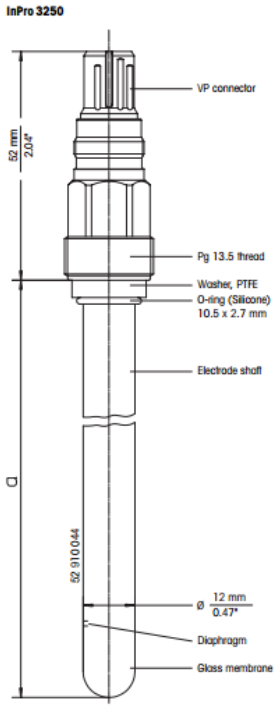

Figure 1 : Schematic of Mettler Toledo pH probe used in fermentation monitoring[24]

Dissolved oxygen probes are widely used to monitor the aeration rate of the fermenter unlike pH it is not possible to take off-line samples for aeration. The probe must be robust to give accurate readings throughout the fermentation. There are two current probe designs available these are galvanic and polarographic. (Figure 2) They both measure the partial pressure of the dissolved oxygen in comparison of saturation of air. Pressure changes can cause variations in the readings but temperature has a greater effect on these readings. The permeability of the membrane can cause a change of 2.5% per ^{o}C. Temperature compensation is inbuilt into the probes and it is better to calibrate these probes after autoclaving. This is achievable for a dissolved oxygen probe as external calibrants are not required. The probe is calibrated by removing oxygen from the fermentation media using nitrogen to achieve a 0% and 100% reading.

Small fermenters tend to use galvanic probes as they are compact and have a relatively low cost. There is a problem with robustness with these probes which make them difficult to use in a large fermenter. A galvanic probe generally has a lead or zinc anode, a silver cathode and then an electrolyte (potassium hydroxide, chloride, acetate or bicarbonate). The probes have a slow response time as mass transfer is slow over

the membrane (Teflon, polyethylene or polystyrene). Rather than measure the dissolved oxygen concentration the electrodes measure the partial pressure.

The membrane within these probes can be removed and replaced if there are issues such as splitting of the membrane at a much lower cost than a new probe and the electrolyte solution can also be replaced. This improves the longevity of the probe thus reducing the cost of running and monitoring a fermentation.

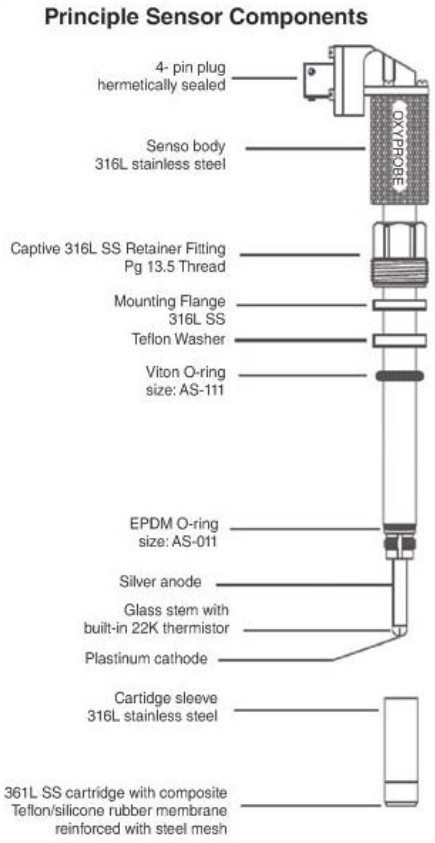

Figure 2 : Schematic of a dissolved oxygen probe's components[25]

The use of NIR and MIR for fermentation monitoring is becoming more widely used with research being carried out into various organisms and monitoring systems. (3.3) The probes used for these measurements are manufactured by various companies including Foss, Bruker and RemSpec or designed in house.[26] Most of these probes follow the same structure with the fibre optic fibres encased in stainless steel housing with either a changeable tip or a changeable mirror. An example of a probe in shown in Figure 3 has an interchangeable tip to allow different path lengths to be used. The tip allows movement of the fermentation broth through the path and does not disturb the agitation of the fermenter.

Figure 3 : Example of NIR probe for fermentation monitoring[27]

There are many different ultrasonic instruments used in various applications that are commercially available from food analysis to dispersion analysis. On-line acoustic monitoring is used in a variety of processes as discussed in 4.2.5.

The probes used for this kind of monitoring can be very simple, for example in food analysis an ultrasonic transducer is attached to a pipe which has the food stuff to be analysed flowing through it. The transducer produces a pulse of ultrasound which travels through the pipe and is reflected back to the transducer by the wall of the pipe.[22]

Low frequency ultrasound detectors are used in the dairy industry to monitor liquid levels within tanks where the liquid or thick foam is detected by the transducer placed at the top of the tank. Probes that are used in the dairy industry must withstand cleaning processes although it does not need to function during a cleaning cycle. The cleaning cycle usually involves water and chemical cleaning which the ultrasound probe can withstand but steam cleaning poses a problem as it can damage the probe including the epoxys and resins within the probe.[28]

At higher frequencies it is possible to measure the liquid level within dairy tanks, using the difference in attenuation when comparing air and liquid. The high attenuating air at frequencies above 1 MHz prevents the ultrasound from being detected by the receiver and so can trigger an alarm system when liquid levels fall below a certain level. Suspended particles and air bubbles cause problems within the measurement as they attenuate the signal between the sensors and to overcome this, the gain of the amplifier is increased. These specialised sensors have been manufactured to work with aerated liquids and suspended solids and can be seen in Figure 4.[28]

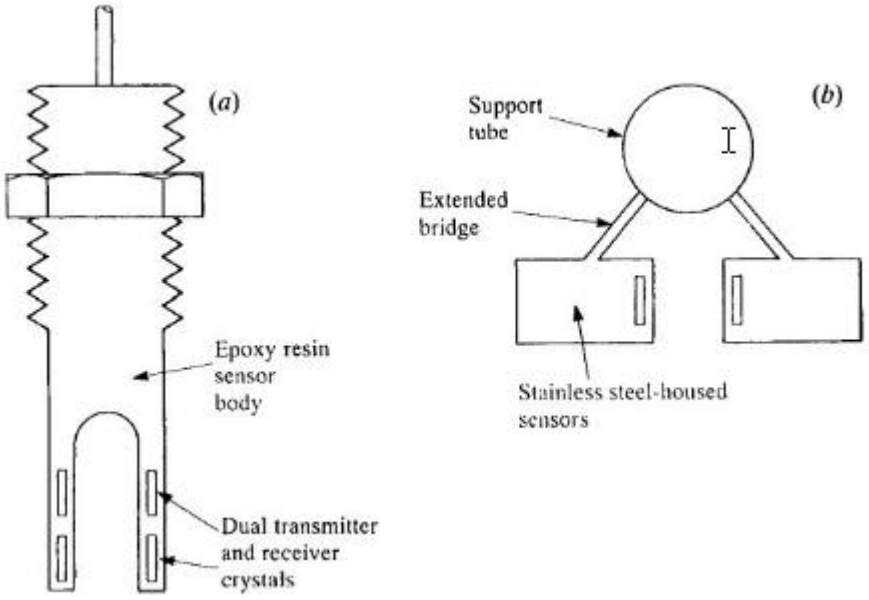

Figure 4 : Specialised sensor design for a) sensor for aerated liquids b) top view of sensor for liquids containing suspended solids[28]

Ultrasound is also used for particle sizing with ultrasonic particle sizers taking measurements of a range of 1-200 MHz which allows a measurement of 10 nm and 1000 µm but adjustments can be made by using custom built systems. These systems use different types of signal including the sinusoidal wave, a tone-burst pulse and a broadband pulse but generally the apparatus used for these techniques is similar with a signal generator, signal analyser and a measurement cell. If a continuous wave is used then a fixed path length or variable path length can be used. The fixed length analyser has two transducers – a transmitter and a receiver which allow a signal to be passed across a fixed path length of the fluid. A variable path length is also possible with a transducer and a reflector plate. The wave travels from the transducer and travels

through the sample and undergoes multiple reflections and reaches the reflector plate which results in a standing wave being formed, calculations can then be carried out to determine the attenuation coefficient of the sample.[29, 30]

1.4 Aims of research

As fermentations are a complex multistage process, monitoring and control plays an important part of identifying when a process is performing sub-optimally. The overall aim of the research was to assess the use of novel on-line measurements including spectroscopy, ultrasound and rheology to provide understanding and optimisation possibilities of biotechnology processes. By developing and assessing these novel on-line instruments, the aim is to improve the processes with the possibility of using these techniques in conjunction with each other to better model the fermentation process and use these models to identify when a fermentation process is performing sub-optimally.

Four main areas of research that will lead to the overall aim:

1. Evaluate the use of near infrared measurements in combination with reference assays for improved process understanding and optimisation of biotechnology processes

2. Evaluate the use of an ultrasound probe for on-line measurement of rheology in biotechnology processes

3. Evaluate the use of a novel refractive index probe for improved process understanding

4. Advance the development of the probe design and application of the novel measurement technology

1.5 Summary

The work represented herein is split into distinct sections. Chapter 1 has set the scene for the challenges of bioprocess monitoring and brief description of possible monitoring techniques. Chapter 2 describes the fermentation process and micro-organisms used in the three experimental studies (*Xanthomonas campestris* and

Escherichia coli). Chapter 3 is the first experimental study of a novel monitoring method examining the use of infrared for monitoring *Xanthomonas* fermentations. Chapter 4 contains the experimental study of the novel acoustic instrument designed by Bioinnovel. The final experimental study is contained in chapter 5 which looks at the novel refractive index probe designed by Stratophase to monitor an *Escherichia coli* fermentation. Each experimental study chapter (3-5) contains the theory and background of the techniques, the experimental parameters as well as the results and discussion. Chapter 6 examines the design of the probes for monitoring a fermentation using the results of the experimental studies and future work that could be carried out.

1.6 References

1. Council, N. R., *Putting Biotechnology to Work: Bioprocess Engineering*. The National Academies Press: Washington, DC, **1992;** 132.

2. McNeil, B.; Harvey, L. M.; Hunter, I., Fermentation technology. The University of Strathclyde: Glasgow, **2009.**

3. McNeil, B.; Harvey, L. M., *Fermentation: a practical approach*. Oxford university press: Oxford, **1990**; 226.

4. Ferreira, L. S.; De Souza, M. B.; Folly, R. O. M., Development of an alcohol fermentation control system based on biosensor measurements interpreted by neural networks. *Sens. Actuator B-Chem.* **2001,** *75* (3), 166-171.

5. Crueger, W., *Biotechnology : a textbook of industrial microbiology*. Sunderland, MA : Sinauer Associates; **1990.**

6. Stanbury, P. F.; Whitaker, A.; Hall, S. J., *Principles of fermentation technology*. 2 ed.; Butterworth-Heinemann: Burlington, **2003**; p 357.

7. Lennox, B.; Montague, G. A.; Hiden, H. G.; Kornfeld, G.; Goulding, P. R., Process monitoring of an industrial fed-batch fermentation. *Biotechnol. Bioeng.* **2001,** *74* (2), 125-135.

8. Montague, G., *Monitoring and control of fermenters*. Rugby, Warwickshire : Institution of Chemical Engineers: **1997.**

9. Sonnleitner, B., Instrumentation of biotechnological processes. *Advances in biochemical engineering/biotechnology* **2000,** *66*, 1-64.

10. Ward, O. P., *Fermentation biotechnology : principles, processes and products*. Milton Keynes : Open University Press: 1**989.**

11. Watson, D. G., *Pharmaceutical Analysis* 2nd ed.; Elsevier: London, **2005.**

12. Arnold, S. A.; Harvey, L. M.; McNeil, B.; Hall, J. W., Employing near-infrared spectroscopic methods and analysis for fermentation monitoring and control - Part 1, method development. *Biopharm. Int.* **2002,** *15* (11), 26-32.

13. Roychoudhury, P.; Harvey, L. M.; McNeil, B., The potential of mid infrared spectroscopy (MIRS) for real time bioprocess monitoring. *Anal. Chim. Acta* **2006,** *571* (2), 159-166.

14. Ulber, R.; Frerichs, J.-G.; Beutel, S., Optical sensor systems for bioprocess monitoring. *Analytical and bioanalytical chemistry* **2003,** *376*, 342-34.

15. Swarbrick, J., *Encyclopedia of Pharmaceutical Technology*. Informa healthcare: **2007**; Vol. 3.

16. Shaw, A. D.; Kaderbhai, N.; Jones, A.; Woodward, A. M.; Goodacre, R.; Rowland, J. J.; Kell, D. B., Noninvasive, on-line monitoring of the biotransformation by yeast of glucose to ethanol using dispersive Raman spectroscopy and chemometrics. *Appl. Spectrosc.* **1999,** *53* (11), 1419-1428.

17. Marose, S.; Lindemann, C.; Ulber, R.; Scheper, T., Optical sensor systems for bioprocess monitoring. *Trends in biotechnology* **1999,** *17* (1), 30-34.

18. Lee, H. L. T.; Boccazzi, P.; Gorret, N.; Ram, R. J.; Sinskey, A. J. In *In situ bioprocess monitoring of Escherichia coli bioreactions using Raman spectroscopy*, 2nd International Conference on Advanced Vibrational Spectroscopy, Nottingham, ENGLAND, Aug 24-29; Elsevier Science Bv: **2003**; pp 131-137.

19. Jeevarajan, A. S.; Vani, S.; Taylor, T. D.; Anderson, M. M., Continuous pH monitoring in a perfused bioreactor system using an optical pH sensor. *Biotechnol. Bioeng.* **2002,** *78* (4), 467-472.

20. Lelong, Ph., Pardo; H. C. D; Cavalie, J. M., Automation of glucose measurement in fermentor broths. *Applied microbiology and biotechnology* **1991,** *36*, 173-177.

21. Kemblowski, Z.; Budzynski, P. *Process rheometry of biological suspensions*, 11th International Congress on Rheology, Brussels, Belgium, Aug 17-21; Moldenaers, P.; Keunings, R., Eds. Elsevier Science Publ B V: **1992**; pp 735-737.

22. McClements, D. J., Ultrasonic Characterization of Foods and Drinks: Principles, Methods and Applications. *Critical reviews in food science and nutrition* **1997,** *37* (1), 1-46.

23. Dzida, M.; Zorębski, E.; Zorębski, M.; Żarska, M.; Geppert-Rybczyńska, M.; Chorążewski, M.; Jacquemin, J.; Cibulka, I., Speed of Sound and Ultrasound Absorption in Ionic Liquids. *Chemical Reviews* **2017,** *117* (5), 3883-3929.

24. Toledo, M., Low-maintenance electrodes for precise pH measurements in the chemical, biotechnology and pharmaceutical industries. http://uk.mt.com/gb/en/home/products/ProcessAnalytics/pH_family_browsw/pH_electrode_browse/InPro3250_3250SG_Aug04_1.html, **2013.**

25. McNeil, B., *Practical fermentation technology*. Chichester, England ; Hoboken, NJ : Wiley: **2008.**

26. Cimander, C.; Carlsson, M.; Mandenius, C. F., Sensor fusion for on-line monitoring of yoghurt fermentation. *Journal of biotechnology* **2002,** *99* (3), 237-248.

27. http://www.electrothermal.com/news.asp?dsl=948. (accessed 27/07/13).

28. Kress-Rogers, E.; Brimelow, C. J. B., *Instrumentation and Sensors for the Food Industry (2nd Edition).* Woodhead Publishing. **2001.**

29. McClements, D. J., Ultrasonic measurements in particle size analysis. *Encylcopedia of analytical chemistry*. **2006.**

30. Challis, R. E.; Povey, M. J. W.; Mather, M. L.; Holmes, A. K., Ultrasound techniques for characterizing colloidal dispersions. *Rep. Prog. Phys.* **2005,** *68* (7), 1541-1637.

2 The fermentation process & micro-organisms

2.1 Fermentation process

2.1.1 Batch fermentation

A batch fermentation is a closed system with the sterilised nutrient solution inoculated at time zero. The incubation then proceeds under the optimum physiological conditions and during the fermentation nothing is added except oxygen, antifoam and acid/alkali for pH regulation. The composition of the medium, the biomass concentration and metabolite concentration changes continually as a result of the metabolism of cells. There are four main stages of the fermentation process (Figure 5):

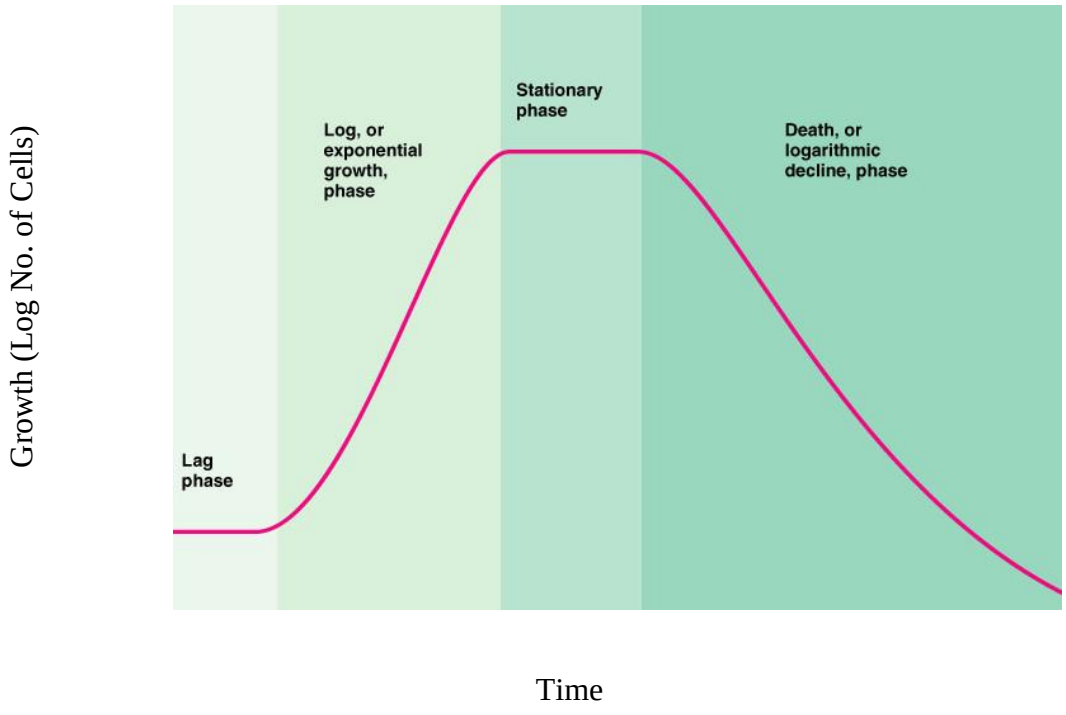

Figure 5 : Schematic of the fermentation process[1]

The lag phase is the period in which the organism undergoes adaptation when the cells are transferred from one medium to another. There is no increase in the number of cells although the cell weight may change. The micro-organisms adapt to their new environment and when the cells are first transferred to a different medium there are several parameters that will change within the media such as the pH, the nutrient supply and growth inhibitors.

The log phase is when the organism is growing at a maximum specific growth rate (μ_{max}) and is most biochemically reactive. The log phase occurs at the end of the lag phase as the cells have adapted to the new media conditions. The growth of cells can now be described as a doubling of cell number per unit time or the doubling of biomass per unit time. The medium alters as the cells uptake substrates and excretes metabolic products. The growth rate will remain constant during the log phase.

The stationary phase is when the organism is not reproducing but there are enough nutrients available to keep the organism alive. This occurs as soon as the substrate is metabolised or a toxic substance has been formed. The growth will slow down or will completely stop. There will be a gradual increase in the biomass or it will remain constant even though the composition of the cells changes. Death phase is when the nutrients have run out and the organism begins to die.[2, 3]

The changing composition in the closed system provides monitoring opportunities for example the consumption of the glucose can be monitored off-line to indicate the 'health' of the fermentation.

2.1.2 Fermenter design

There are many important factors involved in fermenter design, the vessel must provide an environment that is suitable for growth of the culture that is free of contaminants and controllable. The vessel will require aeration, agitation, monitoring and controlling. The reactor must have no connections between non-sterile and sterile parts, minimum flange connections, no dead spaces and have independently sterilisable points. The bioreactor must be made of material that is able to withstand high and low pH, be non-toxic, and steam and pressure tolerant.

A stirred tank reactor (STR) (Figure 6) is the most common and versatile fermenter design; it is an upright cylinder with baffles which prevent vortex mixing. The geometry can be changed as the volume and process requirements are altered. The height and width relationship varies between 2:1 and 6:1. The bottom of the tank has a sparger which allows sterile air to enter. The vertical shaft has one or more impeller which can be top or bottom driven. The number of impellers is dependent on the aspect ratio of vessel. The impellers can be of different designs such as Rushton turbine, marine propellers, multiple

rod or double cone. The stirring and mixing within an STR is an important factor, the fermentation broth is a three-phase system. The liquid phase contains the dissolved salts, substrates and metabolites. The solid phase consists of individual cells, pellets, insoluble substrates or precipitating metabolic products. The gaseous phase is a reservoir for the oxygen supply for CO_2 removal or the adjustment of the pH with gaseous ammonia. A suitable mixing device must be used for the transfer of energy, substrate and metabolite within the bioreactor. The mixing is crucial to the efficiency of the whole fermentation as the transport of any one substrate may affect this. The stirring within a bioreactor allows for the dispersion of air in the nutrient solution and homogenisation must be achieved and the temperature must be the same throughout the fermenter. Immiscible liquids must be dispersed and the microorganisms and solid nutrients equally dispersed.

A point of insertion on the fermenter vessel is a port where there is contact with both the outside and inside of the fermenter vessel. The points of insertion are where there is a possibility of contamination e.g. the sample port. If the sample port becomes contaminated the contamination can remain in the port as well as being transferred to the sample tubes. Therefore, the sample port must be independently sterilisable. There are many advantages to a STR, most fermentation processes can be carried out within the vessel with just minor alterations. For high viscosity fermentation processes the STR is able to mix the process well. However, there are a few disadvantages, the STR may be overly complex for some fermentation systems and there can be issues with sterility.

STRs are widely reported for use in various fermentations. Penicillin production from *Penicillium Chrysogenum* using an STR bioreactor is reported by Rocha-Valdez. (2007)[4] Gas-liquid mass transfer was studied and modelled by Garcia-Ochoa *et al.* (2005) using an STR bioreactor.[5] Garcia-Ochoa *et al.* (2005) were able to model the oxygen mass transfer in the sparged stirred tank reactors as well as predicting the volumetric mass transfer coefficient. STRs were also used in the degradation of 2,4-dichlorophenoxyacetic acid by Kelly *et al.* (1989)[6] As can be seen in the literature stirred tank reactors can be used in a variety of ways.

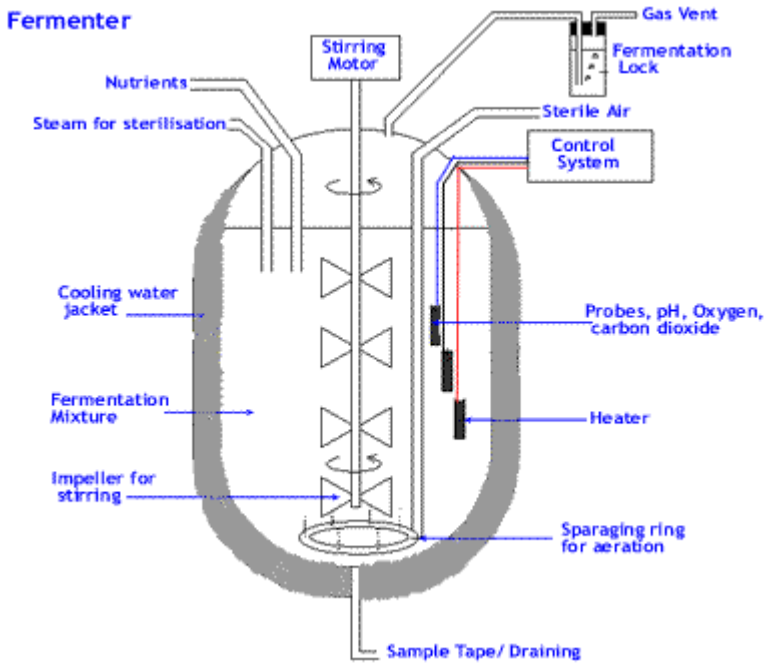

Figure 6: Schematic of a stirred tank fermenter[7]

2.2 Micro-organisms

Two micro-organisms were used for the work discussed in this thesis *Xanthomonas campestris* and *Escherichia coli. Xanthomonas campestris* is of interest as it produces a water soluble exocellular heteropolysaccharide xanthan gum. The properties of the *Xanthomonas campestris* fermentation and the resulting product mean this is an interesting organism to analyse using due to the production of the xanthan gum and its rheological properties including its pseudoplastic nature. (2.2.1.6) *Escherichia coli* is of interest for the work using refractive index as it is a quick growing organism which has been studied by many authors with different techniques so provides a well understood organism for a feasibility with a novel technique. (2.2.2.3)

2.2.1 *Xanthomonas campestris*

Xanthomonas campestris (*X. campestris*) is a phytopathogenic bacterium.[8] *X. campestris* is a genus of the Pseudomonaceae which are plant pathogens.[9] The cells are straight rods which are motile and Gram negative and have a cell envelope similar to that of other gram negative cells.[10] The cells (Figure 7) are usually 0.4-0.7 μm wide and 0.7-1.8 μm long, they also have a single polar flagellum (1.7-3 μm).[9]

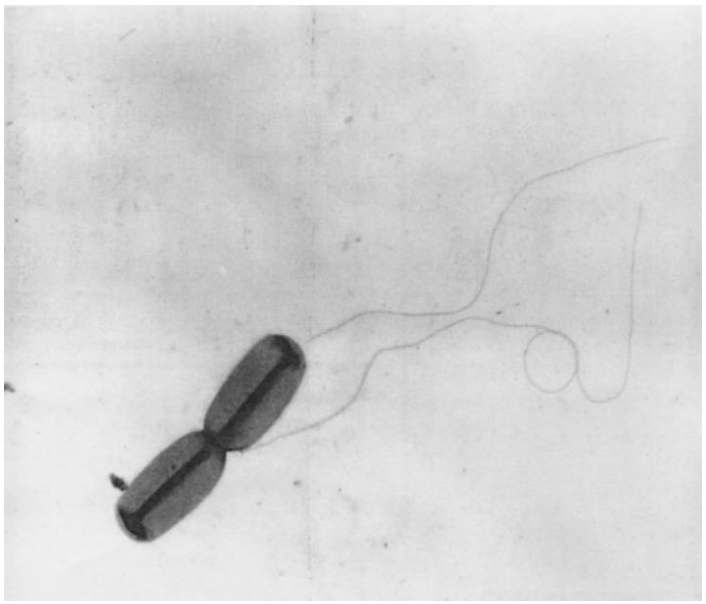

Figure 7 : Transmission electron micrograph of *X. campestris* (x12 000)[9]

Colonies of *Xanthomonas campestris* are yellow, smooth and viscid. This yellow colour is present in all species of *Xanthomonas* such as *X. phaseolis, X. carotae* and *X. malvacearum* but may become absent with degradation of the strain. The yellow colour is due to the Xanthomonadins which are brominated, aryl-polyene, yellow, water insoluble pigments.[11] The cells are grown on complex solid media for 18-20 hours at 25 ^{o}C; the cells can be kept for 14 days before strain preservation must be carried out. To check for strain degradation, the cells are grown for 3 days at 25° ^{o}C after this time bright yellow and round colonies with a diameter of 4-5 mm should be seen. *X. campestris* produces the capsular polysaccharide xanthan gum.[10] The xanthan gum can be seen when stained with India ink and are loosely associated with the cells. All strains can be genetically modified to improve the properties of the xanthan gum for example, product yield, media requirements or to simplify the recovery and purification steps.[12]

2.2.1.1 Xanthan production

Xanthan gum is a water soluble exocellular heteropolysaccharide with a primary structure consisting of repeated pentasaccharide units.[12] Generally the molecular weight of xanthan gum is approximately 2 million although it has been reported as high as 13-50 million.[13] The β−1,4 – linked D-glucose backbone with trisaccharide side chains composed of mannose (β−1,4)− glucuronic acid-(β−1,2)-mannose attached to alternate glucose

residues in the backbone by α-1,3-linkages.[14] The main chain is identical to that of cellulose and the trisaccharide branches are closely aligned with the polymer backbone, it is a stiff chain which can exist as either a single, double or triple helix which reacts to form a complex with polymer molecules (Figure 8).[9]

Xanthan gum is synthesised similar to exopolysaccharide synthesis by other Gram-negative bacteria such as Gellan gum from *Pseudomonas elodea.*[15] The synthetic pathway can be split into three parts:

1. Simple sugars are converted to nucleotide derivatives,

2. An isopentyl pyrophosphate carrier is used to assemble pentasaccharide subunits,

3. The pentasaccharide repeat units undergo polymerisation and are then secreted.

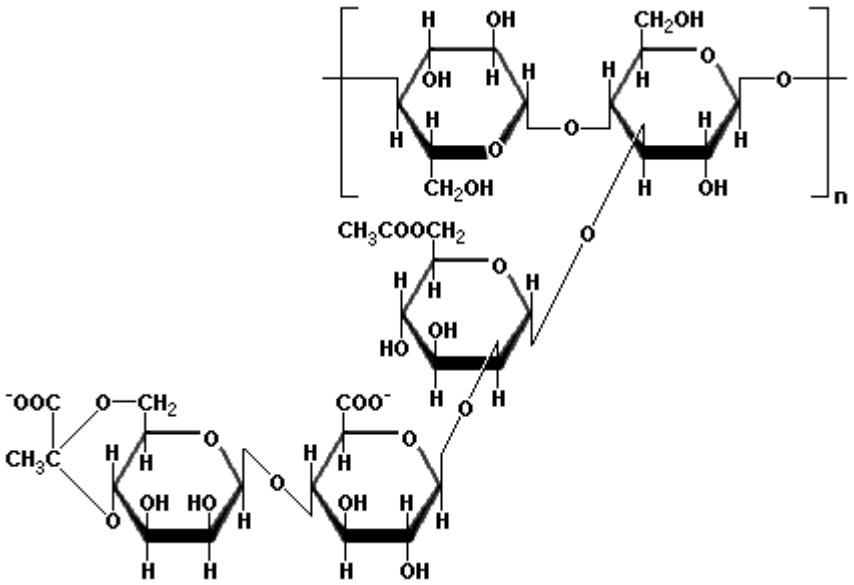

Figure 8 : Structure of xanthan gum repeating unit[16]

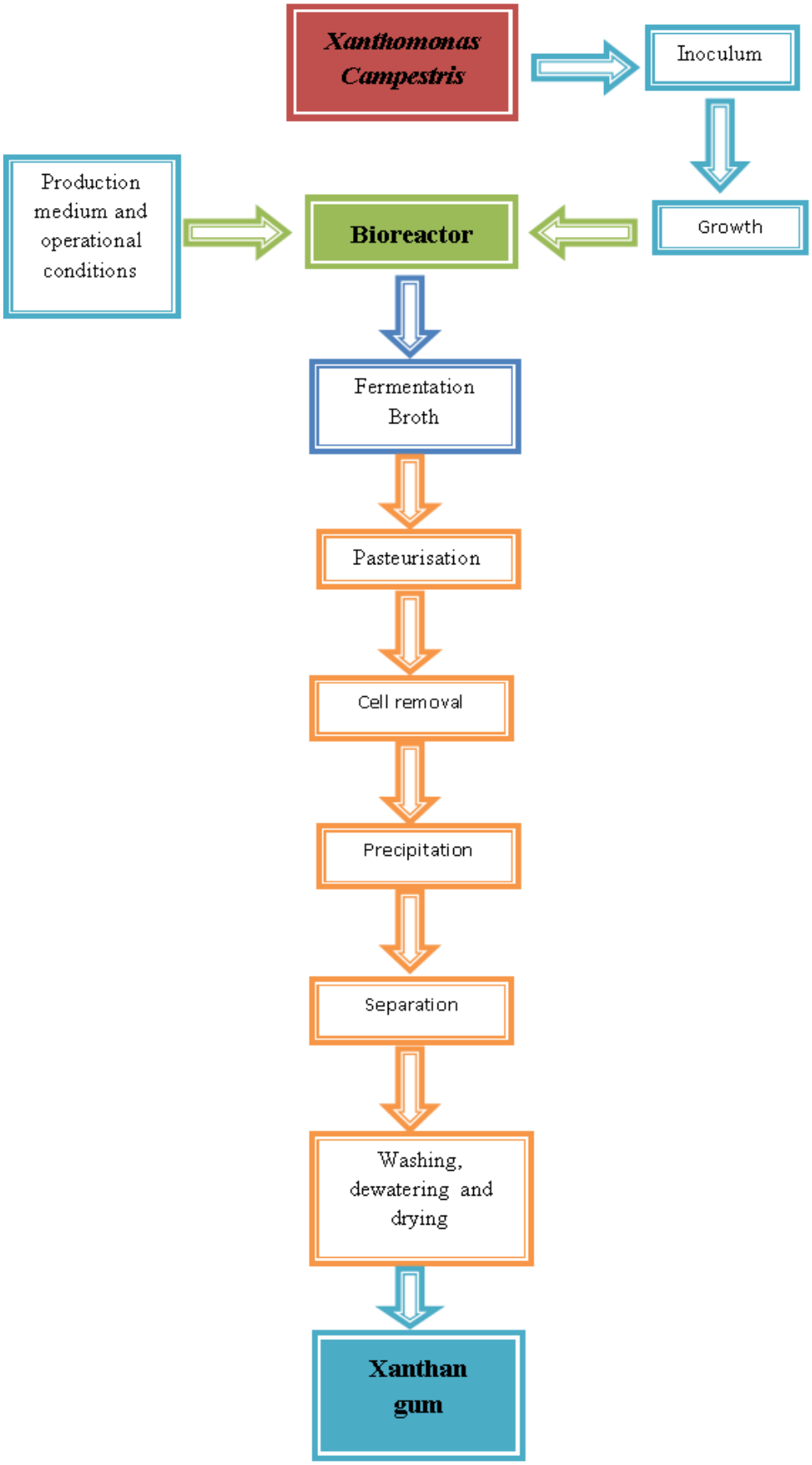

Figure 9 : Outline of the xanthan production process from *X. campestris*

Xanthan is produced generally in a batch fermentation although some work has been carried out with continuous fermentations. The inoculum must be prepared and then this is added to the production media within the bioreactor and the fermentation is carried out (Figure 9) with the xanthan then removed from the fermentation broth.

The batch fermentation has multiple variables which must be considered during the development of a fermentation process. These include the production medium, the operational conditions including the inoculum growth method, temperature and the pH. Once the fermentation is complete the recovery of the xanthan gum can be carried out in many ways.

2.2.1.2 Production medium

There are many possible production media used for xanthan production, all have similarities and often the differences between the media are dependent on the use of the xanthan produced (Table 1). Glucose is commonly used as the sugar for fermentation. The addition point of the glucose was investigated by Amanullah *et al.* (1998) who found that if the glucose was added as a series of pulses after the supplied nitrogen had been exhausted this improved the yield.[17] Lo *et al.* (1997) added glucose initially at a low concentration during the exponential phase and then increased this during the stationary phase. Changing the number of additions affected the xanthan yield with five additions producing a low yield but just two additions gave a high yield and reduced the fermentation time from 120 hours to 100 hours.[18] Rosalam *et al.* (2006) found that a high glucose concentration should be introduced during the stationary phase and that the glucose concentration must be controlled to avoid inhibition by the substrate concentration.[19] Sucrose and hydrolysed starch can also be used as the sugar, however, glucose gives the best product yield, consistency of supply and product quality. There are a few possible reasons for the lower yield and quality including deficiency of certain functional groups resulting in a different metabolic pathway being used. The composition of the nutrient is varied and other by-products could be formed. The unmodified starch could have chemical variants or components which may become inhibitors. There also may be purification problems downstream due to non-reacted compounds and the lower quality of the product. Leela *et al.* (2000) found that glucose gave the highest xanthan

yield with soluble starch giving the lowest yield and maltose producing the second lowest yield.[20]

Nitrogen is also an important nutrient required in the media with nitrogen sources affecting the xanthan product yield. Nitrogen can be provided as either an organic compound or an inorganic molecule.[9] Altering the nitrogen source affects the xanthan yield, ammonia is better for biomass accumulation but higher xanthan yields are found when nitrate is used. When nitrate was used by Letisse *et al.* (2001) 0.79 mmol g^{-1} cells h^{-1} of xanthan was produced while with ammonia only 0.52 mmol g^{-1} cells h^{-1} was produced.[21] A high concentration of nitrogen in the media has no benefit to xanthan production as it is not part of the polysaccharide structure but is used for cell growth and enzyme production.[22] Therefore industrially there must be a compromise between cell growth and xanthan gum production.[19]

Other nutrients must be monitored such as magnesium and phosphate, limiting these results in low pyruvate containing xanthan gum.[9] When phosphorus along with carbon are the limiting nutrients, xanthan gum production is improved.[5] If small quantities of organic acids (e.g. citric acid) are added to the medium, production is enhanced. A nutrient study showed that nitrogen, phosphorus and magnesium influence the biomass accumulation whereas nitrogen, potassium and sulphur influenced xanthan production.[9]

Table 1 : Formulae for production media all masses given in g/L[23]

Nitschke *et al.* (1995)[8]		Sriram *et al.* (1998) [23]		Garcia-Ochoa *et al.* (2000)[9]		Rochoa-Valadez *et al.*	
Glucose	20.0	Glucose	25.0	Sucrose	40.0	Sucrose	40.0
K_2HPO_4	5.0	K_2HPO_4	5.0	K_2HPO_4	2.9	K_2HPO_4	5.0
$MgSO_4.7H_2O$	0.1	$MgSO_4.7H_2O$	0.6	Citric acid	2.1	Citric acid	2.3
Urea	0.4	Urea	0.4	H_3BO_3	$6.0x10^{-3}$	H_3BO_3	$6.0x10^{-3}$
Yeast extract	0.5	Yeast extract	8.0	NH_4NO_3	1.1	Na_2CO_3	0.5
				$MgCl_2$	0.5	Na_2SO_4	$1.1x10^{-1}$
				Na_2SO_4	$8.9x10^{-2}$	$MgCl_2.6H_2O$	$1.6x10^{-1}$
				ZnO	$6.0x10^{-3}$	$FeCl_3$	$1.4x10^{-3}$
				$FeCl_3.6H_2O$	$2.0x10^{-2}$	ZnCl	$6.7x10^{-3}$
				$CaCO_3$	$2.0x10^{-3}$	$CaCl_2.2H_2O$	$1.2x10^{-2}$
				HCl	0.13 mL L^{-1}	NH_4Cl	2.0

2.2.1.3 Operational conditions

2.2.1.3.1 Inoculum

The inoculum development varies in temperature and media requirements. The production of xanthan gum is associated with growth of inoculum as the gum constitutes the capsule. When considering the method of inoculum development, the aim is to increase the cell concentration and minimise the production of xanthan as transport of nutrients is affected by the xanthan around the cells. To suppress the xanthan production multiple stages of inoculum development are used. The micro-organism is transferred from the agar into the YM (Yeast Mold) media (5-7 mL) and incubated for 7 hours. This is then transferred into a larger volume of the media (40-100 mL) containing inorganic salts. This allows the cells to adapt the new conditions that will be encountered in the production phase.[9] The inoculum volume required for the production fermenter varies between 5 and 10 % of the total volume. Other media has been suggest by Papagianni *et al.* (2001) who used a culture medium with 1 %w/v tryptone, 0.5 %w/v yeast, 0.5 %w/v NaCl and 0.2 %w/v glucose.[10] The temperature for the incubation of the inoculum varies between 25 and 28 ˚C.[8, 10, 24] The agitation of the inoculum also varies between 150-180 rpm.[8, 23]

2.2.1.3.2 Temperature

Various temperatures have been used during the fermentation process, for the inoculum stage temperatures varied between 28 and 31 ºC.[9, 14, 24] For xanthan production the temperature range was much greater between 24 and 34 ºC.[9, 19] Different temperatures were found for the best biomass accumulation and the best xanthan production. Casas *et al.* (2000) found that the highest average molecular weight of xanthan was at 25 ºC but the acetate and pyruvate conditions were at their lowest.[25] Garcia-Ochoa *et al.* (2000) found that best biomass accumulation was between 25 and 28 ºC but the best xanthan production was found between 28 and 31 ºC. Moraine *et al.* (1973) found the 28 ºC was the optimal production temperature which is in agreement with Nasr *et al*. (2007) [24, 26] Shu and Yang (1990) found that xanthan was produced with a high yield between 31 and 33 ºC however, this affected the pyruvate content in the gum.[27] Production medium is also a factor when deciding which temperature should be used. Garcia-Ochoa *et al.* (2005)

found that the optimal temperature was 28 ºC with this medium but there was little difference when the process was carried out at 31 ºC.[5]

2.2.1.3.3 Oxygen Transfer rates

Micro-organisms use oxygen as a nutrient for growth, maintenance and metabolite production.[28] Inadequate oxygen supply may cause an aerobic process to operate sub-optimally. The low oxygen supply may also lead to low quality products as well as low product yields. The inadequate oxygen supply is a result of the solubility of the oxygen in the medium and the gas-liquid film resistance for oxygen transport.[23] To enhance the gas-liquid transport many different methods have been attempted including modified reactor design and the design of the impellers and sparger. If the fermentation is viscous or the micro-organism is shear sensitive, then these methods may be ineffective.[23]

As a *Xanthomonas* fermentation is an aerobic process the oxygen supply is a critical factor in the fermentations success. In stirred tank reactors the oxygen transfer rate is influenced by the air flow rate and the stirrer speed. Kessler *et al.* (1993) maintained an air flow rate of 1.6 L/L min^{-1} (x L of air per L of fermentation broth per minute) and did not allow the dissolved oxygen to fall below 10 %.[29] Garcia-Ochoa *et al.* (2009) maintained an air flow rate of 1 L/L min^{-1}.[28] Amanullah *et al.* (1998) used an air flow rate of 0.5 L/L min^{-1} with the dissolved oxygen maintained above 15 %.[30] They also found that the critical dissolved oxygen value is in the range of 6 and 10 %. Funahasi *et al.* (1987) suggested that xanthan production was only affected below 6 %.[31] The quality of the xanthan product from the fermentation is affected by the dissolved oxygen tension (DOT), with restricted oxygen supply the molecular weight of the polymer was lower at lower DOT levels.[32, 33]

The agitation given to the fermentation broth is an integral part of the process as xanthan production is an aerobic process. Papagianni *et al.* (2001) found that as the stirrer speed was increased from 100 to 600 rpm, the xanthan production almost doubled. There is also a similar effect on the cell growth.[10] The problem with *Xanthomonas* fermentation is the viscosity of the broth, as the broth viscosity is increased the mixing becomes more difficult. Kessler *et al.* (1993) carried out a comparison of the impeller type within the fermenter and the fermenter type for xanthan production and aeration.[29] Garcia-Ochoa *et al.* (2013) found that at high stirrer speed, cell damage was caused by hydrodynamic stress and there are changes in morphology at high shear stress.[34] The stirred tank reactors gave

good mixing but there were stagnant zones at a certain distance from the impeller. It was also found that the degree of pyruvilation, acetylation and molecular weight increase with fermentation time.

2.2.1.3.4 pH

The pH is controlled within the fermenter to different extents and with different methods depending on the operator of the fermentation. Harding *et al.* (1995) found that a pH range of 6.2 to 7.6 allowed for the carbon source to be completely used.[14] Kessler *et al.* (1993) maintained the pH to 7 with KOH.[29] This pH was also chosen by Rosalam (2006) who found that a neutral pH was optimum for growth of *X. campestris*. pH control was found to enhance cell growth but had no effect on xanthan production no matter which alkali was chosen for pH control. During production the pH decreases from a neutral pH to around pH 5, because of the acid groups present. If the pH is controlled xanthan production ceases once the stationary growth phase is reached, with no pH control the production will continue past this phase.[19] The viscosity of the xanthan solutions are unaffected by pH change. At a pH of 9 or higher the xanthan is gradually deacetylated and at a pH of 3 or lower the xanthan loses pyruvic acid acetyl groups.[9]

2.2.1.4 Analysis Methods

To determine the success of the xanthan fermentation, process many different analysis methods are used; the viscous properties of the solution are used for rheological measurements. The rheological behaviour was determined by Kessler *et al.* (1993) using a rotoviscometer; the samples were degassed before any measurements were carried out. The fermentation broth was found to obey the power law relationship between shear stress and shear rate.[29] Nitschke *et al.* (1995) measured the viscosity of the sample using a viscometer at 25 ˚C.[8] The cell dry weight is calculated by adding KCl to the fermentation sample, this is then centrifuged and the cells removed and washed before being dried and weighed. The glucose concentration is measured using an enzymatic test.[35] Cell free samples are diluted and added to the glucose reagent and after an incubation time the absorbance is measured using a spectrophotometer.

2.2.1.5 Recovery of Xanthan Gum

A final fermentation broth can contain 10-30 g L^{-1} of xanthan, 1- 10 g L^{-1} of cells and 3 - 10 g L^{-1} of residual nutrients and other metabolites.[36] The Peters *et al.* formula discussed by Habibi *et al*. (2017) formulation followed in 3.5 will result in 18.9 g/L (after 90 hours).[22] The xanthan gum in solution is a hydrophilic colloid which forms a true solution (one phase in thermodynamic equilibrium) in water. The high viscosity of the fermentation broth creates difficulties when trying to remove the biomass, also the high viscosity creates problems for thorough mixing of any reagents in the broth. The broth is often pre-diluted before attempts to remove the polymer take place. To remove the polymer from the fermentation broth, the solubility of the polymer is reduced by adding salts or water miscible non-solvents. Often ethanol and isopropyl alcohol are used to precipitate the polymer. Lower alcohols are often used as these wash out impurities as well as decreasing the solubility to allow phase separation. The volume of the alcohol required is usually ≥ 6 times the volume of broth. The cost of the recovery process and any losses associated must be taken into account when deciding the recovery process for xanthan with a specific use. In the oil industry removal of particles such as the cells is crucial as these may block the porous rock from which the oil is obtained. As a food additive the xanthan must be free from biomass and any reagents used in the recovery process. [9, 22]

2.2.1.6 Properties of xanthan gum

Xanthan gum is an unusual natural polysaccharide as it has functional properties which lead to a broad spectrum of uses.[16] Important xanthan properties:

1. Non-Newtonian behaviour
2. High viscosity at low concentrations
3. Salinity causes little change in the viscosity
4. There is resistance to mechanical degradation
5. Stable over a wide range of temperatures (up to 90 ^{o}C)
6. Biodegradable and so is an environmental friendly product[13]

Xanthan gum is important in the oil industry as it is an additive in drilling fluids. The resistance to thermal degradation and it is compatibility with salt allow it to be used in

the pipes to remove as much oil from the well as possible. The pseudoplasticity of the xanthan gum allows faster penetration of the drill bit as it has a low viscosity when the shear is high but at lower shear rates the viscosity increases.[19]

It is used as a stabiliser within the food industry and can be found in many different food products including salad dressings and dairy products. It can improve the freeze-thaw stability of frozen food products. It is used within the agricultural industry to improve the flow properties of insecticides by uniformly suspending the solid component. It reduces the drift of the pesticide and increases the cling and performance. It is also used in jet injection printing as it disperses, hydrates rapidly and is non-polluting which gives a good colour yield.[9]

2.2.1.6.1 Influence of temperature

Changes in temperature during the reaction can have an effect on the molecular properties of the xanthan polymer. If the temperature is increased the molecular weight of the polymer is lower, which is shown through the intrinsic viscosity of the broth.[10] The viscosity of the broth is dependent on the temperature at which the xanthan is dissolved. There is a decrease in the viscosity as the temperature is increased, however, this is fully reversible between 10 and 80 ^{o}C. The viscosity declines as the dissolution temperature is increased to 40 ^{o}C however between 40 and 60 ^{o}C the viscosity increases with increasing temperature but after 60 ^{o}C the viscosity declines with the increasing temperature.[12]

2.2.1.6.2 Influence of polymer and salt concentration

As the concentration of the polymer in the xanthan solution increases the viscosity of the solution also increases. The reason for this increase in viscosity is the intermolecular interaction and entanglement of the polymer. An increase in the molecular weight of the polymer will also lead to an increase in the viscosity. When a salt is added to the solution the viscosity will decline slightly in low polymer concentrations, this is due to the diminished intermolecular electrostatic forces within the polymer which causes a reduction in the molecular dimensions of the polymer. At high xanthan concentrations or when a large amount of salt is added the viscosity increases, which is likely to be due to the increased interaction of the polymer molecules. When the salt concentration exceeds 0.1 % w/v the changes in the viscosity of the xanthan solution are independent.[9]

2.2.1.7 Conclusions from literature

Xanthan gum is an important industrial polymer which is produced from *Xanthomonas campestris* in a batch fermentation. Xanthan has some important properties such as its non-Newtonian behaviour and high viscosity at low concentrations which may allow monitoring of xanthan gum at low concentrations. Its stability over a wide range of temperatures allows a variety of uses but can also allow analysis by a variety of methods.

There are various combinations of production media and operational conditions that can be used for xanthan production during a *Xanthomonas* fermentation. The composition of the nutrients in the production medium is an important factor and a variation of the Garcia-Ochoa *et al.* (2009) medium will be used during the fermentation with sucrose substituted with glucose. The glucose will be used to improve the product yield.[9]

The *Xanthomonas* fermentation will carried out at 30 °C as it was found that between 28 °C and 31 °C there was little difference in the fermentation as the process was carried out. However, more extreme variations in temperature did have an effect on the productivity.[19] A pH of 7 was chosen for the fermentation as this was found to maintain the xanthan production through the stationary phase.[13] The oxygen transfer rates are important and both the aeration and agitation rate must be considered. An inadequate supply of oxygen will cause the process to operate sub-optimally and a low agitation rate will decrease the production rate. From the literature, the agitation rate for the fermentations will be set at 250 rpm and then cascaded to maintain the correct dissolved oxygen concentration with a constant air flow rate of 1 L/L min^{-1}.[28]

2.2.2 *Escherichia coli*

Escherichia coli (*E. coli*) is often used in biotechnology for assessing novel process analytical tools and their uses in fermentation monitoring. They are often used in lab cultures as they are easily manipulated, simple to grow and difficult to contaminate. *E. coli* is an anaerobic Gram negative, rod shaped bacterium. The cells are typically 2-3 µm long and are 0.5µm in diameter.

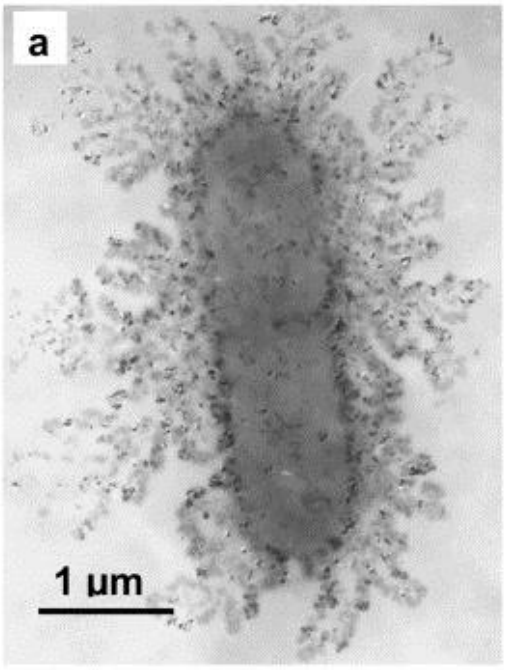

Figure 10: *E. coli* bacterium[37]

2.2.2.1 Production medium

The production medium for *E. coli* fermentations includes the key components as discussed for *Xanthomonas* in 2.2.1.2. As with *Xanthomonas* the actual composition of the media varies greatly, Table 2 illustrates the variation in the medium components.

Table 2 : *E. coli* fermentation media compositions, all masses given in g/L unless otherwise stated

Doak *et al.* (1999)[38]		Macaloney *et al.* (1997)[39]		Castan *et al.* (2002)[40]		Macaloney *et al.* (1994)[41]		Contiero *et al.* (2000)[42]	
NaCl	10	Tryptone	8.57	Tryptone	20	Na_2SO_4	2	Yeast extract	17.5
Tryptone	10	Glycerol	2.8 mL/L	Yeast extract	10	$(NH_4)_2SO_4$	2.46	Tryptone	8.57
Yeast extract	10	Yeast extract	17.15	K_2HPO_4,	2.4 mmol	NH_4Cl	0.5	Glycerol	3.53
Glucose	400	KH_2HPO_4	25	Antifoam	small amount	K_2HPO_4	14.6	K_2HPO_4	25
		NH_4Cl	35	$CaCl_2$,	1 mmol	$NaH_2PO_4.H_2O$	3.6	KH_2PO_4	4.62
		Ampicillin	100 mg/L	$MgSO_4$,	1.2 mmol	$(NH_4)_2$-H-citrate	1	Ampicillin	100 mg/L
		PPG 2000	0.027	Thiamine	0.6 mg/L	$MgSO_4.7H_2O$	1.2	NH_4Cl	5.35
				Glucose	2	Trace element solution	2 mL/L	PPG 2000	75µL/L.
						Thiamine	0.1		

Jensen *et al.* (1990)[43]		McGovern *et al.* (1999)[44]		Zhu *et al.* (2011)[45]		Luli *et al.* (1990)[46]		Arnold *et al.* (2002)[47]	
Yeast extract	20	Glycerol	40	K_2HPO_4	6	Yeast extract	17.15	glucose	25
Glycerol	35	Glucose monohydrate	38.62	KH_2PO_4	3	Tryptone	Jan-00	KH_2PO_4	0.865
Casein hydrolysate	2	Citric acid	3	NaCl	0.5	Glycerol	3.53	K_2HPO_4	7.65
Na_2HPO_4	6	KH_2PO_4	5.55	NH_4Cl	1	K_2HPO_4	25	Tryptone	12
NaCl	10	$K_2HPO_4.3H_2O$	5.6	Yeast extract	5	KH_2PO_4	4.62	Yeast extract	24
$(NH_4)_2SO_4$	10	$NaH_2PO_4.H_2O$	2.25	Glucose	5	NH_4Cl	5.35		
KH_2PO_4	3	$(NH_4)_2SO_4$	1	$MgSO_4$	2 mmol	Ampicillin	100 mg/L		
$MgSO_4.7H_2O$	0.05	NH_4Cl	0.1	$CaCl_2$	0.1 mmol				
$CaCl_2.H_2O$	0.03	$MgCl_2.6H_2O$	1.25	Trace elements	1 mL/L				
Thiamine	0.008	$FeSO_4.7H_2O$	0.02 mg/L						
$FeSO_4$	40 mg	$CaCl_2.7H_2O$	0.02						
Citric acid	20 mg	$MnSO_4.H_2O$	12.9 mg/L						
Trace elements solution	0.5 mL	$ZnSO_4.7H_2O$	8.7 mg/L						
Tetracycline	10 µg	$CoCl_2.6H_2O$	6.45 mg/L						
		$CuCl_2.2H_2O$	3.2 mg/L						
		$Na_2MoO_4.2H_2O$	2,7 mg/L						
		$AlCl_3$	0.8 mg/L						
		H_3BO_3	0.5 mg/L						
		Thiamine HCl	5.00 mg/L						

2.2.2.2 Operational conditions

2.2.2.2.1 Inoculum

Various inoculum preparations were used in the literature with most containing tryptone and yeast extract. Variations in the other components of the media can be seen as well as the conditions in which the inoculum was prepared. Table 3 shows the various inoculum preparation methods for *E. coli* fermentations.

Table 3 : *E. coli* inoculum preparations, all masses reported in g/L unless otherwise stated.

Macaloney *et al.* (1994)[41]		Doak *et al.*(1999)[38]		Macaloney *et al.* (1997)[47]		Castan *et al.* (2002)[40]	
Glycerol	2.8 mL/L	Glucose	25	Glycerol	5.04	Glucose	1 % (w/v)
Tryptone	12.0	Tryptone	12	Tryptone	12.0	Peptone	1 % (w/v)
Yeast extract	24.0	Yeast extract	24	Yeast extract	24.0	Yeast extract	0.5 % (w/v)
KH_2PO_4	2.31	KH_2PO_4	0.87	KH_2PO_4	2.31	NaCl	0.5 % (w/v)
K_2HPO_4	12.5	K_2HPO_4	7.65	K_2HPO_4	12.5	Ampicillin	100 µg/mL
Ampicillin	100 mg/L			Ampicillin	100 mg/L		

2.2.2.2.2 Temperature

The temperature of the fermentation can vary between 30 and 37 ^oC. The lowest temperature for growth was reported by Jensen *et al.* (1990) and Yazdini *et al.* (2002) [43, 49] with Castan *et al.* (2002) using 34 ^oC during their experimentation with *E. coli.*[40] Conteiro *et al.* (2000) reported using 35 ^oC for the fermentation.[42] Sohoni *et al. (2015)* used different temperatures dependent on the bioreactor used. Fed-batch cultivations in a bioreactor was carried out at 32 ^oC. However, shake flask experiments were carried out at 37 ^oC.[50] 37 ^oC is the most common temperature reported in the literature for fermentations.[41, 44, 45, 49, 50, 52-57, 46, 48, 58, 59]

2.2.2.2.3 Oxygen transfer rates

The oxygen transfer rates within an *E. coli* fermentation vary throughout the literature with the focus varying between the dissolved oxygen saturation being maintained at a specific level and aeration rate. The aeration rate varies between 0.4 L/L min and 3 L/L min.[43, 49, 52, 55-57] and the dissolved oxygen rate is also controlled across a wide range of saturation levels of 5 and 50 %. [42-44, 46, 53, 54, 58, 59]

2.2.2.2.4 pH

The pH is maintained in the fermentation with the literature reporting various pH from 6.5 to 7.5. Zhu *et al.* (2011) report the largest pH range with control between 6.5 and 7.5.[52] However, other authors report a much more specific pH, Jensen *et al.* (1990) and Macaloney *et al.* (1997) report a pH of 7.2 [43, 48, 59] and Han *et al.* (1992) report a pH of 7.4.[57] The most common pH reported in the literature is 7 with this maintained throughout the fermentation. [24, 33-34, 37, 39-40, 42-43]

2.2.2.3 Analysis methods

E. coli has been used as an example for many novel monitoring techniques. *In-situ* and at-line monitoring of biomass changes in an *E. coli* fermentation has been carried out by Arnold *et al.* (2002) using near-infrared (NIR), at-line monitoring modeling was successful but the *in-situ* monitoring raised some problems with the matrix.[47] At-line control and fault analysis in an industrial high cell density *E. coli* fermentation using NIR has been carried out by Macaloney *et al* (2000) with the ability to detect bioreactor faults such as dissolved oxygen probe and pH control failure.[41] Mid-infrared (MIR) has also be used to monitor an *E.* coli fermentation using modeling techniques glucose and acetic acid can be monitored using MIR with the errors associated with these models being from the off-line analysis methods rather than the model themselves.[38] Other work has revolved around the concentration of acetic acid and acetate production and the effect that these can have on the production of proteins.[46, 57, 58] Acetate formation in *E. coli* has been monitored using sensors by using the dissolved oxygen response of food transients.[54]

2.2.2.4 Conclusions from the literature

There is a great range in the dissolved oxygen and air flow into the fermentation, the air flow rate chosen for the *E. coli* fermentations was 1 vvm with the dissolved oxygen rate maintained above 20 %. The pH chosen for the fermentation was pH 7 which would be regulated by 2 M sodium hydroxide and 1 M sulfuric acid solutions. There is a large variation in the components of a fermentation medium and the formulation chosen for the *E. coli* fermentation within this thesis was chosen from previous work carried out on this specific strain of *E. coli* and by previous members of the Strathclyde Fermentation Centre.[60]

2.3 References

1. Fermentation process. **2005,** *2009*, Process of fermentation.

2. Crueger, W., *Biotechnology : a textbook of industrial microbiology*. Sunderland, MA : Sinauer Associates: **1990.**

3. McNeil, B.; Harvey, L. M.; Hunter, I., Fermentation technology. The University of Strathclyde: Glasgow, **2009.**

4. Rocha-Valadez, J. A.; Albiter, V.; Caro, M. A.; Serrano-Carreon, L.; Galindo, E., A fermentation system designed to independently evaluate mixing and/or oxygen tension effects in microbial processes: development, application and performance. *Bioprocess and biosystems engineering* **2007,** *30* (2), 115-122.

5. Garcia-Ochoa, F.; Gomez, E., Prediction of gas-liquid mass transfer coefficient in sparged stirred tank bioreactors. *Biotechnol. Bioeng.* **2005,** *92* (6), 761-772.

6. Kelly, M. P.; Hallberg, K. B.; Tuovinen, O. H., Biological degradation of 2,4-dichlorophenoxyacetic acid: chloride mass balance in stirred tank reactors. *Applied and Environmental Microbiology* **1989,** *55* (10), 2717-2719.

7. http://click4biology.info/c4b/4/gene4.4.htm.(accessed 04/09/16)

8. Nitschke, M.; Thomas, R., Xanthan gum production by wild-type isolates of xanthomonas campestris. *World J. Microbiol. Biotechnol.* **1995,** *11* (5), 502-504.

9. Garcia-Ochoa, F.; Santos, V. E.; Casas, J. A.; Gomez, E., Xanthan gum: production, recovery, and properties. *Biotechnol. Adv.* **2000,** *18* (7), 549-579.

10. Papagianni, M.; Psomas, S. K.; Batsilas, L.; Paras, S. V.; Kyriakidis, D. A.; Liakopoulou-Kyriakides, M., Xanthan production by Xanthomonas campestris in batch cultures. *Process Biochem.* **2001,** *37* (1), 73-80.

11. Chun, W. W. C., Xanthomonadins, Unique Yellow Pigments of the Genus Xanthomonas. *The Plant Health Instructor.* **2002**.

12. Garcia- Ochoa, F.; Santos, V. E.; Alcon, A., Xanthan gum production - an unstructured kinetic model. *Enzyme Microb. Technol.* **1995,** *17* (3), 206-217.

13. Peters, H. U.; Suh, I. S.; Schumpe, A.; Deckwer, W. D., Modeling of batchwois xanthan production, *Can. J. Chem. Eng.* **1992,** *70* (4), 742-750.

14. Harding, N. E.; Cleary, J. M.; Ielpi, L., *Genetics and biochemistry of xanthan gum production by Xanthomonas campestris*. VCH Publishers, Inc.; VCH Verlagsgesellschaft mbH: 1995; p 495-514.

15. Vendrusculo, C. T.; Pereira, J. L.; Scamparini, A. R. P., Gellan Gum: Production And Properties. In *Food Hydrocolloids: Structures, Properties, and Functions*, Nishinari, K.; Doi, E., Eds. Springer US: Boston, MA, 1993; pp 91-95.

16. http://www.scientificpsychic.com/fitness/carbohydrates2.html. (accessed 26/09/10).

17. Amanullah, A.; Satti, S.; Nienow, A. W., Enhancing Xanthan fermentations by different modes of glucose feeding. *Biotechnol. Prog.* **1998,** *14* (2), 265-269.

18. Lo, Y.-M.; Yang, S.-T.; Min, D. B., Effects of yeast extract and glucose on xanthan production and cell growth in batch culture of *Xanthomonas campestris*. *Applied microbiology and biotechnology* **1997,** *47* (6), 689-694.

19. Rosalam, S.; England, R., Review of xanthan gum production from unmodified starches by *Xanthomonas comprestris* sp. *Enzyme Microb. Technol.* **2006,** *39* (2), 197-207.

20. Leela, J. K.; Sharma, G., Studies on xanthan production from *Xanthomonas campestris*. *Bioprocess Eng.* **2000,** *23* (6), 687-689.

21. Letisse, F.; Chevallereau, P.; Simon, J. L.; Lindley, N. D., Kinetic analysis of growth and xanthan gum production with *Xanthomonas campestris* on sucrose, using sequentially consumed nitrogen sources. *Applied microbiology and biotechnology* **2001,** *55* (4), 417-422.

22. Habibi, H.; Khosravi-Darani, K., Effective variables on production and structure of xanthan gum and its food applications: A review. *Biocatalysis and Agricultural Biotechnology* **2017,** *10*, 130-140.

23. Sriram, G.; Rao, Y. M.; Suresh, A. K.; Sureshkumar, G. K., Oxygen supply without gas-liquid film resistance to *Xanthomonas campestris* cultivation. *Biotechnol. Bioeng.* **1998,** *59* (6), 714-723.

24. Nasr, S.; Soudi, M. R.; Haghighi, M., Xanthan production by a native strain of *X. campestris* and evaluation of application in EOR. *Pak J Biol Sci* **2007,** *10* (17), 3010-3.

25. Casas, J. A.; Santos, V. E.; Garcia-Ochoa, F., Xanthan gum production under several operational conditions: molecular structure and rheological properties. *Enzyme Microb. Technol.* **2000,** *26* (2-4), 282-291.

26. Moraine, R. A.; Rogovin, P., Kinetics of the xanthan fermentation. *Biotechnol. Bioeng.* **1973,** *15* (2), 225-237.

27. Shu, C. H.; Yang, S. T., Effects of temperature on cell-growth and xanthan production in batch cultures of *Xanthomonas campestris Biotechnol. Bioeng.* **1990,** *35* (5), 454-468.

28. Garcia-Ochoa, F.; Gomez, E., Bioreactor scale-up and oxygen transfer rate in microbial processes: an overview. *Biotechnol Adv* **2009,** *27* (2), 153-76.

29. Kessler, W. R.; Popovic, M. K.; Robinson, C. W., Xanthan production in an external circulation loop airlift fermenter. *Can. J. Chem. Eng.* **1993,** *71* (1), 101-106.

30. Amanullah, A.; Tuttiett, B.; Nienow, A. W., Agitator speed and dissolved oxygen effects in Xanthan fermentations. *Biotechnol. Bioeng.* **1998,** *57* (2), 198-210.

31. Funahashi, H.; Maehara, M.; Taguchi, H.; Yoshida, T., Effects of agitation by flat-bladed turbine impeller on microbial-production of xanthan gum *J. Chem. Eng. Jpn.* **1987,** *20* (1), 16-22.

32. Flores, F.; Torres, L. G.; Galindo, E., Effect of the dissolved oxygen tension during cultivation of *X. campestris* on the production and quality of xanthan gum. *Journal of biotechnology* **1994,** *34* (2), 165-173.

33. Suh, I.-S.; Herbst, H.; Schumpe, A.; Deckwer, W.-D., The molecular weight of xanthan polysaccharide produced under oxygen limitation. *Biotechnology letters* **1990,** *12* (3), 201-206.

34. Garcia-Ochoa, F.; Gomez, E.; Alcon, A.; Santos, V. E., The effect of hydrodynamic stress on the growth of *Xanthomonas campestris* cultures in a stirred and sparged tank bioreactor. *Bioprocess and biosystems engineering* **2013,** *36* (7), 911-925.

35. Tosi, S.; Rossi, M.; Tamburini, E.; Vaccari, G.; Amaretti, A.; Matteuzzi, D., Assessment of in-line near-infrared spectroscopy for continuous monitoring of fermentation processes. *Biotechnol. Prog.* **2003,** *19* (6), 1816-1821.

36. Li, P.; Li, T.; Zeng, Y.; Li, X.; Jiang, X.; Wang, Y.; Xie, T.; Zhang, Y., Biosynthesis of xanthan gum by *Xanthomonas campestris* LRELP-1 using kitchen waste as the sole substrate. *Carbohydr. Polym.* **2016,** *151*, 684-691.

37. Sondi, I.; Salopek-Sondi, B., Silver nanoparticles as antimicrobial agent: a case study on *E. coli* as a model for Gram-negative bacteria. *Journal of Colloid and Interface Science* **2004,** *275* (1), 177-182.

38. Doak, D. L.; Phillips, J. A., In situ monitoring of an *Escherichia coli* fermentation using a diamond composition ATR probe and mid-infrared spectroscopy. *Biotechnol. Prog.* **1999,** *15* (3), 529-539.

39. Macaloney, G.; Hall, J. W.; Rollins, M. J.; Draper, I.; Anderson, K. B.; Preston, J.; Thompson, B. G.; McNeil, B., The utility and performance of near-infra red spectroscopy in simultaneous monitoring of multiple components in a high cell density recombinant *Escherichia coli*; production process. *Bioprocess and biosystems engineering* **1997,** *17* (3), 157-167.

40. Castan, A.; Näsman, A.; Enfors, S.-O., Oxygen enriched air supply in Escherichia coli processes: production of biomass and recombinant human growth hormone. *Enzyme Microb. Technol.* **2002,** *30* (7), 847-854.

41. Macaloney, G.; Hall, J. W.; Rollins, M. J.; Draper, I.; Thompson, B. G.; McNeil, B., Monitoring biomass and glycerol in an *Escherichia coli*; fermentation using near-infrared spectroscopy. *Biotechnology Techniques* **1994,** *8* (4), 281-286.

42. Contiero, J.; Beatty, C.; Kumari, S.; DeSanti, C. L.; Strohl, W. R.; Wolfe, A., Effects of mutations in acetate metabolism on high-cell-density growth of *Escherichia coli*. *J. Ind. Microbiol. Biotechnol.* **2000,** *24* (6), 421-430.

43. Jensen, E. B.; Carlsen, S., Production of recombinant human growth hormone in *Escherichia coli:* Expression of different precursors and physiological effects of glucose, acetate, and salts. *Biotechnol. Bioeng.* **1990,** *36* (1), 1-11.

44. McGovern, A. C.; Ernill, R.; Kara, B. V.; Kell, D. B.; Goodacre, R., Rapid analysis of the expression of heterologous proteins in *Escherichia coli* using pyrolysis mass spectrometry and Fourier transform infrared spectroscopy with chemometrics: application to α2-interferon production. *Journal of biotechnology* **1999,** *72* (3), 157-168.

45. Zhu, H. L.; Gonzalez, R.; Bobik, T. A., Coproduction of Acetaldehyde and Hydrogen during Glucose Fermentation by *Escherichia coli*. *Applied and environmental microbiology* **2011,** *77* (18), 6441-6450.

46. Luli, G. W.; Strohl, W. R., Comparison of growth, acetate production, and acetate inhibition of *Escherichia coli* strains in batch and fed-batch fermentations. *Applied and environmental microbiology* **1990,** *56* (4), 1004-1011.

47. Arnold, S. A.; Gaensakoo, R.; Harvey, L. M.; McNeil, B., Use of at-line and in-situ near-infrared spectroscopy to monitor biomass in an industrial fed-batch *Escherichia coli* process. *Biotechnol. Bioeng.* **2002,** *80* (4), 405-413.

48. Macaloney, G.; Hall, J. W.; Rollins, M. J.; Draper, I.; Anderson, K. B.; Preston, J.; Thompson, B. G.; McNeil, B., The utility and performance of near-infra red spectroscopy in simultaneous monitoring of multiple components in a high cell density recombinant *Escherichia coli* production process. *Bioprocess Eng.* **1997,** *17* (3), 157-167.

49. Yazdani, S. Y.; Mukherjee, K. M., Continuous-culture studies on the stability and expression of recombinant streptokinase in *Escherichia coli*. *Bioprocess and biosystems engineering* **2002,** *24* (6), 341-346.

50. Sohoni, S. V.; Nelapati, D.; Sathe, S.; Javadekar-Subhedar, V.; Gaikaiwari, R. P.; Wangikar, P. P., Optimization of high cell density fermentation process for recombinant nitrilase production in *E. coli*. *Bioresour. Technol.* **2015,** *188*, 202-208.

51. Buck, K. K. S.; Subramanian, V.; Block, D. E., Identification of Critical Batch Operating Parameters in Fed-Batch Recombinant *E. coli* Fermentations Using Decision Tree Analysis. *Biotechnology Progress* **2002,** *18* (6), 1366-1376.

52. Zhu, J. F.; Thakker, C.; San, K. Y.; Bennett, G., Effect of culture operating conditions on succinate production in a multiphase fed-batch bioreactor using an engineered *Escherichia coli* strain. *Applied microbiology and biotechnology* **2011,** *92* (3), 499-508.

53. Gnoth, S.; Simutis, R.; Lubbert, A., Selective expression of the soluble product fraction in *Escherichia coli* cultures employed in recombinant protein production processes. *Applied microbiology and biotechnology* **2010,** *87* (6), 2047-2058.

54. Åkesson, M.; Karlsson, E. N.; Hagander, P.; Axelsson, J. P.; Tocaj, A., On-line detection of acetate formation in *Escherichia coli* cultures using dissolved oxygen responses to feed transients. *Biotechnol. Bioeng.* **1999,** *64* (5), 590-598.

55. Andersen, K. B.; von Meyenburg, K., Are growth rates of *Escherichia coli* in batch cultures limited by respiration? *Journal of bacteriology* **1980,** *144* (1), 114-123.

56. Belo, I.; Mota, M., Batch and fed-batch cultures of *E. coli*; TB1 at different oxygen transfer rates. *Bioprocess and biosystems engineering* **1998,** *18* (6), 451-455.

57. Han, K.; Lim, H. C.; Hong, J., Acetic acid formation in *Escherichia coli* fermentation. *Biotechnol. Bioeng.* **1992,** *39* (6), 663-671.

58. Nakano, K.; Rischke, M.; Sato, S.; Märkl, H., Influence of acetic acid on the growth of *Escherichia coli*; K12 during high-cell-density cultivation in a dialysis reactor. *Applied microbiology and biotechnology* **1997,** *48* (5), 597-601.

59. Macaloney, G.; Draper, I.; Preston, J.; Anderson, K. B.; Rollins, M. J.; Thompson, B. G.; Hall, J. W.; McNeil, B., At-line control and fault analysis in an industrial high cell density *Escherichia coli* fermentation, using NIR spectroscopy. *Food Bioprod. Process.* **1996,** *74* (C4), 212-220.

60. Voulgaris, I. Production of novel amine oxidases from microorganisms. Thesis [Ph. D] -- University of Strathclyde, **2011.**

3 Infrared Spectroscopy

Infrared spectroscopy is a common process analysis technique which has been applied across a wide range of industries.[1] Infrared monitoring has previously been used to monitor other fermentation processes including *E. coli* and *Pichia pastoris*.[2, 3] This chapter investigates the use of both near and md infrared to monitor an *X. campestris* fermentation including modeling of the fermentation system using the off-line reference analysis.

3.1 Infrared theory

Infrared spectroscopy investigates the vibrational properties of the molecules studied. Molecular vibrations occur in the mid infrared region (400-4000 cm^{-1}). Combination bands and overtones of these fundamental vibrations occur in near infrared region of 4000-12500 cm^{-1}. Absorption occurs when a quantum of infrared light interacts with the molecule; it may absorb the energy and therefore vibrate faster. This absorption leads to an increase in vibrational energy level. Absorption can occur when the infrared radiation interacts with a molecule undergoing a change in dipole moment and when the incoming infrared photon has sufficient energy for the transition to the next allowed vibrational state. When the light passes through the material it may be selectively absorbed and the remaining part of the light may be partially transmitted and reflected.

A photon with twice or three times the amount of energy necessary to elevate a molecule to the energy level corresponding to a fundamental absorption will cause excitation to the 2^{nd} and 3^{rd} vibrational energy levels, thereby causing a 1^{st} and 2^{nd} overtone. There are few molecules which produce overtones which can be seen in the NIR region and the higher the overtone, the lower the probability of it occurring. An overtone is generally weaker in intensity with a 1^{st} overtone having ½ the energy of the fundamental absorption and the 2^{nd} overtone has a $^1/_3$. A combination band occurs when the absorbed photon excites two or more of the vibrations; the energy of the photon must be equal to the sum of the energies of the coupling vibrations. The intensity of the combination band absorption is inversely proportional to the number of different vibrations that couple.[4]

The amount of light that is absorbed and the wavelength dependent nature of absorption can provide information about the physical and chemical nature of the material. The amount of light absorbed cannot be measured directly and instead it has to be calculated from either the transmitted or the reflected light. The low molar absorptivity of absorption bands in NIR restricts the sensitivity of the technique but it does allow reflectance measurements to be carried out. When the light is passed through the sample it crosses multiple interfaces and at each interface some light is reflected. If the surface is rough this results in reflection in all directions. In biotechnology systems this can be useful for monitoring the changing morphology. The solids within the fermentation broth will cause the light to be scattered in all directions.

IR measurements can be taken in transmission, reflectance and transflectance modes. Transmission mode is when IR radiation is passed through a sample and the transmitted radiation is measured. Reflectance mode measures the IR radiation that is reflected by the sample. Transflectance probes have contact with the sample fluid which separates the emitter or detector at one side and a mirror at the other side. The emitted light crosses the fluid being partially absorbed, transmitted and reflected. Some light does not reach the mirror but is detected due to the reflection from the sample, whereas light that reaches the mirror is reflected back to the detector and this constitutes the transmission component.[5]

$$A = \log_{10} \frac{I_o}{I}$$ **Equation 1**

Absorbance (A) is measured using Equation 1 where I_0 is the incident radiation intensity and I_1 is the intensity of the transmitted radiation. The intensity of the transmitted radiation can be swapped with the intensity of reflected radiation. [5]

When the IR spectra are combined with chemometrics both qualitative and quantitative analysis can be carried out which is useful in various industries including monitoring of biotechnology processes.[6]

3.2 IR Instrumentation

3.2.1 Dispersive spectrometers

A dispersive instrument has a light source which sends light through both a sample and a reference path and through a chopper which moderates the energy that reaches the detector. The light is then directed to a diffraction grating; this separates the wavelengths of light in the spectral range and directs each wavelength through a slit in the detector. Each wavelength is measured one at a time with the slit monitoring the spectral bandwidth and the grating moving to select the wavelength being measured. An external source of wavelength calibration is required.

3.2.2 Fourier Transform spectroscopy

Fourier transform instrumentation is different to dispersive spectrometers and are based on the Michelsen Interferometer (Figure 11).

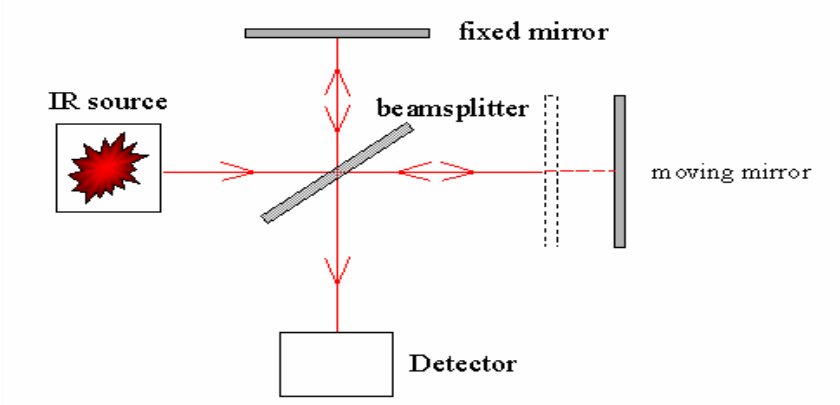

Figure 11 : Schematic of FTIR system[7]

When light strikes the beam splitter, the light is split into two beams which then pass to either the fixed or the moving mirror. The moving mirror oscillates back and forth. When the light is reflected from these mirrors the beam splitter then recombines the light which then passes through the sample. The sample will then absorb the light and this will be detected by the detector. The interference between the light reflecting from the fixed mirror and the energy observed by the detector produces the interferogram.

There are some advantages to this technique as all the spectral elements are measured simultaneously. Thus the spectrum can be obtained very quickly which leads to a better signal to noise ratio when spectra are collected over the same time as dispersive instrument Alternatively it makes it a quicker technique for obtaining a spectrum of the same quality compared to a dispersive instrument. Therefore, FTIR is better for kinetic work and where the signal to noise ratio is poor. There is also no slit for the light to be attenuated and so there is a greater optical throughput and again the signal to noise ratio will be higher than a dispersive instrument.[8]

3.3 IR measurements in biotechnology processes

IR can be used for analysis and control of fermentation processes both small and large scale. [9-11] In most fermentation processes, there are multiple substrates present which can cause problems with designing a IR method for analysis.[12] For in-line analysis, the IR probe is interfaced with a specific fermenter and is inserted into a standard fermenter port. The probes are designed to be resistant to multiple sterilization cycles. When a fermentation is monitored the NIR spectra are collected in either reflectance, transmittance or transflectance mode. For transmittance, the narrow optical path lengths in conjunction with the fluid dynamics of the broth media can make this difficult to implement. IR has yet to be fully exploited due to regulatory problems although IR has been shown to be useful in both aerobic and anaerobic fermentation processes. The organisms that have been investigated and the mode of IR are given in Table 4. When using IR to monitor a fermentation reaction there are many influencing factors, production organism is important, as this will provide information on morphology and the physiological properties. The conditions within the fermenter will also affect the IR measurements. Typical fed-batch bioprocesses involve very close control of one or more nutrients at very low concentrations. MIR spectra provide more useful information than corresponding weaker NIR absorbences. NIR spectroscopy has difficulties generating useful information for analytes at sub g/L concentrations. MIR spectroscopy can distinguish microbes at the strain level and two very closely related chemical species in a biotransformation process. MIR spectroscopy can also determine the concentration of individual sugars in complex mixtures.

Table 4 : Monitoring of different fermentation processes using near and mid infrared

Author	Organism	Infrared Region	Measurement mode	Analysis Method
Arnold *et al.* (2002)[2]	*Escherichia coli*	Near-infrared	Transmission	At-line
Arnold *et al.* (2003)[13]	CHO-K1	Near-infrared	Transmission	*In-situ*
Arnold *et al* (2000)[14]	*Streptomyces fradiae*	Near-infrared	Transmission	At-line
Cavinto *et al.* (1990)[15]	*Saccharomyces cerevisiae*	Near-infrared	Reflectance	On-line
Cimander *et al.* (2002)[16]	*Lactobacillus bulgaricus and Streptococcus thermophilis*	Near-infrared	Reflectance	On-line
Cimander *et al.* (2002)[17]	*Escherichia coli*	Near-infrared	Transmission	*In-situ*
Crowley *et al.* (2005)[3]	*Pichia pastoris*	Near-infrared	Transmission	*In-situ*
Crowley *et al.* (2000)[18]	*Pichia pastoris*	Mid-infrared	ATR	Off-line
Ferreira *et al.* (2001)[19]	*Streptomyces clavuligerus*	Near-infrared	Reflectance	At-line
Finn *et al.* (2006)[20]	*Saccharomyces cerevisiae*	Near-infrared	Transmission	At-line
Ge *et al.* (1994)[21]	*Saccharomyces cerevisiae*	Near-infrared	Reflectance	On-line
Giavasis *et al.* (2003)[22]	*Sphingomonas paucimobilis*	Near-infrared	Transmission	Off-line
Hall *et al.* (1996)[23]	*Escherichia coli*	Near-infrared	Transmission	Off-line
Lewis *et al.* (2000)[24]	Fibroblast cells	Near-infrared	Transmission	*In-situ*
Macaloney *et al.* (1996)[25]	*Escherichia coli*	Near-infrared	Transmission	At-line
Macauley-Patrick *et al.* (2003)[26]	*Gluconobacter suboxydans*	Mid-infrared	ATR	On-line
McShane *et al.* (1998)[27]	Cell-culture	Near-infrared	Transmission	At-line
Mosheky *et al.* (2001)[28]	Saccharomyces cerevisiae	Near-infrared	-	On-line
Navratil *et al.* (2004)[29]	*Lactococcus thermophilus, Lactococcus cremoris, Lactococcus diactylactis and Leuconostoc cremoris*	Near-infrared	Reflectance	On-line
Navratil *et al.* (2005) [30]	*Vibrio cholera*	Near-infrared	Reflectance	On-line
Nordon *et al.* (2008)[31]	*Streptomyces*	Near-infrared	Reflectance	*In-situ*
Rhiel *et al.* (2002)[32]	*Prostate cancer cells*	Near-infrared	Transmission	At-line
Riley *et al.* (1997)[33]	Insect cells	Near-infrared	Transmission	Off-line
Riley *et al.* (1998)[34]	Insect cells	Near-infrared	Transmission	Off-line
Rodrigues *et al.* (2008)[35]	*Streptomyces clavuligerus*	Near-infrared	Transflectance	*In-situ*
Roychoudhury *et al.* (2006)[36]	*Streptomyces clavuligerus*	Mid-infrared	ATR	At-line
Roychoudhury *et al.* (2007)[37]	*Streptomyces clavuligerus*	Mid-infrared	ATR	At-line
Sivakesava *et al.* (2001) [38]	*Lactobacillus casei*	Near & Mid-infrared	ATR- MIR	At-line

Tamburini *et al.* (2003)[39]	*Staphylococcus and Lactobacillus*	Near-infrared	Transflectance	On-line
Tosi *et al.* (2003)[40]	*Staphylococcus xylosus*	Near-infrared	Transflectance	On-line
Triadaphillou *et al.* (2007)[41]	Fungus	Near-infrared	Reflectance	On-line
Vaidyananthan *et al.* (2001)[42]	*Streptomyces fradiae*	Near-infrared	Transmission	At-line
Vaidyanathan *et al.* (2001) [43]	*Penicillium chrysogenum*	Near-infrared	Transmission	At-line
Vaidyanathan *et al.* (1999)[44]	*E. coli, Streptomyces fradiae, Penicillium chrysogenum and, Aspergillus niger*	Near-infrared	Reflectance	Off-line
Vaidyanathan *et al.*(2003)[45]	*Streptomyces fradiae*	Near-infrared	Transmission & reflectance	Off-line
Vaidyanathan *et al.* (2001)[46]	*Penicillium Chrysogenum*	Near-infrared	Transmission	At-line
Yeung *et al.* (1999) [47]	*Saccharomyces Cerevisiae*	Near-infrared	Transmission	On-line

3.3.1 Production organism

The production organism must be considered when the determining the best method of monitoring the fermentation process. The conditions required by the organism vary from anaerobic with low agitation and aerobic with high agitation. Also the biomass concentration produced by the organism and its morphology must be evaluated as these will affect the viscosity and scattering properties of the material. The biomass concentration can be evaluated as an increased biomass concentration will influence the scattering properties and will decrease the light permeability through the system.

Ge *et al.* (1994) monitored *Saccharomyces* cell density by NIR. It was carried out on-line using reflectance measurements. It was found that as the concentration of the biomass increased the backscattered light increased and therefore the spectral absorbance decreased. The second derivative spectra were then used to resolve the spectral overlaps and used to model the biomass concentration.[21] Vaidyanathan *et al.* (2003) carried out a study of 5 different production organisms, three filamentous fungi, one filamentous bacteria and one gram negative unicellular bacteria. The reflectance NIR spectra showed prominent peaks at the same wavelengths for all 5 micro-organisms at 2270-2350 nm and 1650 – 1800 nm. As the identified spectral regions relate to CH, CH_2 and CH_3, these were found to be useful for modelling biomass of these organisms regardless of which organism was used.[45] The regions investigated by both Ge *et al.* (1994) and Vaidyanathan *et al.* (2003) have the potential to be of interest for a *Xanthomonas* fermentation as the CH, CH_2 and CH_3 groups can be found in the glucose and the xanthan gum product.[21, 45]

Morphological properties of the organism will affect the viscosity of the fermentation broth. Tosi *et al.* (2003) also carried out a study of the effects of morphology on the spectra obtained in the region of 700-1800 nm. They found that there was a lack of spectral difference between the rod and spherical shapes. However, there was an overwhelming presence of water and a low final biomass concentration. A calibration model for *S. xylosus* was created to determine acetic acid concentration and this was then used to predict biomass concentration in two other micro-organisms. The model

predicted well for *L. fermentum* and after the addition of external validation steps the model also predicted well for *S. thermophilis*. The external validation steps were thought to be required as lactic acid was produced rather than acetic acid.[40] As *X. campestris* has the same rod shape as *L. fermentum* this would suggest that the morphology of a *X. campestris* should not prevent the ability to monitor the fermentation.

3.3.2 Fermenter conditions

Fermenter conditions will affect the quality of the NIR spectra. There are many variables within the reactor that must be controlled such as agitation rate, aeration rate and temperature.

The flow of the fermentation broth within the fermenter will affect the spectra. Therefore, during the calibration and validation runs, the position of the probe in the fermenter, the agitation and the aeration rates must be kept constant. Ge *et al.* (1994) maintained a constant biomass concentration but increased the agitation rate. There was increased backscattered light this was due to the centrifugal force that push the cells to the reactor walls and/or effects the settling of the particles. However, when the gas flow rate was increased there was a decrease in backscattered light. This was likely to be due to the increased number of air bubbles and therefore a greater fraction of light was transmitted through the bubbles without scattering.[21]

However, Tamburini *et al.* (2003) were in agreement regarding the results of increased agitation rate but with the aeration rate the opposite result was found. Tamburini used an *in-situ* probe rather than an ex-situ probe which may have caused the differences. The air flow rate and agitation caused base line shifts which may be due to the scattering effects of both particles and bubbles. However, an increase in the stirring rate had a greater influence due to the increased movement of the particles and bubbles causing more scattering. The increased stirring rate created more and smaller bubbles which were able to fit through the slit in the probe. The effect of the air flow rate is not as distinct as the added air bubbles produced from the increased air flow rate were larger and so they found it more difficult to fit through the slit in the probe. [39]

Navratil *et al.* (2004) were in agreement with Tamburini *et al.* (2003) and to compensate for the apparent increase in absorbance due to the scattering effects of the bubbles and agitation, they used a correction factor based on a 4th order polynomial equation which was a function of the stirring rate. This correction improved the precision of the predictions of biomass concentration.[29]

To maintain the oxygen levels with the *X. campestris* fermentation the agitation rate will be increased so consideration must be taken of the backscattered light caused by the agitation. As the gas flow rate will be maintained in the *X. campestris* fermentation, the fraction of light transmitted through the bubbles should remain constant.

Temperature changes affect the vibration intensity of molecular bonds and therefore the NIR spectrum of a sample will be influenced by temperature variation. Where water is the major component, as it is in fermentation processes, the effect of changes in temperature is especially noticeable. Temperature affects the degree of hydrogen bonding. An increase in temperature leads to a decrease in the number of hydroxyl groups involved in the hydrogen bonding therefore the absorption band of the free hydroxyl increases. These changes influence the wavelengths where the overtones and combinations occur. [48] Arnold *et al.* (2002) studied a more complex fermentation reaction which had a sudden increase in temperature followed by gradual increases. They found that the spectral changes were difficult to predict due to this variance in temperature. It was found that over time and with the biomass growth it was difficult to distinguish the effects of temperature alone. If the spectra are derivatised the analyte can be distinguished despite the changes in temperature. Temperature can also be included in the model as an independent variable.[2] The temperature in the *X. campestris* fermentation is maintained so no effects of temperature change should be seen in the collected spectra.

3.3.3 Instrument settings

The choice of probe is an important factor to be considered in the monitoring of fermentation systems using IR. The initial low biomass concentration allows transmitted light to be measured but as the biomass increases there may be a

requirement to change to reflected light because of the high number of particles in the system. As both transmission and reflection measurements may be required a transflectance probe may be the most suitable. However, the results obtained from a transflectance probe may be difficult to interpret.[5] Crowley *et al.* (2005) used a path length of 0.5mm for transmission measurements of *Pichia pastoris*, however, at high biomass concentrations (>64g/L) reflectance measurements were taken as the transmission signal became blocked.[3]

The path length required will depend on the physical properties of the broth. An opaque fluid with a high biomass concentration will require a shorter path length to allow the signal to be detected whereas measurements in a clear solution can be made using a longer path length. As the path length is increased the absorbance is also increased which can become a problem in many fermentations where water is the dominant peak. A long path length however, may be required to determine peaks in the region between 1600 and 1800 nm but can lead to saturation at the 1400 and 1900 nm (water peaks). Arnold *et al.* (2002) investigated path lengths of 0.5 mm and 2 mm and found that an increased path length had problems with bubbles which interfered with the signal and therefore reduced the reproducibility of the results.[2] For monitoring of the *X. campestris* fermentation off-line a path length of 0.5 mm to obtain the optimal spectra and try to compensate for the dominant water peaks.

3.3.4 Sampling

The method of monitoring the fermentation with IR can be carried out in three ways, off-line, at-line or on-line. For off-line analysis, the sample is removed manually and transported to a central lab. The advantages to this are the economic benefits of shared staff and equipment and complex sample preparation can be carried out. However, there is a low frequency of sampling associated with this method. At-line analysis also involves manual sampling. The measurement is made with a dedicated analyser and operator and only simple sample preparation can be carried out. It also requires robust and reliable instrumentation. At-line has a faster sampling rate than off-line analysis but is a less efficient use of instrumentation.

For on-line analysis, the sample is taken from the process stream and introduced to the analyser automatically. The signal can be intermittent or continuous depending on the analyser process. The analyser is located near the process and this allows a fast response time. In-line analysis involves analysis *in-situ* with a probe. There is no separate sampling line and is generally faster than on-line. When developing a method for monitoring a particular fermentation, measurements are often carried out at-line first and then further developed into on-line/in-line.

When in-line sampling is carried out the probe must be able to withstand the pressure and temperature of sterilization also the biomass particles, stirring and aeration may affect the probe. The signal must be optimized and the probe cannot be changed without disrupting sterility. Above 2100 nm it was found that the noise from the fibres had an effect on the quality of the spectra. The biomass was also found to absorb strongly between 2260 and 2270 nm. It was also found that when transferring the model from at-line to *in-situ* measurements the lower wavelength regions must be optimized to obtain a satisfactory model.[2] The noise found by Arnold *et al.* (2002) was not found by other authors.[24, 35] Rodrigues *et al.* (2008) gathered a large number of scans to maximize the signal to noise ratio.

External circulation loops were used by Holm-Nielsen *et al.* (2008), Vaccari *et al.* (1994) and Gonzalez- Vara *et al*. (2000)[49, 50, 51] These allowed the spectra to be removed from the fermenter which would remove effects of agitation and aeration from the sample. There is also increased flexibility in sampling as the loop can be attached to different bioreactors. However, problems were found with dead zones being created and artefacts remaining in the sampling loop. The external circulation loop was also a possible source of contamination and sterility issues within the fermenter. Attaching the probe to the wall of the fermenter was also tried by Ge *et al.* (1994) and Cavinato *et al.* (1990) to measure cell density and ethanol, respectively. An advantage of placing the probe on the outside of the fermenter is that it is not in direct contact with the fluid so can be placed after sterilization. However, it must be reflectance measurements that are taken and it is unclear whether this is actually representative of the broth as the particles maybe more concentrated at the outer edges

of the fermenter.[15, 21] For the work in this chapter, samples were taken and all measurements were carried out off-line.

3.3.5 Calibration models

Multivariate analysis techniques are used to interpret complex spectra obtained using NIR & MIR. These techniques include principal component analysis, multivariate linear regression and partial least squares regression. Modelling techniques including PLS can be used to quantitatively model and predict a measured parameter such as glucose concentration.[52, 53]

3.3.5.1 Principal Component Analysis (PCA)

Using PCA, spectra can be shown as scores, loading and a residual matrix which represents the data not captured. Data is pre-processed before PCA is carried out and this can include mean centring where a mean is calculated for each variable and this mean is subtracted from every variable in the column or auto-scaled where the mean value is subtracted from each variable and then the variable is divided by its standard deviation. This step is important as when not completed the first principal component (PC1) will represent the average of the spectra and not the variance in the data set. The principal components that follow are orthogonal to the first and they are effectively constrained by PC1 and so more components will be required to capture the variation in the data set. To demonstrate how similar or different the samples are from each other the scores values are used. The correlation between individual data points are shown in the loading values. There will be several sets of scores and loading that's will be used to categorise large data sets with the 1st PC capturing the largest variation in the data. The data can be 'over-fitted' if too many component are selected.

3.3.5.2 Multiple Linear Regression (MLR)

MLR can be used as a predictive analysis to explain the relationship between one continuous dependent variable from two or more independent variables. These independent variables can be continuous or categorical. Certain assumptions must be made before completing MLR. The data must be normally distributed and a linear

relationship is assumed between the dependent and independent variable. MLR fits a line through a multi-dimensional space of data points. The simplest form has 1 dependent and 2 independent variables. MLR has three major uses:

- Identify the strength of the effect that the independent variables have on a dependent variable
- Forecast effect or impacts of changes i.e. the understanding of how much the dependent variable will change when the independent variables are altered
- Predicting the trends and future values. MLR can be used to obtain point estimates

When selecting data for MLR, it is important to consider model fit. If too many independent variables are added to the model this may lead to an 'over=fit' model.

3.3.5.3 Partial Least Squares (PLS)

PLS can also be used to build quantitative models to predict the properties of a sample provided it is in the range of the data used in the calibration data. The data is split into the X and Y block, the X block represents the multivariate measurement such as spectra and the Y block represents a property that can be measured in the lab e.g. glucose concentration. PLS also uses scores & loadings and these are calculated for the data matrices X & Y. The structure of the model is similar to PCA models, however, there are differences in the way scores & loadings are calculated.[54]

3.3.5.4 Modelling errors

A calibration set is determined and the errors associated with these models determined, the standard error of calibration (SEC) or the root mean squared error of calibration (RMSEC). These are the errors associated with the calibration model when it is built and the calibration data is predicted. A standard error of prediction (SEP) can also be determined as well as a root mean squared error of prediction (RMSEP). These are the prediction errors associated with a calibration model ability to predict a test or validation data set. The RMSEP represents the predictive ability of the model with unseen data. Before a calibration model can be created, the spectra require pre-

processing such as mean centring, derivatisation, multiplicative signal correction (MSC) and standard normal variate scattering (SNV). These techniques reduce the effects of baseline shifts and to deconvolute broad overlapping peaks. Derivatisation is carried out by various authors with the 2nd derivative spectra more commonly used. Arnold *et al.* (2002) used the 2nd derivative spectra to deconvolute the overlapping peaks and reduce the baseline shift seen in the raw spectra.[2] Rodrigues *et al.* (2008) found that these baseline shifts were related to the physical properties within the sample which caused the light to be scattered more with the fermentation sample. All the spectra were mean centred, however, different further pre-processing techniques were carried out dependent on the analyte being modelled.[35] Tamburini *et al.* (2003) also used the 2nd derivative spectra to combat the baseline offsets as these are mainly due to light scattering induced by the increasing density of cells in the culture broth.[39] As the authors have found, derivatised spectra will be analysed for the results described in this chapter to ensure baseline shifts are corrected for.

3.3.6 Calibration models of fermentation processes

IR models have been built for many different microorganisms using either NIR or MIR. NIR spectroscopy has the advantage over MIR as it allows analysis to be carried out *in situ* without sample preparation and it is possible to set an optical-fibre probe in the fermentation. NIR allows longer path lengths in comparison to MIR where the light penetrates a small distance. However, MIR models are often simpler to build and have smaller errors and require fewer latent variables in the models. This section will discuss the types of models that have been built for different fermentations and the considerations that must be taken for building models.[55]

When modelling there are three possible samples that can be used, synthetic mixtures, representative fermentation samples and semi-synthetic samples. Synthetic mixtures are used by various authors to determine analyte concentrations in fermentation runs. McShane *et al.* used synthetic samples when creating a model to predict the concentration of glucose, lactate and ammonia. However, they combined the synthetic samples with cell culture media samples to improve the robustness of the model.[27] Riley *et al.* (1998) also used a combination of synthetic and media samples for the

determination of glucose and glutamine.[34] This approach was also adopted by Lewis *et al.* (2000) who monitored glucose using both synthetic and media samples; the synthetic samples model was poor but with the addition of a few real media samples the models were more robust.[24] Rhiel *et al.* (2002) used synthetic samples for the first calibration model, however, when real samples were added to the model these were outside the calibration set and a new calibration model was required.[32] When real fermentation samples are used for modelling, matrix interactions can be accounted for which cannot be done with synthetic or semi-synthetic samples. Also the environmental and physiological factors can be taken into account.[39] Arnold *et al.* (2002) had a greater confidence in transferring models when real fermentation samples were used and no pre-treatment was required for this transfer.[2] For this work real fermentation samples will be used for modelling to account for the matrix interactions and to produce as representative a model as possible.

The optimum wavelength region for modelling must be determined; Arnold *et al.* (2002) found that three main absorption bands were observed when the spectra of the biomass was collected from an at-line experiment. One of these bands was then selected for the *in-situ* model. The strong absorbance of the water peaks can make it difficult to determine the correct wavelength region so some authors have used the spectra of anhydrous analytes to identify the right bands that would be useful in modelling.[2] Rhiel *et al.* (2002) used a modified grid search to optimise the spectral range. A series of broad regions were selected and these were narrowed to smaller ranges with widths of 100, 200, 300 and 500 cm^{-1}. The performance of each band was determined using the prediction error, the best broad band was then optimised by performing step wise expansion and contracting the range systematically.[32] Triadaphillou *et al.* (2007) used dimension-wise selection to choose the optimum wavelength region. Model wise elimination was carried out with subset selection. The focus was placed on the subset selection which created different subset of variables and then this subset's performance was validated. Interval partial least-squares (*iPLS)* models were created for the spectral subintervals of equal width and their performance was compared to the global model, the comparisons were all based on the RMSECV values.[41] Water peaks will have to be considered in the *X. campestris* fermentation and

before models are built, identification of the appropriate regions will be found using standard solutions of some of the components of the media.

To determine the robustness of the models from batch to batch, Vaidyanathan *et al.* (2001) produced a model for monitoring oil and tylosin production in *S. fradiae*. This model used at-line transmittance measurements as the reflectance measurements taken showed poorer results. After two years an external validation was carried out and the model appeared to be robust after that period of time. To determine the robustness of a model for predicting mycelia biomass, total sugars and ammonium in a *P. chrysogenum* process, analyte and background matrix variations were artificially introduced. To challenge the model, further experimental parameters were also changed; the number of impellers was increased within a smaller tank. These changes were likely to introduce some morphologic changes. The experiments were also carried out over a six-month period to randomize uncontrollable differences. The change in the scale appeared to affect the biomass models as the morphology of the microorganisms was likely to be different. This illustrates the need for an external validation set to identify useful models and any anomalies that occur within them.[46]

Rodrigues *et al.* (2008) have developed a calibration model with a performance that was independent of scale and the bioreactor used. This was carried out using an on-line transflection probe in both pilot and industrial scale bioreactors. This *Streptomyces clavuligerus* fermentation was particularly challenging to monitor as the process is run under vigorous agitation and aeration rates. The filamentous bacteria grow as branch structures which result in high viscosity of the liquid phase and non-Newtonian behaviour of the broth. The rheological properties of the culture liquids will vary during the cultivation time, between batches and also with reactor scale.[35] The challenges that Rodrigues *et al.* encountered may be found within the *X. campestris* fermentation as the resulting broth will have a high viscosity and is also non-Newtonian. However the authors were able to combat these challenges in the model which would suggest that these techniques could be applied to the modelling of the *X. campestris* fermentation.

Streptomyces was used in the work carried out by Chung *et al.*, (1996) who built a PLS calibration model to identify glutamine, glucose, ammonia, lactate and glutamate. Various wavenumber regions were used for these models and the number of factors varied between eight and twelve. All the results from the calibration model are shown in Table 5. The high frequency noise and baseline variations were removed during pre-processing using Fourier filtering and a calibration model was built. However, there was little improvement in the prediction ability but the number of factors was reduced (Table 6).[56] This work demonstrates the ability of NIR to be used to build a PLS model glucose and ammonia concentration within a fermentation, these two analytes will be investigated further in the work described in this chapter.

Table 5 : Calibration model results for glutamine, ammonia, glucose, lactate and glutamate with no pre-processing[56]

Analyte	Range (cm^{-1})	Factors	Standard error of calibration (g/L)	Standard error of prediction (g/L)	Mean percentage error (MPE)
Glucose	4320-4800	12	0.61	0.53	5.73
Glutamine	4320-4700	12	0.29	0.25	5.09
Ammonia	4300-4850	12	0.27	0.25	6.49
Lactate	4300-4500	8	0.34	0.61	6.50
Glutamate	4250-4850	12	0.27	0.56	8.38

Table 6 : Calibration model results for glutamine, ammonia, glucose, lactate and glutamate with pre-processing

Analyte	Range (cm^{-1})	Factors	Standard error of calibration (g/L)	Standard error of prediction (g/L)	MPE
Glucose	4270-4800	6	0.79	0.54	6.98
Glutamine	4320-4850	10	0.36	0.24	4.13
Ammonia	4300-4850	10	0.31	0.31	8.03
Lactate	4320-4500	8	0.37	0.62	7.72
Glutamate	4250-4500	11	0.32	0.48	7.23

Giavasis et al. (2003) built a regression (PLS) model based on the 2nd derivative spectra for determination of gellan and biomass in a *Sphingomonas paucimobilis* fermentation. The authors did not use the region below 5400 cm^{-1} due to water peaks in this region as the water peaks are highly absorbing. The wavenumber range used was wide and a low number of factors were used to build the model which reflects the number of contributors that can influence the spectra. The correlation coefficients found were

0.949 and 0.98157 for biomass and gellan respectively. The root mean squared errors were found to be 0.439 and 0.769. Problems that had to be overcome during the measurements were the viscosity of the sample, optical density of the sample and the fact that air bubbles tend to become trapped in the gellan-biomass water network. The gellan is not dissolved in the water phase of the process fluid but on the cell surface a mass of cell and polysaccharide collects and so the signals of biomass are disturbed. The range of biomass concentration is low and so the accuracy of the primary assay is crucial for the model's performance.[22] The effects of the water peaks have to be taken into consideration in the *X. campestris* fermentation as these may dominate the spectra so as Giavasis found the region below 5400 cm^{-1} may need to be discarded.

Biomass as well as other analytes, acetate, glycerol and ammonium were modelled within an *E. coli* fermentation.[23] The concentrations were determined using either multiple least squares regression (MLR) or PLS. Acetate models were built using the 2^{nd} derivative spectra and when compensation was made for overlapping peaks the r^2 value increased. The reference method again was the largest source of error and when the model was validated the results were found to compare well with the reference analysis results. The calibration model results are contained in Table 7 including the regression method used and the errors associated as well as the number of samples taken.

Table 7 : Calibration model for *E. coli* fermentation analytes and the associated error[23]

Analyte	Number of Samples	Regression model (wavelength selected)	R^2	Standard error of calibration
Acetate	104	MLR (1684 2318 nm)	0.991	1.2 g/L
Ammonium	168	PLS (3 factors 2030-2380 nm)	0.996	13 mM
Biomass	155	PLS (5 factors 2030-2380 nm)	0.993	1.2 g/L
Glycerol	64	MLR (2048 2274 nm)	0.945	1.1 g/L

Roychoudhury et al. (2006) monitored a *Streptomyces clavuligerus* fermentation which showed filamentous growth in a four phase fluid (oil, water, gas and solids) using MIR. A horizontal attenuated total reflectance (HATR) crystal was used with an effective path length of 10.1 μm at 1000 wavenumbers, these measurements were

carried out in triplicate and the spectra where derivatised to determine the key analytes (1st derivative) and the biomass (2nd derivative). These were then used to develop models of ammonia, glucose, methyl oleate and biomass. A low concentration of ammonia was produced which led to it being masked by more abundant analytes. Glucose and methyl oleate had been previously modelled in simpler systems with an r^2 value of 0.975 and a standard error of prediction of 0.56 gL^{-1}. In this more complex system, when first modelled in a previous study the errors were much higher at 2.92 and 2.77 gL^{-1}. In this study, the model built had a much smaller standard error of prediction of 0.38 gL^{-1} with an r^2 of 0.991. For biomass determination the viscosity and the light scattering behaviour of the filamentous culture must be considered, the r^2 was 0.940 and a standard error of calibration of 0.490 gL^{-1}, when an external calibration was carried out the r^2 value increased to 0.971 and standard error of calibration of 0.39 gL^{-1}.[36] Full results of the modelling performed on the *Streptomyces* fermentation are shown in Table 8. The use of MIR by Roychoudhury *et al.* has demonstrated that it is possible to model using PLS ammonium, glucose and biomass, the wavenumber regions could be used to monitor a *X. campestris* fermentation and low standard error of calibrations are found.

Table 8 : Modelling results for analytes of *Streptomyces* fermentation[36]

Analyte	Wavenumber regions (cm^{-1})	Model (deriv.)	Factors	Calibration r^2	Standard error of calibration (g/L)	Validation r^2	Standard error of Validation (g/L)
Ammonium	900-1450	PLS (1st)	6	0.991	0.014	0.991	0.013
Glucose	950-1470	PLS (1st)	5	0.952	0.69	0.975	0.56
Methyl Oleate	1150-1850	PLS (1st)	6	0.981	0.56	0.991	0.38
Biomass	1050-1750	PLS (2nd)	5	0.940	0.49	0.971	0.39

Sivakesava *et al.* (2001) carried out a comparison of monitoring a lactic acid fermentation using both MIR and NIR. The organism that was used for this study was *L.casei*, the MIR measurements were carried out using an FT-MIR ATR probe, and the NIR was carried out using reflectance measurements. Three analytes were studied; these were glucose, lactic acid and cell density. Using the FT-MIR spectra, the model accurately predicted all 3 analytes with 1st derivative spectra reducing the number of factors involved (Table 9). The errors associated with these models are small and so the model appears to be robust. With the NIR spectra, again, it was possible to model

and predict the analytes. However, the standard error of calibration was higher and more factors were required compared to the MIR (Table 10). Therefore, it was determined that it is possible to obtain more accurate predictions from MIR data than NIR data.[38] While the errors and number of factors are higher for the glucose using NIR suggesting MIR would be the more appropriate technique, the number of factors for the lactic acid when using NIR are in fact smaller with a difference of nine factors for the PCR model. The errors associated with the reduced number of factors are larger than the MIR results but these errors are smaller than the errors found by other authors.[26] For cell density, the number of factors when dealing with the raw spectra are much smaller for NIR and MIR with the errors associated the same of similar. This would suggest that either MIR or NIR could be used for the modelling of cell density. The comparison of the two techniques to model the same solution is of interest as the *X. campestris* fermentations will also be analysed by both NIR and MIR and a comparison of the error of the models built with the two techniques compared.

Table 9 : MIR modelling results for three analytes of a *L. casei* fermentation[38]

Analyse	Wavenumber region (cm^{-1})	Model (derivative)	Factors	Calibration r^2	Standard error of calibration (g/L)	Validation r^2	Standard error of prediction (g/L)
Glucose	950-1165	PLS	6	0.98	2.72	0.97	2.94
		PLS (1^{st})	4	0.98	2.50	0.98	2.92
		PCR	9	0.98	2.61	0.98	2.77
		PCR (1^{st})	6	0.98	2.39	0.98	2.77
Lactic acid	1400-1800	PLS	12	0.97	0.69	0.98	0.56
		PLS (1^{st})	7	0.96	0.74	0.98	0.53
		PCR	16	0.97	0.74	0.97	0.64
		PCR (1^{st})	10	0.96	0.84	0.96	0.38
Cell density	1350- 1650	PLS	12	0.93	0.23	0.93	0.32
		PLS (1^{st})	8	0.93	0.23	0.88	0.37
		PCR	17	0.93	0.25	0.92	0.33
		PCR (1^{st})	14	0.92	0.25	0.87	0.37

Table 10 : NIR modelling results for three analytes of a *L. casei* fermentation[40]

Analyte	Wavenumber region (cm^{-1})	Model (derivative)	Factors	Calibration r^2	Standard error of calibration (g/L)	Validation r^2	Standard error of prediction (g/L)
Glucose	950-1165	PLS	11	0.90	8.42	0.91	7.86
		PLS (1^{st})	11	0.88	9.18	0.89	8.41
		PCR	7	0.85	9.60	0.82	9.23
		PCR (1^{st})	20	0.73	16.32	0.69	17.21
Lactic acid	1400-1800	PLS	7	0.91	1.41	0.84	1.80
		PLS (1^{st})	9	0.91	1.50	0.88	1.50
		PCR	7	0.81	2.06	0.74	2.38
		PCR (1^{st})	13	0.75	2.56	0.70	3.42
Cell density	1350- 1650	PLS	6	0.94	0.24	0.96	0.38
		PLS (1^{st})	7	0.93	0.26	0.93	0.38
		PCR	6	0.94	0.25	0.96	0.39
		PCR (1^{st})	13	0.83	0.29	0.78	0.68

Roychoudhury et al. (2006) found that MIR is a significant technique in bioprocess monitoring but it has some limitations. Like many other techniques it is often used as a secondary technique so accuracy is determined by the reference assay and it also has limited multiplexing advantages. The advantages of MIR spectroscopy include rapidity of measurement, flexibility in application and there is potential to include process variations through chemometrics. MIR has advantages over competing techniques such as NIR spectroscopy, for example the ability to quantify analytes present at limiting levels and potentially to identify aspects of product quality (e.g. folding patterns).[57] The spectral resolution is also higher than NIR which allows the possibility of more information to be determined from the spectra.

3.4 Conclusions from infrared literature

Infrared spectroscopy can be used for analysis and control of fermentations process on different scales. The multiple substrates cause a problem for designing an IR method for analysis. Not only will multiple analytes cause problems for the IR method design but also operating conditions must be taken into consideration.[53] Tosi *et al.* demonstrated that models can be built on organisms with the same morphology of *Xanthomonas* and the morphology should not prevent a representative sample being taken. The conditions within the fermenter do need to be considered when monitoring using IR techniques as the agitation rates and air flow rates may affect the spectra. The agitation rate and air flow rate required for a *Xanthomonas* fermentation may cause some problems when using an NIR *in-situ* probe as air bubbles may become trapped in the path.[39] As the temperature is maintained at a constant temperature, the effect of changing temperature on the signal will not have to be considered. Sivakesava *et al.* (2001) compared MIR with NIR using *L. casei* and found that MIR gave the more accurate results with MIR standard error of calibration and number of factors for accurate prediction being lower than that of NIR suggesting that MIR may be a better choice for fermentation monitoring.[38] This comparison alongside the work of Roychoudhury *et al.* suggests that MIR may be the more robust technique for monitoring of fermentations. However, the spectral resolution of NIR suggest it is worth investigating further. The choice of probe and the method of monitoring are also important factors that must be considered. The resulting biomass concentration from the fermentation process may require reflectance measurements rather than transmission and investigation into the optimum path length may need to be carried out.[35] There are numerous examples of MIR and NIR models being built for other micro-organisms which would suggest that the analytes being considered in this work should be able to be modelled with low errors.

3.5 Aims of monitoring of an *X. campestris* fermentation

The main aim of the *X. campestris* work was to find potential novel ways to monitor the fermentation. From previous work, it has been seen that infrared can be used to monitor the fermentation process.[58] However, no work has been carried out to monitor

a *X. campestris* fermentation. To determine possible monitoring methods the following smaller aims will be investigated

1. The potential for off-line reference analysis to produce a model for monitoring

2. The potential for near infrared measurements to be taken of the *X. campestris* fermentation. Ge *et al.* (1994) and Vaidyanathan *et al.* (2001) identified spectral regions for biomass monitoring which may be of interest from other organisms.[21, 43] However, the rheological properties of a *X. campestris* fermentation may also affect the ability of NIR measurements to be taken.[35]

3. The potential for mid infrared measurements to be taken of the *X. campestris* fermentation. Authors have used both MIR and NIR to monitor fermentation systems and many of the same experimental factors have to be considered for both regions.[26, 57]

4. The possibility of using modelling techniques on the spectroscopy data to produce a model for *X. campestris* fermentation monitoring. From previous work carried it out has been seen to be possible to monitor the biomass of a fermentation using actual fermentation samples and it has also been shown to be possible to monitor the products of the fermentation.[2, 32, 46, 59] Various methods had been used to build calibration models to cover a wide range of analytes some of which are present in *X. campestris* fermentations using PLS and/or MLR.[23, 56, 36]

3.6 Experimental

3.6.1 Instrumentation

A Bioflo 110 fermenter/bioreactor (New Brunswick Scientific, Edison, NJ, US) with a 10 L glass vessel was used for the *Xanthomonas* fermentations.

3.6.1.1 NIR

Off-line NIR measurements were taken using a Foss (Foss, Eden Prairie, Mn, USA) NIRsystems 6500 in reflectance and transmission mode, the path length will be denoted within each experiment. The instrument is a post dispersive grating spectrometer which uses a multimode analyser, which is, equipped with both transmittance and reflectance measurement capabilities (3.2.1). The wavelength region scanned was 600-1760 nm and the detector was a thermoelectrically cooled semiconductor photodiode detector – InGaAs. NIR measurements were obtained at 2 nm intervals and in total 32 scans were collected per spectrum. The samples were analysed with an air background and all samples were measured at room temperature and scanned in triplicate. The 6500 was run using Vision (Thermo Fisher Scientific, Waltham, Ma, USA) software and the raw data was read into Matlab R2015b for further analysis.

3.6.1.2 MIR

MIR measurements were taken using a Thermo Nicolet Avatar 360 FT-IR (Thermo Fisher Scientific, Waltham, MA, USA) using the ZnSe crystal. 32 scans were taken at 4 cm^{-1} resolution. Spectra were collected in triplicate. Omnic software was used to collect the spectra and further analysis was carried out using Matlab R2015 software.

3.6.1.3 UV-Vis

A BioMate 5 UV-Visible Spectrophotometer (Thermo Fisher Scientific, Waltham, MA, USA) was used for optical density measurements. The absorbance spectra were measured at 600 nm for each sample.

3.6.2 Inoculum

A *Xanthomonas campestris* plate was prepared using stock culture of *X. campestris* ATCC 13951 streaked onto an agar plate. The agar solution (Table 11) was prepared and then corrected to pH 7 using 1 M NaOH.

Table 11 : Agar solution formula for *Xanthomonas* fermentations

Chemical	Mass (g/L)
Agar bacteriological (Oxoid Ltd, Cambridge, U.K.)	20
Glucose (Merck, Darmstadt, Germany)	4
Malt extract (Fluka, St Louis, MO, USA)	10
Yeast extract (Fluka, St Louis, MO, USA)	4

One single growing colony of *Xanthomonas campestris* from a 48 hours old X. campestris plate was transferred to 20 mL of sterile YMG medium (Table 12) in a 100 mL shake flask and incubated in an orbital shaker at 28°C for 24 hours. The solution was agitated at a rate of 200 rpm. The solution was then transferred into a 500 ml shake flask containing 170 mL of main media (Table 13). A 10% v/v inoculum was used to seed the fermenter for the production of xanthan gum.

Table 12 : YMG broth formula

Chemical	Concentration (g/L)
Glucose (Merck, Darmstadt, Germany)	10
Malt extract (Fluka, St Louis, MO, USA)	3
Yeast extract (Fluka, St Louis, MO, USA)	3
Peptone (Fluka, St Louis, MO, USA)	5

3.6.3 Fermenter

The 10L fermenter was set up as shown in Figure 12 and had a total working volume of 6.4L.

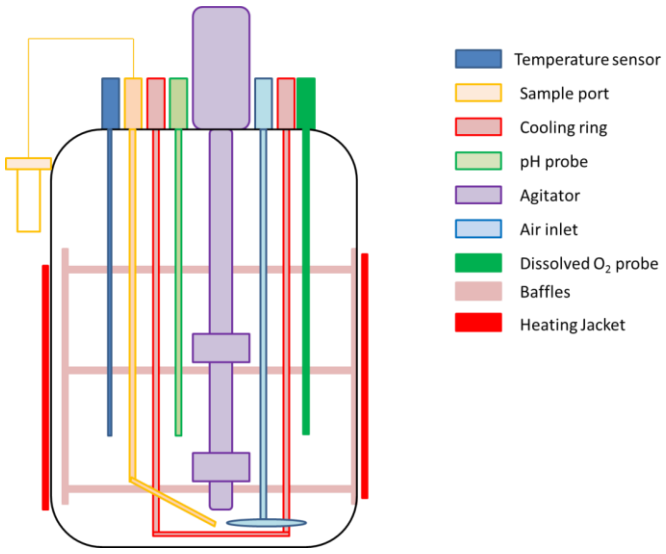

Figure 12 : Schematic of fermenter set up for *Xanthomonas* fermentations

3.6.4 Media and glucose solutions

The media was prepared using the formula shown in Table 13. The media was prepared following the method of Peters *et al.* (1989) in two parts; the glucose solution was prepared and autoclaved separately before adding to the rest of the media under sterile conditions.[60] Both the media and glucose were pH corrected before autoclaving.

Table 13 : Media formula as described by Peters *et al.* (1989) for *X. campestris* fermentation[60]

Chemical	Concentration (g/L)
$C_6H_{12}O_7$ (Sigma, St Louis, MO, USA)	55
$C_6H_8O_7$(BDH/ VWR, Lutterworth, UK)	2.3
KH_2PO_4 (Sigma, St Louis, MO, USA)	5
Na_2SO_4 (Sigma, St Louis, MO, USA)	0.114
$ZnCl_2$ (Sigma, St Louis, MO, USA)	0.0067
Na_2CO_3 (Fluka, St Louis, MO, USA)	0.5
NH_4Cl (Sigma, St Louis, MO, USA)	2
$CaCl_2.2H_2O$ (Sigma, St Louis, MO, USA)	0.012
H_3BO_3 (Sigma, St Louis, MO, USA)	0.006
$FeCl_3$ (Sigma, St Louis, MO, USA)	0.0014
$MgCl_2.6H_2O$ (BDH/ VWR, Lutterworth, UK)	0.163

3.6.5 Reaction conditions

3.6.5.1 Temperature

The temperature within the fermenter was regulated to 28 ˚C using a cooling ring and the heated jacket.[61]

3.6.5.2 pH

In the large volume fermenter, the pH was maintained at pH 7 using 2 M NaOH and a 10% v/v H_2SO_4 solution. The solutions were pumped into the fermenter as required.

3.6.5.3 Air supply

Air was continually pumped into the fermenter vessel at 0.33 L/L min^{-1} and the agitation rate set at 300 rpm for the start of the fermentation. The dissolved oxygen was maintained at 30% by controlling the agitation rate. To prevent foaming within the fermenter, polypropylene glycol (Sigma, St Louis, MO, USA) was added (1 mL/L) to the media before inoculation.

3.6.6 Monitoring

3.6.6.1 NIR

Near- infrared measurements were taken off-line in the Foss 6500. The samples were measured in both reflectance and transmission. The path length of the cuvette was 0.5 cm unless stated otherwise. Further details are found in 3.6.1.1

3.6.6.2 MIR

Mid-infrared measurements were taken off-line with the Avatar. Samples were measured using the zinc selenide crystal. Further details are found in 3.6.1.2

3.6.6.3 Optical density measurements

The samples taken from all three fermenter types were used to measure optical density. 1 mL of the sample was transferred to a semi-micro cuvette for analysis in the UV-Visible spectrometer where single wavelength analysis was carried out 600 nm.

3.6.6.4 Biomass concentration

Triplicate measurements taken on 1 mL of each fermentation sample. The sample was centrifuged for 30 mins at 10,000 rpm and then washed with water and centrifuged for 10 minutes at 10,000 rpm. The Eppendorf was placed into the oven for 24 hrs to dry and then desiccated until weights were taken to ensure a dry constant weight was measured.

3.6.6.5 Xanthan concentration

A cell free sample was obtained by centrifuging the fermentation samples for 30 mins at 10,000 rpm. 3 mL of the cell free sample was added to 15 mL of propanol and placed into the fridge for an hour. The solution was then filtered on pre-weighed filter paper. The filters were dried for 25 minutes in the microwave on the thaw setting and then placed in the oven for 30 minutes to dry. The filters were then placed into a desiccator until the filter paper could be weighed again this was to ensure that a dry constant weight could be taken.

3.6.6.6 Glucose reference analysis

Glucose measurements using the YSI 2700 SELECT Biochemistry analyser (Yellow Springs, OH, USA).

3.6.6.7 Viscosity measurements

Rheological characterisation was carried out by mixing 5 ml of the fermentation sample with 5 ml of 1.5 % w/v xanthan solution. The fermentation samples were mixed with the standard solution as the viscosity of the fermentation samples alone were not within the detection limits of the instrument. Not all fermentation samples were

analysed due to the volume of sample required for this analysis. A Rheomat RM180 rotational viscometer (Maple Instruments, Toronto, Canada) was used to calculate the viscosity of the samples.

3.6.7 Data analysis tools

The spectroscopic data was analysed using Matlab version 2015b (The Mathworks, Natick, USA). Additionally, PLS_toolbox version 8.1 (Eigenvector research Inc., Wenatchee, USA) was used for modelling. All spectra were mean centred before any modelling was carried out.

3.7 Results

3.7.1 Off-line reference analysis

Five X. campestris fermentation reactions were performed. To understand the fermentation process, off-line reference analysis was carried out. As discussed in sections 3.6.4 & 3.6.5, all five fermentations were carried out under the same experimental conditions and with the same formulation of media and glucose. However, according to the off-line reference data, they all performed differently. A summary of the key performance characteristics of the five fermentation reactions is given in Table 14. The following section discusses the analysis of the off-line reference data for optical density, glucose, biomass and xanthan concentration in detail and attempts to build models from these results.

Table 14 : The performance characteristics of the five *X. campestris fermentations*

Fermentation Number	Performance characteristics obtained from off-line analysis
1	Low xanthan production, low biomass production
2	Slower biomass production & glucose consumption
3	Low biomass production, little glucose consumption
4	High biomass production
5	High biomass & xanthan production

The optical density is measured during a fermentation to monitor the growth of the organism as the fermentation progresses. The optical density is a common method to quantify the concentration of substances, as the absorbance is proportional to the concentration of the absorbing species in the sample. The *X. campestris* fermentation samples contain biomass which will absorb the light as well as the yellow pigment Xanthomonadin which is produced during the fermentation. The optical density measurements from the *X. campestris* fermentations are shown in Figure 13. It can be seen from the 5 fermentations that the optical density of the fermentation broth increased as the fermentation progressed in all 5 fermentations with fermentation 5 showing a much higher absorbance than the other fermentations this could be due to the production of xanthan within the fermenter, this would cause an increase in the optical density of the samples as well as the increase in the biomass.

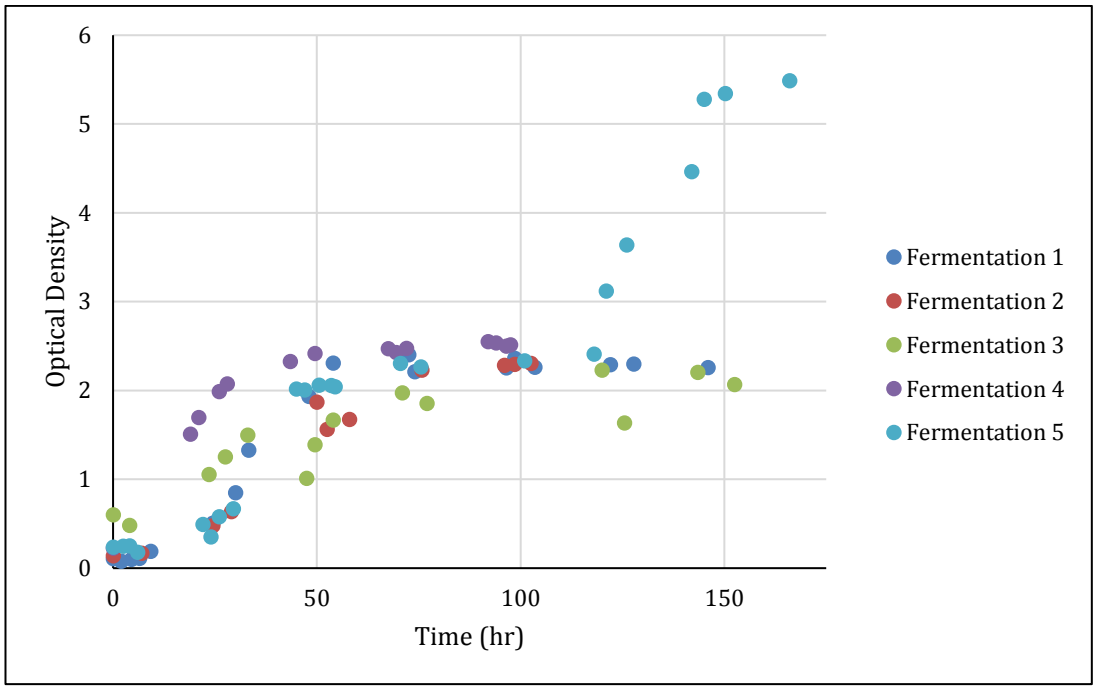

Figure 13 : Optical density measurements at 600 nm of five *X. campestris* fermentations

As glucose is consumed during the fermentation, it can be used as an indicator of the growth of the organism. It can be seen for fermentation 4 & 5 when the off-line glucose analysis are analysed that the glucose decreases throughout the fermentation as the organism uses the glucose for growth.[62] When fermentation 4 & 5 are compared (Figure 14), the glucose is consumed in both fermentations with the glucose

completely consumed by 45 hours in fermentation 5 and 69.5 hours in fermentation 4. The success of fermentation 5 can also be seen in both the rheological changes of the fermentation broth (Figure 18) and the optical density (Figure 13). However, the glucose concentration shown in Figure 14 is lower than expected as 55 g/L was introduced at the start of the fermentation.

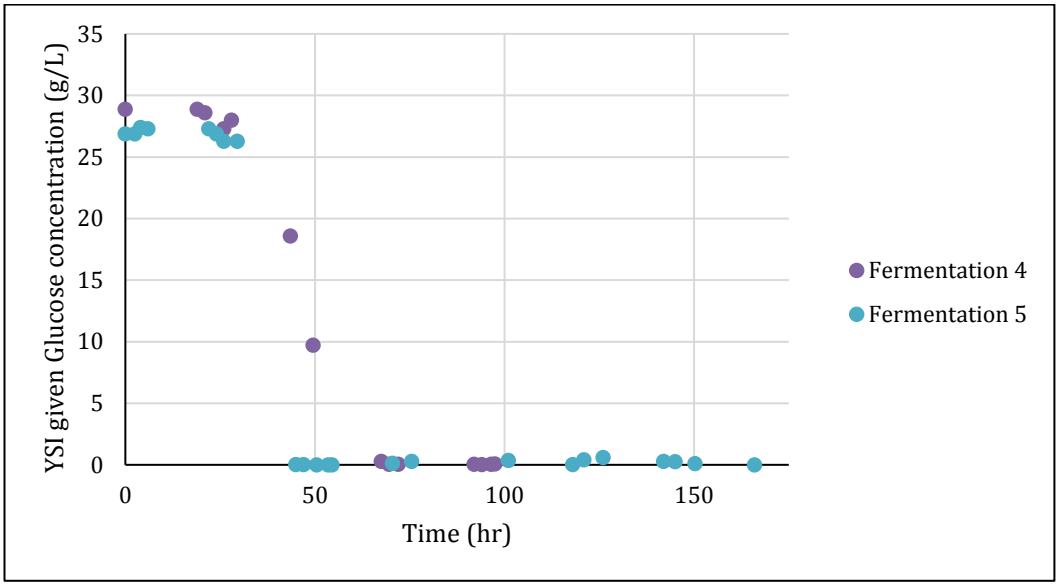

Figure 14 : YSI measured glucose concentration of *Xanthomonas* fermentations 4 & 5

These results are from the YSI and to determine the accuracy of the glucose measurement further experiments were carried out on calibration samples using the YSI. The glucose standard solutions used in 3.7.1 were used to correlate YSI glucose reading to actual concentration. These calibration experiments demonstrated that the glucose concentration calculated by the YSI is lower than the actual concentration of the solution. Using the calibration curve (Figure 15) to calculate the fermentation's measured glucose concentration the calculated glucose concentration is still lower than the expected value, which may suggest the concentration is lower in the fermenter at the start of the fermentation than expected. This lower starting concentration is consistent across all the fermentations. The reliability of the glucose reference measurements could be improved in future work by using another method such as UV-vis spectrophotometry or HPLC which have been used to by other authors to determine the glucose concentration.[40, 57] These methods appear to have been much more reliable and provided the expected glucose concentrations.

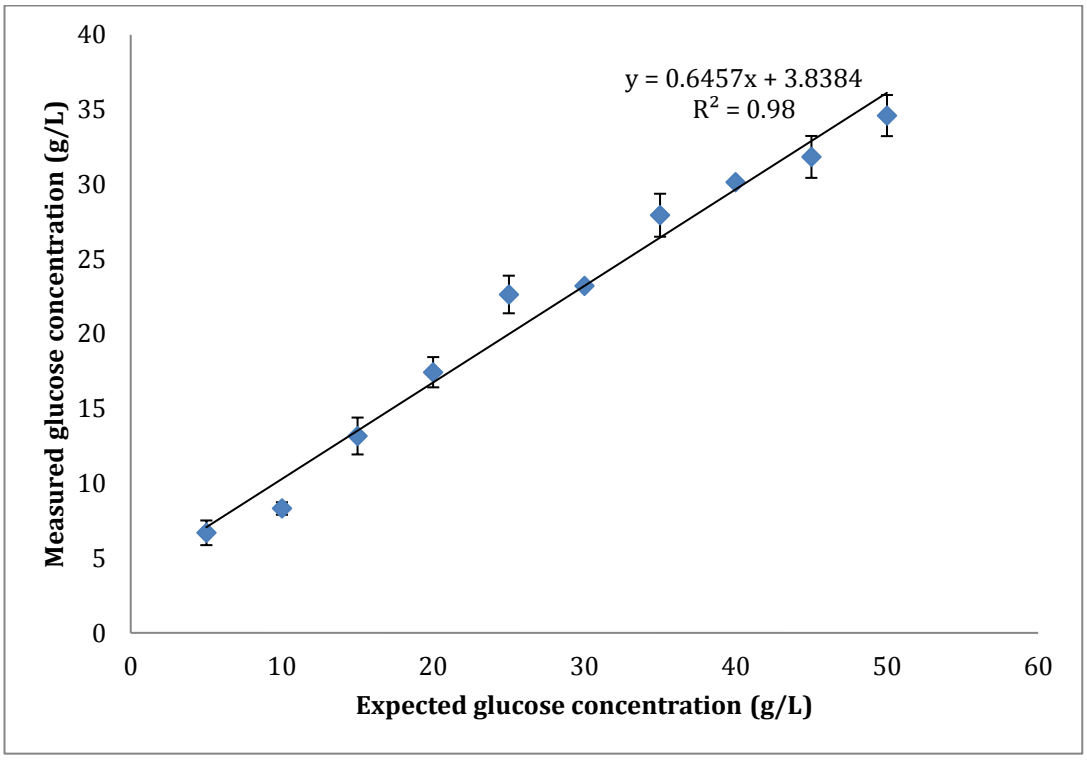

Figure 15 : Measured glucose concentration on YSI in comparison to the concentration of the standard solution prepared

An increase in the biomass concentration can be seen as the fermentation progresses. (Figure 16) This increase in biomass correlates to both the consumption of glucose (Figure 15) and the increase in optical density. (Figure 13) In fermentation two, the increase in biomass becomes significant much later than in fermentation one. The increase in biomass concentration of fermentation 5 has a different profile with a long lag phase and then a sharp increase in the concentration, this is not reflected in any of the other off-line measurements taken, and the optical density undergoes a significant increase at the time that the biomass concentration increases. This may be due to the reference technique were the biomass is not being separated from the media completely and so these are not accurate measurements of the biomass. This is also shown through comparison of the biomass concentration found in fermentation five to fermentation one to four, in fermentation 1-4 the highest biomass concentration was found to be 7 g/L whereas fermentation five it was found to be 40 g/L. This measured concentration of biomass is higher than expected, the concentration of biomass found

by Gilani *et al.* (2011) was much lower. The measured biomass in these experiments will be due to multiple factors, the error associated with them due to the small masses measured and the variation between the replicates, this error will be discussed later in 3.6.6.4 and more significantly the incomplete removal of the xanthan polymer from the mass that was measured. In future experiments a more reliable method of measuring the cell biomass will need to be used to ensure that all the xanthan is removed such as the method used by Giliani *et al.* (2011).[63]

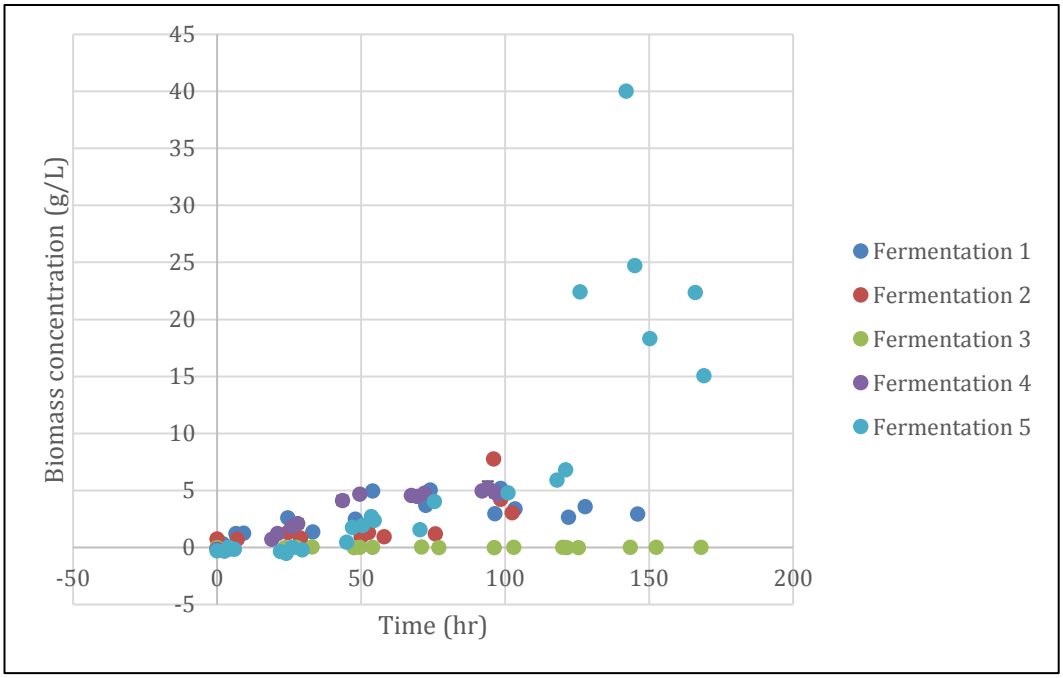

Figure 16 : Biomass concentration measured during the *Xanthomonas* fermentations

Accurately measure the concentration of xanthan produced during the fermentation was found to be challenging. The procedure as described in 3.6.6.5 was used to calculate the xanthan concentration, The xanthan was found at the start of the fermentation which is not expected (Figure 17), only fermentation one was found to have no xanthan but this was found across the whole experiment which again is not expected. Gomashe *et al.* (2013) found that xanthan gum was produced at a maximum of 3.5 g/L at 30 ^{o}C after 120 hrs and no xanthan was found at 0 hrs. The measurements were only taken in this study every 24 hours so the first measurement of xanthan concentration was taken after 24 hours and the concentration of xanthan was found to be 1.75 g/L at 30 ^{o}C. These experiments were carried out using molasses as the carbon

source and Leela *et al.* compared sugar sources and for glucose the maximum xanthan yield was 14.744 g/L. From the experimental results it is obvious that the reference method from the recovery of xanthan gum is not giving an accurate measurement. The increased xanthan yield is likely due to the xanthan not being completely removed from the cells and so the measured masses are a combination of cell material and the xanthan itself. In future experiments the procedure described by Leela *et al*. (2000) would be employed to determine if this would give more accurate results. Leela *et al.* (2000) used the centrifuge for a longer period to separate remove the cells and then also used during the isopropanol step unlike the procedure used in these experiments which only relied on chilling the samples.[20]

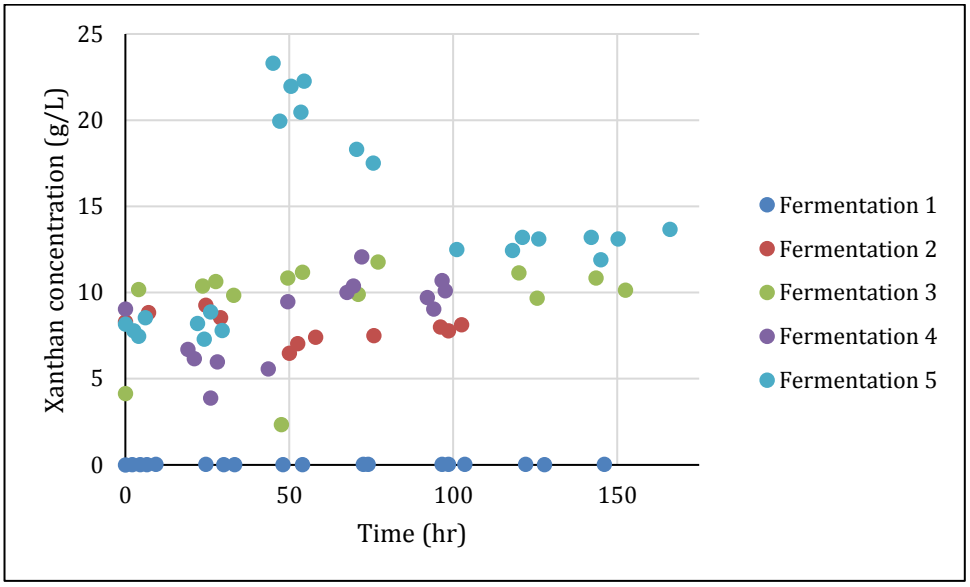

Figure 17 : Xanthan concentrations measured using reference analysis from 5 *Xanthomonas* fermentations

As the calculated concentrations of xanthan concentration are not accurate, the decision was taken to only look at the trends of the xanthan concentration rather than the actual measurements. For example in fermentation 4, the xanthan concentration seen in the fermentation is similar to fermentations 1-3 with a measured concentration of 9g/L at the start of the fermentation (Figure 17). However, if the first three samples are disregarded an increase in xanthan concentration can be seen for samples starting

at 26 hours and there is an increase as the fermentation progresses. Again this is not a robust reference method due to the presence of the xanthan at the start of the process.

The xanthan concentration found in fermentation 5 is also higher than found in other fermentations (Figure 17). Again 9g/L of xanthan is recorded at the start of the fermentation but in this fermentation the concentration of xanthan is the highest in fermentation 5 which is also seen in the viscometer results (Figure 18) as the increased concentration of xanthan is the cause of the increase in viscosity. The fermentation samples also show a decrease in viscosity as the shear rate is increased.

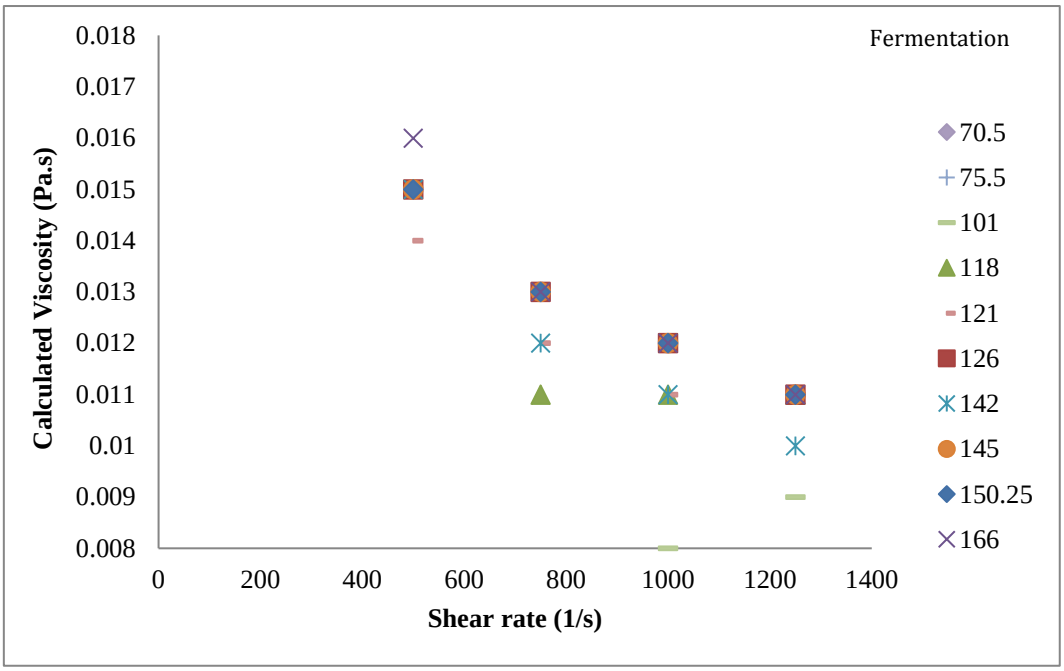

Figure 18 : The calculated viscosity vs sheer rate of *Xanthomonas* fermentation no 5

From the results of the off-line reference analysis it can be seen that the fermentations progressed as expected with an increase in the optical density and biomass and the decrease of glucose concentration. These results do lead to questions regarding the reliability of the reference techniques and the effects this will have on the modelling of these analytes and their use as a reference for the modelling of the NIR and MIR. In future experiments alternative reference methods should be used such as UV-vis and HPLC to determine the glucose concentration as well as taking care to completely separate the biomass and the xanthan product before any measurements are taken.

As a fermentation is a complex system to begin with a simple model could potentially be built from the analyte data described previously. The glucose and optical density measurements are standard reference analysis which are quick and simple to do without the need for large quantities of sample or sample preparation. The biomass and xanthan concentration analysis are more time consuming and difficult to obtain accurate results. As the biomass and xanthan measurements are a more challenging analysis principal component analysis and multiple linear regression modelling using the glucose and optical density measurements was carried out to predict the biomass and xanthan concentrations. PCA and MLR were chosen as they can be used to identify the correlation between the reference measurements and build a simple predictive model to identify the trends.

For the biomass model, an analysis of the principal components was carried out. In Figure 19, the loadings plot of principal component one (PC1) can be seen, this principal component accounts for 76.12% of the variation within the model. Variable 1 is the glucose measurements, variable 2 is the biomass measurements and variable 3 is the optical density of the fermentation broth. From the loadings plot it can be shown that PC1 is most strongly correlated with the biomass measurements and optical density with the glucose measurements being anti-correlated, this is an expected result as the fermentation progresses the glucose is consumed by the micro-organism, which increases the broth's biomass and the optical density.

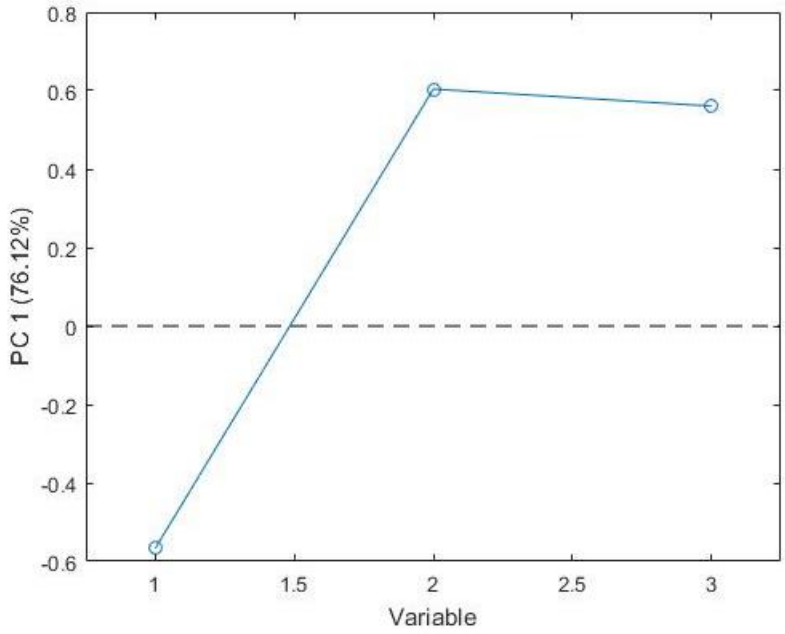

Figure 19 : Loadings plot of principal component 1 in the principal component analysis of fermentations 1-4 to predict the biomass concentration from *Xanthomonas* fermentations

Principal component two (PC2) is mainly associated with the glucose and optical density measurements due to the loading values. The biomass loading is small in PC2 as this analyte is not as strongly associated. (Figure 20)

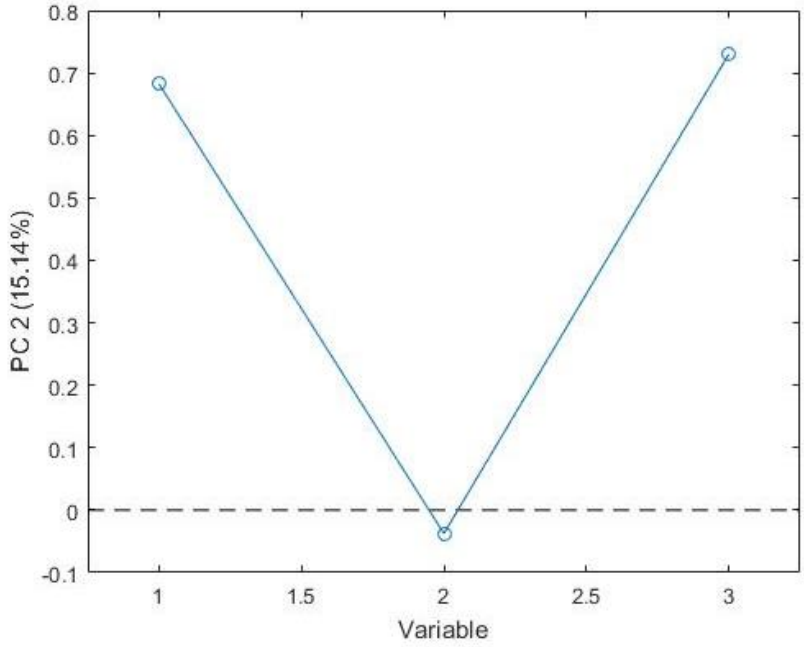

Figure 20 : Loadings plot of principal component 2 in the principal component analysis of fermentations 1-4 to predict the biomass concentration from *Xanthomonas* fermentations

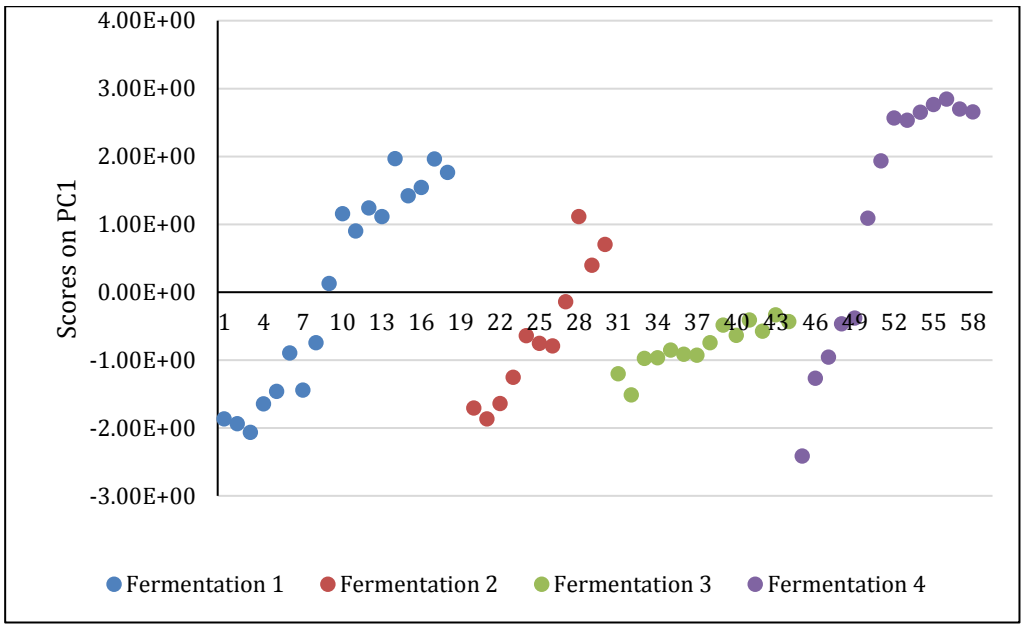

Figure 21 : Scores plot of principal component 1 in the principal component analysis of fermentations 1-4 to predict the biomass concentration from *Xanthomonas* fermentations

When the scores plot of PC1 are analysed (Figure 21), higher concentrations of biomass are seen in the later samples of all the fermentations with fermentation 3 showing the lowest concentration of biomass, which can be seen in the measured fermentation values. (Figure 16). The principal component analysis confirmed the expected correlation of optical density and anti-correlation of glucose.

Using fermentations 1-3 as the calibration data in the MLR analysis, a model was built using the glucose and optical density measurements. The model details are given in Table 15 and when this model is used to predict fermentation 4 the predictions are within the error associated with predictions for all samples apart from 43.5 and 49.5 hours. (Figure 22) The model is used to predict the first 100 hours of the process due to the availability of data for the later stages of the fermentations. Fermentations 2 & 4 were only run for 100 hours. The RMSEC of the model is 1.23 g/L which when compared to the experimental results of a maximum concentration of 6 g/L during the fermentation process is a 20% error associated with the maximum value. This RMSEC is high and further fermentations would hopefully reduce this to give a more accurate model and also a more accurate reference method would also hopefully reduce this error.[23]

Table 15 : MLR model details for Biomass predictions using fermentations 1-3

Pre-processing	Auto scale
RMSEC	1.22743 g/L
RMSECV	1.27507 g/L

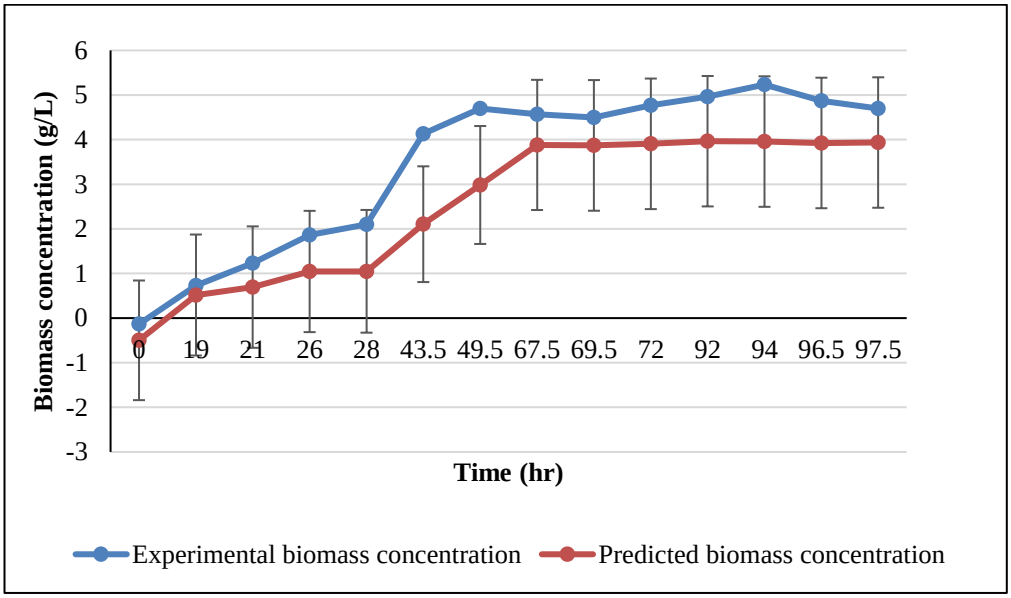

Figure 22 : MLR model biomass concentration predictions for fermentation 4 using fermentations 1-3

Biomass had previously been modelled by Hall *et al.* (1996) for an *E. coli* fermentation. The authors describe issues with the reference method and the contribution these made to the error for their model. However, the errors associated with the PLS predictive models compared well with the errors from the reference methods that were used to build the model.[23] Although for a different organism, the same issues could apply to the *X. campestris* fermentation. Perhaps with more fermentations with longer running times and accurate biomass concentrations within the fermenter, the model would become more robust. As a starting model, the above model allows a prediction of the biomass concentration which would remove the need for the time consuming biomass extraction from the fermentation samples.

For the xanthan principal component analysis, the loadings plot of principal component one (PC1) can be seen in Figure 23, this principal component accounts for 62.25% of the variation within the model. Variable 1 is the glucose measurements, variable 2 is the xanthan measurements and variable 3 is the optical density of the fermentation broth. From the loadings plot it can be shown that PC1 is most strongly correlated with the glucose concentration and the xanthan concentration and optical density are anti-correlated with the glucose concentration as with the biomass principal component analysis this is expected within the fermentation as the organism grows.

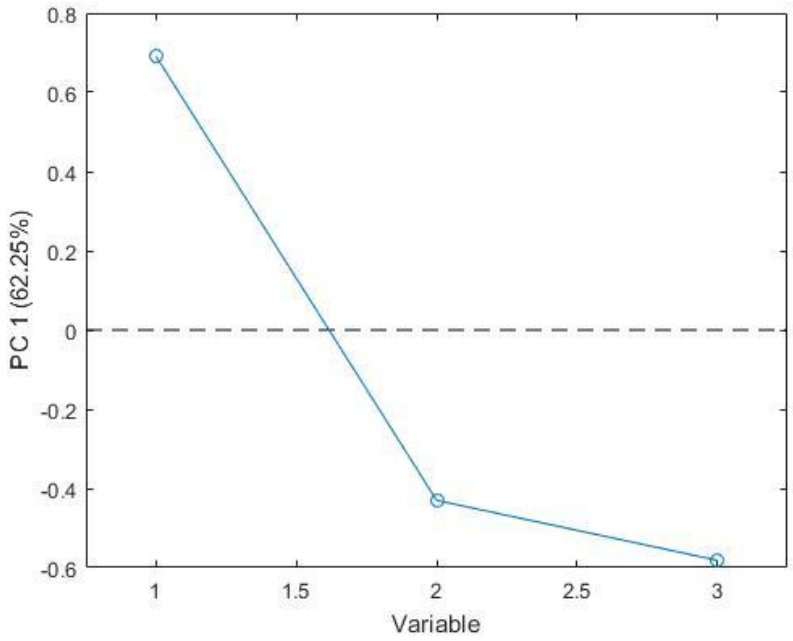

Figure 23 : Loadings plot of principal component 1 in the principal component analysis of fermentations 2-5 to predict the xanthan concentration

Principal component two (PC2) is mainly associated with the xanthan and optical density measurements. The glucose loading is small in PC2 as this analyte is not as strongly associated. (Figure 24) In PC2 the xanthan concentration and optical density results are anti-correlated with each other.

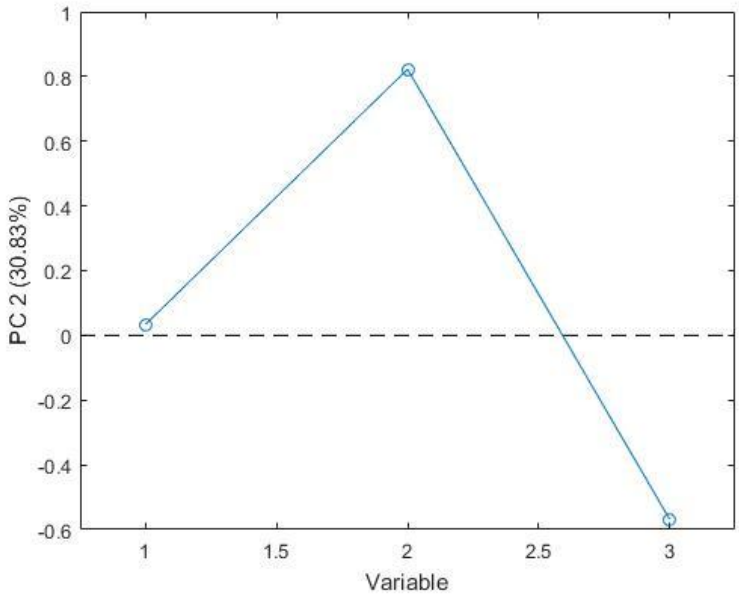

Figure 24 : Loadings plot of principal component 2 in the principal component analysis of fermentations 2-5 to predict the xanthan concentration

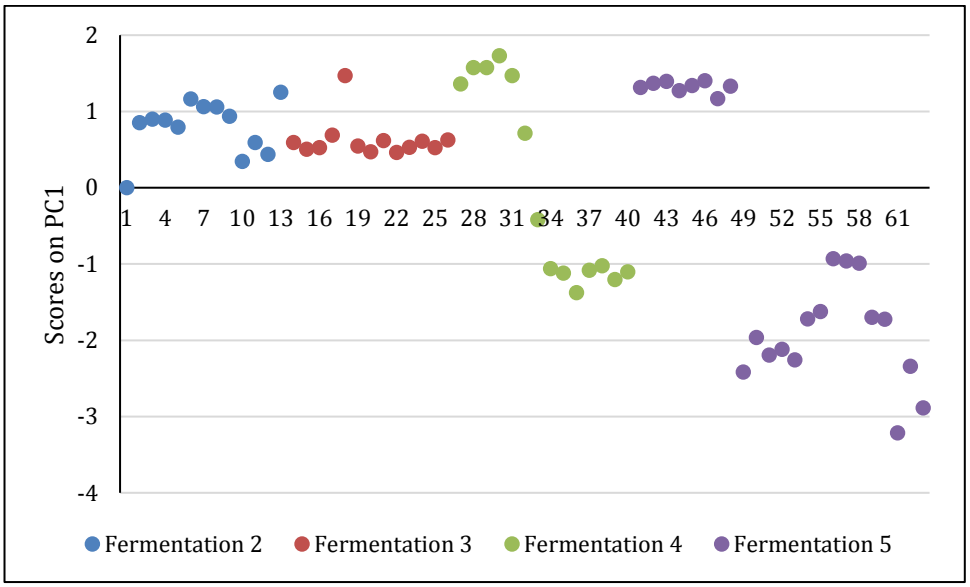

Figure 25 : Scores plot of principal component 1 in the principal component analysis of fermentations 2-5 to predict the xanthan concentration

When the scores plot of PC1 are analysed (Figure 25), higher concentrations of glucose are seen in the early samples of all the fermentations with fermentation 4 & 5 showing the large drop in concentrations of glucose, which can be seen in the measured fermentation values. (Figure 42) In PC2 (Figure 26), the xanthan concentration can be seen to increase as the fermentation progress in fermentations 4 & 5 which is also seen

in the fermentation results. (Figure 17) Both PC1 and PC2 scores show the trend of the fermentation.

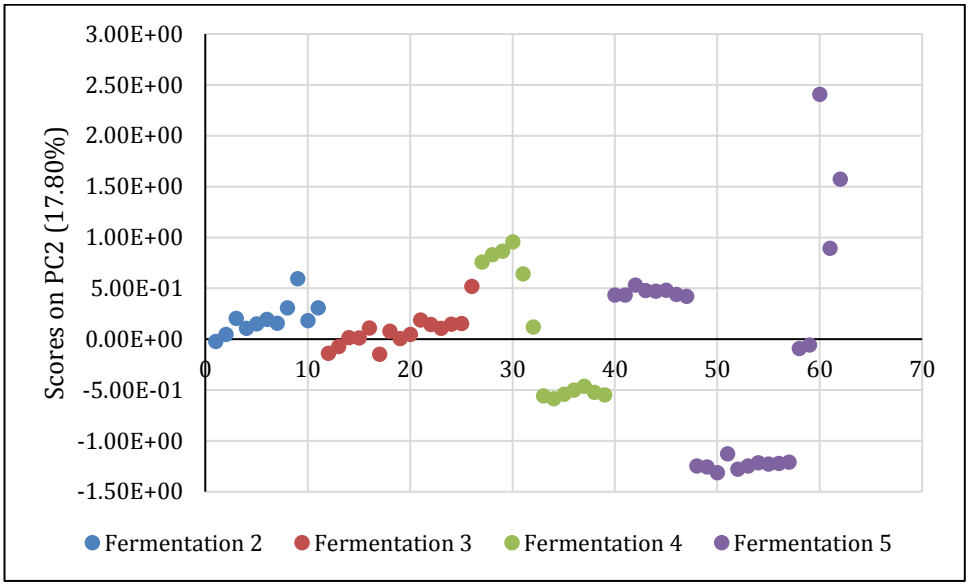

Figure 26 : Scores plot of principal component 2 in the principal component analysis of fermentations 2-5 to predict the xanthan concentration

Using fermentations 2, 3 & 5 as the calibration data in the MLR analysis, a model was built using the glucose and optical density measurements. These fermentations were selected due to the results of the xanthan reference analysis as fermentation 1 had been discounted due to the lack of xanthan measured in the sample and fermentation 4 was chosen to be the predicted fermentation. The model details are given in Table 16 and when this model is used to predict fermentation 4 the predictions are generally within the error associated with predictions and the trend of the xanthan concentration is as would be expected. Again the RMSEC value is high in comparison to the measured value (2.67 g/L compared to a maximum 12.5 g/L), a more reliable model would have a smaller RMSEC and RMSECV The large error and the non-fit of the model is likely to be due to the unreliability of the starting xanthan concentrations used to build the model and to get a more accurate model the further investigation mentioned in 3.7.1 would need to be carried out. Another factor to consider is the low concentration of xanthan in the system. Vaidyanathan *et al.* (2001) modelled a penicillin fermentation and the low concentration of penicillin in the fermenter caused larger errors on the model than desired.[46]

Table 16 : MLR model details for xanthan predictions using fermentations 2, 3 & 5

Pre-processing	Auto scale
RMSEC	2.67434 g/L
RMSECV	2.78555 g/L

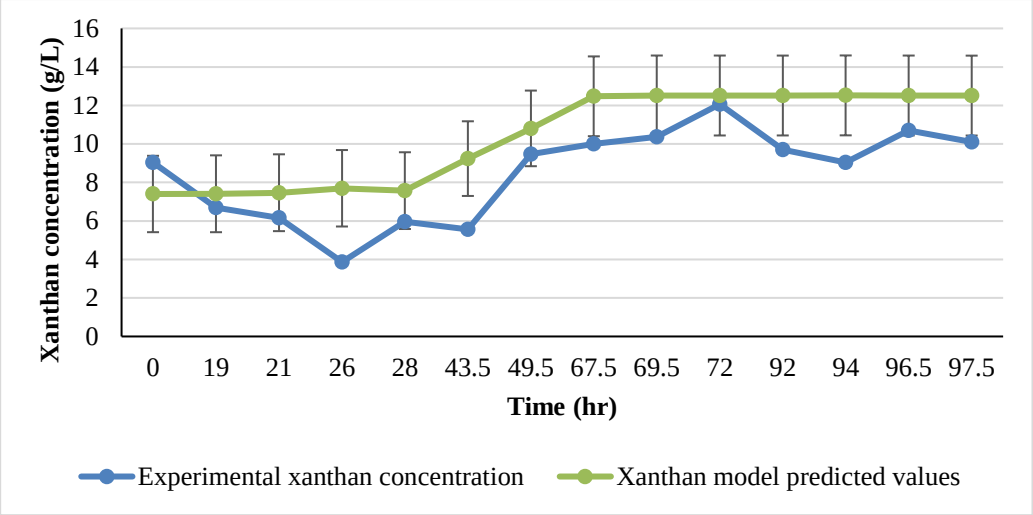

Figure 27 : MLR model xanthan concentration predictions for fermentation 4 using fermentations 2, 3 & 5

In Figure 27, it can be seen that the model predicts the general trend of the xanthan production. However, the model has a smooth increase in the xanthan concentration whereas fermentation 4 has the initial drop of concentration between 0 and 26 hours and also the model does not replicate the higher xanthan concentration at 92 hours. To improve the accuracy of the xanthan model, further fermentations could be added which may help provide a more accurate prediction but also to improve the reference method used to calculate the concentration of the xanthan in the fermentation.

The models produced of the xanthan and biomass have large errors associated with them and further work will need to be carried out to improve the robustness of these models including establishing better reference techniques for the analysis.

3.7.2 Infrared monitoring of the fermentation

A simple MLR model has been demonstrated using the off-line analyte analysis. These models are simplistic and to better understand a fermentation process, on-line monitoring would be advantageous. One possible method for monitoring and modelling a *X. campestris* fermentation is the use of an infrared probe which could be inserted into the fermenter to allow this. This on-line monitoring would allow for changes in certain analytes to be monitored in real time and reduce the need for as much off-line analysis. This technique has been carried out by multiple authors on a variety of organisms as discussed in 3.3.5.

3.7.2.1 Standard solution analysis

Near and mid infrared spectra were collected of standard solutions of xanthan gum and glucose standard solutions, these measurements were taken to understand which regions in the spectra to analyse further and understand the effects of the concentration range within the fermenter on the spectra collected.

To determine the spectrum from xanthan gum, a spectrum was collected using a Foss on-line 6500, with a transflectance probe with a path length 2mm. The spectrum (Figure 28) shows peaks at ~6750-7250 cm^{-1} and ~8250-8750 cm^{-1}. When these absorbences are compared to a water spectrum (Figure 28) it can be seen that the first overtone of the O-H stretch (6750-7250 cm^{-1}) from the backbone of the xanthan gum will be masked by the water that is present in the media. However, the peak at ~8250-8750 cm^{-1} should be visible when the measurements of the fermentation broth are carried out. This peak can be attributed to the second overtone of the C-H bonds found within the xanthan.

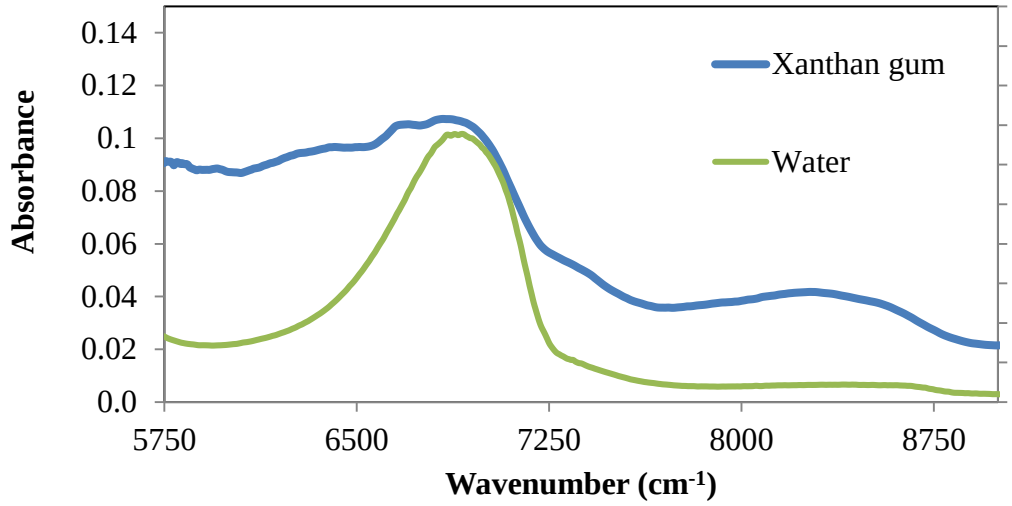

Figure 28 : NIR spectra of xanthan gum from Foss on-line NIR transflectance probe and water using an Antaris II FT-NIR system (Thermo Fisher Scientific, Waltham, MA, USA)

Xanthan standard solutions were made with a concentration range of 0-2% wt./v aqueous solutions. This concentration range does not cover the full range of xanthan concentrations found in industrial fermentations, Garcia-Ochoa *et al.* (2000) found that the fermentation broth contains 10-30 g/L of xanthan (1-3% wt/v).[64] Due to the technique used to prepare the standard solutions, no solutions of higher concentration were prepared as it became difficult to dissolve the xanthan to form a consistent solution. The NIR transmission spectra are dominated by the water peaks and no contribution from the xanthan can be seen.

As can be seen in Figure 29, the reflectance spectra show the water peaks predominantly, one region 6400-6900 cm^{-1} does show changes in the first derivative. This region relates to the CH, CH_2 and CH_3 2nd overtone region. However, this change does not appear to be correlated to the concentration of xanthan. 0.5% and 1.5% xanthan concentrations are together and the 1 and 2% xanthan concentrations are together.

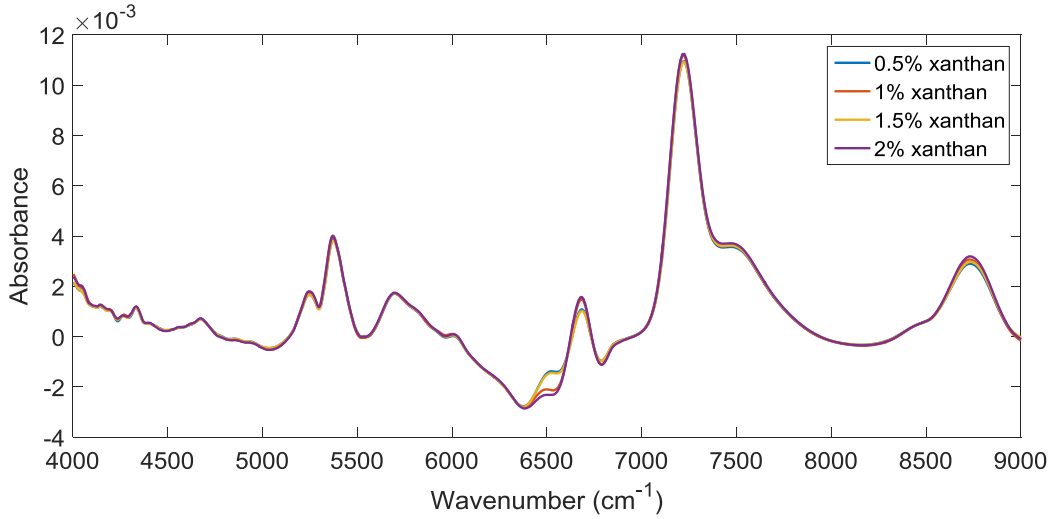

Figure 29 : NIR first derivative reflectance spectra of 0.5-2%wt/v xanthan standard solutions

When the MIR spectra of the xanthan solutions are analysed there are some slight changes seen in the same region (980-1180 cm^{-1}) as the glucose solutions this is due to the contribution from the C-O and C-C in the xanthan. (Figure 8). The peaks are not as defined as the glucose and the change in absorbance not as large. Mudoi *et al.* (2013) found many more peaks in the MIR analysis of the extracted xanthan however, the water peaks dominate the xanthan standard solution measurements.[65]

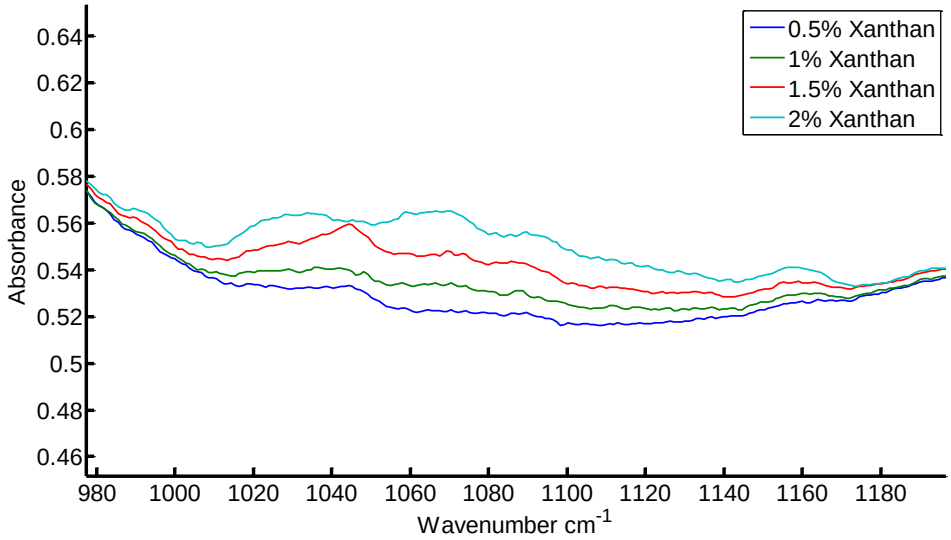

Figure 30 : MIR spectra of 0.5-2% wt/vol xanthan standard solutions in the region of 980-1180 cm^{-1}

Glucose standard solutions were prepared in water with a concentration range of 0-50 g/L and measured in the NIR in both the reflectance and transmission mode using a 0.5 cm cuvette. In the reflectance mode, the raw spectra show little change when the glucose is measured with the water peaks dominating the spectra (Figure 31). When derivative spectra are analysed – a contribution from the 1st overtone OH can be seen ~6710 cm^{-1} and a contribution from the CH and CH_2 within the glucose between 5650-5814 cm^{-1}. Chung *et al.* (1996) have found the region 4320-4800 cm^{-1} to be useful in the modelling of glucose in fermentation samples, however this region was not found to be useful in these experiments.[56] There was little variation in the spectra and upon further analysis this could not be correlated to the concentration of glucose in the samples. However, Giavasis *et al.* (2003) did not use any region below 5400 cm^{-1} due to contributions from the water peaks.[22]

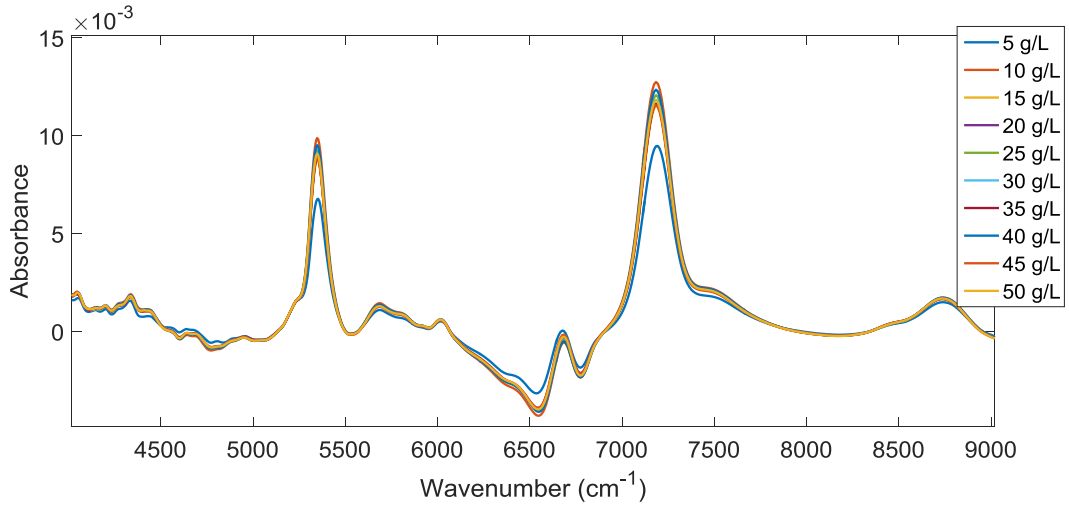

Figure 31 : First derivative NIR spectra of glucose standard solutions (5-50 g/L)

When the MIR spectra of the glucose solutions are analysed there are regions of interest which show changes as the glucose concentration increases. In the 980 -1180 cm^{-1} region there is a distinct spectral pattern (Figure 32) that increases in absorbance as the glucose concentration increases which was also seen by Meinke *et al.*[66] (2008) These peaks are attributed to the C-O and C-C stretching within the glucose molecule (Figure 33) and are assigned in

Table **17**.[67]

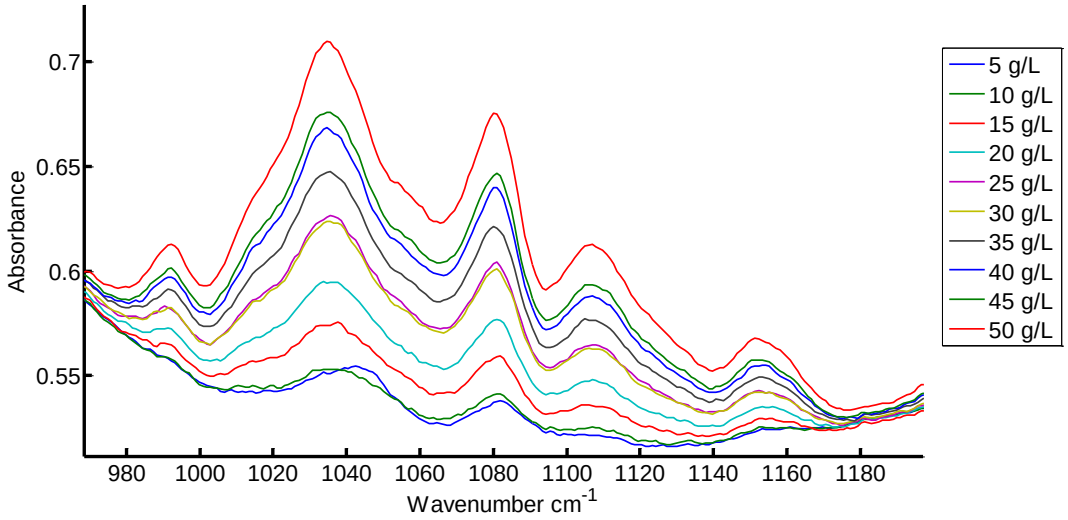

Figure 32 : MIR spectra of 5-50 g/L glucose standard solutions in the 980-1180 cm^{-1} region.

Table 17: Peak assignments of MIR spectra in the region of 980-1180 cm^{-1}

Peak (cm^{-1})	Attributed stretch
990	CO + CC
~1030	CO
1080	CO + CC
1110	CO
1150	CO + CC

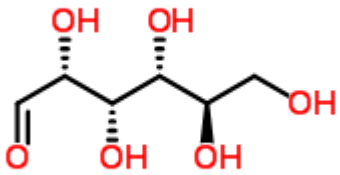

Figure 33 : D-(+)- Glucose molecule[68]

From the results of the standard solution analysis, the regions of interest for MIR for both the xanthan and glucose is 980-1180 cm-1 this region shows the C-O and C-C stretching and these groups are present in both the glucose and xanthan. Water peaks dominate the NIR spectra, however, the 6400-6900 cm^{-1} region should be investigated further as changes were seen in the derivatised xanthan spectra. From the literature, other regions that should be explored in future work are 4320-4800 cm^{-1} for glucose monitoring.

3.7.2.2 Off-line fermentation infrared analysis

Both the xanthan and the glucose standard solutions show potential for monitoring fermentation samples. The MIR appears to be the more promising spectroscopy technique as the water in the standard solutions obscured the contributions from the xanthan and the glucose in the NIR spectra. In the following work, off-line NIR and MIR analysis was carried out on the fermentation broth samples.

When NIR analysis was carried out on the fermentation broths (Table 14), the water peaks are dominant in both the reflectance and transmission modes similar to those of the standard solutions. When the reflectance spectra are derivatised, three possible regions of interest 5675-5727 cm^{-1}, 6535-6622 cm^{-1} and 8620-8770 cm^{-1} are seen. (Figure 34)

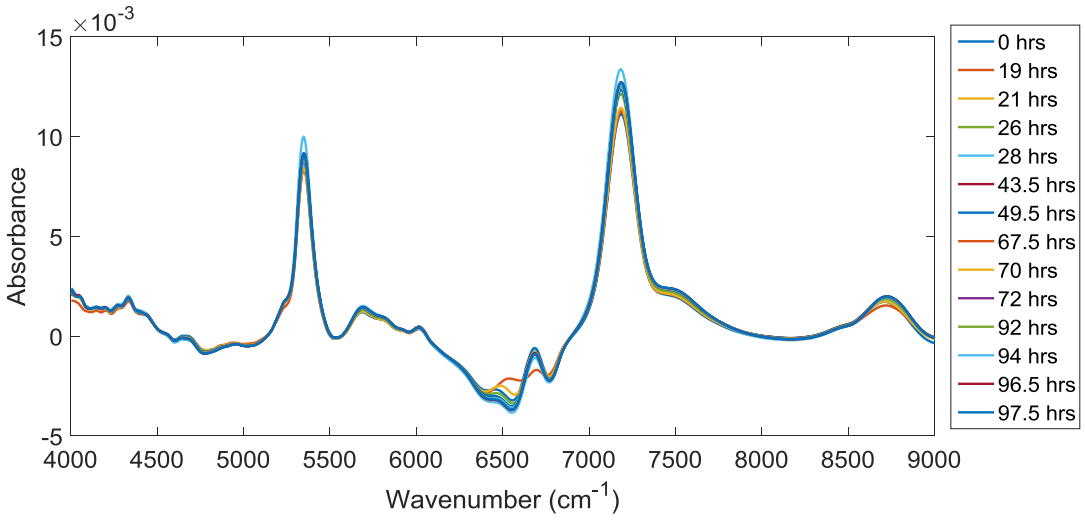

Figure 34 : NIR first derivative reflectance spectra for fermentation 4

When the peak at 8710.8 cm^{-1} is examined closely, the increase can be seen as the fermentation progresses and then reaches a plateau during the fermentation. This is seen in both fermentations 4 & 5 (Figure 35). This peak is associated with second overtone CH_3 and CH_2 which would suggest that there is no more increase in CH_3 and CH_2 later in the fermentation. This region has been used to model the biomass of other fermentations by Vaidyanathan *et al.* (2000) regardless of which organism is used.[14] This would suggest this region could be of interest for modelling of a *Xanthomonas*

fermentation but the contribution of the xanthan to this region would need to be considered.

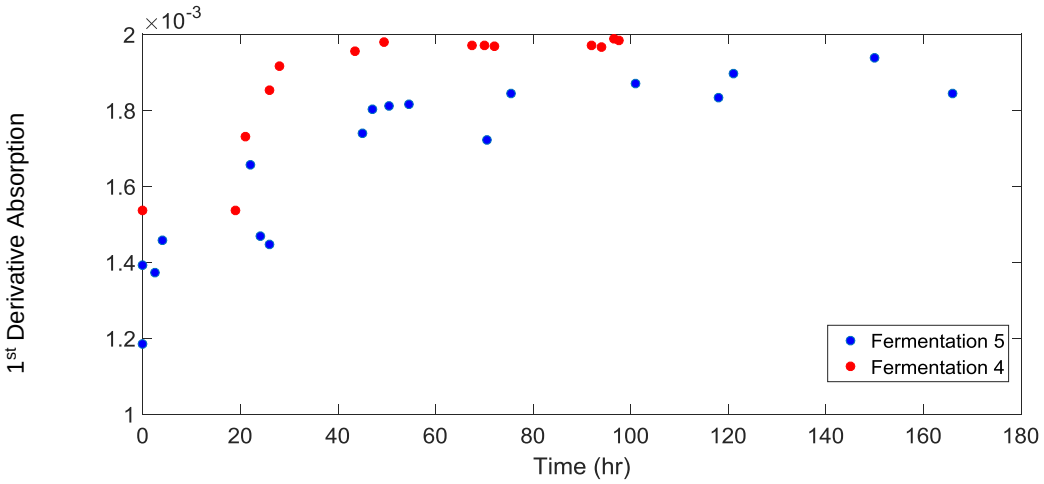

Figure 35 : NIR first derivative reflectance spectra at 8710.8 cm^{-1} in fermentation 4 & 5

The same can be said of CH and CH_2 first overtones that are seen between 5650-5814 cm^{-1}; this is seen in fermentations 4 & 5 (Figure 36) and can be attributed to both the glucose and the xanthan produced.

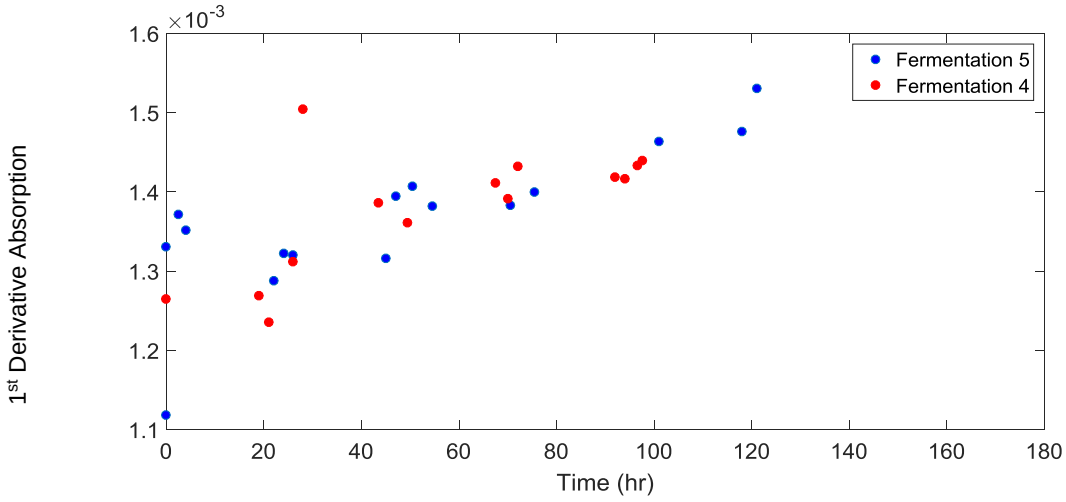

Figure 36 : NIR first derivative 5681.82 cm^{-1} of fermentations 4 & 5

At 6570.3 cm^{-1}, the second overtone N-H region, a decrease can be seen as the fermentation progresses (Figure 36) when this is compared to the spectra from ammonium chloride standard solutions, the same peaks can be seen in this region (Figure 38). Ammonium chloride is used within the starting medium as the nitrogen

source for the fermentation; this is consumed during the fermentation. Ammonia nitrogen has been used by Hue *et al.* (2014) to determine cocoa fermentation levels successfully using NIR in the same region. Hue *et al.* (2014) were monitoring NH_3 production rather than consumption.[69] However, they were able to show that the changes in N-H can be monitored during the fermentation. This would suggest that the changes in the ammonium chloride levels in a *Xanthomonas* fermentation could possibly be used to monitor the progress of the fermentation.

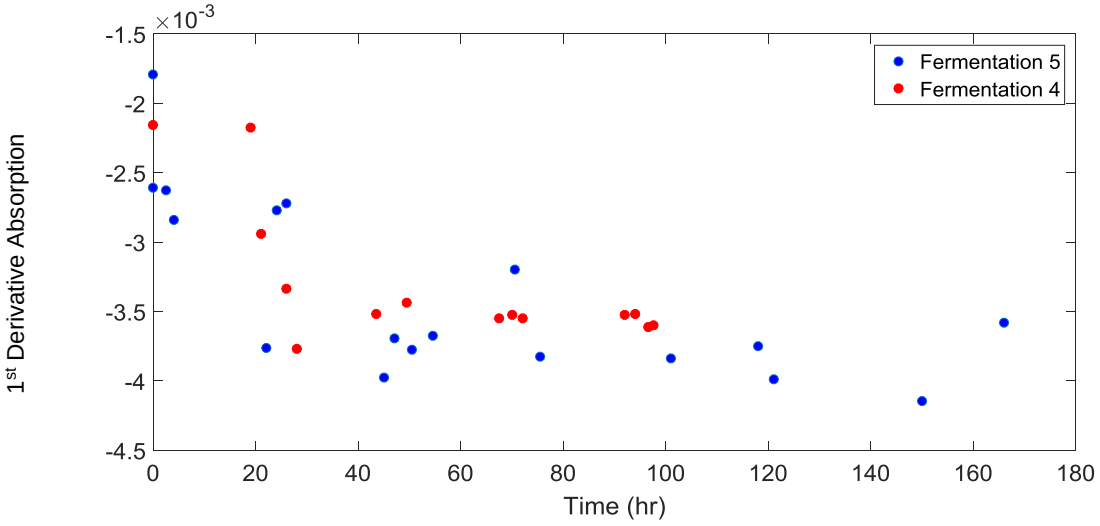

Figure 37 : NIR first derivative spectra at 6570.3 cm^{-1} for fermentations 4 & 5

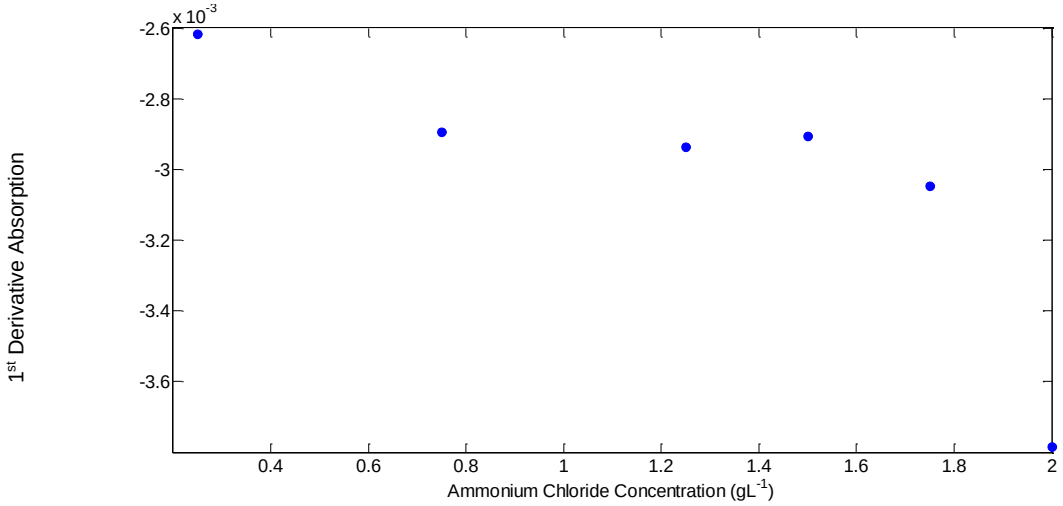

Figure 38 : NIR first derivative at 6570.3 cm^{-1} of ammonium chloride standard solutions (0.2-2g/L)

When the fermentation MIR spectra are considered, the region of interest is 960 - 1180 cm^{-1} (Figure 39) as this is the region seen in the glucose standard solutions. (Figure 32) This region was used by Roychoudhury *et al.* (2006) to model glucose in a *Streptomyces* fermentation and by Sivakesava *et al.* (2001) to monitor a *L. casei* fermentation.[38, 57] In this region, the fermentations can be considered in two groups, fermentation 1 & 2 and fermentation 4 & 5. Taking fermentations 1 & 2, the spectra show the same spectral pattern as glucose with 5 peaks, the absorbance of these peaks decreases as the fermentation progresses, this would suggest that the glucose is being consumed as the fermentation progresses which is also shown in the glucose reference analysis.

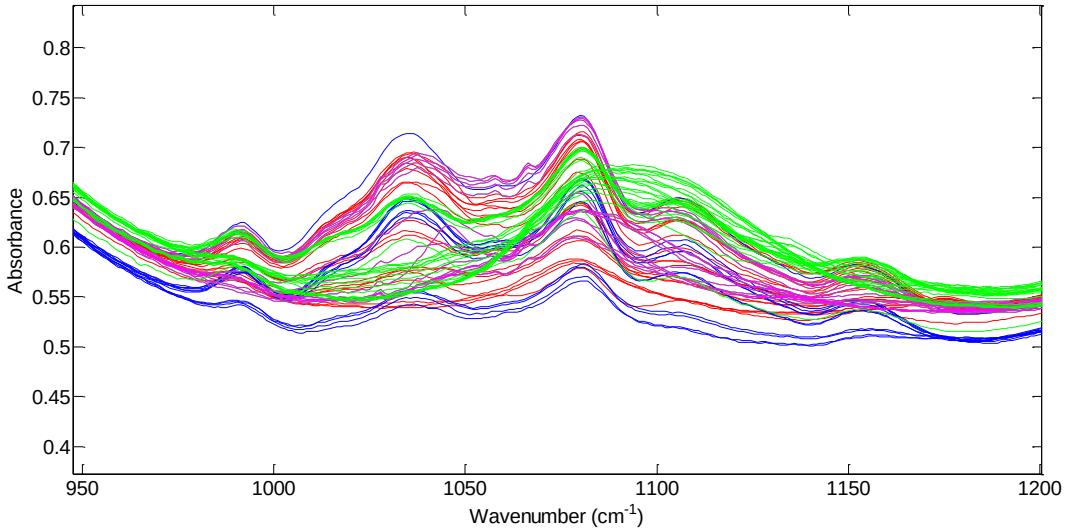

Figure 39 : Comparison of MIR spectra of fermentations 1 (blue), 2 (red), 4 (pink) & 5 (green)

In fermentations 4 & 5, the spectra are slightly different with the same 5 peaks from the glucose seen at the start of the fermentation but then an added peak is seen at 1080 cm^{-1}. These peaks do not appear until after the glucose has been consumed (Figure 40) which correlates to the production of xanthan in Figure 17 and can be linked to the changes in rheology (Figure 18). This peak can be attributed to the xanthan production and when only this peak is considered in fermentation 4 & 5, it can be seen the fermentation that produced the most xanthan has the highest absorbance. (Figure 41)

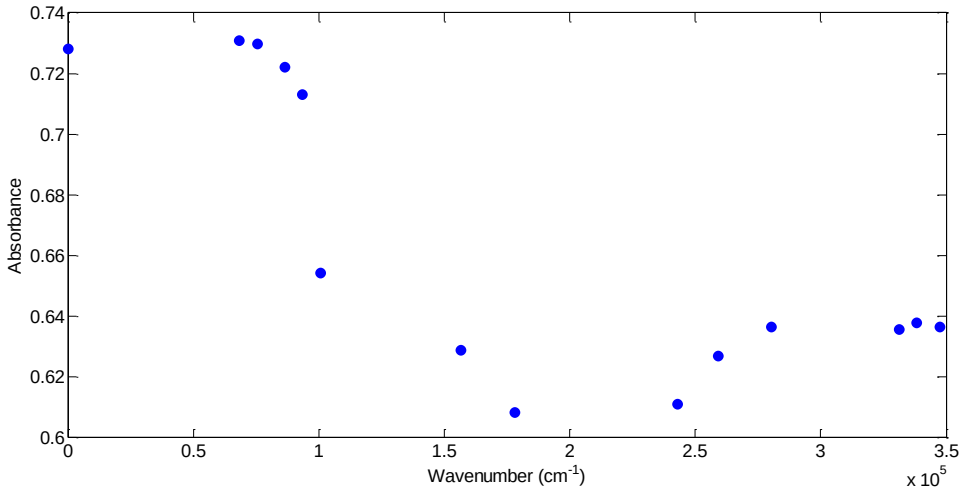

Figure 40 : MIR raw spectra at 1080 cm^{-1} for fermentation 4

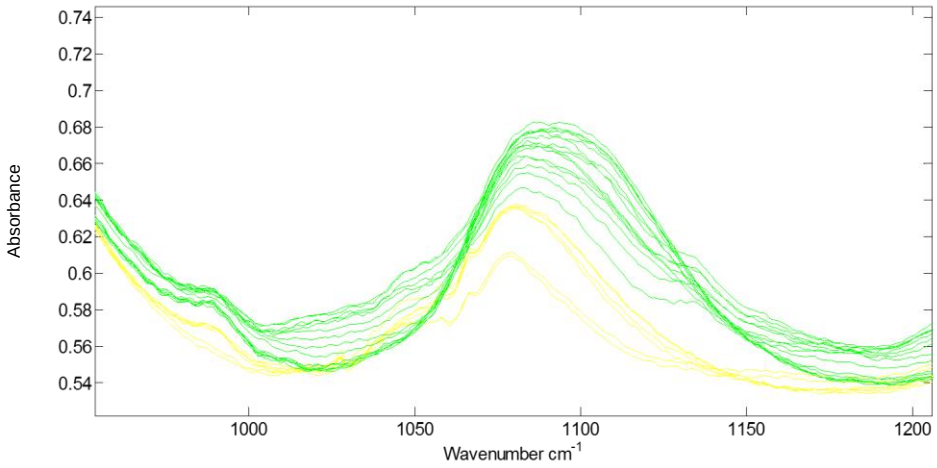

Figure 41 : Comparison of fermentation 4 (yellow) and 5 (green) in the region of 1000-1150 cm^{-1}

From the results of the fermentation infrared analysis there are a few regions of interest which may allow models to be built. In the NIR spectra, three possible regions were identified, 5650-5814 cm^{-1}, 6570.3 and 8710.8 cm-1. These have been attributed by other authors to ammonium, glucose and biomass respectively and also were found in the standard solution analysis in Figure 17. From the MIR spectra the 960-1180 cm^{-1} region looks promising as a region to monitor both xanthan production and glucose consumption. Again this region was found to be of interest by other authors as well as from the standard solution analysis.[56, 40]

From the literature it can be seen that it is possible to monitor glucose consumption during a fermentation reaction using MIR with Roychoudhury *et al.* (2008) carried out PLS modelling on the glucose consumption of *S. clavuligerus* and Sivakaseva *et al.* (2001)[36, 38] carried out both PLS and PCR modelling on *L. casei.* All these models used the same region as identified during the *X. campestris* fermentation as showing changes during the fermentation (Figure 17). A PCA and PLS model was designed to monitor the glucose levels in the fermentations. There were some difficulties with creating this model in large part due to the reference method with the YSI producing variable readings as described in 3.6.6.6. while these fermentations were only measured using this technique, others have used UV-vis spectrophotometers or HPLC to determine the glucose concentration which would have given more reliable results and hopefully improved the prediction accuracy of the models.[36, 40]

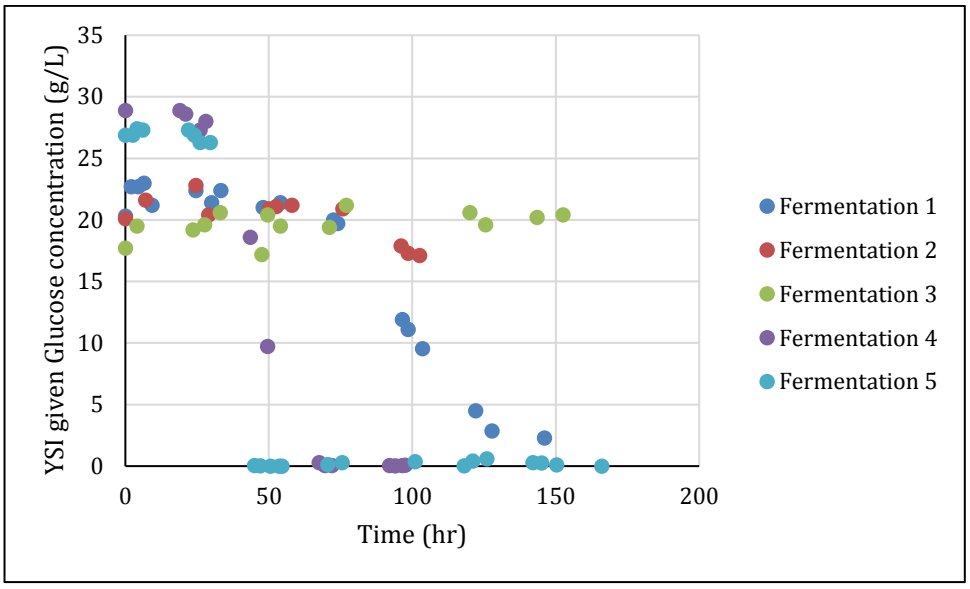

Figure 42 : YSI measured glucose concentration of all 5 *Xanthomonas* fermentations

As can be seen in Figure 42, the glucose consumption varied especially when comparing fermentations 1 and 2 and fermentations 4 and 5 both the PLS and PCA model were designed using the MIR region - 996-1200 cm^{-1}.

A PCA model using first derivative spectra in this region which had been mean centred was created using 5 principal components. Looking at fermentation 1,3,4 and 5, the first principal component captures 59.46% of the variance within the data set however

when the component scores are plotted against the sample number (Figure 43) – it appears that the model is in fact showing the glucose consumption or non-consumption as seen in fermentation 3.

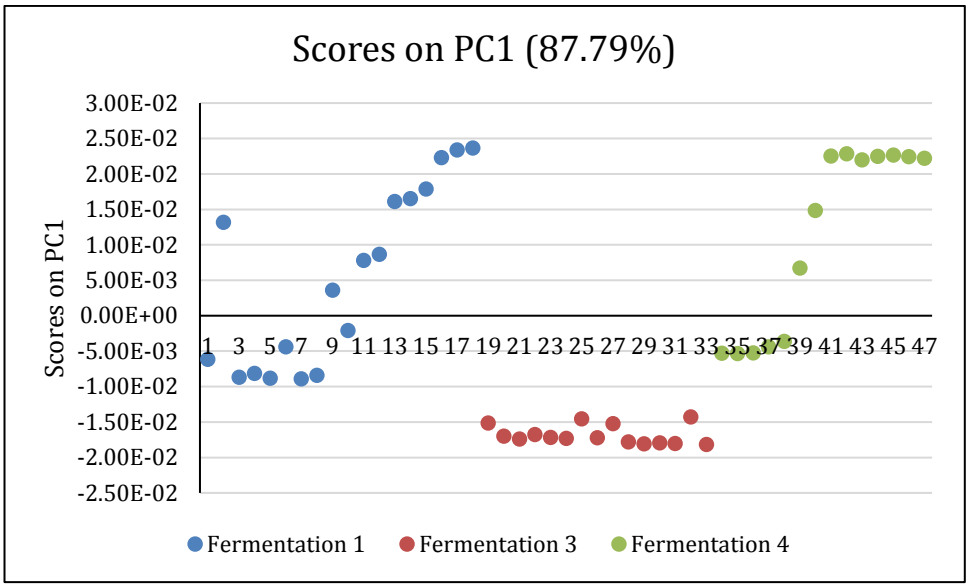

Figure 43 : Scores on PC1 MIR first derivative glucose region spectra - fermentations 1, 3 & 4

Using fermentations 1 and 4, a 1st derivative PLS model was designed using two latent variables. This model had a RMSEC of 2.78 g/L and an RMSECV: 3.50 g/L. These errors are larger than those found by Roychoudhury *et al* (2007) and as referenced in 3.7.1 and as discussed previously other reference methods may have reduced this error and provided a better model.[37] The model was then used to predict the concentration of glucose within fermentations 5. It can be seen that the model predicts the trend of the glucose consumption during the fermentation however; the actual calculated concentration is lower than the YSI concentration. This is also seen when the glucose standards are predicted, the trend is the same but the values are consistently lower (Figure 44).

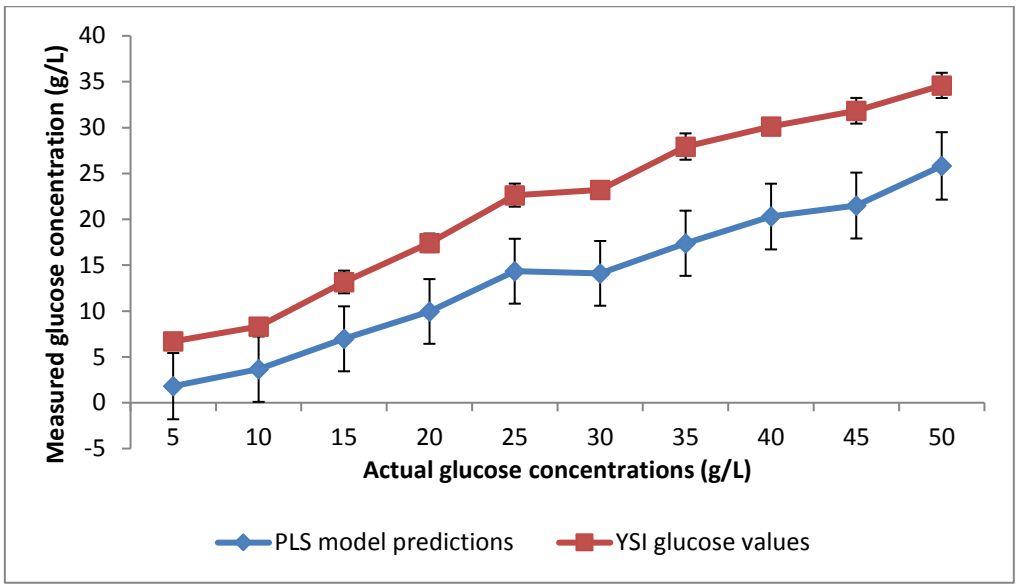

Figure 44 : PLS model prediction of glucose standard concentrations

The PLS model was able to predict the decrease in concentration of glucose in fermentation 5 (Figure 45). There are some higher than expected glucose values in the later stages of the fermentation. It is likely due to the model assuming that these peaks were due to glucose when in fact these are contributions from the xanthan produced during the fermentation which produce peaks in the same region.

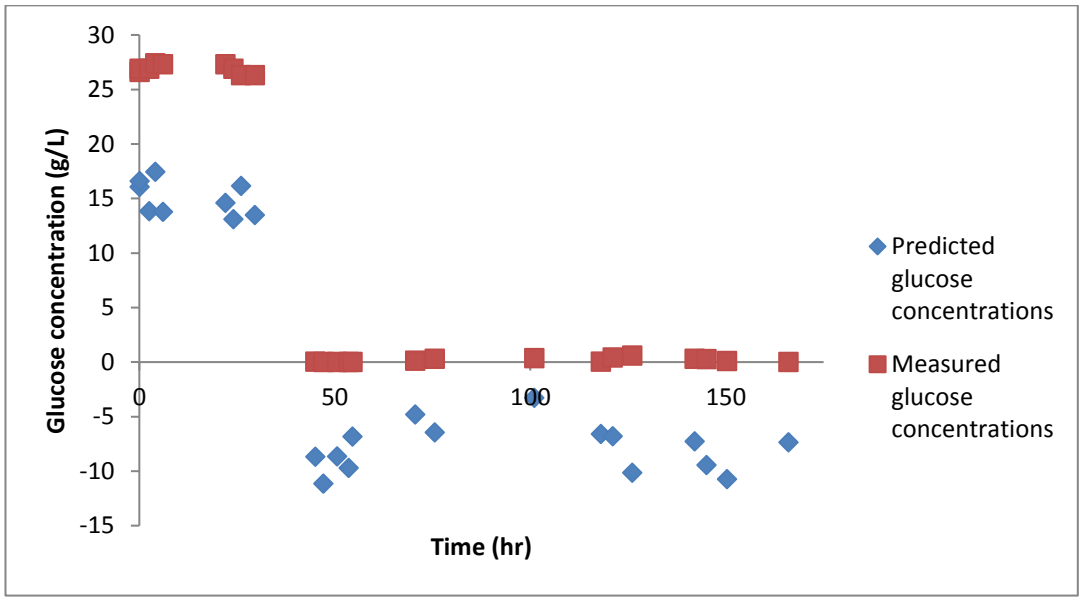

Figure 45 : Predicted and measured glucose concentrations for fermentation 5 using MIR PLS model

The lack of accuracy in the prediction of the model is likely to be due to errors associated with the model and further work would have to include a more reliable glucose reference method and additional fermentations to improve the model.

When a reflectance NIR PLS model was built using the 1st derivative spectra in the region – 8333 and 9090 cm^{-1}, the glucose predictions were not as accurate. The predicted concentrations are opposite to those expected. The RMSECV was much higher than the MIR models when using both the standards within the model and some of the fermentation results. The water peaks are dominating and the small changes in the NIR spectra due to the glucose are not representative in the models. The region used for these NIR models were not used by the authors described in 3.3.5,[27, 33, 56] this may be due to the difficulties with the water peaks and the small changes contributed by the glucose.

As the xanthan reference analysis was poor and xanthan was only seen in the fermentation 4 & 5 MIR spectra, producing a robust model is difficult to produce. Using just one fermentation and xanthan reference values it was possible to produce an example. The model had used 3 variables and has a RMSECV of 2.128 g/L and was used to predict the xanthan concentration in fermentation 5. (Figure 46) Although the measured values are significantly higher than the predicted values, the general trend of the fermentation can be seen. With an unreliable xanthan reference method as described in 3.7.1, the xanthan concentrations are higher than expected with a maximum expected xanthan concentration within the fermenter of 18.5 gL^{-1} and upon visual examination of the fermentation broth it appeared to have a low viscosity and the predicted values of 10gL^{-1} are a more realistic measurement of the fermentation broth.[64] However, until a better reference method can be determined and there are more xanthan producing fermentations it would be difficult to determine if the predicted values are those expected. A model based on the NIR spectra was not possible due to the small changes seen due to the xanthan.

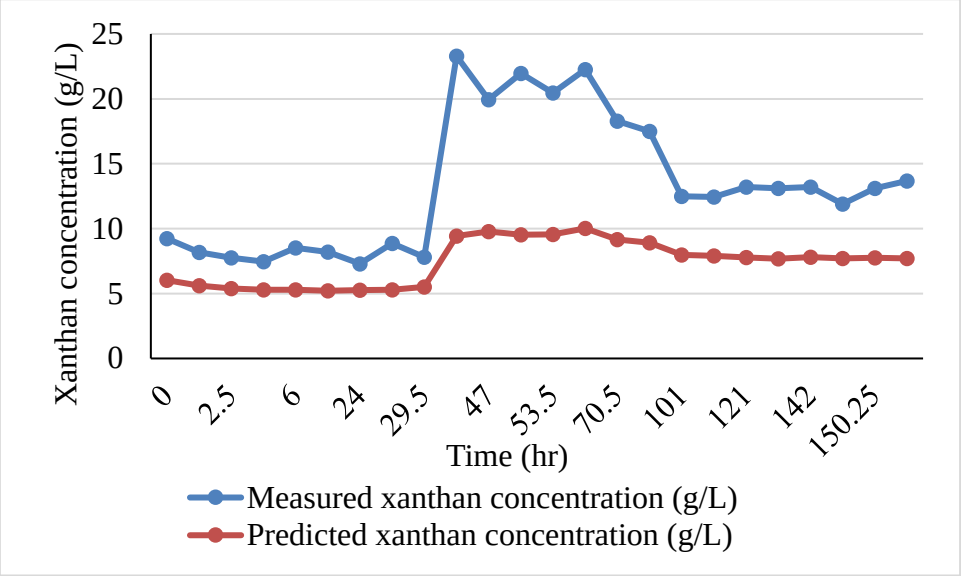

Figure 46 : Measured and predicted xanthan concentrations of fermentation 5 using fermentation 4 MIR spectra

3.8 Conclusions

A *Xanthomonas* fermentation is a difficult reaction with many sources of error and variation between fermentations. A simple MLR model was produced to predict the concentrations of the xanthan and biomass concentrations within the fermenter using optical density and glucose measurements. However, this model had limited success as the errors associated with the predictions are high, while the general trend of the biomass concentration can be seen the actual concentrations predicted are not robust The reasons for the high error may be due to the poor reference method used and further work would need to be carried out to produce more fermentations with a reliable measurement technique. The increase in the number of fermentations available would also allow a robust model to be built as more fermentations could be used for calibration. It is also possible to monitor the change in glucose concentration as the fermentation proceeds if the region of 980 -1200 cm^{-1} is examined. The glucose concentration decreases during the fermentation and using the calibration model it is possible to monitor the glucose concentration with the MIR spectra. The glucose model could be made more robust by a more accurate reference technique and further fermentations that include a change in starting glucose concentrations. Using the NIR

spectra to predict the glucose concentration proved more difficult with larger RMSEC values and negative predictions.

The production of xanthan can also be monitored within the same region with a new peak produced due to the xanthan being formed; this becomes more difficult to model as the xanthan reference method is not as robust as the glucose reference method. The fermentation samples also produced a small concentration of xanthan so a more productive fermentation may produce large enough concentrations of xanthan to compensate for the larger errors with the reference method. A MIR model was created to determine the concentration within the fermenter with predictions on fermentation 5, the reference method did cause some problems within the model but the predicted values are closer to expected xanthan concentrations for this fermentation. The NIR model produced a predicted increase in glucose concentration; however, these values were a negative concentration.

It can be seen from both the glucose and xanthan modelling that a robust reference method must be used to determine fermentation concentrations to allow the building of accurate models and that the MIR spectra produce better models with negative values and inverted values being found in the NIR models.

Further fermentations would need to be carried out to determine the robustness of the models and also a better set of xanthan reference results may allow the better creation of xanthan models.

3.9 References

1. *Near-infrared Spectroscopy*. 1st ed.; Wiley-VCH: Weinheim, 2002; p 348.

2. Arnold, S. A.; Gaensakoo, R.; Harvey, L. M.; McNeil, B., Use of at-line and in-situ near-infrared spectroscopy to monitor biomass in an industrial fed-batch Escherichia coli process. *Biotechnol. Bioeng.* **2002,** *80* (4), 405-413.

3. Crowley, J.; Arnold, S. A.; Wood, N.; Harvey, L. M.; McNeil, B., Monitoring a high cell density recombinant Pichia pastoris fed-batch bioprocess using transmission and reflectance near infrared spectroscopy. *Enzyme Microb. Technol.* **2005,** *36* (5-6), 621-628.

4. Osbourne, B. G.; Fearn, T.; Hindle, P. H., *Practical NIR spectroscopy*. Pearson Education: Harlow, 1986; p 227.

5. Cervera, A. E.; Petersen, N.; Lantz, A. E.; Larsen, A.; Gernaey, K. V., Application of Near-Infrared Spectroscopy for Monitoring and Control of Cell Culture and Fermentation. *Biotechnol. Prog.* **2009,** *25* (6), 1561-1581.

6. Yves Roggo, P. C., Lene Maurer, Carmen Lema-Martinez, Aureile Edmond and Nadine jent, A review of near infrared spectroscopy and chemometrics in pharmaceutical technologies. *Journal of pharmaceutical and biomedical analysis* **2007,** *44* (3), 683-700.

7. http://www.fc.up.pt/pessoas/peter.eaton/tutorial/sld011.htm. (08/11/10).

8. Hagman, A.; Sivertsson, P., The use of NIR spectroscopy in monitoring and controlling bioprocesses. *Process Control Qual.* **1998,** *11* (2), 125-128.

9. Pollard, D.; Buccino, R.; Connors, N.; Kirschner, T.; Olewinski, R.; Saini, K.; Salmon, P., Real-time analyte monitoring of a fungal fermentation, at pilot scale, using in situ mid-infrared spectroscopy. *Bioprocess and biosystems engineering* **2001,** *24* (1), 13-24.

10. Alves-Rausch, J.; Bienert, R.; Grimm, C.; Bergmaier, D., Real time in-line monitoring of large scale Bacillus fermentations with near-infrared spectroscopy. *Journal of biotechnology* **2014,** *189*, 120-128.

11. Pollard, D.; Kirschner, T.; Salmon, P., Rheological characterization of a fungal fermentation for the production of pneumocandins *Bioprocess and biosystems engineering* **2002,** *24* (6), 1615-7605.

12. Arnold, S. A.; Harvey, L. M.; McNeil, B.; Hall, J. W., Employing near-infrared spectroscopic methods and analysis for fermentation monitoring and control - Part 1, method development. *Biopharm. Int.* **2002,** *15* (11), 26-32.

13. Arnold, S. A.; Crowley, J.; Woods, N.; Harvey, L. M.; McNeill, B., In-situ near infrared spectroscopy to monitor key analytes in mammalian cell cultivation. *Biotechnol. Bioeng.* **2003,** *84* (1), 13-19.

14. Arnold, S. A.; Crowley, J.; Vaidyanathan, S.; Matheson, L.; Mohan, P.; Hall, J. W.; Harvey, L. M.; McNeil, B., At-line monitoring of a submerged filamentous bacterial cultivation using near-infrared spectroscopy. *Enzyme Microb. Technol.* **2000,** *27* (9), 691-697.

15. Cavinato, A. G.; Mayes, D. M.; Ge, Z. H.; Callis, J. B., Noninvasive method for monitoring ethanol in fermentation processes using fiberoptic near-infrared spectroscopy *Anal. Chem.* **1990,** *62* (18), 1977-1982.

16. Cimander, C.; Carlsson, M.; Mandenius, C. F., Sensor fusion for on-line monitoring of yoghurt fermentation. *Journal of biotechnology* **2002,** *99* (3), 237-248.

17. Cimander, C.; Mandenius, C. F., Online monitoring of a bioprocess based on a multi-analyser system and multivariate statistical process modelling. *J. Chem. Technol. Biotechnol.* **2002,** *77* (10), 1157-1168.

18. Crowley, J.; McCarthy, B.; Nunn, N. S.; Harvey, L. M.; McNeil, B., Monitoring a recombinant Pichia pastoris fed batch process using Fourier transform mid-infrared spectroscopy (FT-MIRS). *Biotechnol. Lett.* **2000,** *22* (24), 1907-1912.

19. Ferreira, L. S.; De Souza, M. B.; Folly, R. O. M., Development of an alcohol fermentation control system based on biosensor measurements interpreted by neural networks. *Sens. Actuator B-Chem.* **2001,** *75* (3), 166-171.

20. Finn, B.; Harvey, L. M.; McNeil, B., Near-infrared spectroscopic monitoring of biomass, glucose, ethanol and protein content in a high cell density baker's yeast fed-batch bioprocess. *Yeast* **2006,** *23* (7), 507-517.

21. Ge, Z. H.; Cavinato, A. G.; Callis, J. B., Noninvasive spectroscopy for monitoring cell-density in a fermentation process *Anal. Chem.* **1994,** *66* (8), 1354-1362.

22. Giavasis, I.; Robertson, I.; McNeil, B.; Harvey, L. M., Simultaneous and rapid monitoring of biomass and biopolymer production by *Sphingomonas paucimobilis* using Fourier transform-near infrared spectroscopy. *Biotechnol. Lett.* **2003,** *25* (12), 975-979.

23. Hall, J. W.; McNeil, B.; Rollins, M. J.; Draper, I.; Thompson, B. G.; Macaloney, G., Near-infrared spectroscopic determination of acetate, ammonium, biomass, and glycerol in an industrial *Escherichia coli* fermentation. *Appl. Spectrosc.* **1996,** *50* (1), 102-108.

24. Lewis, C. B.; McNichols, R. J.; Gowda, A.; Cote, G. L., Investigation of near-infrared spectroscopy for periodic determination of glucose in cell culture media in situ. *Appl. Spectrosc.* **2000,** *54* (10), 1453-1457.

25. Macaloney, G.; Draper, I.; Preston, J.; Anderson, K. B.; Rollins, M. J.; Thompson, B. G.; Hall, J. W.; McNeil, B., At-line control and fault analysis in an industrial high cell density *Escherichia coli* fermentation, using NIR spectroscopy. *Food Bioprod. Process.* **1996,** *74* (C4), 212-220.

26. Macauley-Patrick, S.; Arnold, S. A.; McCarthy, B.; Harvey, L. M.; McNeil, B., Attenuated total reflectance Fourier transform mid-infrared spectroscopic quantification of sorbitol and sorbose during a Gluconobacter biotransformation process. *Biotechnology letters* **2003,** *25* (3), 257-260.

27. McShane, M. J.; Cote, G. L., Near-infrared spectroscopy for determination of glucose lactate, and ammonia in cell culture media. *Appl. Spectrosc.* **1998,** *52* (8), 1073-1078.

28. Al Mosheky, Z.; Melling, P. J.; Thompson, M. A., In situ real-time monitoring of a fermentation reaction using a fiber-optic FT-IR probe. *Spectroscopy* **2001,** *16* (6), 15-20.

29. Navratil, M.; Cimander, C.; Mandenius, C. F., On-line multisensor monitoring of yogurt and Filmjolk fermentations on production scale. *J. Agric. Food Chem.* **2004,** *52* (3), 415-420.

30. Navratil, M.; Norberg, A.; Lembren, L.; Mandenius, C. F., On-line multi-analyzer monitoring of biomass, glucose and acetate for growth rate control of a *Vibrio cholerae* fed-batch cultivation. *J. Biotechnol.* **2005,** *115* (1), 67-79.

31. Nordon, A.; Littlejohn, D.; Dann, A. S.; Jeffkins, P. A.; Richardson, M. D.; Stimpson, S. L., In situ monitoring of the seed stage of a fermentation process using non-invasive NIR spectrometry. *Analyst* **2008,** *133* (5), 660-666.

32. Rhiel, M.; Cohen, M. B.; Murhammer, D. W.; Arnold, M. A., Nondestructive near-infrared spectroscopic measurement of multiple analytes in undiluted samples of serum-based cell culture media. *Biotechnol. Bioeng.* **2002,** *77* (1), 73-82.

33. Riley, M. R.; Rhiel, M.; Zhou, X. J.; Arnold, M. A.; Murhammer, D. W., Simultaneous measurement of glucose and glutamine in insect cell culture media by near infrared spectroscopy. *Biotechnol. Bioeng.* **1997,** *55* (1), 11-15.

34. Riley, M. R.; Arnold, M. A.; Murhammer, D. W., Matrix-enhanced calibration procedure for multivariate calibration models with near-infrared spectra. *Appl. Spectrosc.* **1998,** *52* (10), 1339-1347.

35. Rodrigues, L. O.; Vieira, L.; Cardoso, J. P.; Menezes, J. C., The use of NIR as a multi-parametric in situ monitoring technique in filamentous fermentation systems. *Talanta* **2008,** *75* (5), 1356-1361.

36. Roychoudhury, P.; Harvey, L. M.; McNeil, B., At-line monitoring of ammonium, glucose, methyl oleate and biomass in a complex antibiotic fermentation process using attenuated total reflectance-mid-infrared (ATR-MIR) spectroscopy. *Anal. Chim. Acta* **2006,** *561* (1-2), 218-224.

37. Roychoudhury, P.; McNeil, B.; Harvey, L. M., Simultaneous determination of glycerol and clavulanic acid in an antibiotic bioprocess using attenuated total reflectance mid infrared spectroscopy. *Anal. Chim. Acta* **2007,** *585* (2), 246-252.

38. Sivakesava, S.; Irudayaraj, J.; Ali, D., Simultaneous determination of multiple components in lactic acid fermentation using FT-MIR, NIR, and FT-Raman spectroscopic techniques. *Process Biochem.* **2001,** *37* (4), 371-378.

39. Tamburini, E.; Vaccari, G.; Tosi, S.; Trilli, A., Near-infrared spectroscopy: A tool for monitoring submerged fermentation processes using an immersion optical-fiber probe. *Appl. Spectrosc.* **2003,** *57* (2), 132-138.

40. Tosi, S.; Rossi, M.; Tamburini, E.; Vaccari, G.; Amaretti, A.; Matteuzzi, D., Assessment of in-line near-infrared spectroscopy for continuous monitoring of fermentation processes. *Biotechnol. Prog.* **2003,** *19* (6), 1816-1821.

41. Triadaphillou, S.; Martin, E.; Montague, G.; Nordon, A.; Jeffkins, P.; Stimpson, S., Fermentation process tracking through enhanced spectral calibration modeling. *Biotechnol. Bioeng.* **2007,** *97* (3), 554-567.

42. Vaidyanathan, S.; Matheson, L.; Mohan, P.; Harvey, L.M.; McNeil, B., Assesment of near-infrared spectral information for rapid monitoring of bioprocess quality *Biotechnol. Bioeng.* **2001,** *74* (5), 376-388.

43. Vaidyanathan, S.; Harvey, L. M.; McNeil, B., Deconvolution of near-infrared spectral information for monitoring mycelial biomass and other key analytes in a submerged fungal bioprocess. *Anal. Chim. Acta* **2001,** *428* (1), 41-59.

44. Vaidyanathan, S.; Macaloney, G.; McNeil, B., Fundamental investigations on the near-infrared spectra of microbial biomass as applicable to bioprocess monitoring. *Analyst* **1999,** *124* (2), 157-162.

45. Vaidyanathan, S.; White, S.; Harvey, L. M.; McNeil, B., Influence of morphology on the near-infrared spectra of mycelial biomass and its implications in bioprocess monitoring. *Biotechnol. Bioeng.* **2003,** *82* (6), 715-724.

46. Vaidyanathan, S.; Macaloney, G.; Harvey, L. M.; McNeil, B., Assessment of the structure and predictive ability of models developed for monitoring key analytes

in a submerged fungal bioprocess using near-infrared spectroscopy. *Appl. Spectrosc.* **2001,** *55* (4), 444-453.

47. Yeung, K. S. Y.; Hoare, M.; Thornhill, N. F.; Williams, T.; Vaghjiani, J. D., Near-infrared spectroscopy for bioprocess monitoring and control. *Biotechnol. Bioeng.* **1999,** *63* (6), 684-693.

48. Cozzolino, D.; Liu, L.; Cynkar, W. U.; Dambergs, R. G.; Janik, L.; Colby, C. B.; Gishen, M., Effect of temperature variation on the visible and near infrared spectra of wine and the consequences on the partial least square calibrations developed to measure chemical composition. *Anal. Chim. Acta* **2007,** *588* (2), 224-230.

49. Holm-Nielsen, J. B.; Lomborg, C. J.; Oleskowicz-Popiel, P.; Esbensen, K. H., On-line near infrared monitoring of glycerol-boosted anaerobic digestion processes: Evaluation of process analytical technologies. *Biotechnol. Bioeng.* **2008,** *99* (2), 302-313.

50. Vaccari, G.; Dosi, E.; Campi, A. L.; Gonzalezvara, A.; Matteuzzi, D.; Mantovani, G., A near-infrared spectroscopy technique for the control of fermentation processes- an application to lactic-acid fermentation *Biotechnol. Bioeng.* **1994,** *43* (10), 913-917.

51. Gonzalez-Vara, A.; Vaccari, G.; Dosi, E.; Trilli, A.; Rossi, M.; Matteuzzi, D., Enhanced production of L-(+)-lactic acid in chemostat by Lactobacillus casei DSM 20011 using ion-exchange resins and cross-flow filtration in a fully automated pilot plant controlled via NIR. *Biotechnol. Bioeng.* **2000,** *67* (2), 147-156.

52. Pripp, A. H., Application of Multivariate Analysis: Benefits and Pitfalls. In *Statistics in Food Science and Nutrition*, Springer New York: New York, NY, 2013; pp 53-64.

53. Pham, P. J.; Hernandez, R.; French, W. T.; Estill, B. G.; Mondala, A. H., A spectrophotometric method for quantitative determination of xylose in fermentation medium. *Biomass and Bioenergy* **2011,** *35* (7), 2814-2821.

54. Miller, J.; Miller, J., *Statistics and Chemometrics for Analytical Chemistry, 4th Edition*. 4th ed.; Pearson: 2000.

55. Watari, M., Applications of near-infrared spectroscopy to process analysis using fourier transform spectrometer. *Optical Review* **2010,** *17* (3), 317-322.

56. Chung, H.; Arnold, M. A.; Rhiel, M.; Murhammer, D. W., Simultaneous measurements of glucose, glutamine, ammonia, lactate, and glutamate in aqueous solutions by near-infrared spectroscopy. *Appl. Spectrosc.* **1996,** *50* (2), 270-276.

57. Roychoudhury, P.; Harvey, L. M.; McNeil, B., The potential of mid infrared spectroscopy (MIRS) for real time bioprocess monitoring. *Anal. Chim. Acta* **2006,** *571* (2), 159-166.

58. Scarff, M.; Arnold, S. A.; Harvey, L. M.; McNeil, B., Near Infrared Spectroscopy for bioprocess monitoring and control: Current status and future trends. *Critical reviews in biotechnology* **2006,** *26* (1), 17-39.

59. Arnold, S. A.; Matheson, L.; Harvey, L. M.; McNeil, B., Temporally segmented modelling: a route to improved bioprocess monitoring using near infrared spectroscopy? *Biotechnol. Lett.* **2001,** *23* (2), 143-147.

60. Peters, H.-U.; Herbst, H.; Hesselink, P. G. M.; Lünsdorf, H.; Schumpe, A.; Deckwer, W.-D., The influence of agitation rate on xanthan production by Xanthomonas campestris. *Biotechnol. Bioeng.* **1989,** *34* (11), 1393-1397.

61. Garcia- Ochoa, F.; Santos, V. E.; Alcon, A., Xanthan gum production - an unstructured kinetic model. *Enzyme Microb. Technol.* **1995,** *17* (3), 206-217.

62. Amanullah, A.; Satti, S.; Nienow, A. W., Enhancing Xanthan fermentations by different modes of glucose feeding. *Biotechnol. Prog.* **1998,** *14* (2), 265-269.

63. S.L., G.; G.D., N.; H.D., H.; H., Z., Kinetic models for xanthan gum production using Xanthomonas campestris from molasses. *Chemical Industry and Chemical Engineering Quarterly* **2011,** *17* (2).

64. Garcia-Ochoa, F.; Santos, V. E.; Casas, J. A.; Gomez, E., Xanthan gum: production, recovery, and properties. *Biotechnol. Adv.* **2000,** *18* (7), 549-579.

65. Mudoi, P.; Bharali, P.; Konwar, B. K., - Study on the Effect of pH, Temperature and Aeration on the Cellular Growth and Xanthan Production by Xanthomonas campestris Using Waste Residual Molasses. **2013,** - *3* (- 3), -.

66. Meinke, M.; Mueller, G.; Albrecht, H.; Antoniou, C.; Richter, H.; Lademann, J., Two-wavelength carbon dioxide laser application for in-vitro blood glucose measurements. *Journal of Biomedical Optics* **2008,** *13* (1).

67. Ibrahim, M.; Alaam, M.; El-Haes, H.; Jalbour, A. F.; Leon, A. d., Analysis of the structure and vibrational spectra of glucose and fructose. *Ecletcia Quimica* **2006,** *31* (3), 15-21.

68. http://www.chemspider.com/Chemical-Structure.96749.html (10/08/13).

69. Hue, C.; Gunata, Z.; Bergounhou, A.; Assemat, S.; Boulanger, R.; Sauvage, F. X.; Davrieux, F., Near infrared spectroscopy as a new tool to determine cocoa fermentation levels through ammonia nitrogen quantification. *Food Chem.* **2014,** *148*, 240-245.

4 Acoustic Monitoring

Acoustic monitoring is currently being used in multiple industries, with the food industry carrying out research into further acoustic monitoring techniques. Ultrasound can provide information on the fundamental properties of the material; the main advantages of ultrasound are that it is rapid, non-destructive and can be applied to systems that are concentrated and optically opaque. These advantages are similar to those of the NMR, however ultrasound has additional advantages of price and the adaptability for on-line measurements. The non-destructive nature of the technique and the ability to apply to an optically opaque system could be useful for the monitoring of fermentation processes. There are various methods of ultrasound measurement, including pulse-echo, through transmission and continuous wave which all have different advantages and disadvantages depending on the sample being measured.

Rheometers were first used in the 19th century to measure electric current. They are more traditionally used to measure the flow of liquids such as paints, oils and polymers. Rheometers are used in the medical industry to study the flow of blood and can also be used for measuring molten poly(methyl methacrylate) resins.[1] As fermentation broths can display changes in viscosity due to the product of the process, rheological monitoring may help to understand the progress of a reaction or identify when a product has been formed.

Bioinnovel have designed a novel acoustic probe which may be able to monitor a fermentation. This new probe can potentially combine the acoustic measurements with rheological measurements to model fermentations which show significant rheological changes such as *X. campestris.*

4.1 Acoustic Theory

In ultrasound measurements, a high frequency sound wave is propagated through the material. The type and degree of interaction between the sound wave and the material are used to obtain information about the properties of the material.

4.1.1 Ultrasonic wave

Ultrasonic waves can be applied to materials in many different ways. When an oscillating stress wave is applied perpendicular to a materials surface, a compression wave is generated as the layers of the material move in the same direction as the stress wave. When the stress wave is applied parallel to the material's surface a shear wave is generated as the layers of the material move perpendicular to the propagating wave. (Figure 47) When the wave is removed the energy which was stored as ultrasound is released and the material returns to its equilibrium position. Hence, ultrasound (at low powers) is non-destructive.[2]

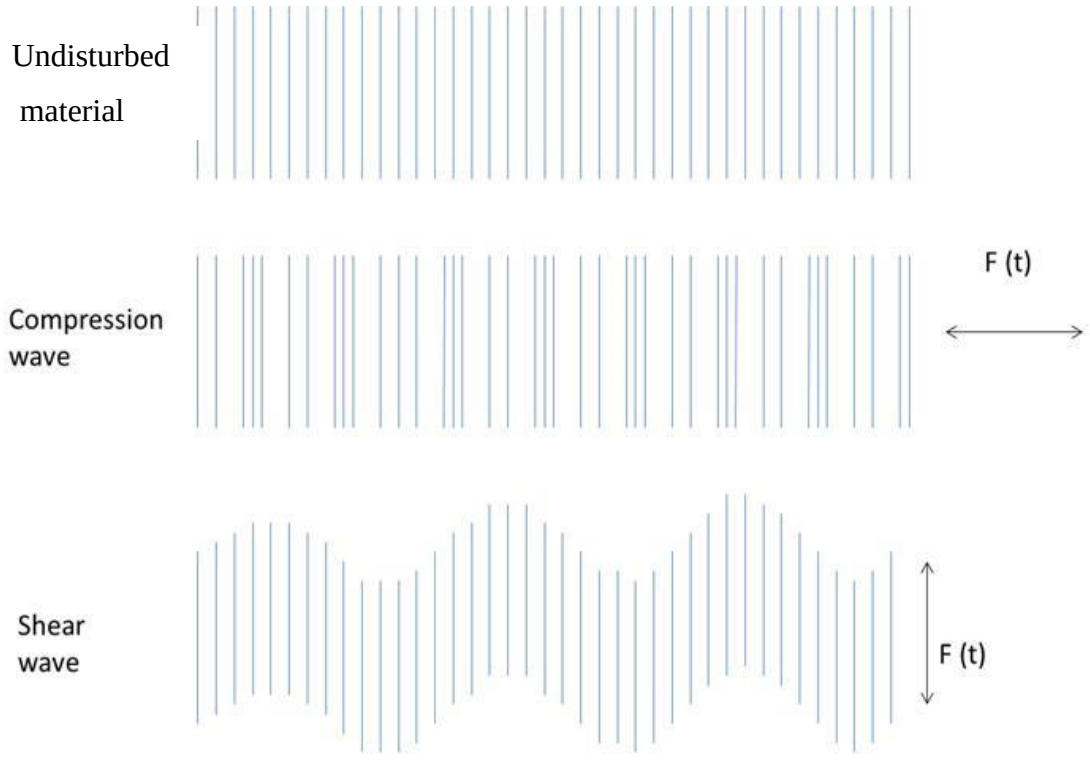

Figure 47 : Ultrasonic waves propagate through materials as either a compression or shear wave, dependent on the acoustic pressure F (t)[2]

As an ultrasonic wave is propagated through a material, the amplitude of the wave is altered with the time and distance travelled. This change in amplitude can be attributed to the different physical properties of the material such as temperature, pressure and density, these changes are dependent on the material used. The wave can be characterised by its amplitude and frequency, which are experimental parameters, and the wavelength and attenuation co-efficient, which are frequency dependent characteristics of the material. Wavelength and frequency relate to the ultrasonic velocity, which is a characteristic property of the material.

4.1.2 Ultrasonic velocity and attenuation

The physical and ultrasonic properties of a material, are related to each other and this relationship can be determined using Equation 2.

$$\left(\frac{\boldsymbol{k}}{\boldsymbol{\omega}}\right)^{\mathbf{2}} = \frac{\boldsymbol{\rho}}{\boldsymbol{E}} \qquad \text{Equation 2}$$

where k = complex wave number of the material

ω = angular frequency

ρ = density

E = elastic modulus

The complex wave number, k can be used to relate the measureable ultrasonic properties of attenuation and velocity, to the bulk physical properties such as density (Equation 3).

$$\boldsymbol{k} = \frac{\boldsymbol{\omega}}{\boldsymbol{c}} + \boldsymbol{i\alpha} \qquad \text{Equation 3}$$

where c = velocity

α = attenuation coefficient

The ultrasonic velocity (c) in a material is the distance travelled by the ultrasonic wave in a unit of time. It can be determined using Equation 4, where the time taken (t) for the wave to travel a known distance (d) is measured.[3]

$$c = \frac{d}{t}$$ Equation 4

The ultrasonic velocity can also be calculated by measuring the wavelength of ultrasound (λ) at a known frequency (f) (Equation 5).

$$c = \lambda . f$$ Equation 5

When a material has a low attenuation, Equation 2 can be simplified to Equation 6

$$\frac{1}{c^2} = \frac{\rho}{E}$$ Equation 6

Equation 6 relates the ultrasonic velocity to two physical properties of the material, elastic modulus and density. A less dense material allows the wave to travel through the material quicker. However, the ultrasonic velocity in solids is higher than that of liquids as the difference in moduli of the solids and liquids is greater than the difference in densities. Phase changes can be monitored using the change in velocity of ultrasound in solids, liquids and gases due to the differing properties of the materials.

When an ultrasonic wave passes through a material, its amplitude will change due to the attenuation. Adsorption and scattering are the two main sources of attenuation and all materials will attenuate the wave to some extent. In both heterogeneous and homogenous materials adsorption is important; some of the energy from the ultrasound wave is converted to other forms and will eventually become heat. In heterogeneous materials the ultrasound wave is scattered in different directions when it comes into contact with a particle. The wave is then not detected by the receiver as the direction of the propagation of the wave has changed even though the energy remains stored as ultrasound. The attenuation coefficient of a material can be calculated using Equation 7.

$$A = A_0 e^{-\alpha x}$$ Equation 7

where A = amplitude of the wave

A_0 = initial amplitude of the wave

x = distance travelled through material

4.1.3 Interaction of ultrasound with matter

4.1.3.1 Ultrasonic adsorption and relaxation

Energy is absorbed by a material as an ultrasonic wave passes through it and so the waves amplitude decreases. The main forms of adsorption of ultrasound in gases and liquids are thermal conduction, viscosity and molecular relaxation. For solids, overall adsorption may be affected by other physical mechanisms.

When mechanical energy in the wave is converted into other physicochemical mechanisms already in existence in the material it is adsorption. Some energy will be lost as heat, this energy loss is due to regions of high and low temperature in the material (thermal conduction) or due to the movement of molecules in the material as the wave passes through (viscosity). Classical adsorption (Equation 8) in a liquid is the contribution of the sum of the thermal conductivity and the viscosity to the overall adsorption by the liquid.

$$\alpha_{classical} / f^2 = 4\pi^2 / \rho\, c\, (4\eta/3 + (1-\psi)\tau / C_p) \qquad \text{Equation 8}$$

where η = viscosity

τ = thermal conductivity

ψ = ratio of specific heat capacities

C_p = specific heat capacity at constant pressure

$4\eta/3$ = contribution of viscous losses

$(1-\gamma)\tau / C_p$ = contribution of heat conduction losses

ρ = density

If a solution is in dynamic equilibrium, an ultrasonic wave will cause the local temperature and pressure to change and thus the equilibrium will be altered. The relaxation time is measured as the time taken for the solution in dynamic equilibrium to change to the new equilibrium.

4.1.3.2 Ultrasound and interaction with particles

The extent of the scattering of the ultrasonic wave when it is in the presence of particles in solution is determined by the wavelength (λ) of the ultrasound used and the dimensions of the particle (d) in the solution. The scattering of ultrasound can be divided into three regions[4]

1. Long wavelength limit (LWL) where the particle size is much smaller than the ultrasonic wavelength ($d < \lambda /10$)

2. Intermediate wavelength regime (IWR) where the particle size is approximately similar to the ultrasonic wavelength ($\lambda /10 < d < 50 \lambda$)

3. Short wavelength limit (SWL) where the particle size is much greater than the ultrasonic wavelength ($d > 50 \lambda$)

4.1.4 Measurement techniques

The choice of measurement system is dependent on the material being tested, the property being measured, the equipment available, desired speed and accuracy, and if it is to be used for off or on-line monitoring.

4.1.4.1 Pulsed techniques

Pulsed techniques are most widely used, easy to operate and are rapid and non-invasive.

4.1.4.1.1 Pulse–echo technique

An electrical pulse of the appropriate frequency, amplitude and duration is generated by a signal generator, which is then converted into an ultrasonic pulse by the transducer. The transducers convert electrical energy into mechanical energy and vice-versa. The most common type of transducer contains a single piezoelectric crystal which can generate an electrical potential when they are deformed along an axis. When choosing a transducer, the range of frequencies, diameter and acoustic matching must

be considered. If the crystal is highly dampened, it is a broadband transducer which can be used with very narrow pulses. The ultrasonic wave is propagated through the sample until it reaches the other side of the measurement vessel and it is then reflected back to the transducer. The transducer is now the receiver and converts the ultrasound wave back into an electrical signal which can be displayed on an oscilloscope. When the echoes are analysed the velocity, attenuation and impedance of a sample can be determined.[5]

Velocity is calculated using Equation 9.

$$\boldsymbol{c = \frac{2d}{t}} \qquad \text{Equation 9}$$

where d = cell length

t = time between successive echoes

The attenuation coefficient (Equation 7) is determined by measuring the decrease in amplitude of successive echoes. The specific acoustic impedance of a sample is determined by measuring the fraction of ultrasound that is reflected from the boundary between the measurement cell and the sample.

4.1.4.1.2 Through Transmission (Pitch – catch)

In through transmission measurements, two transducers are used where one acts as the generator and the other acts as the receiver. The sample is placed between the transducers and the time of flight and amplitude of the ultrasonic pulse is measured. The ultrasonic velocity and attenuation coefficient can be determined by this method. The ultrasonic velocity is calculated using Equation 4, where the time taken for the pulse to travel between the transducers given by t and d is the distance between the two transducers. The attenuation coefficients can be calculated relative to a calibration sample, which is analysed prior to the sample of interest using Equation 10.[6]

$$a = 20\ log_{10}\left(\frac{A_w}{A_s}\right)$$ Equation 10

where A_w = amplitude of the calibration signal

A_s = amplitude of the sample signal

4.1.4.2 Continuous wave

A measurement cell containing the sample is placed between an ultrasonic transducer and a reflector plate. The reflector plate must be capable of moving vertically through the sample. A sine wave of desired frequency and amplitude is generated by a signal generator to the transducer. The resulting ultrasonic wave generated by the transducer propagates through the sample and is reflected back by the reflector plate. This wave is reflected back and forth between the front face of the transducer and the reflector plate. As the reflector plate is moved, the amplitude of the standing waves, produced by the sample, detected by the transducer go through a series of maxima and minima due to the movement of the plate. The velocity and attenuation are calculated by the resulting signal.[7]

4.2 Rheological theory

4.2.1 Viscosity

Viscosity (η) is the measure of the resistance to flow. This is related to the concept of shear stress.[8] Shear stress is when a force is applied which causes the material to shear or twist; Newton's postulate relates shear stress (σ) and shear strain (γ) to the viscosity through (Equation 11)

$$\sigma = \eta\gamma$$ Equation 11

This postulate can be explained through an example of two parallel plates (geometries), each with area, A, and a distance apart, d, and the gap is filled with the fluid which is to be sheared (Figure 48).[8]

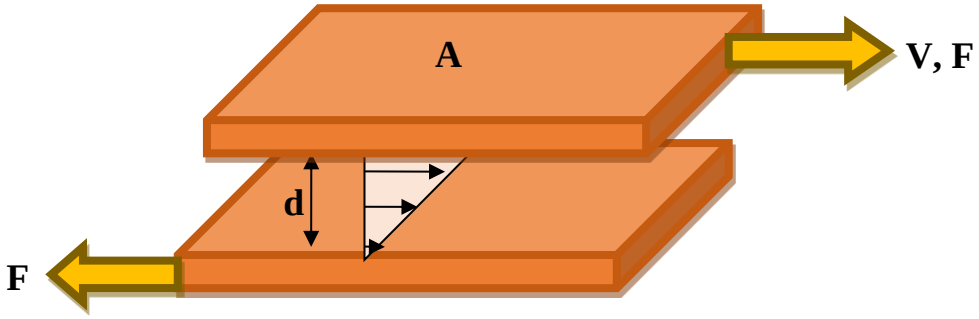

Figure 48 : Schematic of forces applied

When the top geometry moves with velocity, V, and the bottom geometry does not move, this leads to the fluid experiencing different shear forces throughout the liquid and there will be a velocity gradient equal to V/d. This gradient is known as the shear strain rate ($\dot{\gamma}$) which is measured in s^{-1}.[9]

The shear stress is measured in Pascals and is the force required per unit area to produce the plate motion. When an external stress is applied to a fluid, the high mobility of the molecules causes the fluid to deform. This deformation will continue until the stress is removed. However, the rate of deformation will be slowed by the internal friction forces hindering the movement of the molecules. From this, an equilibrium state is reached where there is a constant rate of external stress producing a constant rate of deformation.[10]

4.2.2 Fluids

There are two main classes of fluid in rheometery; Newtonian and non-Newtonian.

4.2.2.1 Newtonian

The simplest fluids have a direct relationship between viscosity and shear stress. Shear rate has no effect on this relationship. These are called Newtonian fluids. There are several properties that a Newtonian fluid must have:

- when shearing is finished, the stress in the fluid must fall to zero immediately,

– the shearing viscosity must produce the same results each time, no matter how long the resting time between the measurement times is, and;

– the viscosities measured by different types of deformation are always proportional to one another.

4.2.2.2 Non-Newtonian

Non-Newtonian fluids have a viscosity which varies with different shear rates. The viscosity is a function of shear rate as opposed to a coefficient and so Newton's postulate becomes (Equation 12)

$$\boldsymbol{\sigma = \gamma . \eta . \dot{\gamma}} \qquad \text{Equation 12}$$

The function $\eta . \dot{\gamma}$ is now not constant with shear rate but if the other conditions hold, the fluid can be termed a generalised Newtonian fluid.

A shear thinning material shows a decrease in viscosity with increasing shear rate. At very low and high shear rates, the viscosity reaches a constant value and these are referred to as the lower and upper Newtonian regions. Shear thinning is observed in solutions containing macromolecules such as celluloses. The macromolecules align in the direction of the shear stress vector when the stress is applied and they exhibit a reduced resistance to flow, so there is a decrease in viscosity. A pseudoplastic material has properties similar to a shear thinning material, however, it has a limiting high shear rate.[8] As the shear rate is reduced there is an increase in the viscosity of the solution, however, the rate of increase in the viscosity will reduce and therefore a constant velocity will be achieved even with a further reduction in shear rate. A xanthan gum solution is an example of a shear thinning fluid. The properties of xanthan gum solutions is discussed in 2.2.1.

A shear thickening material is one in which the viscosity increases as the shear rate increases. Shear thickening is typical flow behaviour of pastes and suspensions where there are high concentrations of particles (>50%).[11] Shear thickening materials have relatively simple flow patterns.[8]

4.2.3 Models

There are many models that can be used to describe the rheological properties of a material. The curve shown in Figure 49 can be described with various model equations such as the cross and power laws (Equation 13 & Equation 14).

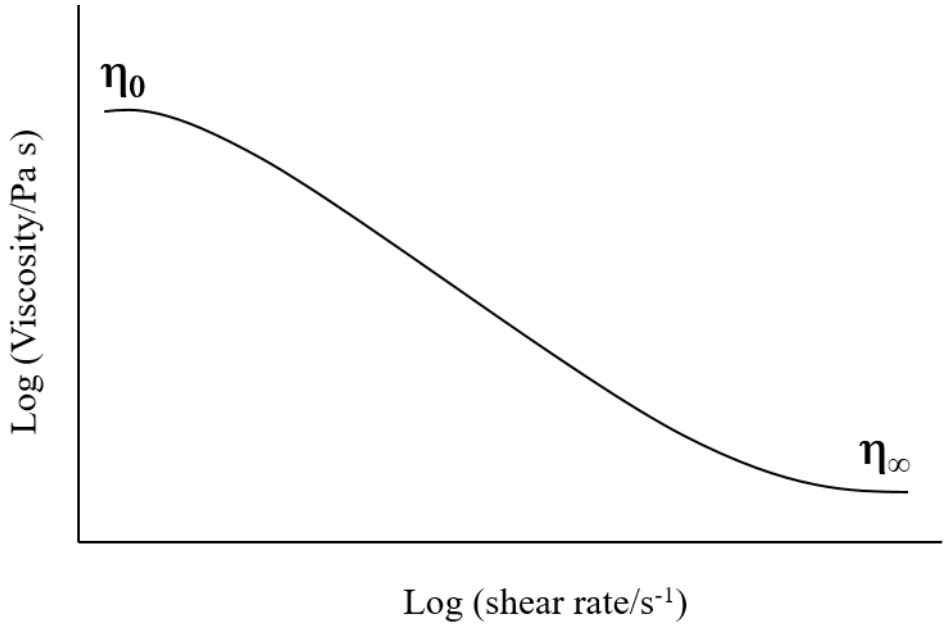

Figure 49 : An example of a shear thinning curve

When describing the curve in **Figure 49** a function must be found that satisfies multiple conditions:

1. When the shear rate is very small, the viscosity must be constant, η_0
2. When the shear rate is very large, the viscosity must be constant, η_∞
3. The viscosity must also change smoothly between these two points

These conditions, plus equations that predict the shape of the general flow curve (viscosity *vs.* shear rate), need at least four variable parameters.

The Cross model

$$(K\dot{\gamma})^m = \frac{\eta_0 - \eta}{\eta - \eta_\infty} \qquad \text{Equation 13}$$

where: η_0 and η_∞ are the viscosities at very high and low shear rates

K is a constant parameter with dimensions of time

m is a dimensionless constant

However, when $\eta << \eta_0$ and $\eta >> \eta_\infty$ the cross model reduces to:

$$\eta(\dot{\gamma}) = K_2\,\dot{\gamma}^{n-1} \qquad \text{Equation 14}$$

This is the power law model (Equation 14), where n = power law index and K_2 is the 'consistency' with units Pa s^n. The power law model can be used to describe a xanthan solution.

4.2.4 Rheological measurements

4.2.4.1 Creep Experiments

A constant shear stress is applied to the sample over a defined length of time and then removed. The shear strain is recorded as a function of time. The shear stress used should cause deformation in the sample but it should not destroy any internal structure within the sample.[11] An example of a creep and recovery curve is shown in Figure 50, the first stage of the graph shows the up curve where the stress is applied to material and the sample is deformed which increases the compliance, in the second stage of the graph, stress is removed and the relaxation of the material is measured.

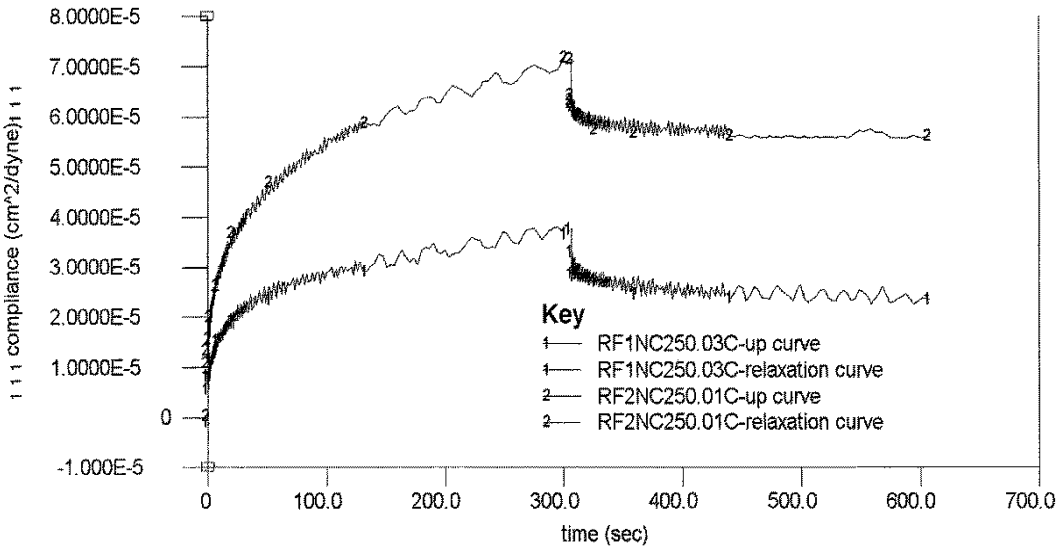

Figure 50 : Example of creep and recovery curve of example solder pastes[12]

4.2.4.2 Oscillation experiments

The elastic properties of materials such as xanthan gum[13] and starch solutions can be measured. Oscillatory measurements (Figure 51) can be used to obtain data on the deformation behaviour of fluids at very low strains and hence on their rest structure. A sinusoidal stress is applied to the fluid and the resulting sinusoidal strain is measured.[8] When an elastic material is measured the response will be in phase with the applied stress. For a viscous material the response will be 90° out of phase.

If linear viscoelasticity applies, the response of the target fluid under the oscillation can be divided into a viscous and an elastic component. The principle of the technique is to measure the phase lag, and the amplitudes of the stimulus are response signals and use[8] them to calculate the magnitudes of the viscous and elastic components.

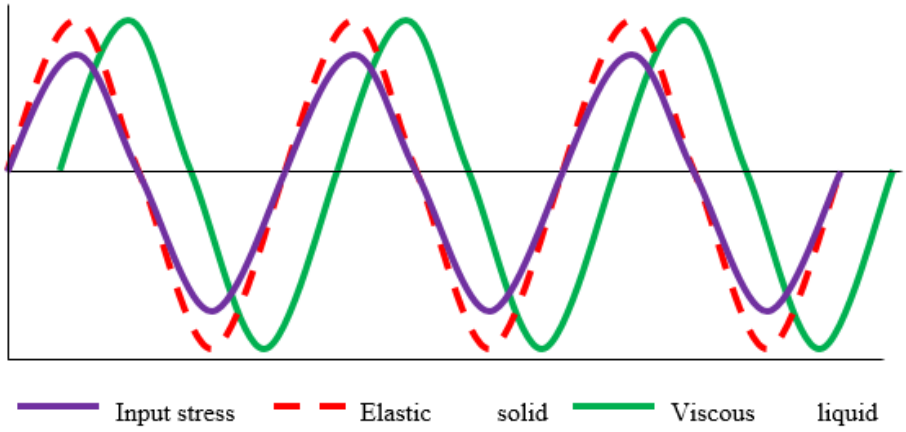

Figure 51 : Example oscillatory measurement signals

The elastic modulus or storage modulus G' is defined as:

$$G' = \sigma_0 \cos(\delta) / \gamma_0 \qquad \text{Equation 15}$$

Where σ_0 = amplitude

δ = phase lag

The viscous modulus or loss modulus G'' is defined as:

$$G'' = \sigma_0 \sin(\delta) / \gamma_0 \qquad \text{Equation 16}$$

Most rheometers can measure the phase difference between the input and output signals. When measuring over a range of shear rates, shear stresses or time, a number of other parameters can be calculated.[8]

1. Shear modulus

$$G = \sigma^2 / N_1 \qquad \text{Equation 17}$$

Where $N_1 = \frac{2 \times force\ separating\ plates}{cross\ sectional\ area}$

σ = shear stress

2. Relaxation time – real fluids have a spectrum of relaxation times, and the magnitude of λ_M (relaxation time) based on the Maxwell model, can be regarded as a minimum value.

$$\lambda_M = \frac{viscosity}{shear\ modulus} \qquad \text{Equation 18}$$

3. Recoverable shear strain (γ_1) – when a viscoelastic fluid is sheared, part of the deformation is lost through frictional viscous flow and the part due to elastic forces is recoverable.

$$\gamma_1 = N_1/\sigma \qquad \text{Equation 19}$$

4.2.4.3 Flow experiments

Flow curves are usually measured at a constant temperature; the temperature must be regulated within the rheometer as heat is produced during measurement due to shear heating.[14] Flow curves (Figure 52) measure the changes in the shear stress as the shear rate is increased; this gives the information regarding flow properties and can be used to identify the fluid type.[15]

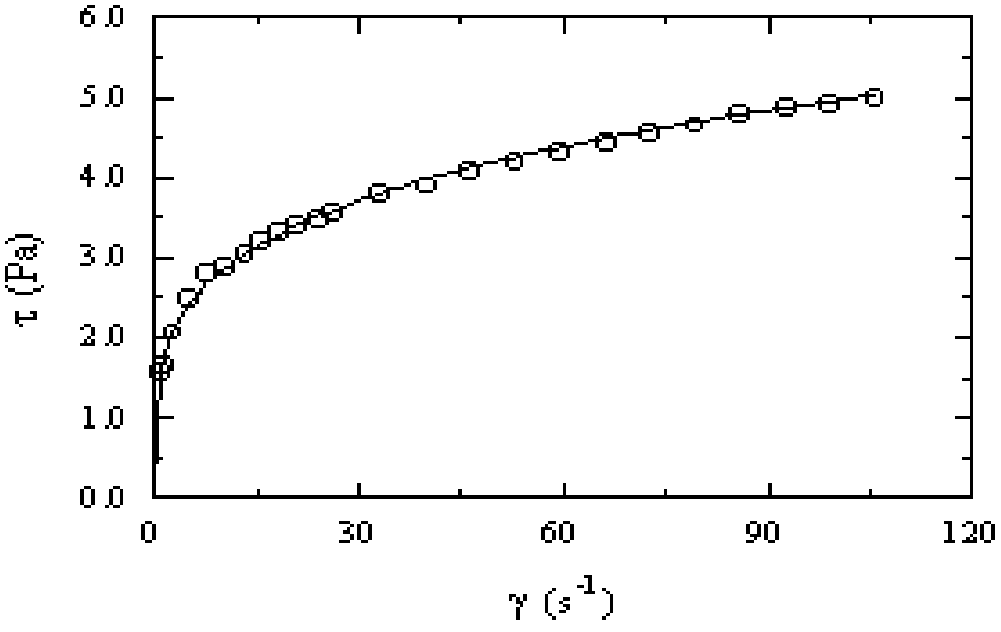

Figure 52 : Example of flow curve for xanthan 0.4 %[16]

4.2.5 On-line acoustic monitoring

On-line sensors must be capable of rapid and precise measurements and ideally be non-destructive and non-invasive. They must also be robust and be able to withstand changes in temperatures and pressures. For the monitoring of food production, a pulse of ultrasound is generated by the transducer and this then travels through the pipe and is reflected back to the transducer by the back wall of the pipe. The ultrasonic velocity and attenuation coefficient of food are determined by measuring the time-of-flight and amplitude of the received echo.[2]

Ultrafiltration (UF) has been generally recognised as one of the most effective methods for the concentration and separation of bio products and is used in the pharmaceutical and food industries. Funke *et al.* (2010) showed that the permeate flux has a minimum at pH 4.5-5 during UF of hydrochloric acid casein whey. Also investigated was the effect of pH and ionic environment on the UP of protein solutions. They observed that flux varied with pH; in the presence of salts, the flux at pH 5 was substantially increased, whereas at pH 2 and 10, it was substantially lowered. In addition to the decline in flux, the retention of protein generally increases with time. The development of a non-destructive technique to detect the absorption and build-up of the protein layer on a membrane surface in real time and under realistic operation conditions is of considerable interest. An ultrasonic technique was developed to monitor the deposition and growth of the protein layers at varying pH values. Both the attenuation and the velocity provide useful quantitative information about the properties of deposited protein layers, such as density and thickness. [17, 18]

The ability of ultrasonic spectroscopy to determine the particle size distribution of colloidal suspensions has been demonstrated; the technique can characterise colloidal suspensions which are concentrated and optically opaque. On-line determination of particle size distributions of colloidal suspensions during processing is a very important technique. The technique could be used to monitor the efficiency of a processing operation in real time, which could lead to a major improvement in the manufacture of many colloid based materials. One problem to overcome when monitoring colloidal suspensions is the presence of small gas bubbles which can

obscure the signal from colloidal particles because of their ability to strongly scatter ultrasound.[19]

Ultrasound Doppler techniques can be used to measure streaming velocities in biological fluids as well as in water. Ultrasound has the advantage that it can be used in non-transparent fluids and is a relatively inexpensive technique.[20]

Bamberger at al[21] produced an ultrasound probe that could determine the fluid density and solids concentration in food processing by measuring reflections at the fluid sensor interface, and the velocity and attenuation of the signal. This probe was non-invasive and self-calibrating as acoustic impedance is unaffected by changes in the pulser voltage. These ultrasonic measurements were found to be robust for determining the fluid density and particulate concentrations in the liquid foodstuffs.

Henning *et al.* (1999) designed an acoustic sensor that can be used in industrial processes, which can characterise liquid mixtures, for uses such as monitoring of waste water treatment processes, determination of concentration relations in beer, and measurements of fat and solid non-fat concentration in the dairy industry.[22] If the liquid's composition is known, then it is possible to determine the properties of the material. The sensor system has good accuracy in density measurements.

Banchet *et al.*(1999) have used pitch-catch acoustic measurements to determine the non-linear parameter (B/A) in alkanols.[23] A model determined by Germain *et al.* (1989) was used to determine the parameter using the transmission coefficients, acoustic absorption coefficients and frequencies of the measured solutions.[24] This method was found to be in agreement with other values of B/A in the literature.

Ultrasonic reflectance spectroscopy was used by Kulmyrzaev *et al.* (2000) to detect changes in the bubble characteristics in aerated foods. These bubbles are distributed in the liquid or solid matrices e.g. bread and whipped cream.[25] Ultrasound has been shown to be able to determine the size and concentration of the air bubbles in very dilute systems. Kulmyrzaev *et al.* (2006) measured the ultrasonic velocity and attenuation of the bubbly liquid and the bubble properties were determined using an appropriate theory. Good agreement between the theoretical calculations and the

experimental calculations were found. Where a concentrated suspension is used, adjustments will have to be made as the system complexity increases. Even with these limitations, it may be that ultrasonic measurements are a useful on-line measurement system for aerated food samples.[26]

Ultrasound measurements can also be used to measure blood velocity non-invasively and can diagnose blood vessel disease.[27] It was found that ultrasound can be used to characterise the blood flow but also to detect disease induced changes in the flow of the blood.

Sayan *et al.* (2002) illustrated the effect of particle size and suspension density on the ultrasonic velocity.[28] Changes in the solid concentration and particle size were made to model solutions e.g. NaCl and the ultrasonic velocity was measured using an immersion sensor. A relationship between the particle concentration and ultrasound velocity was found e.g. increasing the particle concentration from 0-80 g caused an increase in velocity of 2.5%.

Ultrasound is used for a variety of food analysis such as ascertaining, the crispiness of biscuits, where the ultrasound was used in pitch catch mode and the ultrasound signal was sent across the biscuit. A correlation between the elastic modulus and the ultrasonic velocity was found.[29] Ultrasound can also be used to determine the quality of meat by measuring the velocity of the ultrasound signal through live animals or carcasses. Lean meat has a significantly different velocity than fat and this allows the determination of the quality.[30] Ultrasonic velocity can also be used to determine the shell thickness of eggs and also the differences between the egg yolk and white which can be used for quality control.[31] For fruits and vegetables, there is a difficulty as there are air spaces in the fruit which exhibit resonant behaviour at various ultrasound frequencies. Therefore, many fruits and vegetables have very large attenuation coefficients and their ultrasonic velocities are lower than air e.g. banana. This high attenuation at frequencies used normally for ultrasound monitoring has been overcome by using higher ultrasonic intensities, lower frequencies or slicing the fruit. However, these solutions cause problems as the high intensities may damage the fruit, lower frequencies may be less accurate and slicing the fruit destroys the sample.[32]

4.2.6 Process control rheometery and on-line measurement of rheology in biotechnology processes

Process control is an important factor in many industrial processes. The advantage of using rheology for process control is that there can be considerable savings in time and effort. A control system can be introduced to alter the process when the viscosity reaches an unacceptable level. A good on-line viscometer will measure a representative sample of the process so it must be taken at an appropriate point in the process and the sample must pass continually through a responsive viscometer at a reasonable speed. The results from both off-line and on-line measurements should be relatable.[33] On-line viscometers make the same measurements as off-line viscometers; these include measurements of drag on rotating geometries or stationary objects in the flow, the speed of falling/pulled objects and the pressure-drop or flow-rate down conduits or through orifices. The energy absorbed by vibrating elements, spheres, rods and blades can also be measured.

Biotechnology processes are crucial to the pharmaceutical industry with biopharmaceuticals having a significant impact in the fight against some of the most distressing human diseases. The rheological properties within the fermentation broth can lead to better understanding of the process and thus allow better control. Process rheometers have been commercialized, but only with limited success. Disadvantages such as the low rate of data acquisition and difficulty of cleaning associated with these instruments have thus created widespread scepticism towards an in-line process rheometer, which therefore tend to be rather short lived on the market and are in many cases applicable to only a limited number of materials.

Kemblowski *et al.* (1990) measured the rheological properties of mycelial fermentation broths. During fermentation the biomass concentration and the morphology of the micro-organisms changes, which leads to changes in the rheological properties of the broth. The changes in the rheological properties of the fermentation broth influence the hydrodynamics of the bioreactor which can influence the mass and heat transfer. Mycelial fermentation broths are non-homogenous and contain settling particles which cause difficulties when measuring with traditional methods.[34] The

Metzner-Otto method determines the torque on the shaft of the impeller in the fermentation vessel. However, there are disadvantages associated with this method including a narrow range of laminar flow,[35] which is flow without turbulence, which may be overcome by using helical ribbon impellers.[36] Kemblowski *et al.* (1990) found that an on-line rheometer is a sensitive tool for monitoring fermentation processes and could also be used for control purposes.[34]

In filamentous micro-organism fermentations, the complex morphology of the micro-organisms causes variations in the viscosity of the broth. The morphology of the micro-organism is influenced by a variety of factors such as agitation speed and dissolved oxygen concentration so it is difficult to relate broth rheology to all aspects of morphology. At high microbial concentrations, the hyphae get tangled which results in a highly viscous suspension. These broths can be characterized by the shear rate dependent viscosities and by a yield stress. When there is a low biomass, the broth will often be Newtonian like. The power-law model can be used to describe the flow behaviour of the fungal fermentation *P. chrysogenum* broth. The impact of microbial growth on the broth rheology can be seen from a study of the dependence on the power-law parameters k and n on the biomass concentration, which tend to increase rapidly with biomass concentration.[37, 38]

Leduy *et al.* (1974) carried out a study on the rheological properties of a non-Newtonian fermentation broth using *Pullularia pullulans* which produces a polysaccharide. The rheology measurements were taken off-line and were able to demonstrate the change in the viscosity of the broth from Newtonian to pseudoplastic. *Xanthomonas* also produces a polysaccharide (2.2.1) which suggests that the rheological measurements from a *Xanthomonas* fermentation could also demonstrate the changes in Newtonian behaviour of the broth.[39]

On-line rheometery has been used in the polymer industry to monitor polymer processing; Covas *et al.* (2006) produced an on-line rotational rheometer that was used to measure multiple materials including silicon oil and polypropylene.[40] The rotational rheometer was a cone and plate design that allowed measurements to be taken at high temperatures (275 ^{o}C). Blends of polymers were analysed and the on-line rheometer

was more accurate in determining the structural changes in the blend than the off-line system.

Rheology has also been used in the food industry. Food rheology is usually the measurement of the behaviour of liquid foodstuffs, although, recent developments in solid and liquid measurements have led to the development of new rheometers and on-line analysis. The rheometer designed by Salas-Bringas *et al.* (2007) has a complex geometry due to the shaft shape. Measurements were carried out on polybuthene-1 as a model solution.[41] Models were then developed using these measurements to determine the viscosity of the material using torque and rotational speed with average shear stress and mean shear rate. The accuracy of the prediction of a simple model was found to be ± 25 Pa s over a large range of viscosities. If a higher accuracy is required, then a more complex model would have to be designed.

4.3 Combination rheology and ultrasound

Some work has been carried out on the combination of rheology and ultrasound. An ultrasonic shear rheometer was used by Saluja *et al.* (2005) This work is based on the analysis of impedance of a quartz crystal which can vibrate at megahertz frequencies.[42] The ultrasonic shear rheometer has the advantage of measuring the viscoelastic properties of protein solutions at low frequencies, which when used with oscillatory rheometers can destroy the solution structure. The ultrasonic shear rheometer can also detect the difference in rheological solutions at two ionic strengths. This technique is non-destructive and requires micro-litre sample volumes. It can also be used to monitor the visco-elasticity of a solution including kinetic studies.

Wiklund *et al.* (2007) evaluated both the ultrasonic velocity profiling (UVP) and the in-line ultrasonic velocity profiling with pressure drop (UVP-PD) rheometery methods for non-invasive, rheological characterization of complex model and industrial suspensions with size distributions ranging from sub-microns up to several cm. Rheological properties were measured in-line and compared with off-line measurements using a conventional rheometer. For the off-line measurements, concentric cylinder geometries were used and measurements were taken over a range of temperatures and shear rates corresponding to the flow loop. Particles larger than 1

mm caused a problem and were removed before any measurements were taken due to the gap restriction.[43]

To validate the in-line UVP-PD method, the flow curves and rheological parameters determined by fitting to models such as the power law model were compared to the off-line measurements. Good agreement was found between the UVP-PD and off-line measurements, where the particle size was smaller than the shear gap in the concentric cylinder. Off-line rheometers were found to produce unrealistic results in comparison to UVP-PD when the particles larger than the shear gap were removed as this affected the rheological properties of the system.

Instantaneous velocity profiles and the rheological properties of systems with a wide range of particle sizes, distributions and shapes were obtained, more than had been previously stated in the literature. A maximum concentration of particles was found to be 30% w/w for UVP and UVP-PD measurements. The UVP-PD method offers a very efficient tool for process monitoring and quality control in industrial practice, as changes in rheology, both gradual and rapid, can be continuously monitored in-line.

When a comparison was carried out between UVP and conventional rheological measurements on simple Newtonian model fluids and highly concentrated, opaque, non-Newtonian industrial fluids containing particles of different shapes and sizes ranging from μm to several cm, the results showed excellent agreement between the two methods. Only one solution caused problems as the particles within the solution were again too large to be used with the conventional rheometer. UVP allows real time, in-line rheometery based on simultaneous measurements of fluid velocity profiles. The measurements are rapid, non-destructive and non-invasive.[43]

4.3.1 Conclusions from rheology and acoustic literature

Acoustics have been used to monitor many different processes, the conditions in which the acoustic sensors can work would allow the monitoring of a fermentation. The use of ultrasonic spectroscopy has the potential to monitor these reactions, although, the air bubbles within the fermenter may cause difficulties.[19] This is discussed further in 1.3. However, the work carried out by Kulmyrzaev *et al.* (2000) could be adapted to monitor the changes in the fermentation broth.[25]

As ultrasound can be used with non-transparent fluids this will allow measurements to be taken during a *X. campestris* fermentation. This fermentation is progresses from a pale yellow broth to a very viscous bright yellow broth which has the consistency of custard.[20]

On-line process rheometery is challenging as cleaning the system and the low rate of data acquisition has led to scepticism. However, Kemblowski *et al.* (1992) were able to monitor a fermentation process and found that it has the potential for fermentation monitoring.[44] Leduy *et al.* (1974) were able to measure the changes in the rheological properties of a non-Newtonian fermentation broth which has the potential to be replicated for *Xanthomonas.*[39] The morphology of the fermentation broth will play a large part in the ability to monitor rheological changes, a *X. campestris* fermentation is a promising organism to monitor due to the viscosity of the broth during xanthan production. Some studies have combined rheology and ultrasound, these have used UVP and UVP-PD rheometery methods.[45] However, the Bioinnovel probe would combine the rheology and ultrasound through modelling.

4.3.2 Aims of acoustic monitoring and rheological measurements

The main aim of the acoustic and rheology work was to determine the ability of the novel probe in monitoring the fermentation process, including monitoring analyte consumption and the possibility to combine rheological measurements. To determine this the following smaller aims will be investigated:

1. System characterisation of the new probe to determine system parameters and understand the probe design

2. Analyse model solutions to identify changes in the velocity and attenuation coefficient

3. Analyse the rheological properties of xanthan gum to allow combination of techniques in the future

4.4 Experimental

4.4.1 Equipment set up

The prototype probe designed by Bioinnovel is composed of two Panametrics NDT (Waltham, MA, USA) 10 MHz pencil transducers held at a distance of 30 mm apart via a steel cylinder (Figure 53).

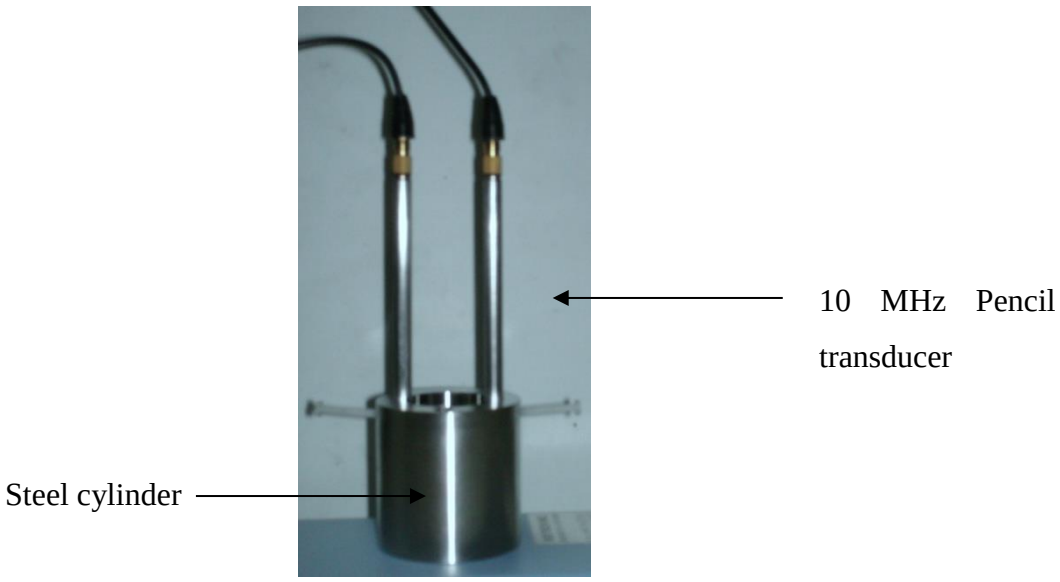

Figure 53 : Prototype probe designed by Bioinnovel

These pencil transducers are connected to a Panametrics NDT pulser/receiver model number 5077PR with or without (Figure 54) a Panametrics NDT preamplifier. An Agilent (Santa Clara, CA, USA) 54642A oscilloscope was used to capture all acoustic signals.

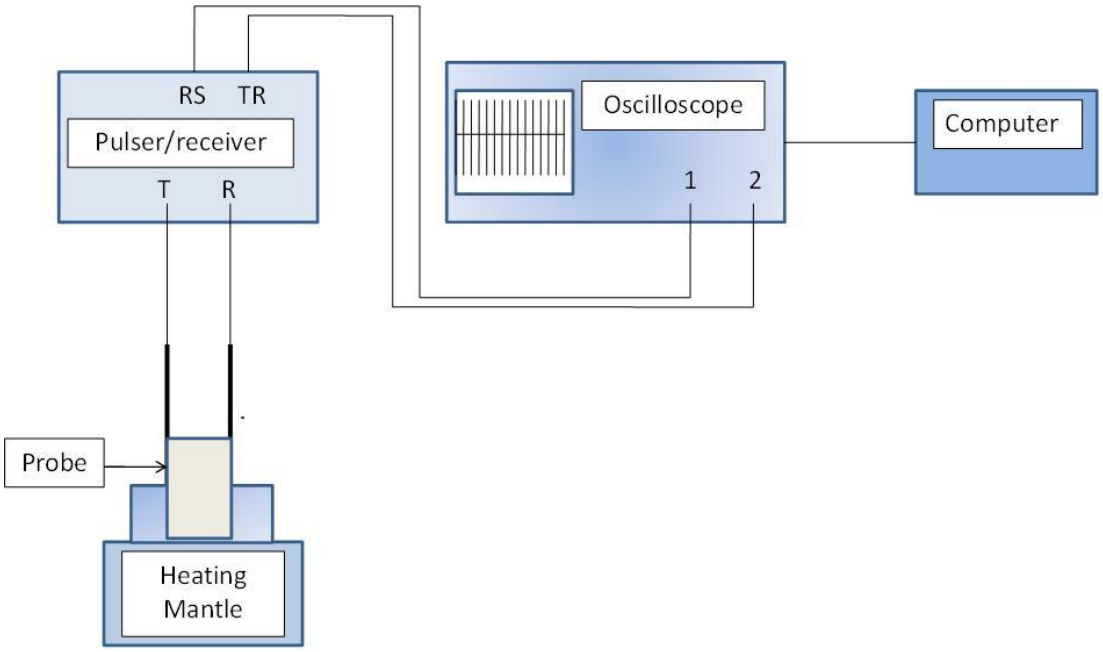

Figure 54 : Schematic of experimental set up with no preamplifier

T=transmit output, R= received pulse, TR= trigger pulse, RS=received signal

In Figure 54, one of the transducers is connected to the transmit (T) output on the pulser/receiver. The pulse is then sent across the sample and the second transducer receives the signal. The received pulse (R) is transferred to the pulser/ receiver and then connected to channel 1 on the oscilloscope via the received signal (RS) port on the pulser/ receiver. The trigger pulse (TR) is produced by the pulser/receiver and is connected to channel 2 on the oscilloscope. The signals are displayed on the oscilloscope screen and after data capture are transferred to the computer using a GPIB/USB interface. Due to the fragility of the probe especially the connections of the transducers to the ring, this probe was only deployed off-line with the sample being placed in a beaker on the heating mantle to maintain temperature.

4.4.2 Software

The computer was connected to the oscilloscope via an Agilent 82357A USB/GPIB interface. Signals were saved in binary format using Agilent Intulink software. The binary files were then read into Matlab R2007B for further analysis.

4.4.3 Signal analysis

The pulse repetition rate used throughout the experiments was 500 Hz, with a sampling rate of 50 MHz for measurement of the model solutions. This sample rate will allow accurate prediction of the peak minimum and maximum as the transducers used in these experiments are 10MHz so to meet the Nyquist sampling rate a sampling rate of at least 20MHz must be used.[46] Twenty-five signals are captured at once Time (s)

Figure 55); both the trigger (channel 2 on oscilloscope) and the received signal were collected (channel 1 on the oscilloscope).

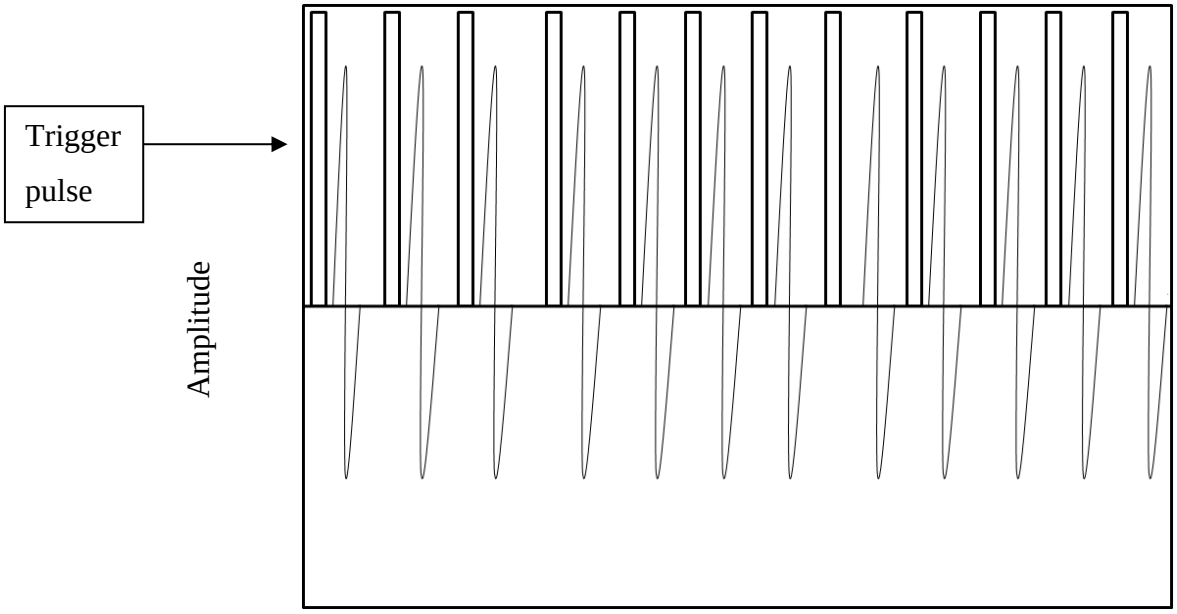

Figure 55 : Schematic of oscilloscope display

When a pulse is generated at the transmit transducer, a trigger pulse is generated simultaneously by the pulser/receiver. The receive transducer measures the ultrasound wave after propagation through the sample. The time between each trigger pulse and its associated receive signal can be used to determine the velocity of the ultrasound wave. The amplitude of the receive signal can be used to calculate the attenuation coefficient.

4.4.4 Velocity

4.4.4.1 Theoretical calculations

An example signal is shown in Figure 56 where the trigger pulse is shown in green and the sample signal in blue. The points at which the trigger pulse starts and at which the signal amplitude is at its most negative were identified. The difference between these points was identified and this was then multiplied by the sampling rate to convert points to time. This gave the time taken for the signal to travel across the sample, which was then used in Equation 20 to calculate the velocity.

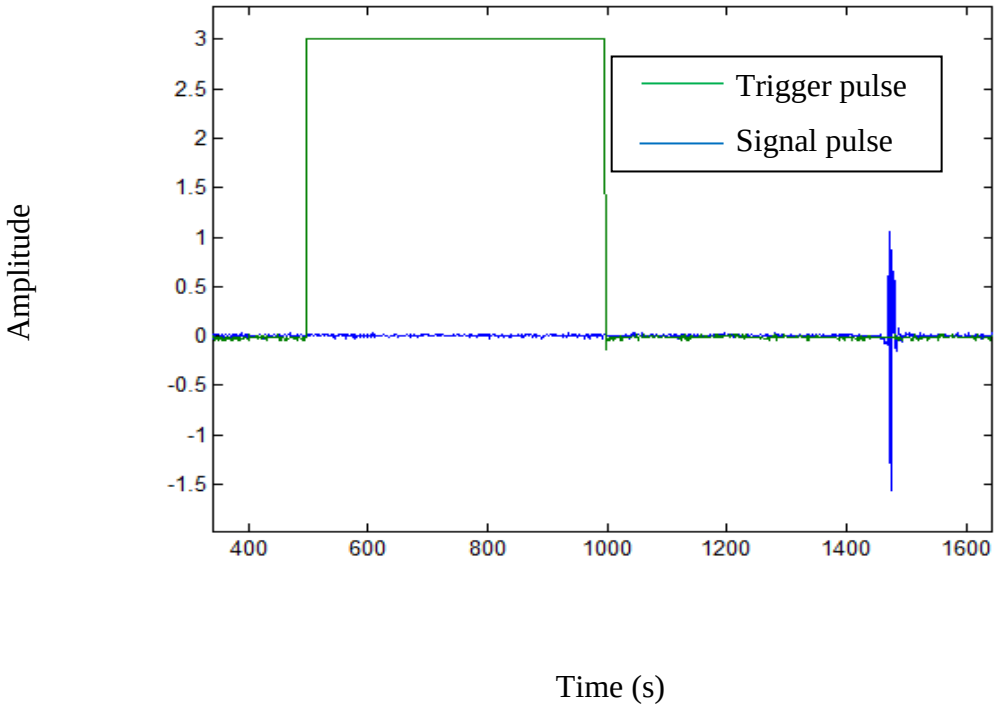

Figure 56 : One example signal for water

The velocity was calculated using Equation 20

$$c = d/t \qquad \text{Equation 20}$$

Where: c = velocity (ms^{-1})

d = distance between the transducers (m)

t = time for the signal to travel through the sample

The distance between the transducers was 30 mm. However, to account for small variations in the position of the transducers in the holder, a 25°C water sample was measured at the start of each experimental session and as the speed of sound in water at 25°C is reported in the literature as 1496 ms^{-1}, this was used to calculate the actual distance between the two transducers.[47]

4.4.4.2 Experimental calculations

For the calculation of velocity, the time at which the trigger pulse started was determined, as was the time at which the minimum peak amplitude occurred for the sample signal. These were then used to calculate the velocity along with the distance between the transducers which was determined experimentally using a water sample.

For example, a water sample was measured and the following data was obtained:

Trigger pulse (points)	Sample peak minimum (points)	Difference between start of trigger pulse and peak minimum (points)	Difference between start of trigger pulse and peak minimum (s)
50962	49995	967	1.93E-05

The known velocity of water at 25 °C is 1496 ms^{-1} and rearranging Equation 20 allows calculation of the path length:

$$d = v \times t \qquad \text{Equation 21}$$

Therefore:

d = 1496 x 1.93x10-5

= 0.0289m

The distance was calculated for all 25 water signals obtained in one measurement and the measurement was repeated three times. The average distance was determined from the 75 signals.

4.4.5 Attenuation coefficient

4.4.5.1 Theoretical calculations

The attenuation coefficient for the sample relative to water was calculated using the peak to peak voltage of the water and sample signals. An example signal is shown in Figure 57; the time of the signal has no effect on the attenuation so the trigger pulse was not required for the calculation and therefore the time values on the x axis are from when the first pulse is received.

$$\alpha = 20 \log_{10}\left(\frac{A_w}{A_s}\right) \qquad \text{Equation 22}$$

Where: α = attenuation coefficient (dB)

A_w = amplitude of the water signal (peak to peak voltage (V))

A_s = amplitude of sample signal (peak to peak voltage (V))

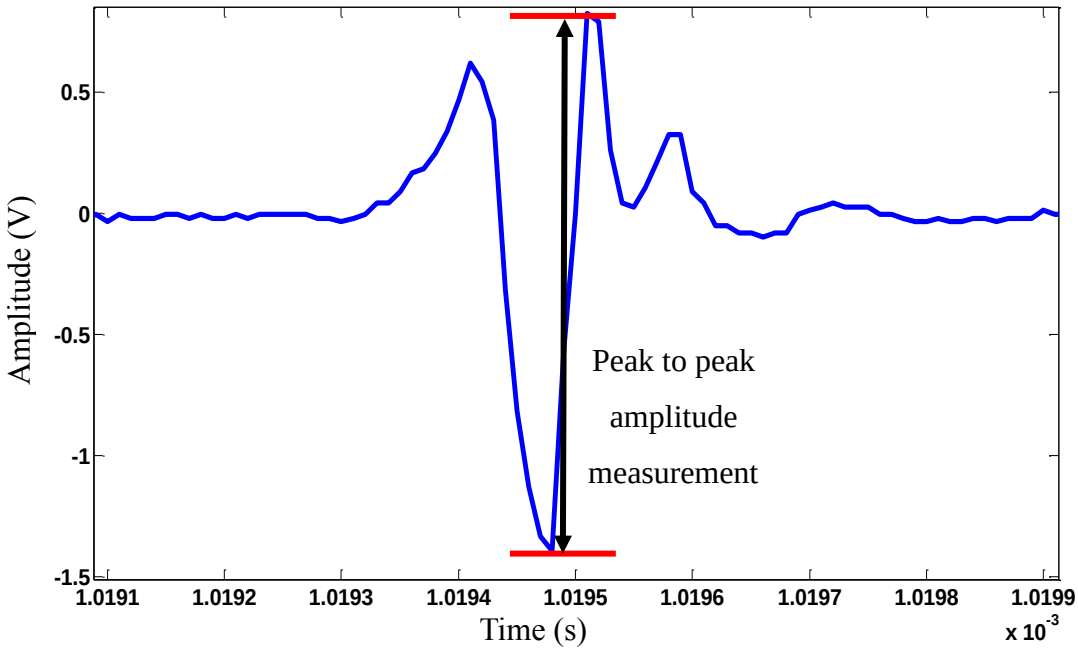

Figure 57 : Peak to peak measurement of signal

4.4.5.2 Experimental calculations

For the attenuation calculations, the maximum and minimum peak amplitudes for the sample signal were determined to calculate the peak to peak voltage. The peak to peak difference was subsequently calculated for each of the twenty-five signals captured in one measurement and three repeat measurements were conducted. The peak to peak voltage for the water signal acquired prior to that of the sample was also calculated. The attenuation coefficient was determined using Equation 22. The attenuation coefficients, from peak to peak voltages of the water (A_w) and the sample (A_s) can be calculated from:

1. The amplitude of each sample signal is compared to the amplitude of each water signal i.e. 75 sample signals are compared to 75 water signals.

2. The amplitude of each sample signal is compared to the average water signal of each repeat i.e. 25 sample signals compared to 1 average from the corresponding repeat of water.

3. The amplitude of each sample signal is compared to the average water signal of all three repeats i.e. 75 sample signals are compared to 1 water value.

4. The average of the twenty-five sample signals in one repeat compared to the average of the water signal of each repeat i.e. 3 sample values are compared to 3 water values.

5. The average of all twenty-five sample signals in one repeat compared to the average water signal of all three repeats i.e. 3 sample values are compared to 1 water value.

For calculation of the attenuation coefficient for the model solutions method 2 was used.

4.4.6 System characterization

For characterisation of the acoustic system, the experimental parameters (unless otherwise stated) in Table 18 were used.

Table 18 : Parameters for system characterisation

Sample	Distilled water
Temperature of sample	25 ^{o}C
Pulse repetition frequency	500 Hz
Pulser voltage	100 V
Transducer frequency	10 MHz
Gain	20 dB
High pass filter	Out
Low pass filter	Full
Sample rate	100MHz

The high pass filter (HPF) allows either the complete bandwidth of the instrument (1 kHz to 35 MHz) to be used (out setting) or will filter above (1 MHz). The low pass filter will allow either the complete band width to be displayed or a 10 MHz cut off frequency. For characterisation of the system, the low pass filter was set to allow the complete bandwidth through. Within the time domain, the system was characterised by optimising the gain, voltage and the filter combination. Within the frequency domain the frequency content of the pulse generated by the pulser/receiver was determined alongside the effect of temperature on the signal.

To determine the repeatability of the system, five measurements of distilled water were taken with the probe in place. This provides an estimate of the measurement variability. Five repeat measurements of distilled water were also made but the probe was removed and replaced. This provides an estimate of the additional variation associated with the removal and replacement of the probe. Within the system repeatability study, there are three types of variation associated with the repeatability of the system:

1. Short term variation within the twenty-five signals in each repeat

2. Longer term variation within the five repeats

3. Probe removal variation which is the variation associated with the removal and replacement of the probe between measurements.

4.4.7 Analysis of model solutions

4.4.7.1 Sample preparation

Model solutions of xanthan, agar, glycerol and starch in distilled water were prepared for analysis. The range of concentrations for glycerol, agar and starch was from 1-5 % wt./v. The concentrations chosen to represent concentrations that may be found in a fermentation where possible. However, due to the viscous properties of the solution, for xanthan, the concentration range was 0.1 – 2% wt./v.

Table 19 : Sample preparation

Sample	Weight of sample (g)	Volume of water (ml)	Concentration of solution (% wt./v)
Glycerol (Sigma, St Louis, MO, USA))	0.4991	50	1.00
	1.1124	50	2.22
	1.5287	50	3.06
	2.0167	50	4.03
	2.5255	50	5.05
Starch from Potato (Sigma, St Lois, MO, USA)	0.4995	50	1.00
	0.9976	50	2.00
	1.4844	50	2.97
	1.9844	50	3.97
	2.4445	50	4.89
LB Agar [Lennox L Agar] (Sigma, St Louis, MO, USA)	1.0010	100	1.00
	1.9950	100	2.00
	3.0112	100	3.01
	4.0068	100	4.01
	4.9942	100	4.99

Xanthan Gum (Sigma, St Louis, MO, USA)	0.1153	100	0.12
	0.5027	100	0.50
	0.9999	100	1
	1.9933	100	1.99

4.4.7.2 Acoustic

Using the parameters identified as optimum during system characterisation, the model solutions (at 25 ºC) were analysed.

Table 20: Experimental parameters for model solutions

Sample	Distilled water
Temperature of sample	25 ºC
Pulse repetition frequency	500 Hz
Pulser voltage	100 V
Transducer frequency	10 MHz
Gain	30 dB
High pass filter	Out
Low pass filter	Full
Sample rate	50 MHz

Before any measurement was undertaken on a model solution, three water replicates were measured as a control to check that the system was working correctly and for use as a reference for the attenuation calculations. Water replicates were also taken between samples. The starch solutions required constant agitation with a magnetic stirrer as the starch did not dissolve in the distilled water.

4.4.8 Rheological measurements of xanthan model solutions

Three xanthan solutions were prepared with the concentrations of 0.1, 0.5 and 1% wt./vol for all rheological testing with the cone and plate rheometer. An AR-100 (New Castle, DE, USA) rheometer with a 4 cm parallel plate geometry was used for model solution testing.

For creep analysis the solution was heated to 25 ^{o}C in the conditioning step. The sample then had a stress applied of 1 Pa for a maximum of time of 20 minutes. The stress was then removed and so the shear stress was 0 Pa.

Flow measurements were carried out with the shear rate being increased from 0.2-2000 s^{-1} for ten minutes and then reduced from 2000 – 0.2 s^{-1}; the temperature was again held at 25^{o}C. A frequency sweep step was carried out with the angular frequency being decreased from 500 to 0.05 rad s^{-1}. The solution was given 1 minute to equilibrate at each step. A second frequency sweep step was carried out with the angular frequency being increased from, 0.05 to 500 rad s^{-1} with the same equilibration time.

4.5 Results

4.5.1 System Characterisation

When the system was characterised, the gain of the transmit signal was varied from 1 to 59 dB with the pre-amplifier connected, the signals were saturated. When the signals are saturated, the intensity information will be lost and so these do not accurately represent the material being measured. A signal should have the shape as described in Figure 57.

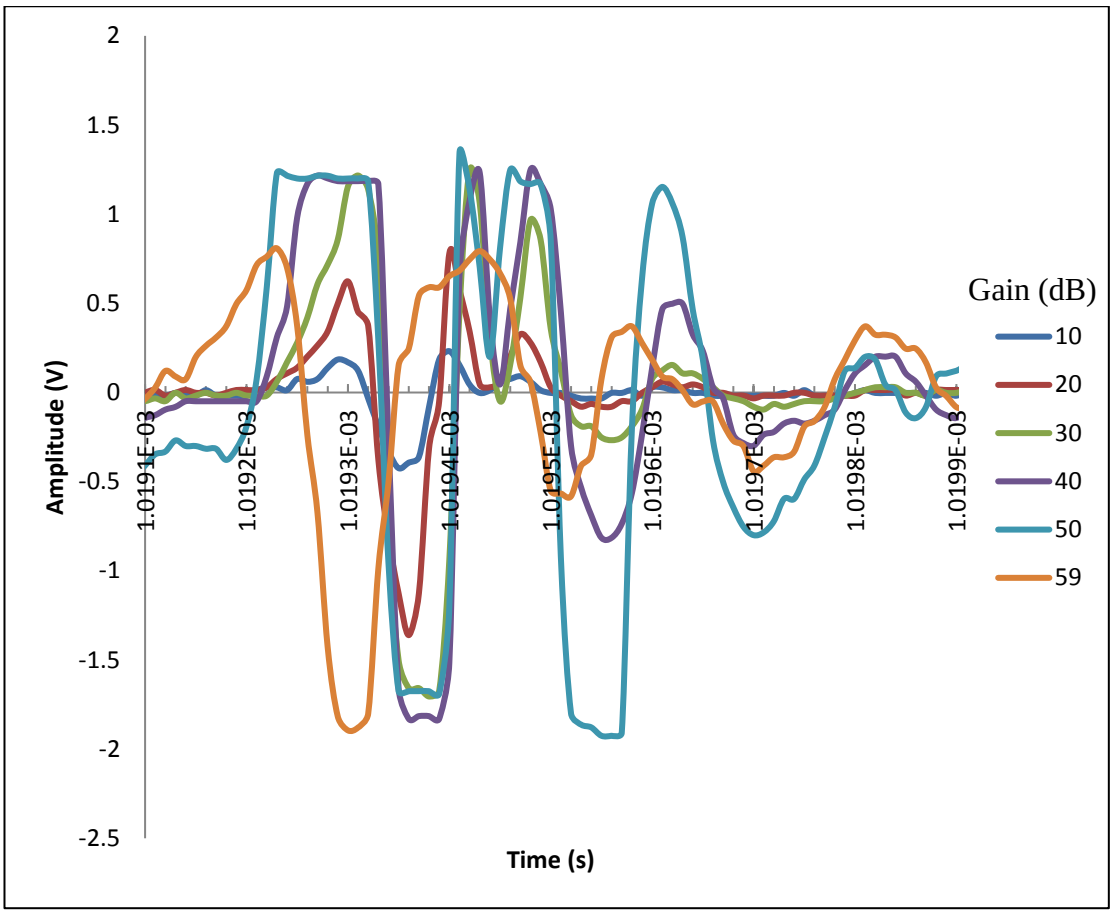

Figure 58 : Variation in gain without pre-amplification

When the gain of the transmit signal was varied (without the pre-amplifier), the amplitude was saturated above 30 dB (Figure 58). When comparing the signals obtained for water with a gain of 10, 20 and 30 dB, the signal obtained with a gain of 20 dB produces the best shape of signal and so this gain was used for the analysis of the model solutions. The voltage analysis led to the selection of 100 V as the higher voltages caused the signal to become saturated. When certain combinations of filters are used, the signal becomes unclear and so the out and full filters were used.

The transmit frequency was varied between 3 and 10 MHz and the FFT of the received signals were calculated. There is a peak at 5 MHz irrespective of the transmit frequency. For the lower frequencies there is also a peak at approximately 12.5 MHz. As the transducers are designed to operate at 10 MHz, this suggests that the pulses generated by the pulser/receiver contain a significant portion of the signal at 5 MHz.

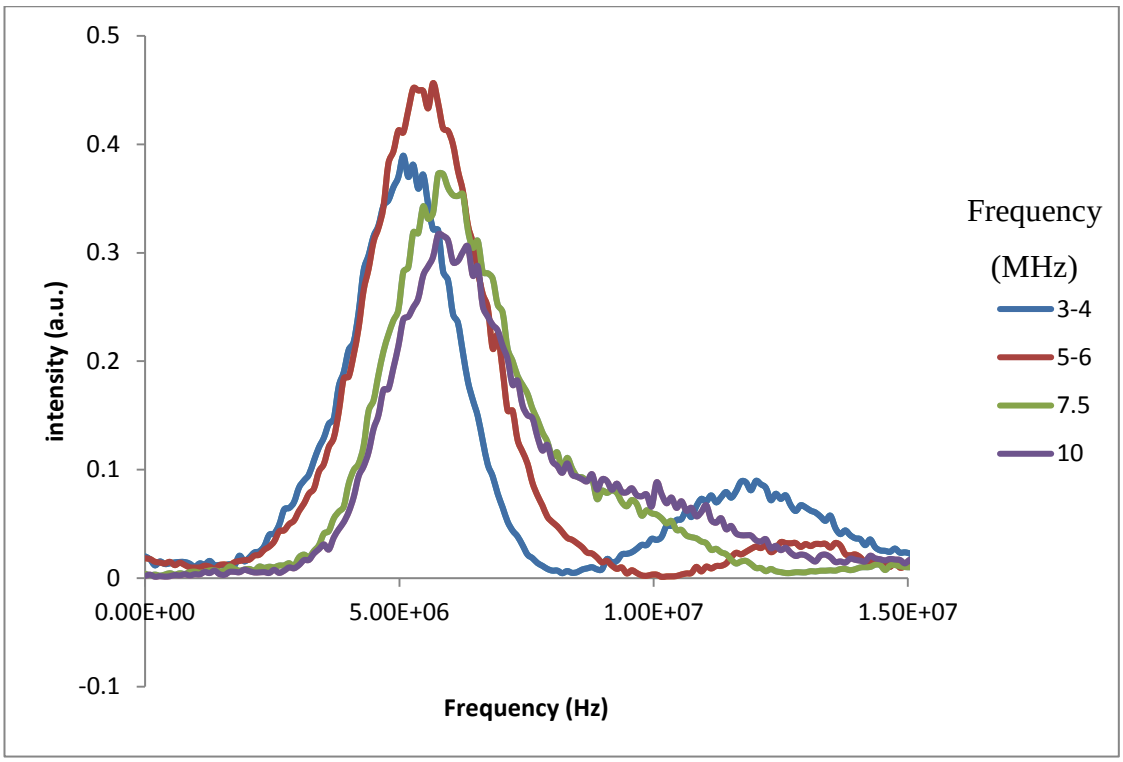

Figure 59 : Frequency content analysis

From the repeatability study, it can be seen that the there is little variation in the amplitude of the signal or the velocity of the signal between when the probe is removed and replaced, or kept in place. The peak to peak voltages and velocities are shown in Table 21; the RSD values are small for both the peak to peak voltage and velocity of the in place and removed samples. The difference in variation between the two sets of measurements is also small, with no statistical difference at 95% confidence level - this means that the error associated with the removal and replacement of the probe is insignificant.

Table 21 : Comparison of peak to peak voltages and velocities with and without removal of probe

	Peak to peak voltage (V)	std. Dev. (V)	RSD (%)	Velocity (m/s)	std. Dev (m/s)	RSD (%)
In place	2.896	0.018	0.618	1542.386	1.593	0.103
Removed	2.925	0.026	0.884	1545.619	2.827	0.183

The temperature at which microorganisms grow optimally varies between organism and strain. When water at various temperatures is analysed, the amplitude of the signal

is not affected by the change in temperature. However, there is an effect on velocity. When the temperature was varied between 25 and 43°C (Table 22), it can be seen that the velocity of the signal increases as the temperature increases, which is in agreement with the literature. Smith *et al.* (1954) also found the same effect of temperature on velocity measurements in water.[48] The variation of temperature on the velocity is due to the thermodynamic properties of the water and its isothermal compressibility.

From the relative standard deviation (RSD) values (Table 22) it can be seen that there is little variation over the 25 signals at each temperature.

Table 22 : Velocity at various temperatures

Temperature (°C)	25	26	27	33	35	37	39	43
Velocity (ms^{-1})	1496.3	1494.4	1499.8	1512.0	1514.4	1517.0	1526.5	1531.2
Std. deviation (ms^{-1})	0.62	0.76	0.78	1.11	0.97	0.78	3.51	3.06
RSD (%)	0.04	0.05	0.05	0.07	0.06	0.05	0.23	0.20

From the system characterisation work it can be seen that working without the pre-amplifier produces an un-saturated signal and that the gain for the experiments should be set to 20 dB and a voltage of 100 V as again the signal becomes saturated. From the frequency study it can be seen that the pulses generated contain a significant portion of the signal at 5 MHz. There is no statistically significant effect of removing and replacing the probe from the sample or when between readings with the probe in-situ. As the velocity of the samples are affected by the change in temperature, all further experiments will take place on a heating mantle to maintain a temperature of 25 °C.

4.5.2 Model solutions analysis

Using the parameters identified in the system characterization, 4 fermentation analytes were analysed at various concentrations which mimic the concentrations in the

different phases of different microorganism fermentations.[49] Using the conditions as described in 4.4.7.

4.5.2.1 Glycerol

Example signals from the glycerol solutions are shown in Figure 60; as the concentration of the glycerol solution increases, the signal is detected earlier.

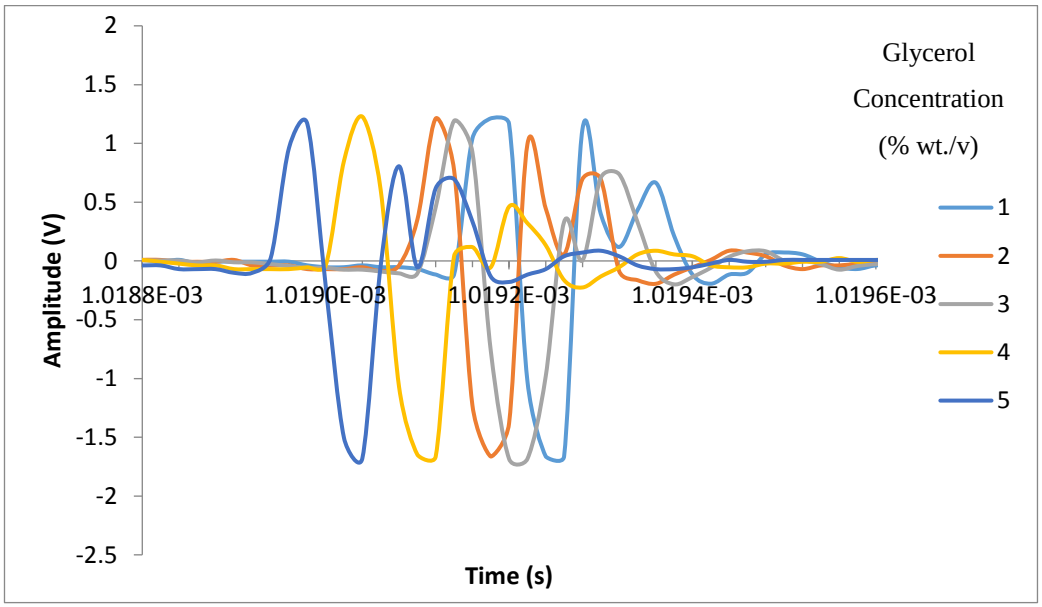

Figure 60 : Acoustic signals for 1-5% glycerol in water

In Figure 61, the velocity increases as the concentration increases. Gulseren *et al.* (2007) found the speed of sound in glycerol to be ~1500 ms^{-1} at these low concentrations.[50] This was at a lower temperature (20 ^{o}C) than that used experimentally. Gulseren *et al.* (2007) found that as the temperature increased, the velocity also increased, therefore the higher calculated values found experimentally in Figure 61 can be related to the higher temperature employed. When further measurements were taken on glycerol solutions with concentrations of up to 100%, this increase in velocity was seen with increasing concentration (Figure 62). For pure glycerol, the speed of sound is 1904 ms^{-1}; experimentally the velocity was calculated to be 1914 ms^{-1} with a standard deviation between the three repeats of 2.19 ms^{-1}. Calculation of the attenuation coefficients of the glycerol solutions was not carried out due to the higher concentration signals being saturated.

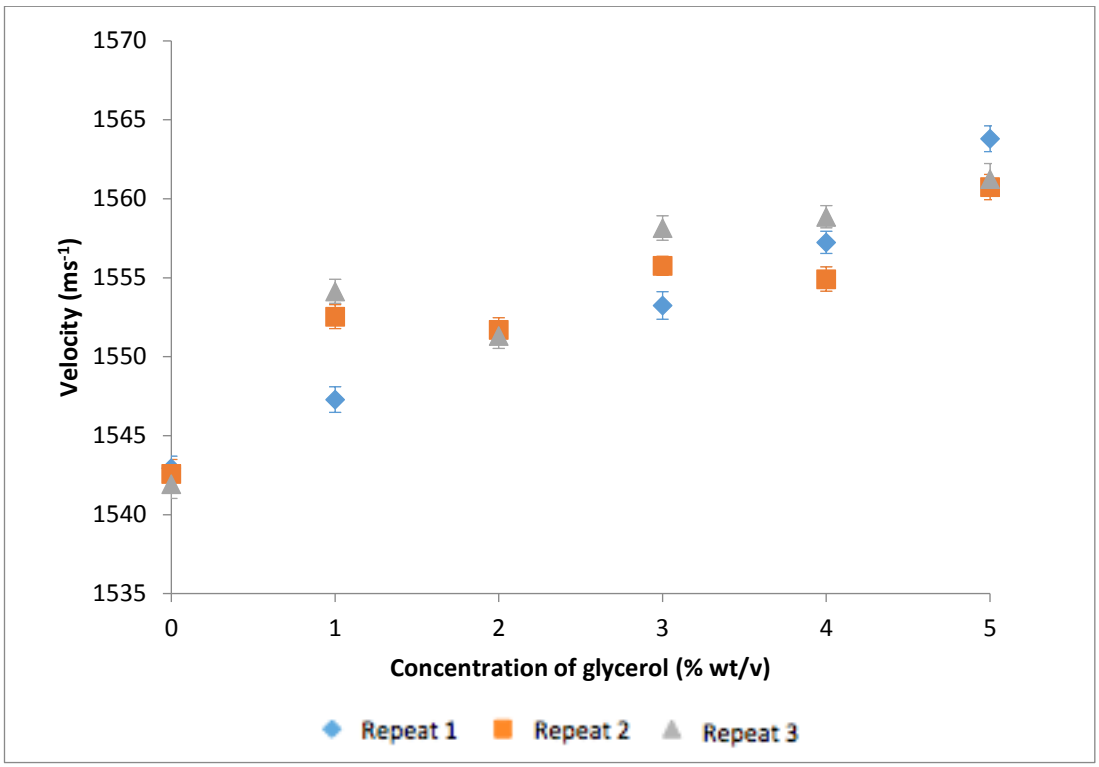

Figure 61 : Speed of sound in glycerol solutions (1-5 %) for 3 repeats and their associated standard deviations ± 1 (n=25)

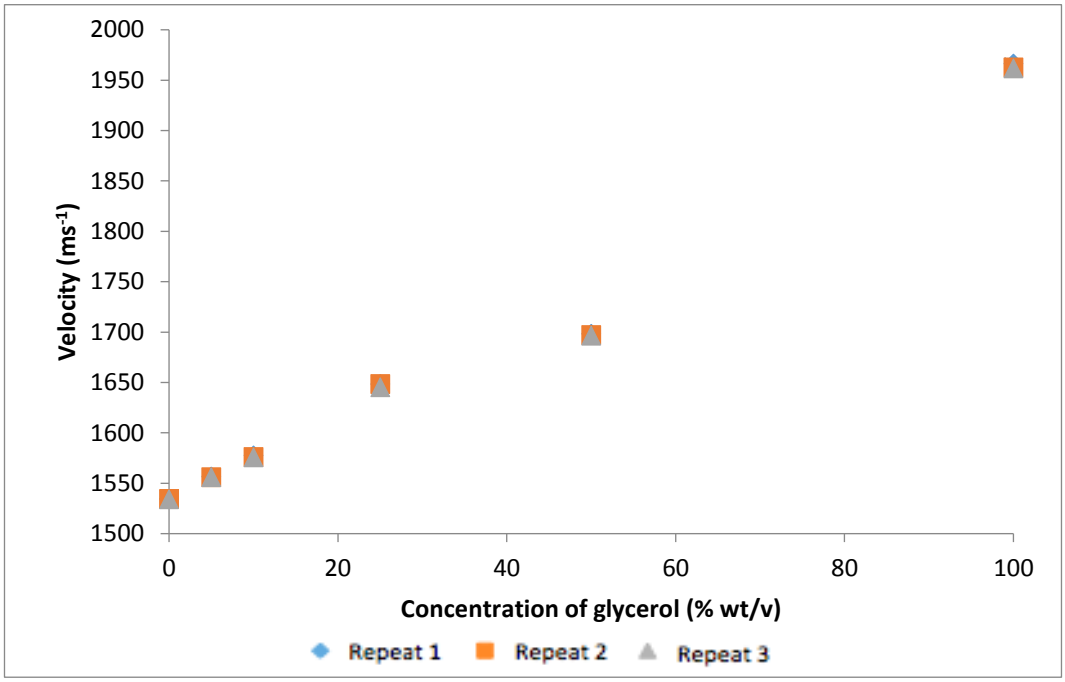

Figure 62 : Average velocity of glycerol in water at concentration ranges 5-100% - 3 repeats

4.5.2.2 Starch

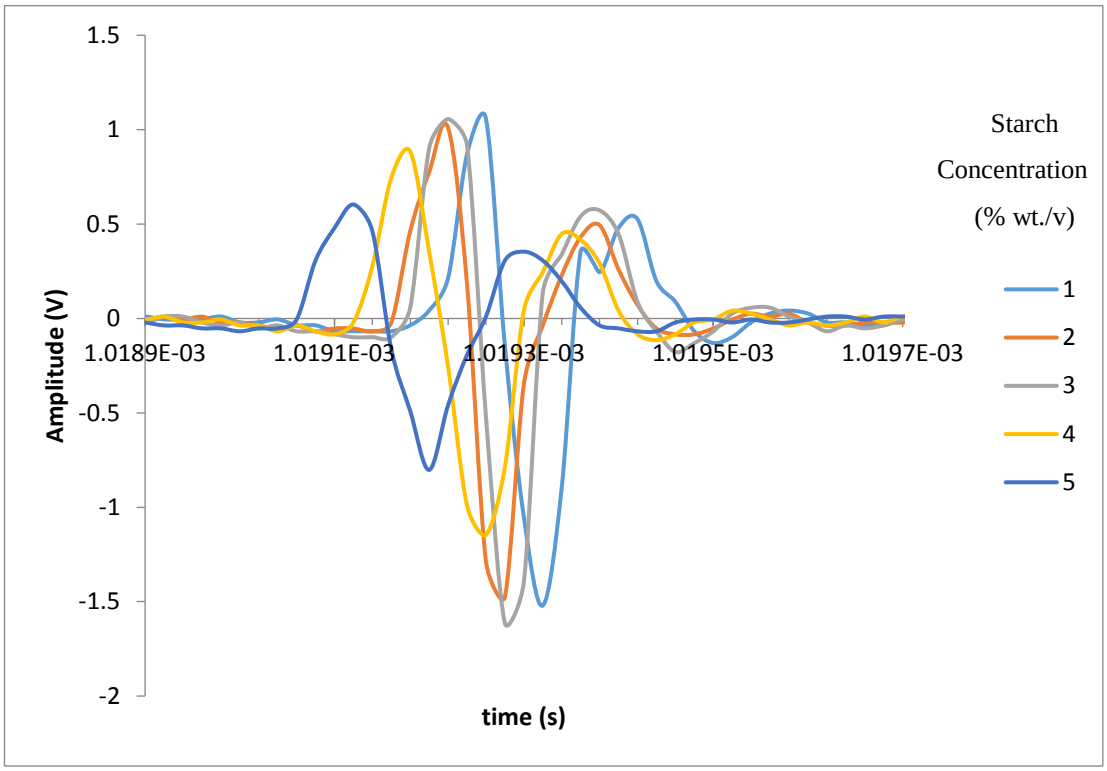

Figure 63 : Acoustic signals for 1-5% starch in water

The signals shown by the starch solutions (Figure 63) illustrate that both the velocity and the attenuation coefficient vary with concentration. The amplitude of the signals decrease as the concentration of starch increases and the time for the signal to be measured also decreases as the concentration increases.

The velocities calculated for the starch solutions show a decrease at low concentrations and then an increase as the concentration increases, the increase is not as clear as with the glycerol solutions with greater ranges of velocities seen at each concentration. The variation within the velocity is shown in Table 23. This could be due to variation in the level of agitation which was necessary to suspend the starch particles in water. There will also be a greater variation in the velocity as there will be scattering of the ultrasound by the particles which will vary the propagation distances.

Table 23 : Average of three repeats Starch velocity measurements and their associated standard deviations

Concentration (% wt./v)	Velocity (ms^{-1})	Std dev. (ms^{-1})	RSD (%)
1	1545.85	2.43	0.16
2	1544.19	0.38	0.02
3	1543.99	0.49	0.032
4	147.84	2.57	0.17
5	149.46	0.80	0.05

In Figure 64, the ratio of average velocity of the solution to velocity of water is plotted against the concentration of the starch solution - the result is a parabola which is in agreement with the findings of Urick.[51] Urick (1947) found that there is a parabolic relationship between the ratio of the sample velocity and water to the concentration of the solution, where particles are present (particle size of 0.4 and 5μm). The reason for this change is that as an ultrasonic wave is propagated through the solution, the variation of the solids changes the density and compressibility of the solution, which will change the velocity and attenuation of the acoustic signal.

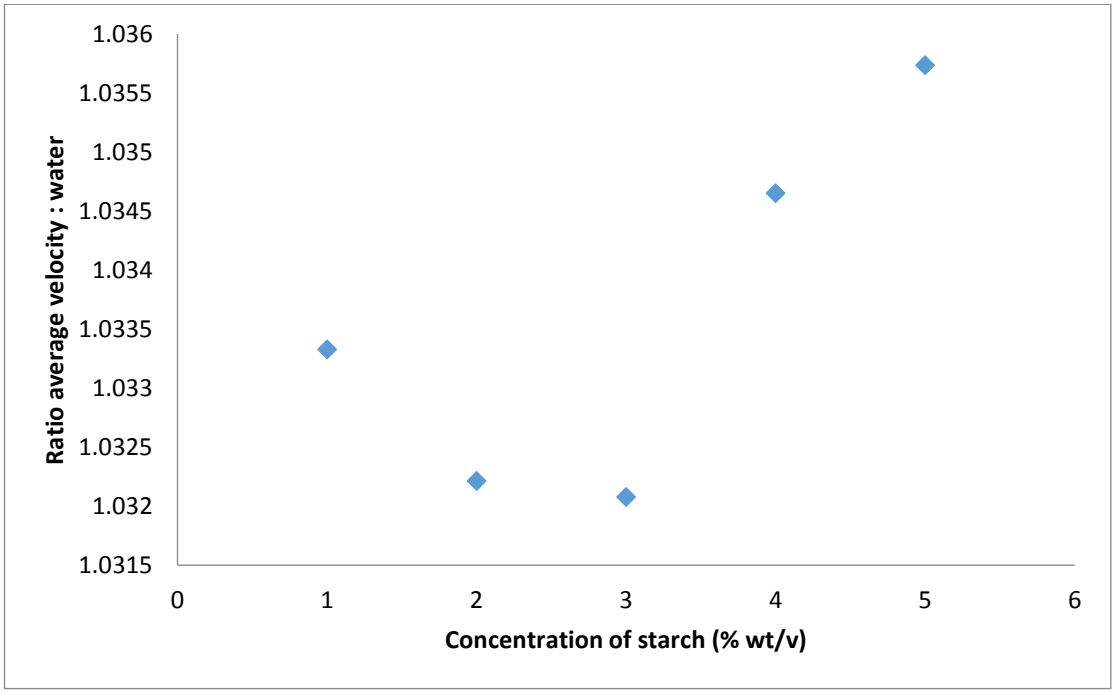

Figure 64 : Ratio of average velocity of starch/water against concentration

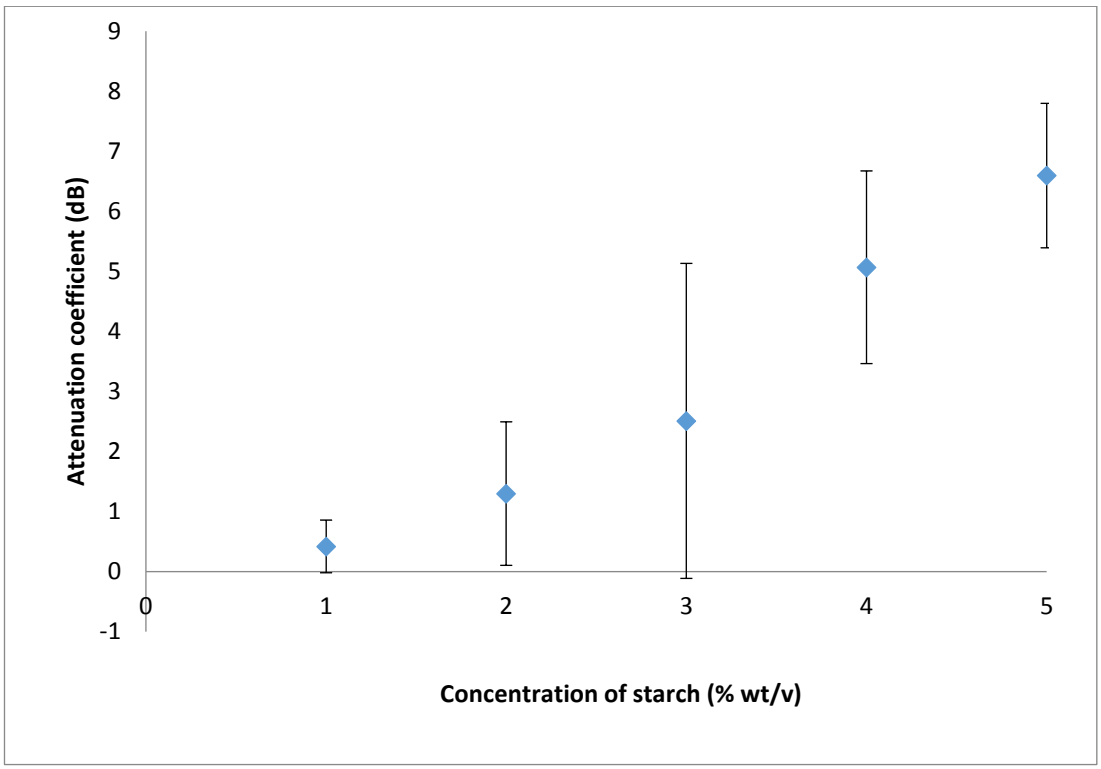

Figure 65 : Average of 3 repeats attenuation coefficient relative to water for starch solutions and their associated std dev ±1 (n=3)

In Figure 65, the attenuation coefficients for the starch solutions are shown including the std deviation associated with these measurements. The attenuation coefficients of the starch solutions show an increase as the concentration increases. This is due to the particles within the solution which scatter the wave in a different direction to the incident wave. As the concentration is increased the number of particles in the solution increases and so the wave is scattered more. However, the error associated with these measurements is high and further experiments would have to be carried out to try to reduce the error. The agitation of the starch particles contribute to the variation between the results as the number of particles in between the transducers will vary for each reading. In the literature, Koltsova *et al*, (2010) reported the attenuation coefficient of a 1 % starch solution to be 0.1 dB at 3 MHz, which is close to the calculated value in the experiments when taking into consideration the differences in experimental set up including the frequency of the signal.[52]

4.5.2.3 LB Agar

The amplitude of the signals from the LB agar liquid model suspensions does not appear to be affected by the change in concentration. However, the concentration increase appears to have an effect on the speed of the signal.

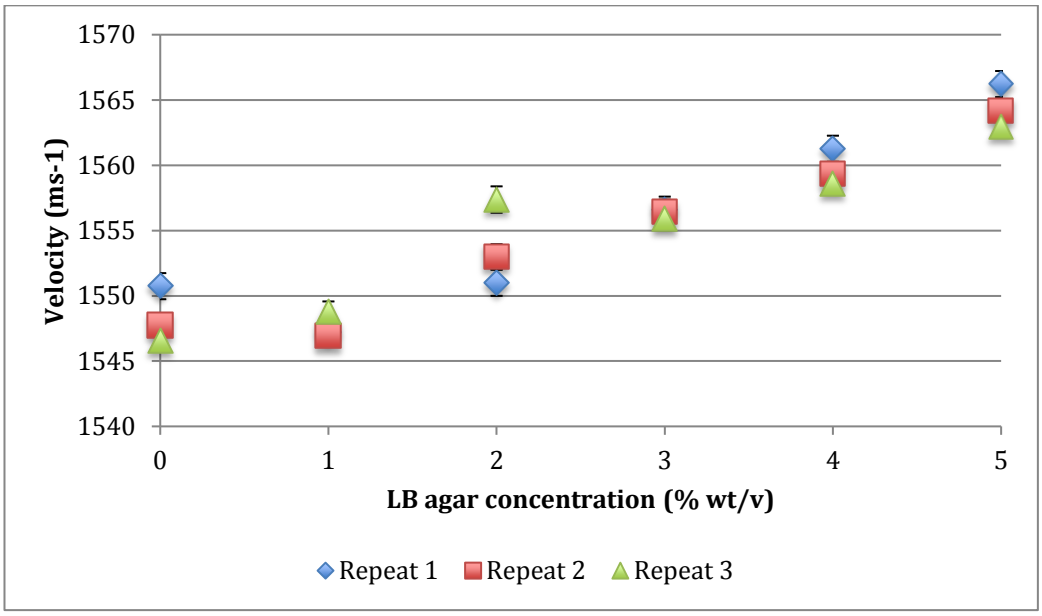

Figure 66 : Velocity at various concentrations of agar - 3 repeats and their associated standard deviation ±1 (n=25)

The speed of sound in the agar suspensions increases as the concentration increases. A 2% suspension has a velocity of approx. 1554 ms^{-1} with a standard deviation of 3.26 ms^{-1}. This is slightly higher than the value reported in the literature of 1540 $ms^{-1;}$ this may be due to the literature value using a 2% solution pressed into a disk rather than as a suspension.[65, 53] Again, this change in velocity can be related to Equation 23.

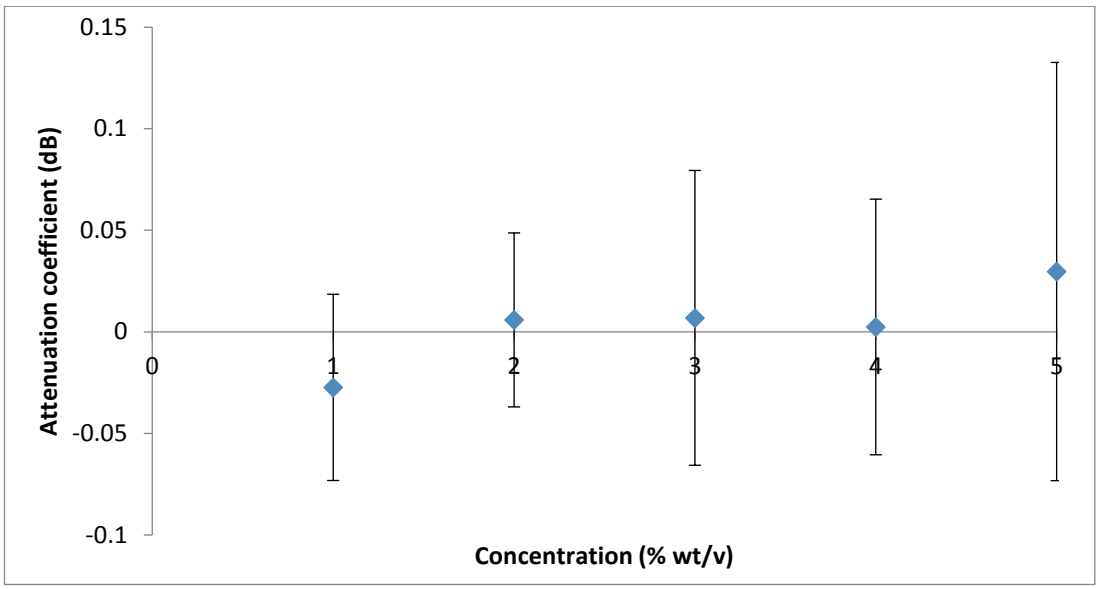

Figure 67 : Average attenuation coefficients relative to water for agar at all concentrations for 3 repeats and their associated std dev ±1 (n=3)

The errors associated with the attenuation coefficients are high with large relative standard deviation between the repeats in comparison to the peak to peak values as shown in Table 24. At higher concentrations the attenuation coefficients may be affected, however in fermentation systems the concentration of agar is low ~2-3% during the inoculum growth.[54, 55, 54]

Table 24 : Agar attenuation coefficients - comparison of standard deviations

Concentration (% wt./v)	Attenuation coefficient (dB)	Std dev (dB)	RSD (%)	Peak to peak voltage (V)	Std Dev (V)	RSD (%)
1	-0.027	0.046	-170.37	2.894	0.027	0.93
2	0.006	0.043	716.67	2.860	0.030	1.04
3	0.007	0.073	1042.85	2.859	0.027	0.94
4	0.002	0.063	3150	2.860	0.022	0.77
5	0.030	0.102	340	2.840	0.011	0.39

4.5.2.4 Xanthan

Xanthan model solutions were investigated by both acoustic monitoring like the other model solutions but these solutions were also investigated rheologically. This was done to allow a combination of the infrared monitoring discussed in Chapter 3 to allow real time monitoring of a *X. campestris* fermentation by a combination of multiple techniques

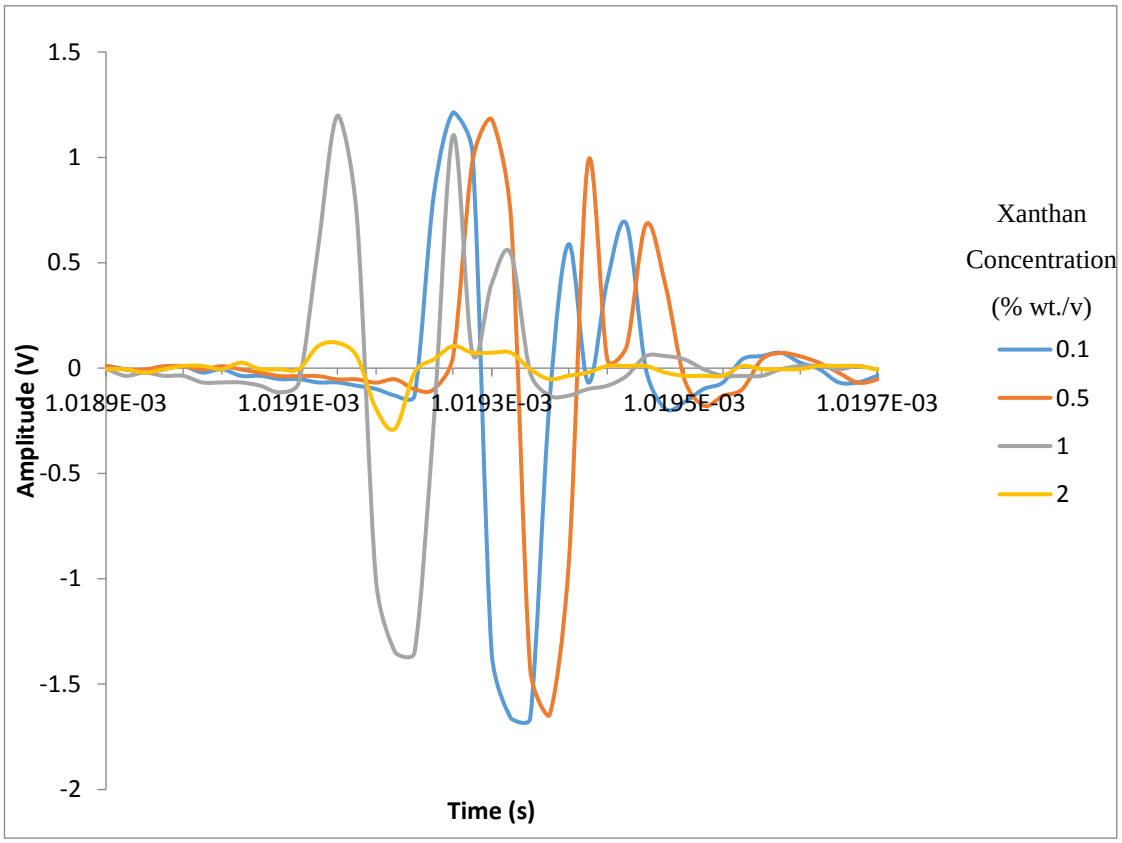

Figure 68 : Acoustic signals for 0.1, 0.5, 1 and 2 % xanthan in water

Example signals from xanthan solutions are shown in Figure 68. As the concentration of the xanthan solution changes, both the amplitude of the signal and the time of signal detection change. From the signals observed, the amplitude of the 2 % solution is significantly reduced.

Table 25 : Comparison of attenuation and peak to peak voltages and their standard deviation for xanthan solutions

Concentration (% wt./v)	Attenuation coefficient (dB)	Std dev	RSD (%)	Peak to peak voltage (V)	Std dev	RSD (%)
0.1	0.026	0.030	116.470	2.831	0.004	0.142
0.5	0.043	0.020	46.292	2.830	0.004	0.135
1	0.037	0.029	77.419	2.828	0.016	0.550
2	1.274	1.781	11.532	0.291	0.081	27.890

In Figure 69, the average attenuation coefficient of the three repeats of the xanthan solutions are displayed. The attenuation coefficient of the 2% solution is 1.274 dB, while the attenuation coefficient of the 1% solution is 0.037 dB. The errors associated with the values are high due to the small value of the attenuation coefficient. A 2% wt./v solution of xanthan was found by Rahalkar *et al.* (1986) to have an attenuation coefficient of 175 dB m^{-1} at 5 MHz; the difference in attenuation coefficient could be due to the difference in frequency in which the measurements were taken, or a potential problem with the setup of the probe.[56]

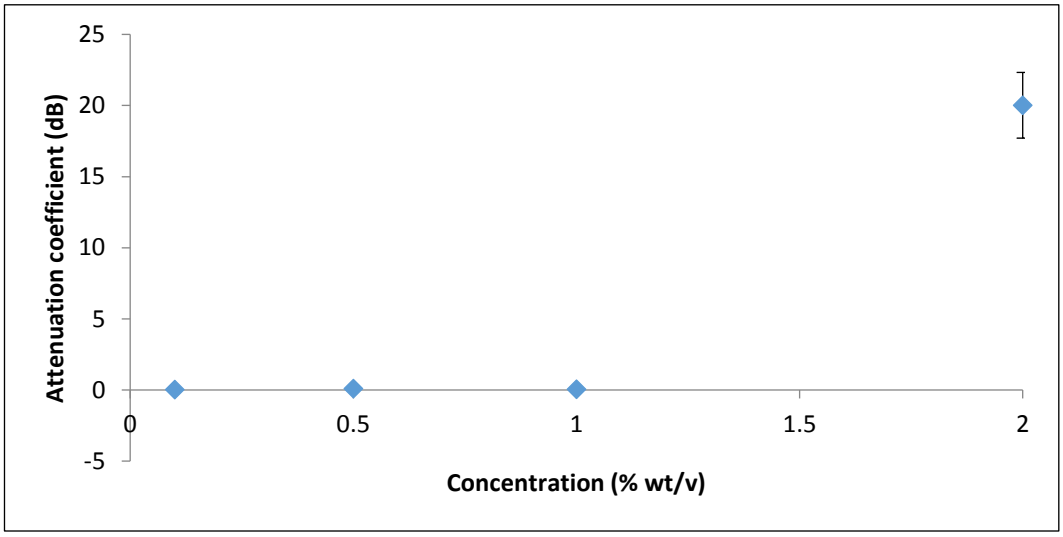

Figure 69 : Average attenuation coefficients relative to water for xanthan repeats, the error bars denote ± 1std dev. (n=3)

The error associated with the attenuation coefficients are large due to the peak to peak voltages of the water and sample being very close. When the amplitudes are divided, the result is close to one - when this is inserted into the calculation, the log value is close to zero at these low values as can be seen in Figure 70; when there is a small variation in the value there is a large change in the log value.

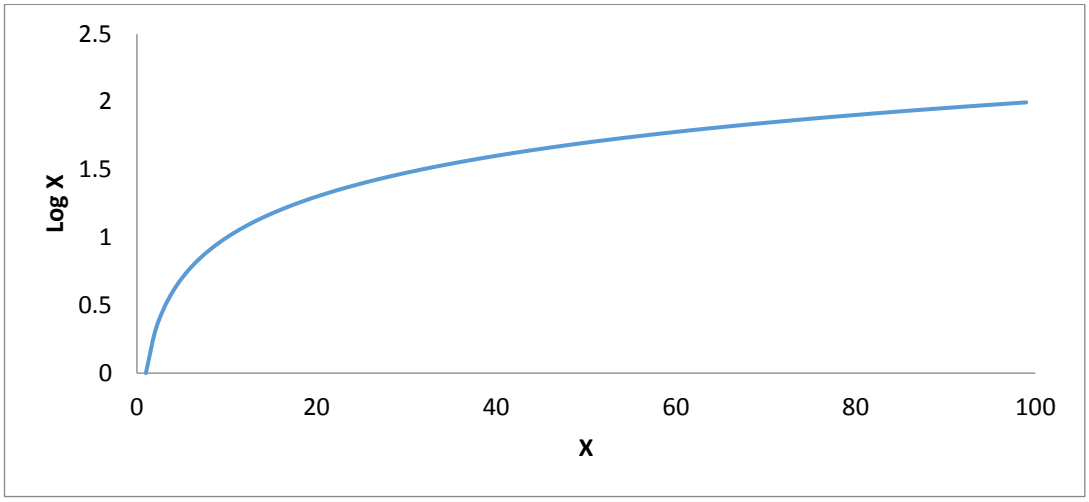

Figure 70 : Log graph

In Figure 71, the velocity increases as the concentration increases, except at 0.5%; this may be due to the solution being analysed on a separate day from the other xanthan solutions or an error occurring during preparation. Pakzad *et al.* (2008) found the speed of sound in xanthan gum to be 1564 ms^{-1}.[57] The highest velocity found experimentally was 1549 ms^{-1} with a standard deviation between the three repeats of 1.37 ms^{-1}. Although the concentration is not stated in the literature, the values found experimentally and those in the literature are close, which may suggest that the concentration of the solution measured in the literature is higher as the temperature at which the literature value is measured is lower (22 ^{o}C). The velocity at which an ultrasonic wave propagates through a material for low attenuating materials can be calculated using Equation 23.

$$\frac{1}{c^2} = \frac{\rho}{E} \qquad \text{Equation 23}$$

Where c = velocity

ρ = density

E = modulus (in this case the bulk modulus)

As found by Dhiaa, the density of a xanthan solution increases with the increase in concentration and so this affects the velocity according to Equation 23.[58]

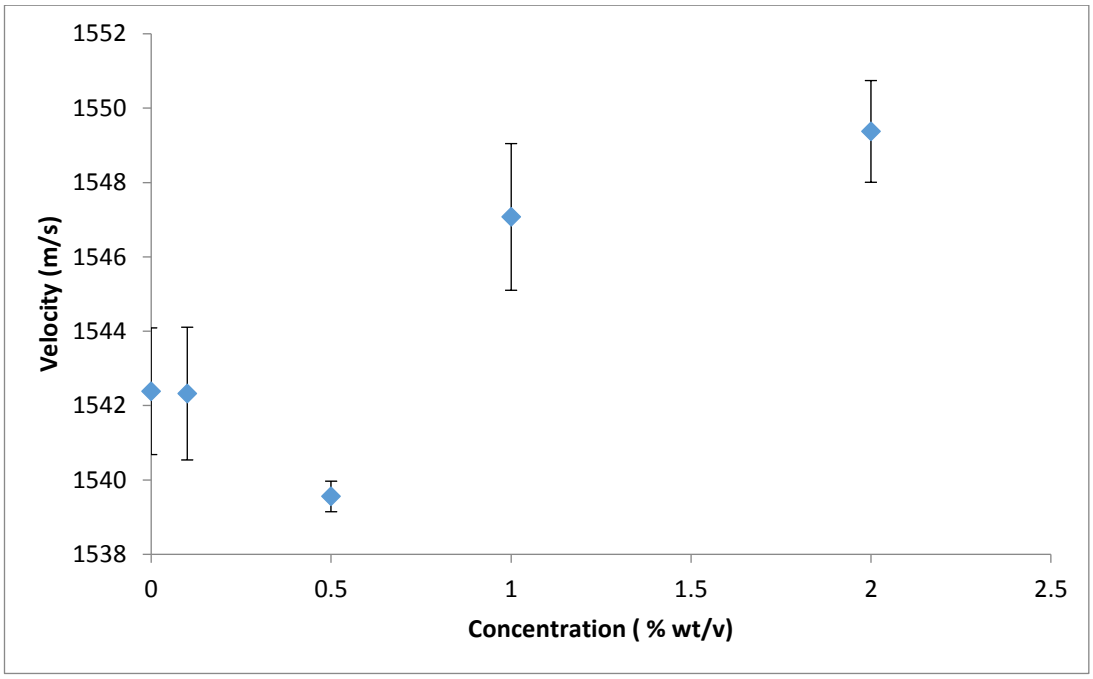

Figure 71 : 0.1, 0.5, 1 and 2 % xanthan solution velocity measurements average of three repeats and their associated standard deviation ± 1 (n=3)

The error associated with the velocity calculation is obtained from the difference in points between the start of the trigger pulse and peak minimum of the sample signal; were calculated, the variation was usually plus or minus one point. This error relates to the digitisation of the signal and so the error associated with the time for the ultrasound to travel from the transmit to the receive transducer can be decreased by increasing the sample rate. This will decrease the time between consecutive points leading to a more accurate determination of velocity.

The analysis of the analytes found that the attenuation co-efficient measurements were unreliable across the 4 analytes, the signals became saturated at high glucose concentrations, there are large errors associated with the LB agar measurements and the 2% xanthan solution has a very large error associated. The attenuation measurements of the starch solutions look more promising with the increase in starch particles in the solution causing changes in the attenuation. However, again large errors are associated with these changes which could be caused by the agitation of the sample and so a consistent sample is not being measured every time. The velocity measurements hold more promise with all 4 analytes showing changes in their velocity as the concentration increases with the results of the experiments closely matching those already in the literature. [50, 52, 57, 53] These results could be carried forward to future experiments where fermentation samples could also be measured using the probe and then the system model in a similar way to 3.7.2.2. In the future the probe could be adapted to be placed inside the fermenter which would allow real time monitoring of the fermentation process. As well as modelling the analyte concentrations, the probe could also be used in conjunction with off-line rheology measurements to provide information on the viscosity of a fermentation which would give insight into the progress of the fermentation.

4.5.3 Rheological measurements

Figure 72 illustrates the flow measurements taken of the xanthan solutions; the increase in shear stress as the shear rate is increased. There are two points on the graph that are outliers from the expected curve - these could be caused by air bubbles within the sample or undissolved particles of xanthan; these would affect the shear stress on the sample. These two points also appear on the viscosity plot (Figure 73), which shows the viscosity decreasing as the shear rate increases. This is a property attributed to pseudoplastic materials, which Zataz *et al.* (1984) found xanthan solutions at low concentrations to display.[59] The 0.5% and 1% solution also follow this pattern and exhibit pseudo plastic behaviour.

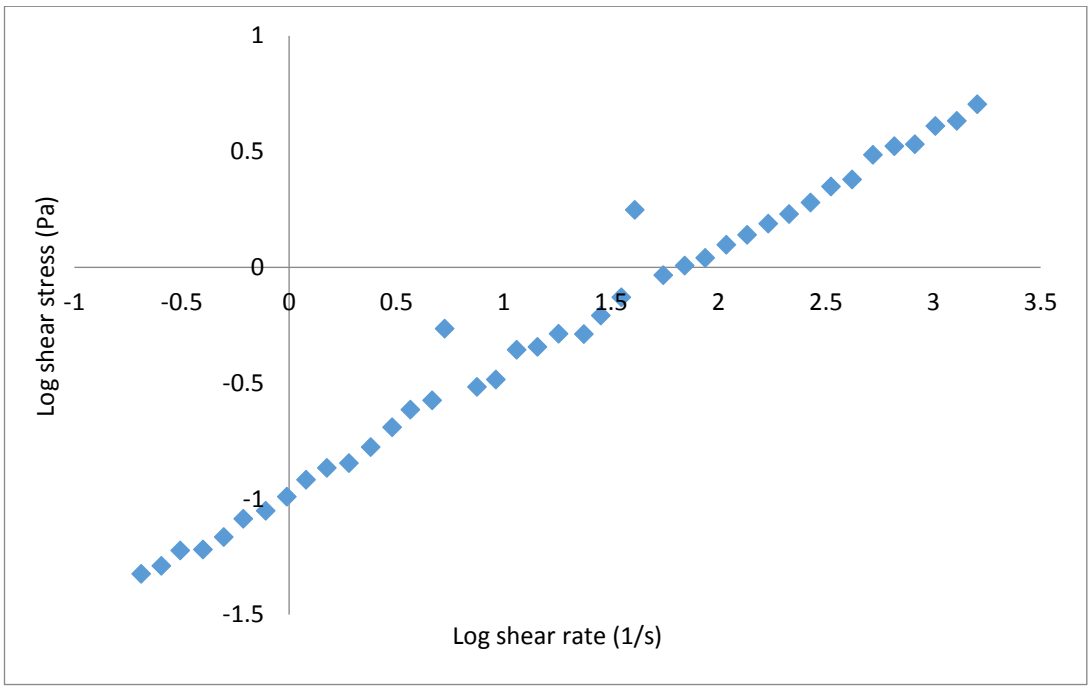

Figure 72 : Log plot of the flow curve for 0.1% xanthan

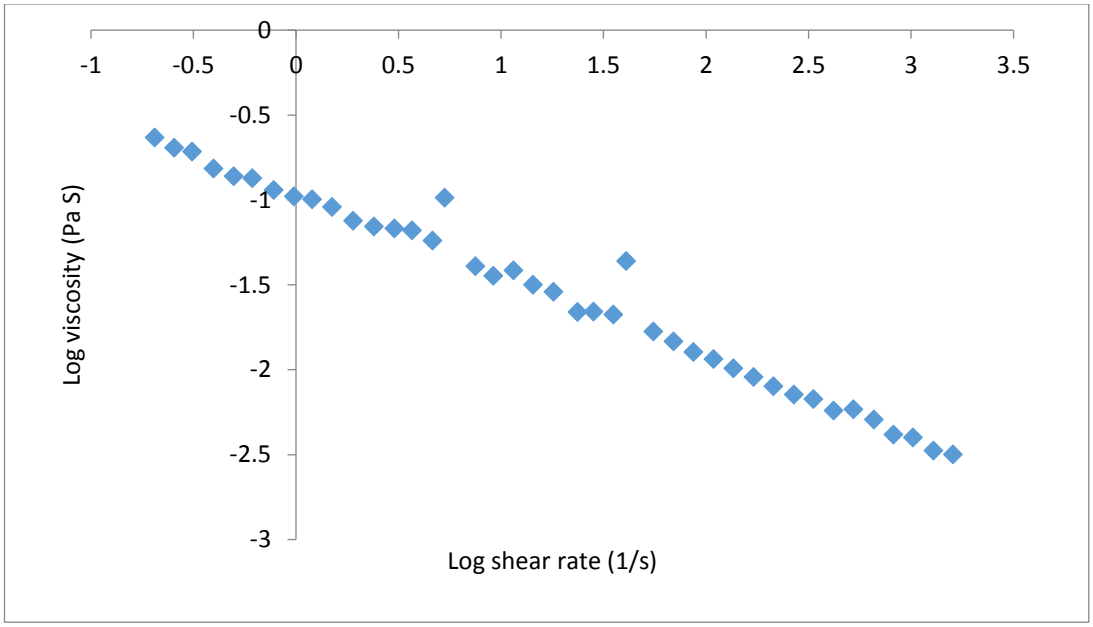

Figure 73 : Log plot of the viscosity vs. shear rate 0.1% xanthan

In Figure 74, the viscosity of the xanthan solution increases as the concentration increases. This viscosity increase can be seen visually but also within the acoustic data, where the velocity increases with the increase in concentration. Again there are two

points which as discussed previously are outliers which could be caused by air bubbles or undissolved particles of xanthan in the solution.

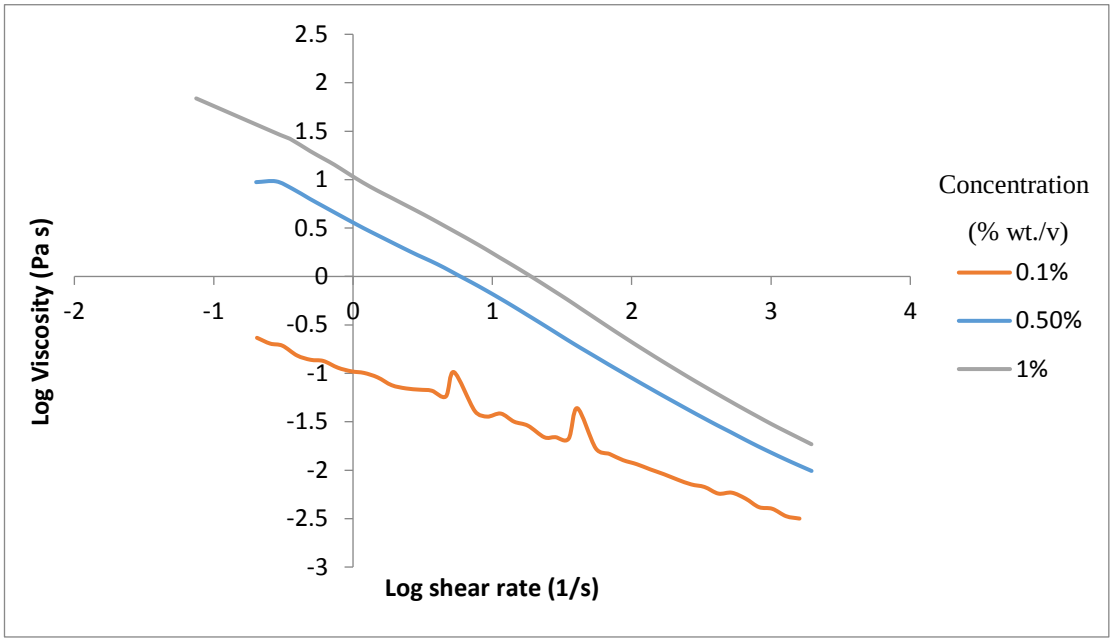

Figure 74 : Combined viscosity data for 0.1-1% xanthan solutions

The elastic modulus (Figure 75) of the solution increases as the concentration is increased. When the angular frequency is increased, the G' also increases. Milas *et al.* (1990) found that with an increase in concentration the G' values also increased.[60]

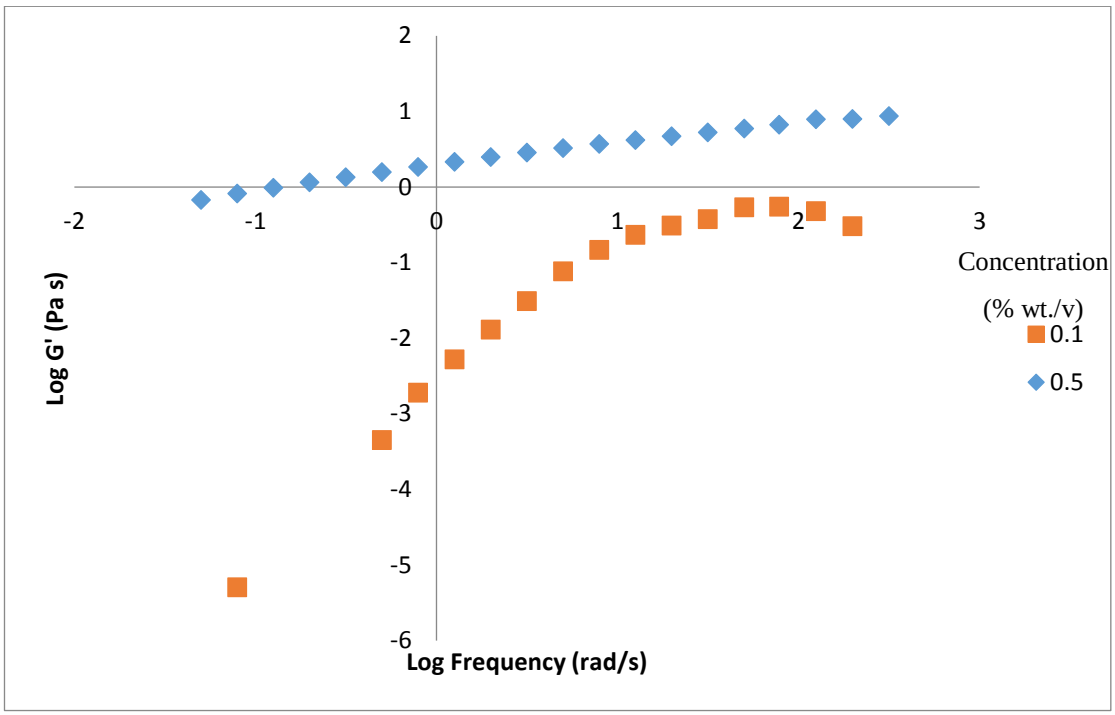

Figure 75 : Comparison of oscillatory data (G') for 0.1 and 0.5 % xanthan

The viscous modulus (Figure 76) follows the same increase with increasing concentration. Milas *et al.* (1990) found that with increasing concentration the G'' value would increase, but also that the cross over point of the two moduli would be at a lower frequency at higher concentration. However, with the results found experimentally, the cross over point is found to occur at a higher frequency when the concentration is increased (Figure 77). This may be due to the same problems as found with the velocity measurements of the 0.5% solution.[60]

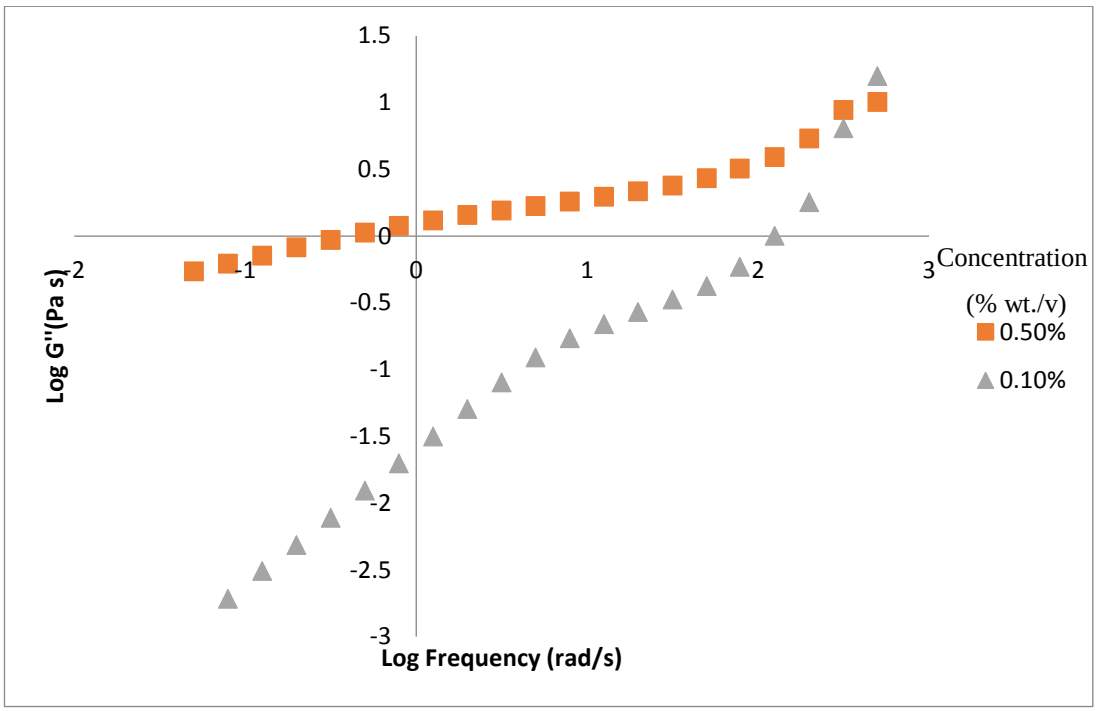

Figure 76 : Comparison of oscillatory data (G") for 0.1 and 0.5 % xanthan

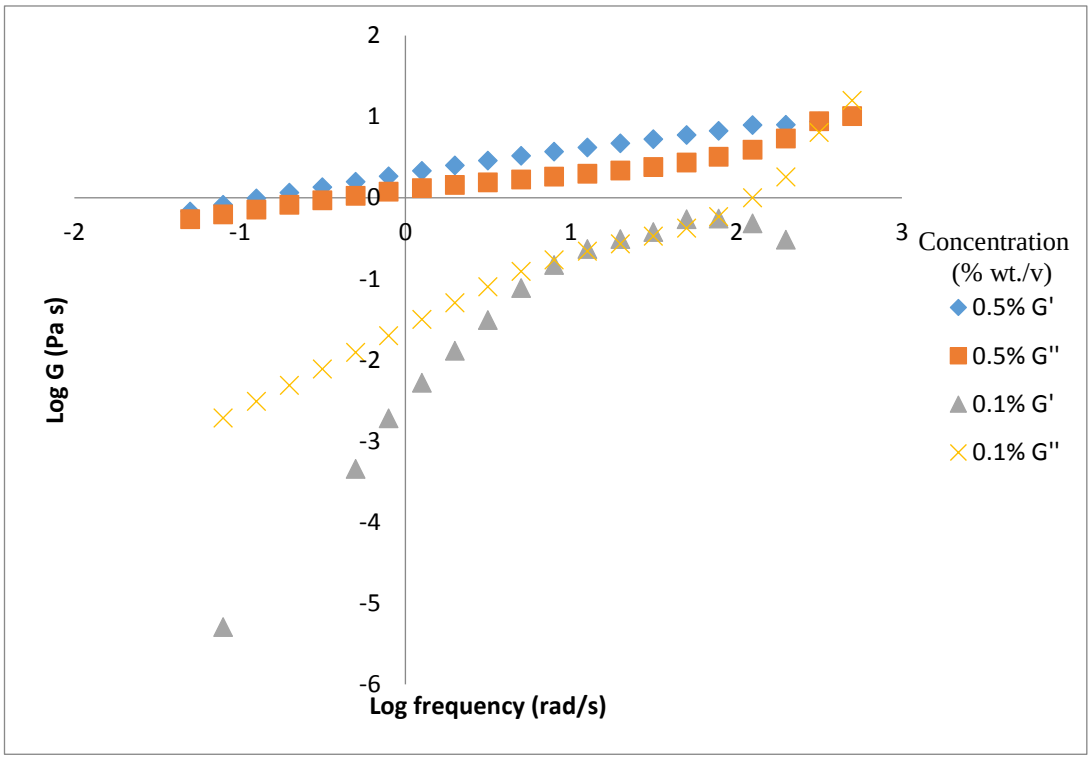

Figure 77 : G' and G" data for 0.1 and 0.5% solution of xanthan

As the velocity is affected by the increase in density of the xanthan solution which is caused by an increase in concentration; this increase in concentration also causes the increase in viscosity of the xanthan solutions. This simple link of the concentration of the xanthan solutions would suggest that it is possible to relate the velocity measurements to the viscosity and other rheological measurements. If the acoustic probe can be designed to take on-line measurements then the velocity measurement would allow the viscosity of the solution and the concentration of xanthan to be calculated. The concentration of the xanthan would be a useful monitoring method for the success of a fermentation and to optimise the process. This would require further investigation with a wider range of xanthan concentrations and a redesign of the probe so that it could be submerged within the fermenter to take on-line measurements. (4.7)

4.6 Conclusions from experimental work

The novel probe designed by Bioinnovel has shown that with all the model solutions there is a trend shown with increasing concentration for agar, xanthan and glycerol; as the concentration increases there is an increase in the velocity. The calculated velocities are similar to the values reported in literature for these solutions. For starch as there are particles present, the relationship between velocity and concentration is slightly different due to a parabolic relationship rather than a linear one. The presence of particles changing the relationship between velocity and concentration could potentially cause problems within a fermentation system, for example the xanthan in a fermentation is found on the cell membrane rather than in solution so the cell may affect the relationship of the xanthan to measured velocity.

Attenuation calculations of the model solutions were found to be less useful than the velocity measurements with these experimental parameters. For agar and starch, attenuation coefficients are not affected by the change in concentration. Glycerol attenuation coefficients could not be calculated due to the saturation of the signal. The attenuation coefficient for xanthan appears to be unaffected by low concentration <1%. However, at the change between one and two percent there is a possible increase in attenuation coefficient, but due to the discrepancy between day 1 and day 2 this would need further investigation. In fermentation systems the xanthan concentration can

reach higher concentrations,[61] so at this concentration there may be some effect on the attenuation coefficient.

With all the model solutions, there is an effect on velocity when the concentration is increased. However, at the low concentrations used, attenuation is insensitive to changes in the concentration of glycerol, xanthan and agar. During the fermentation process, low concentrations of agar are used, which would suggest that measurement of attenuation cannot solely be used to determine the concentration of the system. Xanthan has been reported to reach concentrations of 5% so the attenuation may be affected at these slightly higher concentrations. The attenuation coefficient of the starch solution increases as the concentration is increased. Agitation of the solution causes greater variation in the velocity and attenuation values measured. For glycerol, even when the concentration of the solution was increased to 100% the effect on attenuation was very limited. However, the velocity measurements were found to be in agreement with those stated in the literature and the linear relationship between concentration and velocity levels was observed.

Adaptations in the probe design will have to be made to allow the use of the probe in the fermenter, for example; the probe must have appropriate fixtures to hold the transducers in place that will not be affected by the pressure of the autoclave or be sensitive to agitation. (4.7)

With the changes in the rheological properties of xanthan solutions as the concentration increases, rheology is a possible monitoring method of fermentations. The pseudo plastic behaviour and the other properties would allow measurement of the concentration of the xanthan in a sample. The acoustic measurements and the rheological measurements could be combined to form a model to predict the xanthan concentration, however further work would need to be done on other analyte concentrations and samples to take this further.

4.7 Discussion of potential of acoustic monitoring

Acoustic monitoring certainly has potential for monitoring of fermentation reactions as the change in velocity by changing concentration could be used to monitor the progression of a fermentation. Acoustic monitoring has not been widely used for monitoring of fermentations on-line and this new probe would allow real time information to be gathered on the concentration of substrates in the fermentation broth. For example, a *Xanthomonas* fermentation could be monitored by correlating the change in velocity to the increase in xanthan production. There is also the potential to link the rheological properties of a *Xanthomonas* fermentation to the acoustic changes as an increase in the xanthan concentration in the fermentation broth will lead to a change in the viscosity of the broth. Further work would be required to determine how successful the probe would be when a more complex solution is measured as only one substrate was measured at a time. Also other substrates found in a fermentation broth should also be analysed for example glucose as a carbon source. For the acoustic monitoring to take place on-line then the probe would have to be redesigned, as the current structure would not allow this. To address the issues of the prototype probe, the following issues would need to be addressed:

1. Sterilisability
2. Movement of the transducers
3. Flow of the fermentation broth
4. Sites for cell growth
5. Robustness and longevity
6. Calibration requirements

To allow the probe to be autoclaved it would be beneficial to fit in a standard port on a fermenter lid to be autoclaved in place. The transducers would also have to with stand a temperature of 120 ºC and pressure of 2 Bar. The whole probe to be cost effective would need to be re-used multiple times without damage to the transducers or loss of signal over time.

The transducers would need to be held in place with no chance of movement during the fermentation as there is no way to move them back into the correct position and

dependent on the micro-organism in the fermenter, the agitation rate and turbulence within the fermenter can not only vary dependent on organism but also the point during the fermentation for example the agitation rate of a *Xanthomonas* fermentation can vary between 200 and 750 rpm in a 9.5 L fermentation.

To allow a representative flow of the fermentation broth a horizontal flow, such as those used in the food industry, would allow the impeller within the fermenter to help with movement of the broth past the transducers. If this could not be achieved then a smaller cylinder holding the transducers in place could allow better flow through the broth.

A concern when inserting a probe into a fermentation system would be creating dead zones where the micro-organisms are unable to grow in the same way as the rest of the broth or the potential for biomass to become trapped during the fermentation. In highly viscous broths such as a *Xanthomonas* fermentation then the fluid may become trapped within the sample cylinder. A design such as those used in a settlement tank with a fork shaped set up (Figure 78) may prevent the build up near the transducers and the formation of dead zones.

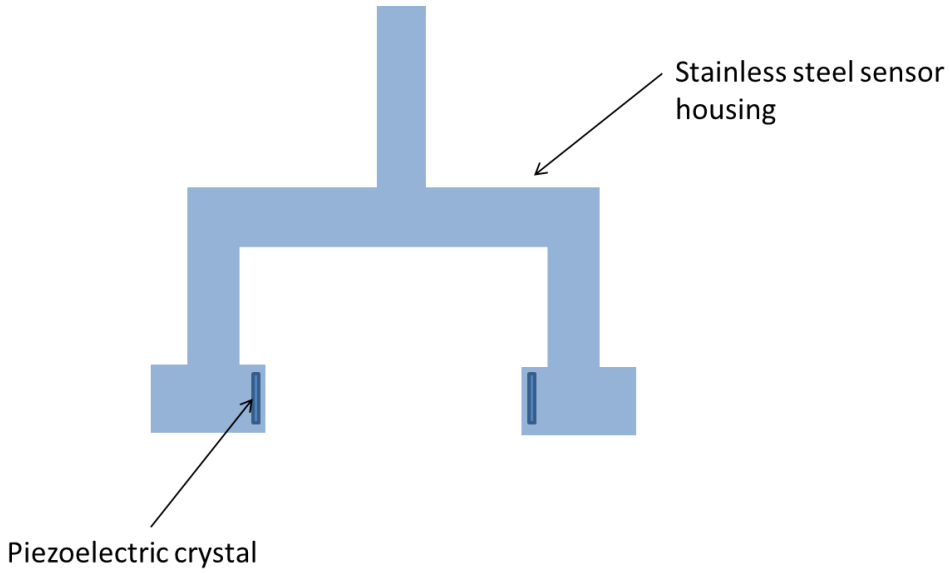

Figure 78 : Settlement tank ultrasound probe set up for measurement of suspended particles in solution

If the probe requires calibration then this must be completed before insertion in the fermenter and autoclaving or be able to be calibrated in place. In the case of the

acoustic monitoring the fermentation media before inoculation can be used as a reference measurement.

Using the NIR probe design, a fixed path length particle sizer and the dip stick probe as a template, a potential probe design is shown in Figure 79, here the transducers suitable for immersion are placed in steel casing which allows the transducers to be held in place and autoclaved within the fermenter. The sensor window allows horizontal flow of the fermentation broth while maintaining a similar set up to Bioinnovel's prototype probe. The acoustic transducers are the major source of investigation as the transducers currently used could not be used to monitor a large proportion of fermentations due to the 8 hour immersion limit. Work would need to be carried out to identify transducers that can be used for a much longer period of time e.g. the 90 hours of a *Xanthomonas* fermentation.

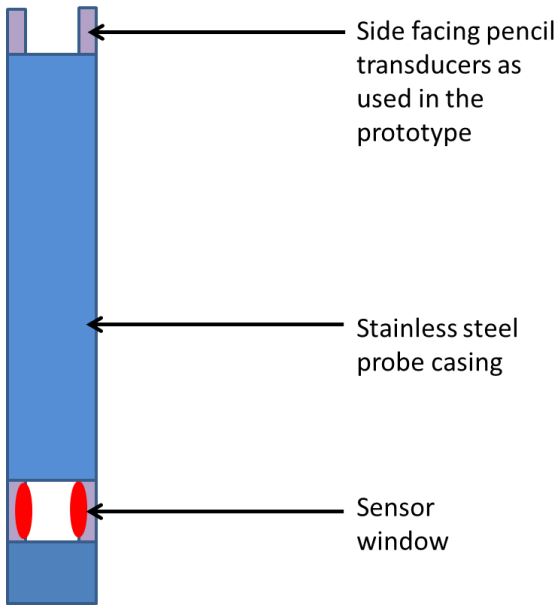

Figure 79 : Potential prototype acoustic probe

4.8 References

1. Stamboulides, C.; Hatzikiriakos, S. G., Rheology and processing of molten poly(methyl methacrylate) resins. *International Polymer Process* **2006,** *21* (2), 155-163.

2. McClements, D. J., Ultrasonic Characterization of Foods and Drinks: Principles, Methods and Applications. *Critical reviews in food science and nutrition* **1997,** *37* (1), 1-46.

3. McClements, D. J., Ultrasonic measurements in particle size analysis. *Encylcopedia of analytical chemistry*, **2006**.

4. Hopper, C. Investigations of novel analytical strategies for monitoring industrially relevant antibiotic fermentation processes. Thesis [Ph. D] -- University of Strathclyde, **2011.**

5. Silva, A.; Perez, N., *Ultrasound Measurement Of The Content Of Solid Particles In Liquid Media Applied To Oil Industry*. 21st International Congress of Mechanical Engineering, Oct 24-28; RN, Brazil, **2011.**

6. Morris, A. S.; Langari, R., Fundamentals of Measurement Systems, *Measurement and Instrumentation*. Butterworth-Heinemann: Boston, **2012**, pp 1-10.

7. Ensminger, D.; Bond, L. J., *Ultrasonics: Fundamentals, Technologies and Applications*. CRC Press: **2011**, p 765.

8. Goodwin, J. W.; Hughes, R. W., *Rheology for chemists An introduction*. 2nd ed., Royal Society of Chemistry, **2008**.

9. Sherman, P., *Industrial rheology with particular reference to foods, pharmaceutical and cosmetics*. Academic Press: London, **1970.**

10. Malkin, A. Y.; Isayev, A. I., 2 - Viscoelasticity. *Rheology Concepts, Methods, and Applications (Second Edition)*, Elsevier: Oxford, **2012**, pp 43-126.

11. Swarbrick, J., *Encyclopedia of Pharmaceutical Technology*. 3rd ed.; Informa Healthcare: New York, **2007,** Vol. 5.

12. Bao, X. H.; Lee, N. C.; Raj, R. B.; Rangan, K. P.; Maria, A., Engineering solder paste performance through controlled stress rheology analysis. *Solder. Surf. Mt. Technol.* **1998,** *10* (2), 26-+.

13. Whitcomb, P.J.,Rheology of Xanthan Gum. *Journal of rheology* **1978,** *22* (5), 493-505.

14. Mezger, T. G., *The rheology handbook: for users of rotational and oscillatory rheometers. 2 ed.*; Vincentz Network GmbH & Co KG,**2006**, p 299.

15. Antonio Vercet, R. O., Pedro Marquina, Simon Crelier and Pascual Lopez-Buesa, Rheological properties of yoghurt made with milk submitted to manothermosonication. *Journal of agricultural and food chemistry* **2002,** *40* (21), 6165-6171.

16. Badino JR., A. C. B.; Facciotti, M. C. R.; Schmidell, W., Construction and operation of an impeller rheometer for on-line rheological characterisation of non-Newtonian fermentation broths. *Brazilian Journal of Chemical Engineering*. **1997,** *14* (4).

17. Funke, M.; Buchenauer, A.; Mokwa, W.; Kluge, S.; Hein, L.; Muller, C.; Kensy, F.; Buchs, J., Bioprocess Control in Microscale: Scalable Fermentations in Disposable and User-Friendly Microfluidic Systems. *Microbial cell factories*. **2010,** *9*.

18. Jianxin Li, R. D. S., G.Y. Chai and D.K. Halbauer, Development of an ultrasonic technique for in situ investigating the properties of deposited protein during crossflow ultrafiltration. *Journal of colloid and interface science.* **2005,** *284* (1), 228-238.

19. Challis, R. E.; Povey, M. J. W.; Mather, M. L.; Holmes, A. K., Ultrasound techniques for characterizing colloidal dispersions. *Rep. Prog. Phys.* **2005,** *68* (7), 1541-1637.

20. Zauhar, G.; H.C.Starritt; Duck, F.A.; Studies of acoustic streaming in biological fluids with an ultrasound Doppler technique. *The British journal of radiology*. **1998,** *71*, 297-302.

21. Bamberger, J. A.; Greenwood, M. S., Non-invasive characterization of fluid foodstuffs based on ultrasonic measurements. *Food research international*. **2004,** *37* (6), 621-625.

22. Henning, B.; Daur, P. C.; Prange, S.; Dierks, K.; Hauptmann, P. *In-line concentration measurement in complex liquids using ultrasonic sensors*, 1st Joint Meeting Ultrasonics International Conference/World Congress on Ultrasonics (UI 99/WCU 99), Lyngby, Denmark, Jun 29-Jul 01; Elsevier Science Bv: Lyngby, Denmark, **1999**; pp 799-803.

23. Banchet, J.; Cancian, J.; Cheeke, J. D. N. *Measurement of the acoustic nonlinearity parameter in 1-alkanols*, 1st Joint Meeting Ultrasonics International Conference/World Congress on Ultrasonics (UI 99/WCU 99), Lyngby, Denmark, Jun 29-Jul 01; Elsevier Science Bv: Lyngby, Denmark, 1999; pp 301-304.

24. Germain, L.; Jacques, R.; Cheeke, J. D. N., Acoustic Microscopy Applied To Nonlinear Characterization Of Biological Media. *Journal of the acoustical society of America.* **1989,** *86* (4), 1560-1565.

25. Kulmyrzaev, A.; Cancelliere, C.; McClements, D. J., Characterization of aerated foods using ultrasonic reflectance spectroscopy. *Journal of food engineering.* **2000,** *46* (4), 235-241.

26. Silberman, E., Sound velocity and attenuation in bubbly mixtures measured in standing wave tubes. *Journal of Acoustical society of America.* **1957,** *29*, 925-935.

27. Fish, P. J., Ultrasonic investigation of blood flow. *Proc. Inst. Mech. Eng. Part H-J. Eng. Med.* **1999,** *213* (H3), 169-180.

28. Sayan, P.; Ulrich, J., The effect of particle size and suspension density on the measurement of ultrasonic velocity in aqueous solutions. *Chem. Eng. Process.* **2002,** *41* (3), 281-287.

29. Povey, M. J. W.; Harden, C. A., An Application Of The Ultrasonic Pulse Echo Technique To The Measurement Of Crispness Of Biscuits. *Journal of Food Technology* **1981,** *16* (2), 167-175.

30. Park, B.; Whittaker, A. D.; Miller, R. K.; Hale, D. S., Predicting Intramuscular Fat In Beef Longissimus Muscle Form Speed Of Sound. *J. Anim. Sci.* **1994,** *72* (1), 109-116.

31. Gould, R. W., Nondestructive Egg-Shell Thickness Measurements Using Ultrasonic Energy. *Poult. Sci.* **1972,** *51* (4), 1460-&.

32. *Oxford English dictionary*, Oxford University press: Oxford, 2008.

33. Arnold, S. A.; Crowley, J.; Vaidyanathan, S.; Matheson, L.; Mohan, P.; Hall, J. W.; Harvey, L. M.; McNeil, B., At-line monitoring of a submerged filamentous bacterial cultivation using near-infrared spectroscopy. *Enzyme Microb. Technol.* **2000,** *27* (9), 691-697.

34. Kemblowski, Z.; Budyzynski, P.; Owczarz, P., On-line measurements of the rheological properties of fermentation broth. *Rheologica Acta.* **1990,** *29* (6), 588-593.

35. Kemblowski, Z.; Sek, J.; Budzynski, P., The Concept Of A Rotational Rheometer With Helical Screw Impeller. *Rheologica Acta.* **1988,** *27* (1), 82-91.

36. Reuss, M.; Debus, D.; Zoll, G., Rheological Properties Of Fermentation Fluids. *Chem. Eng.-London.* **1982,** (381), 233-236.

37. Goudar, C.T.; Strevett, K.A.; Shah, S.N., Influence of microbial concentration on the rheology of non-Newtonian fermentation broths. *Applied microbiology and biotechnology.* **1999,** *51* (3), 310-315.

38. Bechapattarapong, N.; Bai, W. A. A., F.; Moo-young, M., Rheology and hydrodynamic properties of tolypocladium inflatum fermentation broth and its simulation. *Bioprocess and biosystems engineering.* **2005,** *27* (4), 239-247.

39. Leduy, A.; Marsan, A. A.; Coupal, B., A study of the rheological properties of a non-Newtonian Fermentation broth. *Biotechnol. Bioeng.* **1974,** *16* (1), 61-76.

40. Covas, J. A.; Maia, J. M.; Machado, A. V.; Costa, P. In *On-line rotational rheometry for extrusion and compounding operations*, Conference on Rheometry, Apr 10-12; Elsevier Science Bv: Cardiff, WALES, 2006; pp 88-96.

41. Salas-Bringas, C.; Jeksrud, W. K.; Schuller, R. B., A new on-line process rheometer for highly viscous food and animal feed materials. *Journal of food engineering.* **2007,** *79* (2), 383-391.

42. Saluja, A.; Kalonia, D. S., Application of ultrasonic shear rheometer to characterise rheological properties of high protein concentration solutions at microliter volume. *Journal of pharmaceutical sciences.* **2005,** *94* (6), 1161-1168.

43. Wiklund, J.; Shara, I.; Stading, M., Methodology for in-line rheology by ultrasound doppler velocity profiling and pressure difference techniques. *Chemical engineering science.* **2007,** *62* (16), 4277-4293.

44. Kemblowski, Z.; Budzynski, P. *Process Rheometry Of Biological Suspensions*, 11th International Congress on Rheology, Aug 17-21; Moldenaers, P.; Keunings, R., Eds. Elsevier Science Publ B V: Brussels, Belgium, **1992**, 735-737.

45. Stading, J. W. A. M., Application of in-line ultrasound doppler based UVP-PD rheometry method to concentrated model and industrial suspensions. *Flow measurement and instrumentation.* **2008,** *19* (3-4), 171-179.

46. Freeman, R. L., Wiley Series in Telecommunications and Signal Processing. *Telecommunication System Engineering*, John Wiley & Sons, Inc., **2005**,1052-1053.

47. http://www.engineeringtoolbox.com/sound-speed-water-d_598.html.

48. Smith, A. H.; Lawson, A. W., The Velocity of Sound in Water as a Function of Temperature and Pressure. *The Journal of Chemical Physics* **1954,** *22* (3), 351-359.

49. Holm-Nielsen, J. B.; Lomborg, C. J.; Oleskowicz-Popiel, P.; Esbensen, K. H., On-line near infrared monitoring of glycerol-boosted anaerobic digestion processes: Evaluation of process analytical technologies. *Biotechnol. Bioeng.* **2008,** *99* (2), 302-313.

50. Gulseren, I.; Coupland, J. N., Ultrasonic velocity measurements in frozen model food solutions. *Journal of food engineering* **2007,** *79* (3), 1071-1078.

51. Urick, R. J., A sound velocity method for determining the compressibility of finely divided substances. *Journal of applied physics* **1947,** *18*, 983-987.

52. Koltsova, I. S.; Polukhina, A. S.; Deynega, M. A. *Reversible And Irreversible Processes In Biocomposites*, Session Of The Scientific Councol Of Russian Academy Of Science On Acoustics, 15-17 June, **2010.**

53. Browne, J. E.; Ramnarine, K. V.; Watson, A. J.; Hoskins, P. R., Assessment of the acoustic properties of common tissue-mimicking test phantoms. *Ultrasound Med. Biol.* **2003,** *29* (7), 1053-1060.

54. Hayashida, S.; Ohta, K.; Flor, P. Q.; Nanri, N.; Miyahara, I., High-concentration ethanol fermentation of raw ground corn. *Agricultural and Biological Chemistry* **1982,** *46* (7), 1947-1950.

55. Nigam, J. N.; Gogoi, B. K.; Bezbaruah, R. L., Alcoholic fermentation by agar-immobilized yeast cells. *World J. Microbiol. Biotechnol.* **1998,** *14* (3), 457-459.

56. Rahalkar, R. R.; Gladwell, N.; Javanaud, C.; Richmond, P., Ultrasonic behavior of glass-filled polymer-solutions. *J. Acoust. Soc. Am.* **1986,** *80* (1), 33-39.

57. Pakzad, L.; Ein-Mozaffari, F.; Chan, P., Using computational fluid dynamics modeling to study the mixing of pseudoplastic fluids with a Scaba 6SRGT impeller. *Chem. Eng. Process.* **2008,** *47* (12), 2218-2227.

58. Dhiaa, A. H., The temperature effect on the viscosity and density of xanthan gum solution. *KUFA. Journal of Engineering.* **2012,** *3* (2), 17-30.

59. Zataz, J. L.; Knapp, S., Viscosity of Xanthan Gum solutions at low shear rates. *Journal of pharmaceutical sciences* **1984,** *73* (4), 468-471.

60. Milas, M.; Rinaudo, M.; Knipper, M.; Schuppiser, J. L., Flow and viscoelastic properties of xanthan gum solutions. *Macromolecules.* **1990,** *23* (9), 2506-2511.

61. Garcia-Ochoa, F.; Santos, V. E.; Casas, J. A.; Gomez, E., Xanthan gum: production, recovery, and properties. *Biotechnol. Adv.* **2000,** *18* (7), 549-579.

5 Refractive index

Refractive index monitoring is used in a wide variety of industries for various reactions and processes. It is often used in process control in manufacturing, environmental monitoring and quality control of chemical or food industries.[1, 2] Stratophase have designed a novel probe which has the potential to monitor reactions on-line which has previously been used to monitor ethanol fermentations and mammalian cell cultures.[3] However, the probe has not been used to monitor bacterial cell fermentations, this work investigates the possibility of monitoring of this type of fermentation.

5.1 Refractive index theory

Refractive index (RI) is the measurement of the bending of light when it enters a denser medium. The ratio between the sine of the angle of incidence of the light and the sine of the angle of refraction gives the refractive index. (Figure 80)[4]

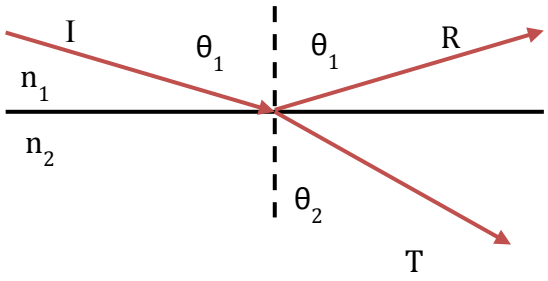

Figure 80 : Light beams are reflected (R) and refracted or transmitted (T) at the

Snell's law (Equation 1) describes this relationship. The absolute angle of refraction is derived by dividing the refractive index relative to air by a factor of 1.00027 which is the absolute refractive index of air.[5]

$$\frac{sin\theta 1}{sin\theta 2} = \frac{\upsilon_1}{\upsilon_2} = \frac{n_1}{n_2} \qquad \text{Equation 1}$$

Where:

θ = angle measured from the normal of the boundary

υ = velocity of light in the respective medium

n = refractive index respective of the medium

The refractive index of a solution or mixture of transparent liquids can be calculated using Equation 2.[6]

$$\boldsymbol{n = n_v + \phi(n_u - n_v)} \qquad \text{Equation 2}$$

Where:

n = RI

n_v = RI solvent

n_u = RI solute

Φ = volume fraction of the solute

5.2 Techniques for measuring RI

Differential refractometry can be carried out with or without the use of an interferometer. When using an interferometer this technique uses a two beam interferometer to determine the refractive of a sample compared with air. The sample with parallel input and output faces is placed within the sample beam with and compared to the reference beam in air. The phase lag caused by the sample is given as $2\pi nz/\lambda_0$ compared to air ($2\pi n_{air}z/\lambda_0$) where z is the sample length and n is the refractive index. The phase difference between the two beams is shown in Equation 3.

$$\boldsymbol{\delta = \frac{2\pi z(n - n_{air})}{\lambda_0}} \qquad \text{Equation 3}$$

The refractive index of air is 1 which allows the refractive index of the sample to calculated using the phase difference. The phase difference is measured by adjusting a calibrated phase compensator in the reference beam to regain zero order fringe or white light fringes. The effect of optical attenuation by a sample decreases the fringe brightness but does not affect the phase and so only the real part of the complex refractive index is measured.[7, 8,9]

McClimans *et al.* (2006) have designed a refractometer which measures the refractive index of solutions using differential refractometry without interferometry. This method is based on total internal reflectance. The refractometer designed used a

divergent laser beam to determine the RI. The advantages of having an instrument without an interferometer include better portability and the ability to record real time changes in RI as often the interferometer methods are designed to measure isotropic samples rather than monitoring processes.[10,11] Laser based methods are also used to study changes of RI in micro channels with the advantages being that they are low cost, have a simple structure and can be used without adding labels to the solutions. There are some limitations on the sensitivity of the instruments due to the small diameter of the channels which can limit the optical path length.[12] White *et al.* defined (2008) a detection limit for refractive index sensors as a method of characterising the performance of RI sensors using both the sensors resolution with its sensitivity. Traditionally sensors are compared on the sensitivity alone but White et al. (2012) find this insufficient for qualitatively characterising the ability of a sensor to both identify and quantify a targeted material in a sample. [13,14]

The methods discussed by Xiong *et al.* (2011) include the transverse laser beam detection method which measures the displacement of the laser beam as it passes through the micro channel.[12] This is a technique that is widely utilised as it has a simple structure and easy optical realisation. There are disadvantages to this method as it has poor sensitivity and there is a limit to the size of micro channel this method can be applied to. This technique has been used to monitor glycerol and saccharose.[15,16]

Krattiger *et al.* (1993) used a hologram based laser RI method which involves a focused laser beam which is divided into two beams after interacting with a holographic image film. (Figure 81) The two laser beams are introduced to the micro channel which produced four areas of interference areas. Two of these interference areas measure the RI change in the micro channel which become the detection signal and two inferences are the reference signal. The detection and analyte signal can be used together for analyte determination. This method has the same sensitivity compared to traditional transference configuration. The disadvantages to this technique are the high cost and the challenging optical realisation. It has been used by Krattiger & Bruno *et al.* (1996) for capillary and chip electrophoresis.[16,17]

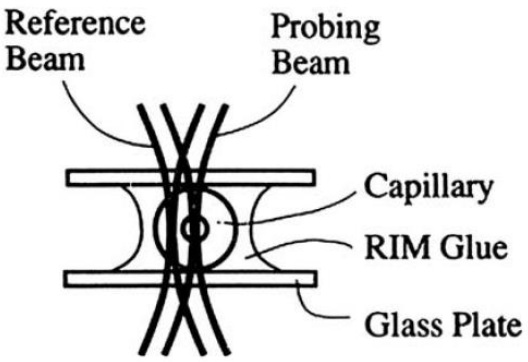

Figure 81 : Schematic of the core part of the hologram laser based refractive index detection.[12]

5.3 RI monitoring

Refractive index monitoring is used in a wide variety of industries for various reactions and processes. It is often used in process control in manufacturing, environmental monitoring and quality control of chemical or food industries.[1,2]

Tubino *et al.* (2014) have used a refractometer which has a conical device attached as a sample cell which acts as a flow cell over the refractometer to analyse changes in RI of biodiesel. The samples pass through a phase separator first to remove the glycerol from the solution and air bubbles as these could affect the measurement due to a smaller volume of biodiesel being in the sample cell. The measured RI values corresponded to the amount of biodiesel in the reaction flask.[18]

Zabala *et al*. (2014) used a refractometer to measure the refractive index of a methanolysis reaction for biodiesel. When measurements were taken using a differential RI detector on-line there were problems due to flow instabilities through the chamber but measurements were taken successfully off-line of the alcoholic phase.[19]

RI detectors are used routinely as the detector for high performance liquid chromatography (HPLC). They are used to analyse samples that lack strong chromophores in the UV or visible regions and are non-fluorescent. The advantages to this technique are the non-destructive nature and it is a concentration dependent bulk

property.[20] Plata *et al*. (2013) used an HPLC to determine the carbohydrates present during a Saccharomyces fermentation.[21]

The RI will be constant for pure substances under standard conditions and is often used analytically as a measure of sugar or the total solids in a solution. RI measurement can also be used to determine the purity of oils.[4] The conversion of soybean oil has been monitored using off-line RI and was found to be an inexpensive and simple method for monitoring the transesterification process.[22] Santos *et al.* (2013) were able to correlate the weight % of the total esters of the soybean oil and the biodiesel mixture to the refractive indices and regression analysis based on the results were performed.[22]

RI has been used in forensic applications with glass refractive indices being compared in forensic cases. The glass refractive index measurements (GRIM) are used to compare known and unknown fragments for matching by RI comparison.[23]

Fibre optics have been used for the monitoring RI changes of various chemicals and processes. Yeh *et al.* (2012) have used an optical time-domain reflector based fibre sensor to monitor different liquid organic chemicals. The RI is detected according to the measured reflected power level of the backscattered light from the optical time domain reflector via a single mode fibre-based sensor. A wide range of chemicals have been analysed including ethyl acetate, THF and cyclohexane.[24] Bacterial growth was measured by a refractive index tapered fibre optic biosensor. Cells were grown on the surface of the sensor and the changes in RI were measured. The specific growth rate of the bacteria was measured by the sensor and it provides many advantages over other methods such as dry weight and optical density including the ability to monitor in real time and label free monitoring of small analyte volumes. [25]

5.4 Conclusions from refractive index literature

There are various instruments that have been designed to monitor the refractive index in various processes. McClimans *et al.* (2006) designed an instrument without an interferometer which allows real time monitoring.[2] This real time monitoring can also be seen in the novel Stratophase system as described in 5.6.1.1. The sensitivity of the instrumentation is important and the novel system must take this into account.[12]

Refractive index measurements have been used to monitor glycerol and saccharose and other pure substances, which provides some insight into the ability of refractive index changes to monitor an *E. coli* fermentation as similar compounds are found within the broth.[16] However, the complexity of the fermentation broth may add some challenges to monitoring due to the combination of the analytes.[19,18]

Certain fermentation conditions may affect the refractive index measurements such as air bubbles and the flow past the sensor; where the probe is situated in the fermenter and the design of the probe will be important in any RI monitoring as discussed in (1.3)

5.5 Aims of refractive index monitoring

The main aim of the RI work was to determine the ability of the novel probe in monitoring an *E. coli* fermentation including monitoring glucose consumption acetic acid and biomass production. *E. coli* was used in these experiments rather than *X. campestris* as it is a simpler organism to grow (2.2.2) and a shorter growth time. To determine this the following smaller aims will be investigated

4. The effect of the fermenter on the functionality of the probe
5. The change in RI measurement by the probe for each analyte
6. The effect of combinations of analytes on the RI measurement
7. The potential for monitoring off-line fermentation samples
8. The potential of monitoring on-line fermentations

5.6 Experimental

5.6.1 Instrumentation

5.6.1.1 Stratophase Instrumentation

The novel system designed by Stratophase (Southampton, UK) can be used on-line to monitor the change in the refractive index during a process including ethanol

fermentation and mammalian cell cultures.[3] The main components of the system are the control unit and the probe which are connected using armoured fibre optic cables. The technology allows the RI to be monitored in the media and this is used to infer changes in its chemical composition. The absolute levels of specific products or metabolites cannot be accurately calculated but the reaction profile can be monitored and rates of change calculated for the process in real time. The system can be used to identify failure points and trigger warnings to allow the operator to fix the problem or discontinue the reaction as well as providing information on the process, such as when maximum product is achieved to allow optimal harvesting leading to a better yield and a reduced process time. As the system operates on non-visible light to enable it to work with glassware fittings, it cannot be used in a direct comparison with conventional RI values which are taken and quoted at a specific wavelength of visible light. Sparrow *et al.* (2009) found that for a shift in the traditional RI equates to a shift of approximately 15 nm in the Bragg wavelength.[26]

5.6.1.1.1 Controls

The RIS lab module is a prototype optical sensor control unit. The control unit allows up to eight independent probes to be connected to the system and monitored at one time. The only information that is transmitted between the control unit and the probe is light with a scan frequency of 2 Hz and a wavelength range of 1510 -1590 nm. The control unit emits broadband light to the optical microchip sensor in the probe. This passive sensing element allows the light to interact with the media and reflects back the changes to the control unit.

5.6.1.1.2 Probe

The sensor is housed in an insertion probe which can be easily introduced into a bioreactor using a standard port. The optical micro sensor is based on the concept of integrated optical circuits. These circuits allow light to be channelled to different locations of the circuit according to a specific design. When the light is at a specific location on the chip it interacts with a very specific wavelength reflector. These reflectors known as Bragg gratings will reflect one wavelength of light and let other wavelengths pass through unaffected. The wavelength of an individual reflector is

defined during the manufacturing process which allows the specific wavelength of light to be correlated to the exact location on the chip. The sensors are designed so that changes on the reflector subtly change the reflected wavelength. The probe directly measures the refractive index of the media by sensing a shift in the wavelength between incident light and the light returning from the media. The signals transmitted using the wavelength of light allows multiple reflectors to be used on one chip with all signals travelling down a single optical fibre.[27] (Figure 82)

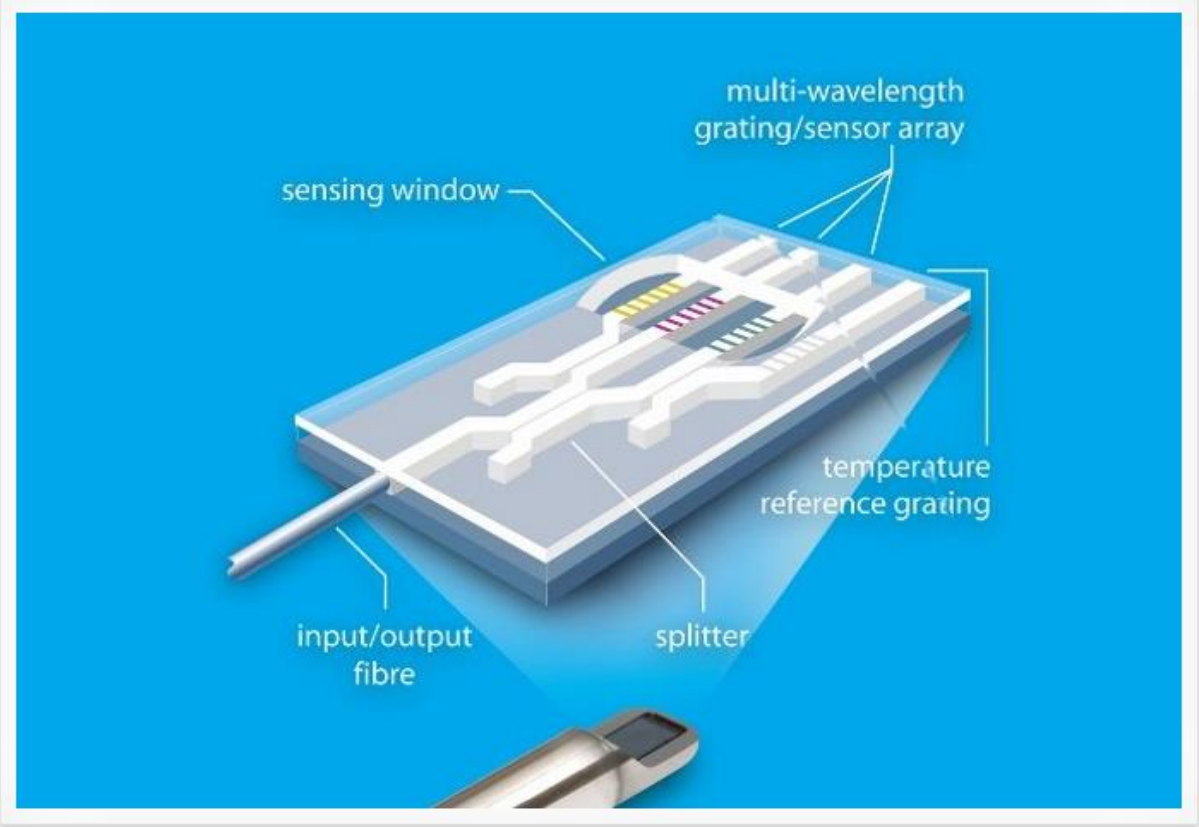

Figure 82 : Stratophase sensing window illustrating the Bragg grating[3]

The Stratophase system was used for all refractive index measurements with two designs of probe used during this work. The first probe design had the sensor encased in stainless steel housing as can be seen in Figure 83. The sensor inset into the probes surface led to the possibility of the probe becoming fouled with biomass becoming trapped in the rim.

Figure 83 : Example of the first design of the Stratophase probe showing the small encased sensing window

The second probe (Figure 84) design had the sensor on the surface on the probe to try and prevent fouling and also led to a larger sensor surface.

Figure 84 : Example of the second design of the Stratophase probe showing the larger sensing window flat on the probes surface

5.6.1.2 Fermenter

A Bioflo 110 fermenter/bioreactor (New Brunswick Scientific, Edison, NJ, USA) with a 10 L glass vessel was used for the fermentations.

5.6.1.3 Off-line analysis

For off-line analysis, the off-gas from the fermenter was measured using an Applikon, (Applikon Biotechnology, Schiedam, Netherlands) gas analyser. A BioMate 5 UV-Visible Spectrophotometer (Thermo Fisher Scientific, Waltham, MA, USA) was used for optical density measurements.

5.6.2 Inoculum

The inoculum protocol used was described by Voulgaris (2011) has been previously optimised for the strain of *E. coli*. (Table 26)[28] The inoculum was incubated for 12 hours at 37ºC and 200 rpm until the optical density at 600 nm reached 0.5.

Table 26 : Inoculum preparation for *E. coli* fermentation as described I Voulgaris (mL).[28]

Salt solution (Table 27)	100
Glucose (50% w/v) (BDH/ VWR, Lutterworth, UK)	10
1M $MgSO_4$ (Sigma, St Lois, MO, USA)	1
Trace elements (Table 28)	1
Karbamycin (0.5 µg/ml) (Sigma, St Lois, MO, USA)	2.5
H_2O	387.5

Table 27: Formulation of salt solution to be used in *E. coli* fermentation media (g/L)

$(NH_4)_2SO_4$ (Sigma, St Lois, MO, USA)	10
K_2HPO_4 (Sigma, St Lois, MO, USA)	73
$NaH_2PO_4.2H_2O$ (Sigma, St Lois, MO, USA)	18
$(NH_4)_2$H-citrate (BDH/ VWR, Lutterworth, UK)	2.5

Table 28 : Formulation of trace element solution to be used in *E. coli* fermentation media (g/L)

$CaCl_2.2H_2O$ (Sigma, St Lois, MO, USA)	0.5
$FeCl_3$ (Sigma, St Lois, MO, USA)	10.03
$ZnSO_4.7H_2O$ (Sigma, St Lois, MO, USA)	0.18
$CuSO_4.5H_2O$ (Sigma, St Lois, MO, USA)	0.16
$MnSO_4.H_2O$ (BDH/ VWR, Lutterworth, UK)	0.15
$CoCl_2.6H_2O$ (BDH/ VWR, Lutterworth, UK)	0.18
$Na_2EDTA.2H_2O$ (Sigma, St Lois, MO, USA)	22.5

5.6.3 Media and glucose solutions

The media used the formulation (Table 29) used by Voulgaris (2011). The media and glucose solutions were autoclaved separately before being sterilely pumped into the fermenter.[28] The working volume within the fermenter was 10L.

Table 29 : Media formulation (g/L)

Glucose (BDH/ VWR, Lutterworth, UK)	11.5
1M $MgSO_4$ (Sigma, St Lois, MO, USA)	2 mL/L
Trace elements	2 mL/L
$(NH_4)_2SO_4$ (Sigma, St Lois, MO, USA)	2
K_2HPO_4 (Sigma, St Lois, MO, USA)	14.6
$NaH_2PO_4.7H_2O$ (Sigma, St Lois, MO, USA)	3.6
$(NH_4)_2$2H-Citrate (BDH/ VWR, Lutterworth, UK)	0.5
Polypropylene glycol (BDH/ VWR, Lutterworth, UK)	0.1 mL/L

5.6.4 Reaction conditions

All conditions chosen for this fermentation were described previously by Voulgaris. (2011)[4] The pH within the fermenter was maintained at 7 using 1M H_2SO_4 and 2M NaOH. The temperature within the fermenter was controlled to 30 ºC using the cold ring within the fermenter and the external heating jacket. The dissolved oxygen within the fermenter was maintained above 30 % by varying the agitation rate between 300 and 750 rpm, the aeration rate was kept constant at 1 vvm.

5.6.5 Monitoring

5.6.5.1 Refractive Index

In the following experiments the shift in Bragg wavelength is measured by subtracting the Bragg wavelength of the background from the Bragg wavelength of the solution in question. This was achieved by placing the probe in the background solution and allowing the signal to steady and then placing the solution of interest and again allowing to settle. The backgrounds used and any deviation from this method of measurement are denoted within the discussion of the results of the experiments.[29]

5.6.5.2 Off-line measurements

5.6.5.2.1 Optical density

During the fermentation, optical density measurements were taken for every sample. All measurements were taken at 600 nm with water as a reference using a BioMate 5

UV-Visible Spectrophotometer (Thermo Fisher Scientific, Waltham, MA, USA) with a path length of 1 cm and water as reference.

5.6.5.2.2 Biomass

1 mL of the sample was placed in a pre-weighed Eppendorf tube. The samples were then centrifuged for 10 minutes at 12,000 rpm. The samples were then rinsed with water and placed in the centrifuge again for 10 minutes at 12, 00 rpm. The samples were then dried and placed in a desiccator to ensure a dry constant weight was measured. All measurements were carried out in triplicate.

5.6.5.2.3 Acetic acid

Acetic acid measurements were taken using a Roche Biopharm kit and the UV-vis spectrometer as described in (3.6.1.3)

5.7 Results

5.7.1 System characterisation

To analyse the use of the Stratophase RI monitoring system for fermentations, first the system was characterised. A series of experiments were run with the probe used off-line. The stability of the probe was tested across a range of pHs using NaOH and H_2SO_4, these were selected as they are used in fermentation reactions as pH regulators. The probe was cleaned and placed in water to get a background reading. The probe was removed and placed in the solution until the wavelength shift reading had stabilised. The probe was then removed, washed with water and placed back in the original beaker of water for another background reading. This was carried out for all pH solutions of different pH.

The shift in the Bragg wavelength is small when the pH is varied. The largest shift is at pH 14 with a change of 68. (Figure 85) In Figure 86 the effects of increasing the concentration of sodium hydroxide causes a larger shift in Bragg wavelength, a corresponding trend of change in RI was found by Wasburn *et al.* (1932) and a large change is seen at the highest concentration which follows the same pattern as the shifts

in Bragg wavelength found experimentally.[30] However, during the course of an *E. coli* fermentation the pH should never rise above 7.5 due to pH control.

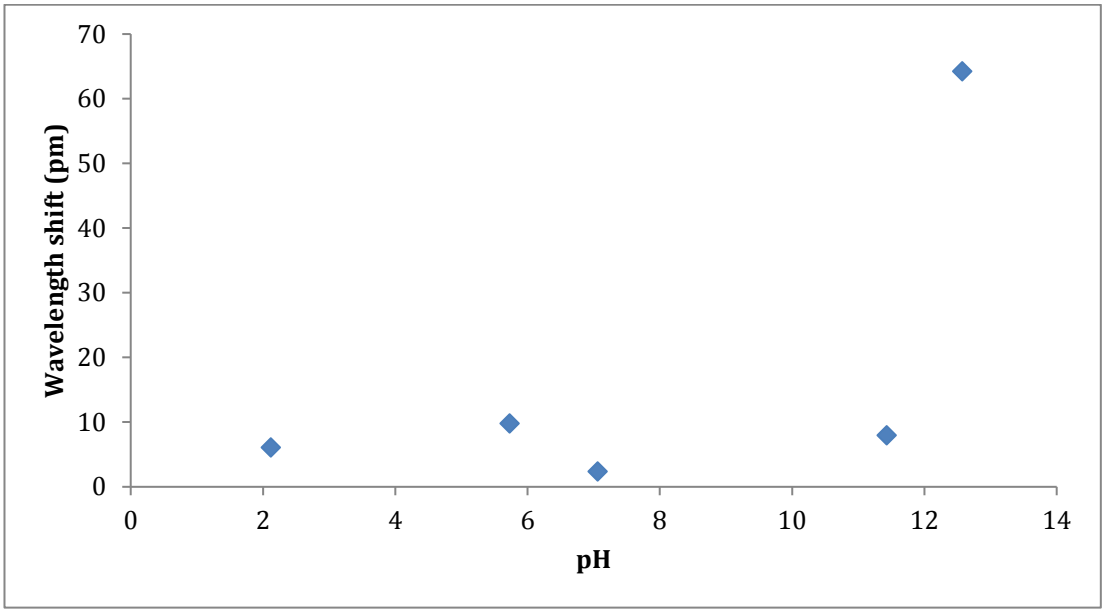

Figure 85 : The effect of pH on the shift of Bragg wavelength of solutions using water as a background measurement

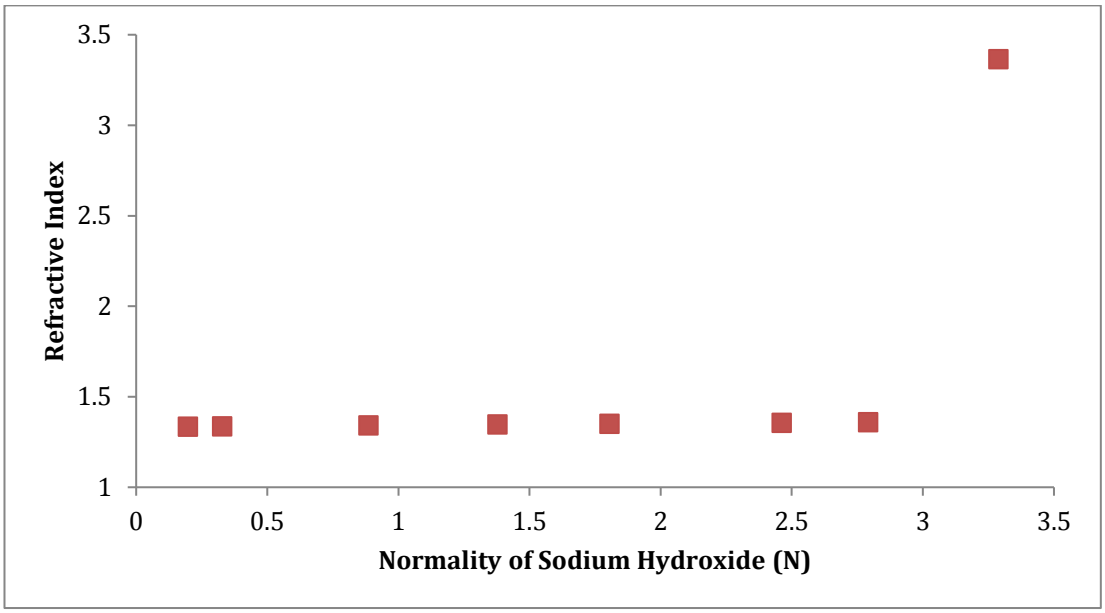

Figure 86 : Effect of increasing concentration of sodium hydroxide on refractive index measurements found by Washburn *et al.* (1932) [30]

The agitation rate within the fermenter could vary between 300 and 750 rpm and with an increase in agitation rate there will be an increase in the number of air bubbles within the fermenter. These air bubbles may affect the Bragg wavelength measurements if they pass through the sensor as the meauremnts are taken as the light would not be refracted. They could also pose the same problem if they were to become trapped within the sensor window of probe design 1 (Figure 83). To test the effects of agitation, the probe was placed in water on a stirrer. The stirrer speed was increased during measurement and the shift in Bragg wavelength was measured. As can be seen in Figure 87, there is a shift in the Bragg wavelength as the agitation rate increases, however, the change is small and that this is likely to be a minor change in the Bragg wavelength compared to other parameters. When no agitation is applied to a water sample, there is a small shift in the Bragg wavelength (Figure 88) but this is smaller than when the agitation is applied and again when compared to other parameters would not have an affect. This was also tested by Sparrow *et al.* who found that the shift was at most 7 pm.[26]

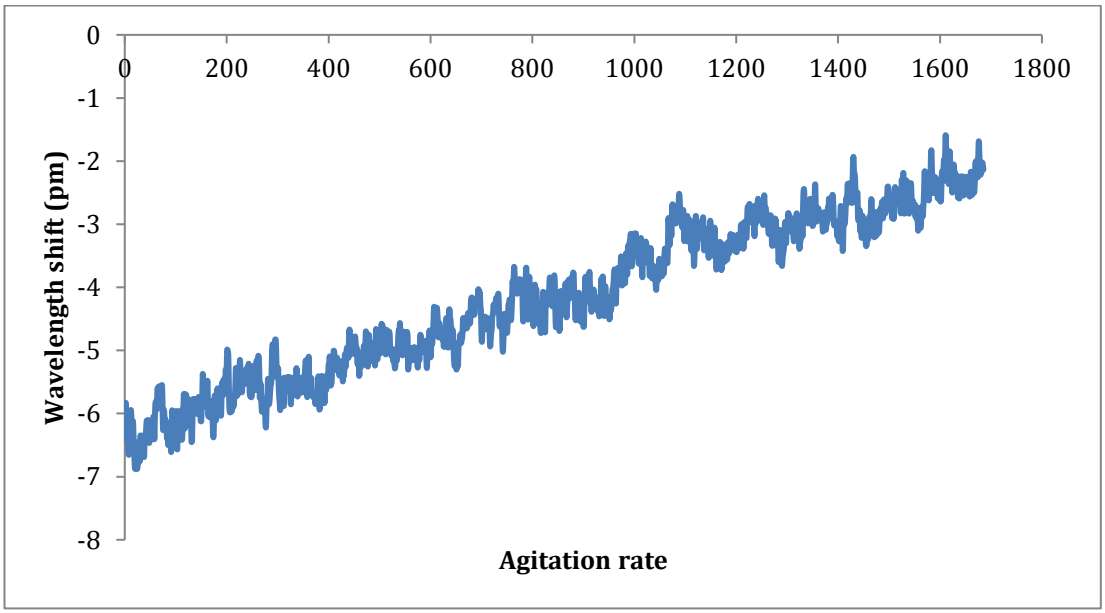

Figure 87 : The change in agitation rate and the effect on the Bragg wavelength measurements

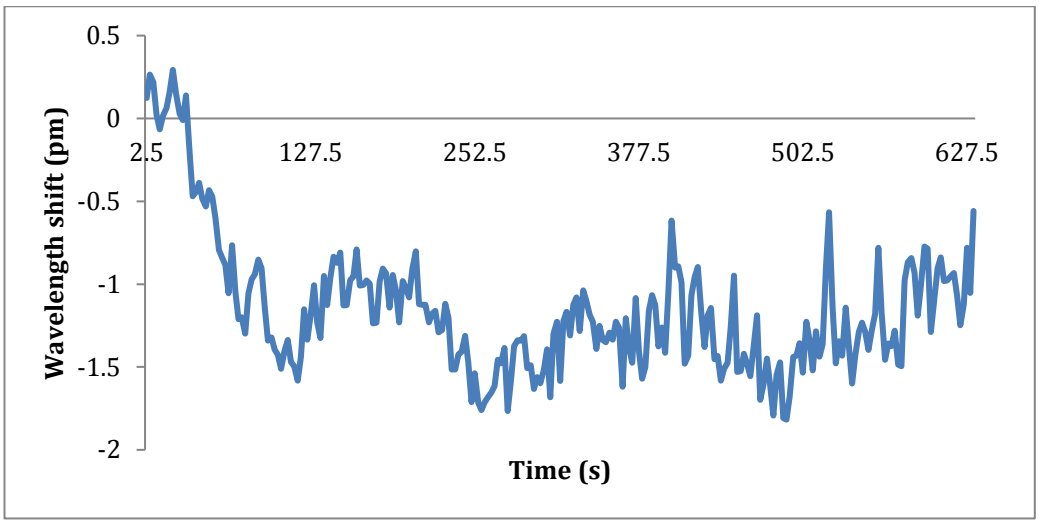

Figure 88 : Shift in the Bragg wavelength when the probe is kept in place in water

The fermenter is continually aerated at a rate of 1 vvm throughout the fermentation with the agitation rate altered to maintain the dissolved oxygen level. The effect of increasing the aeration rate was investigated using air pumped from the fermentation control unit through water with the probe inserted. The shift in Bragg wavelength was calculated over four different aeration rates and is displayed in Figure 89. It can be seen that the shift in Bragg wavelength compared to non-aerated water is between 7 and 14 pm, at 1 vvm the shift in Bragg wavelength would be ~8pm. This change would not be seen as the aeration rate within the fermenter will be constant and the aeration rate will be set before Stratophase probe measurements are taken.

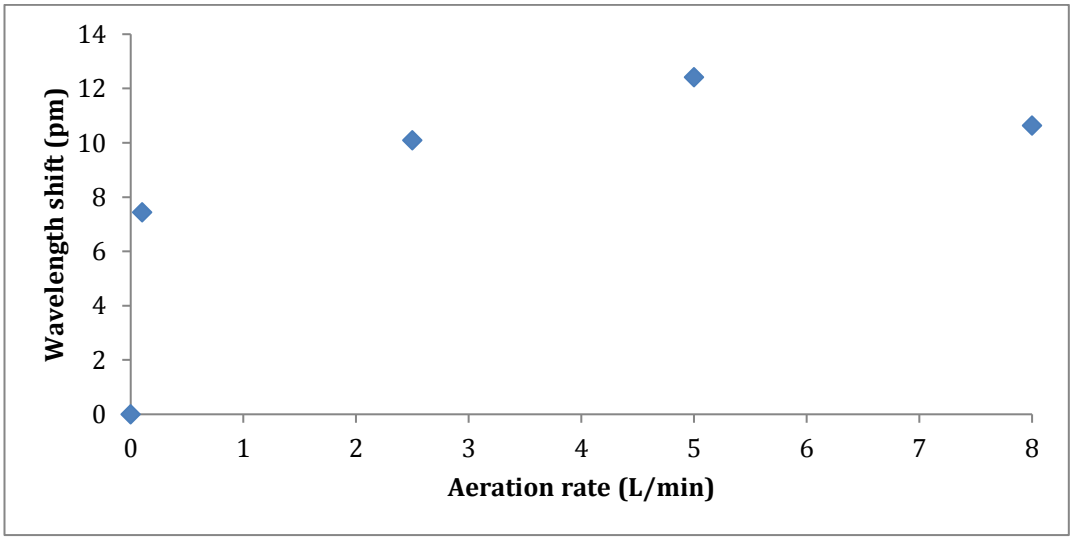

Figure 89 : The effect of aeration rate on the shift of Bragg wavelength

To determine the reproducibility of the Stratophase refractive index measurements, repeat measurements were taken in various solutions including: ethanol, media, water and a glucose solution as well as various combinations of these. In Figure 90, it can be seen that there is little variation between the repeats of the various solutions. When Table 30 is used to compare the standard deviation and relative standard deviation between the three repeats the largest standard deviation is within the glucose measurements and the smallest in the water and ethanol.

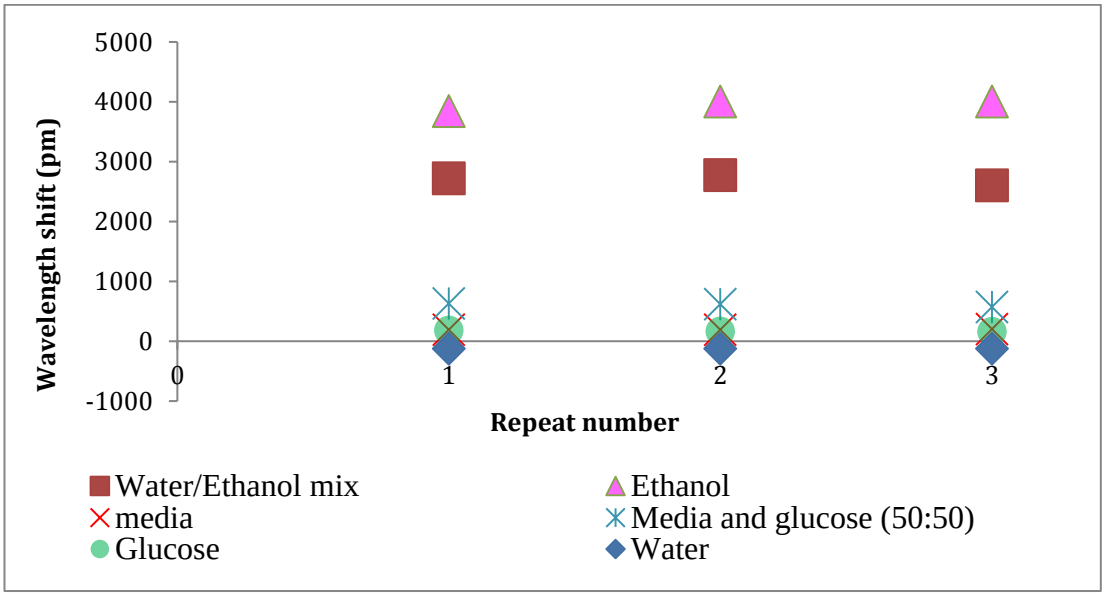

Figure 90 : Reproducibility of Bragg wavelength measurements in various solutions.

Table 30 : Average Bragg wavelength shift change of various solutions including the standard deviation and the % RSD

Solution	Average wavelength shift (pm)	Standard deviation	% RSD
Water/Ethanol (50:50 mix)	2699.58	86.58	3%
Media (prepared as described in 5.6.3)	196.03	7.45	4%
Glucose (15 g/L)	167.71	10.57	6%
Ethanol	3951.90	92.79	2%
Media/Glucose (50:50 mix)	607.70	30.31	5%
Water	-123.20	1.94	-2%

5.7.2 Analyte analysis

From the results of the system characterisation experiments, work was carried out on major components of the fermentation media to determine the shift in Bragg wavelength. Three analytes were chosen for analysis; these were glucose, *E. coli* cell material and acetic acid which would be produced during the course of the reaction. The solutions were prepared as listed in Table 31

Table 31 : Concentration of analyte solutions used in analyte analysis

Glucose (g/L)	Cell material (g/L)	Acetic acid (g/L)
2.5	2.5	0.1
5	10	0.15
7.5	15	0.2
10		0.25
15		0.3

All solutions were then analysed by placing the probe into a water solution as a blank and to determine the baseline. The probe was then placed into the analyte solution and allowed to stabilise. These readings were carried out in triplicate.

For the glucose solutions (Figure 91), with an increase in glucose concentration there is an increase in the shift of Bragg wavelength in comparison to water. Yanus *et al.* (1988) and Yeh (2008) also found this trend to be true for actual RI.[31, 32] If a higher concentration glucose solution has a higher shift in wavelength then it would be expected that the shift of the fermentation broth would decrease as the glucose is consumed during the fermentation. This is found by Campbell *et al.* (2013) where the shift in wavelength decreases in a *S. cerevisiae* fermentation as the glucose is consumed.[33]

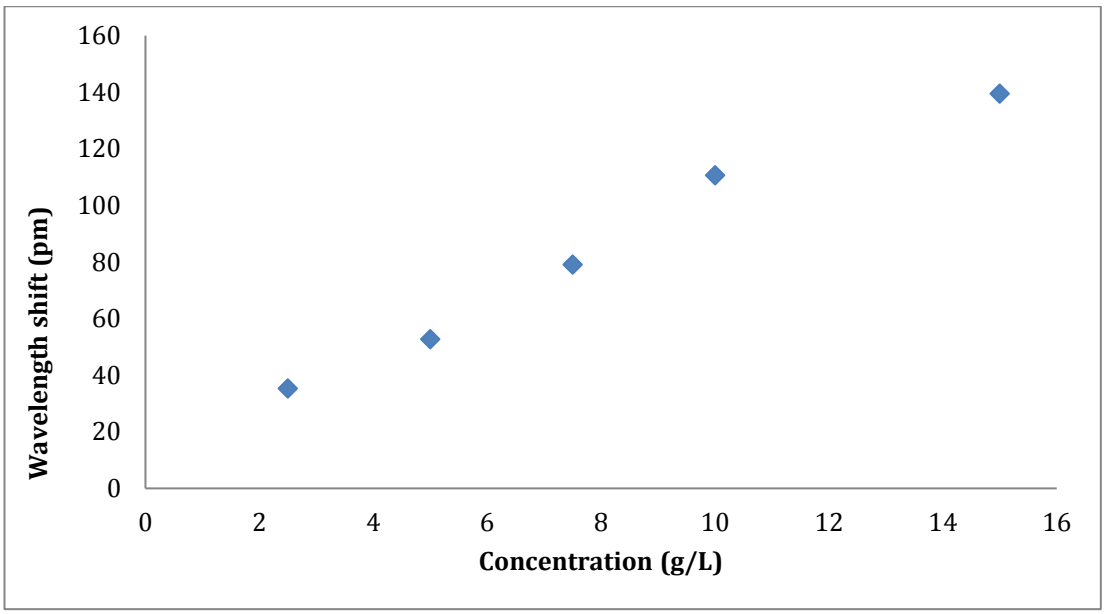

Figure 91 : Glucose in water standard solutions and the shift in Bragg wavelength observed

For biomass in solution, only three concentrations were prepared due to the difficulty in obtaining enough biomass to make the solutions. In Figure 92 it is shown that the increased biomass concentration causes an increased shift in Bragg wavelength. This is expected as the light comes into contact with the biomass it will scatter the light which will cause a shift in the Bragg wavelength. The increased concentration of biomass will cause more diffraction and therefore the shift will increase.[34] As the fermentation progresses the biomass within the fermenter increases which will cause an increase in the wavelength shift.

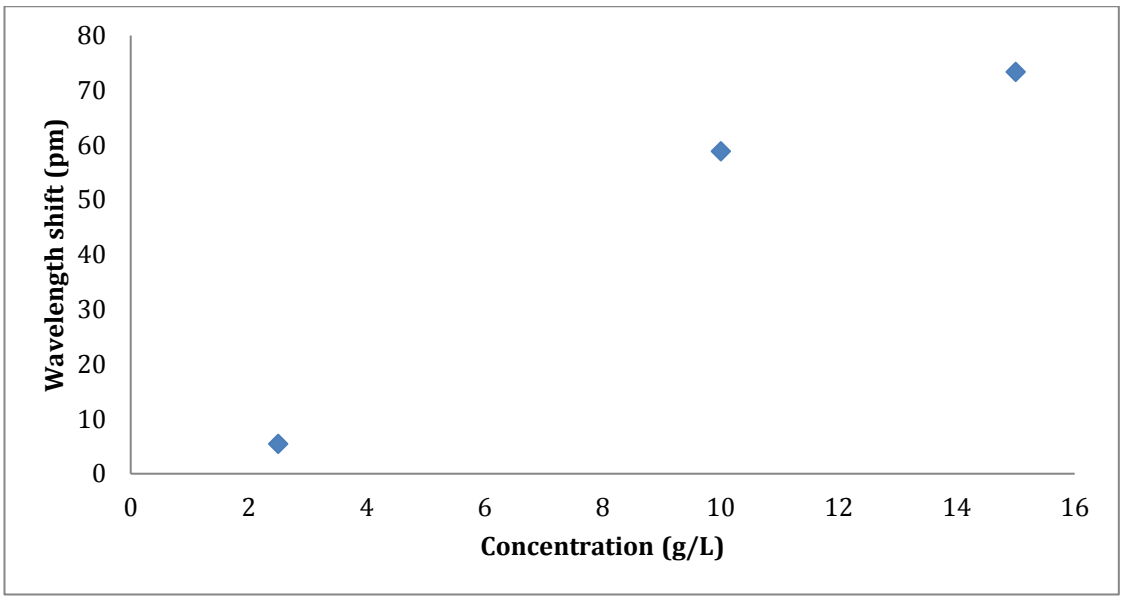

Figure 92 : Biomass in water standard solutions and the PTI changes observed

The acetic acid solutions caused a slight wavelength shift as the concentration was increased. (Figure 94) One possible reason for the small increase would be due to the standard solution concentrations being so low. When this is compared to traditional RI measurements, as the acetic acid concentration only increases slightly in the concentration ranges measured in the experiment. A 0.1% w/w solution has the RI also increases at very high concentrations of acetic acid the refractive index begins to decrease.[35] These concentrations were chosen to replicate the concentration of acetic acid that would be found within the fermenter. This shift is not as large as the shift produced by glucose or even the biomass, during the course of the fermentation the acetic acid concentration will increase and this will cause a small increase in the wavelength shift. This is unlikely to have an effect during the fermentation because of the low acetic acid concentrations.

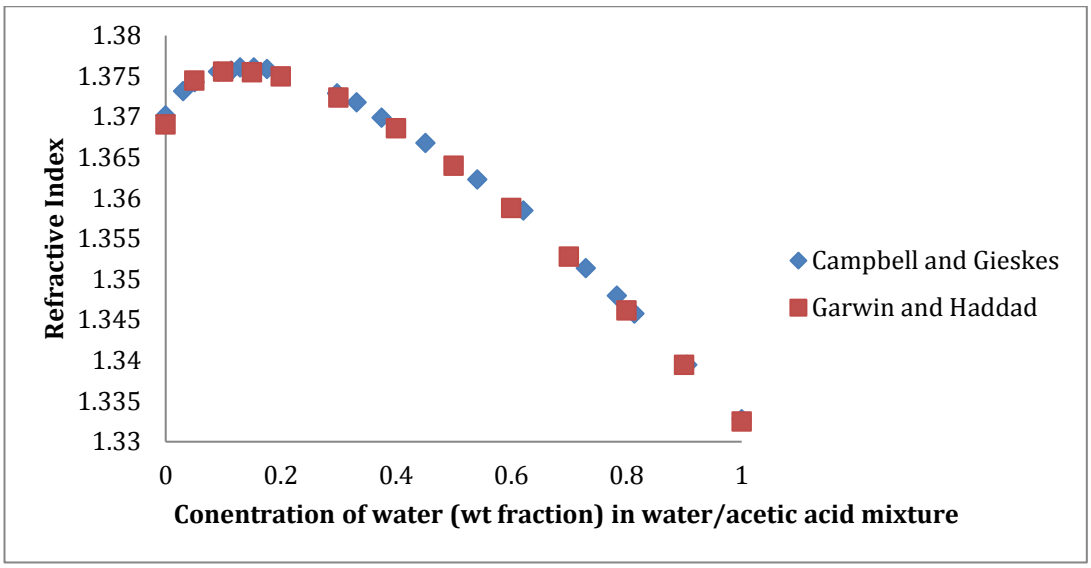

Figure 93 : Comparison of acetic acid/water mixture refractive indexes found by Campbell & Gieskes and Garwin & Haddad (1992) [35]

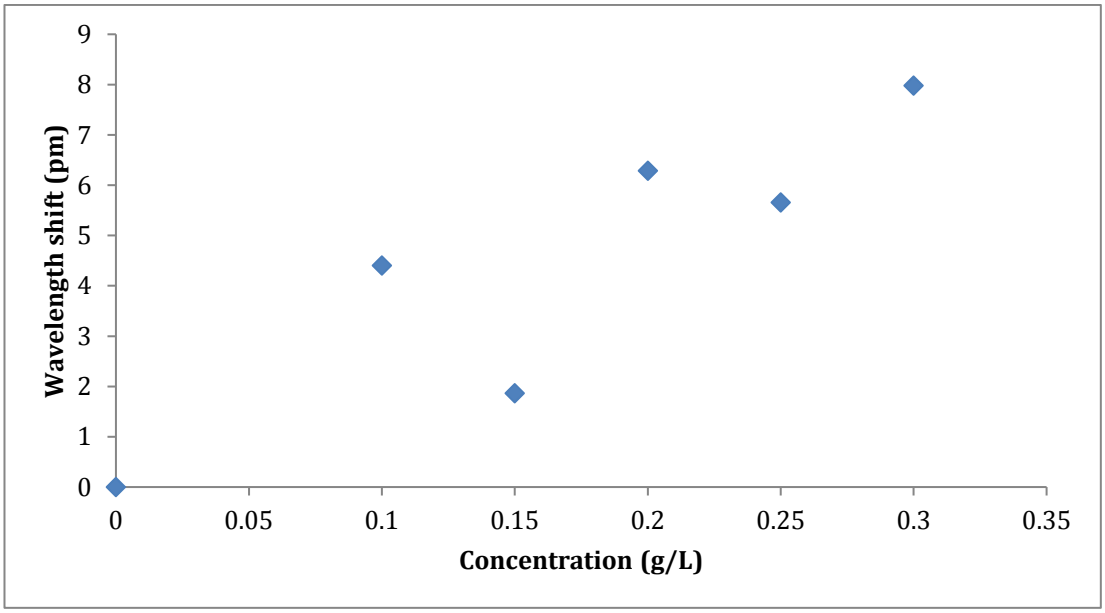

Figure 94 : Acetic acid standard solutions and the observed shift in Bragg wavelength

From the results seen of the individual analytes, during the course of the fermentation the glucose concentration decrease will cause a decrease in the Bragg wavelength shift but the production of acetic acid and the increase in biomass concentration will cause an increase in the Bragg wavelength shift. To determine the effect of the combination of these changes mixtures were prepared and analysed. Three concentrations of each analytes were used as described in Table 32. The mixtures were a 50:50 mix

Table 32 : Concentration of three analytes used in combination to assess the Bragg wavelength shift seen within the fermenter

Concentration (g/L)	Glucose	Biomass	Acetic acid
Low	2.5	2	0.1
Middle	7.5	10	0.2
High	15	15	0.3

When the glucose/biomass solutions were analysed the results were not as expected. (Figure 95) The expectation was that as both the biomass and glucose caused an increase in the wavelength shift that this would lead to the same effect when they are combined with the 15 g/L biomass/15 g/L glucose having the largest wavelength shift.

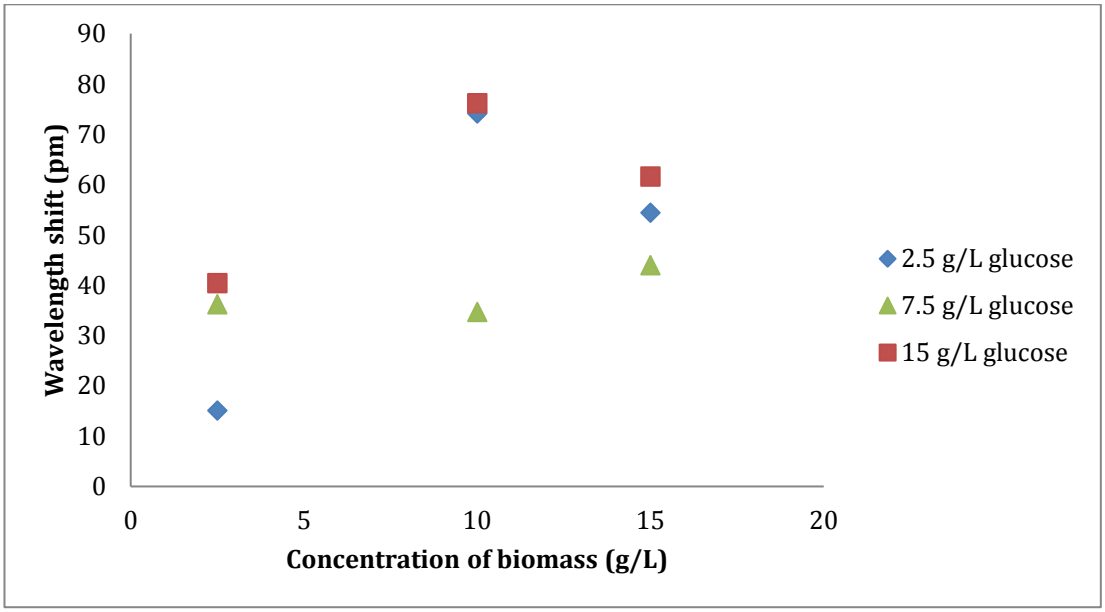

Figure 95 : Wavelength shift measurements of glucose/biomass solutions

The predicted trend is shown in Figure 96 with an increase in the wavelength shift as the concentration of both solutions increased. The predicted values were calculated by using the formula for calculating the refractive index of a mixture as described by Reis *et al.*[36] (2010) In the measured results the wavelength shift is not as large as expected and the highest RI of 2.5 and 15 g/L of glucose are found at 10 g/L biomass. Although the highest RI of 7.5 g/L is found to be at 15 g/L the trend is still not as expected with the middle concentration of glucose having the lowest wavelength shift. This could be

due to the biomass solutions being unrepresentative of the solution more mixing may be required which would affect the wavelength shift.

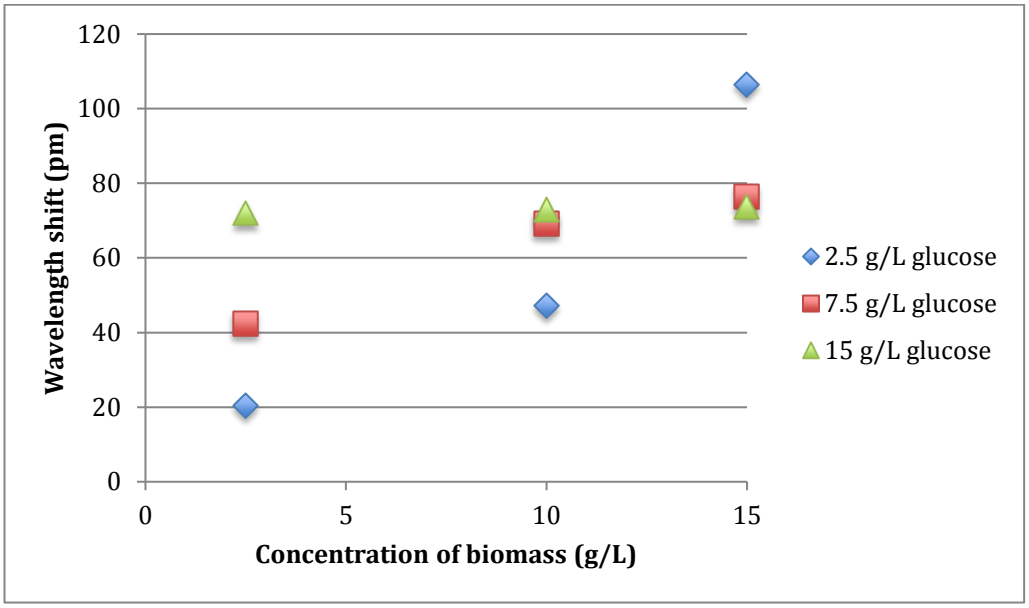

Figure 96 : Predicted change in the wavelength shift of the biomass/glucose solutions

When acetic acid and biomass solutions are examined it would be expected that the trend would be seen in Figure 97. The expected trend was calculated using the refractive index of mixtures formula. The slight increase in the wavelength shift for acetic acid combined with the increase for biomass would lead to a slight increase in the wavelength shift as the concentration of acetic acid is increased but the shift caused by the biomass would be the major contributor.

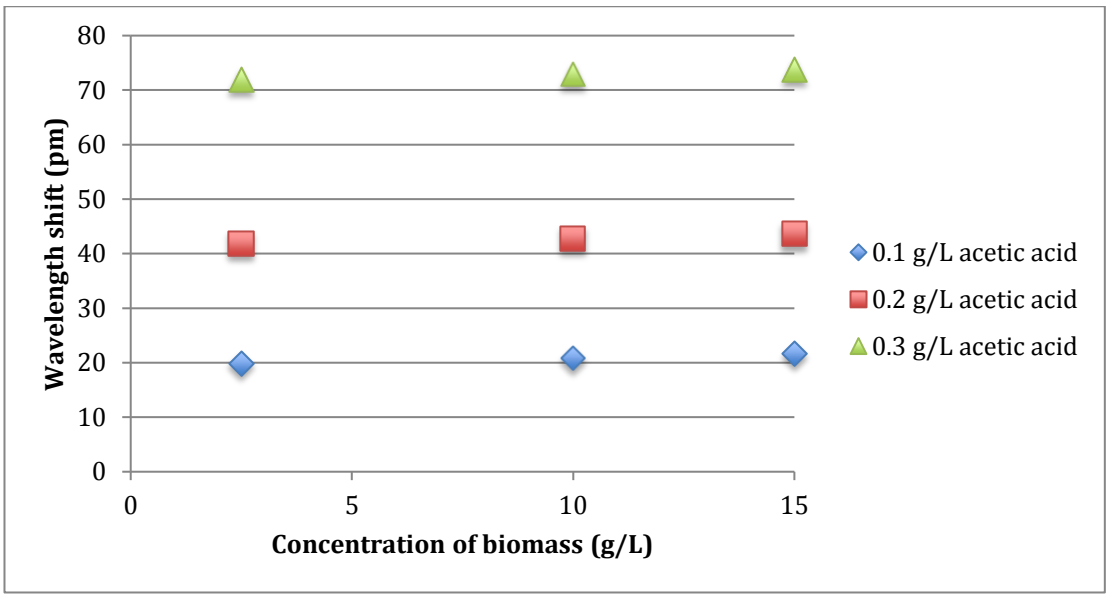

Figure 97 : Predicted change in wavelength shift of the biomass/acetic acid solutions

However, when the mixture is analysed for the lowest concentration of acetic acid the trend is as expected, although, the starting wavelength shift is lower than expected. For 0.2 g/L acetic acid the complete opposite is seen with a decrease in the Bragg wavelength which cannot be explained from the previous results again this could be due to the incomplete mixing of the solutions. At 0.3 g/L of acetic acid the increase in the wavelength shift is seen as expected.

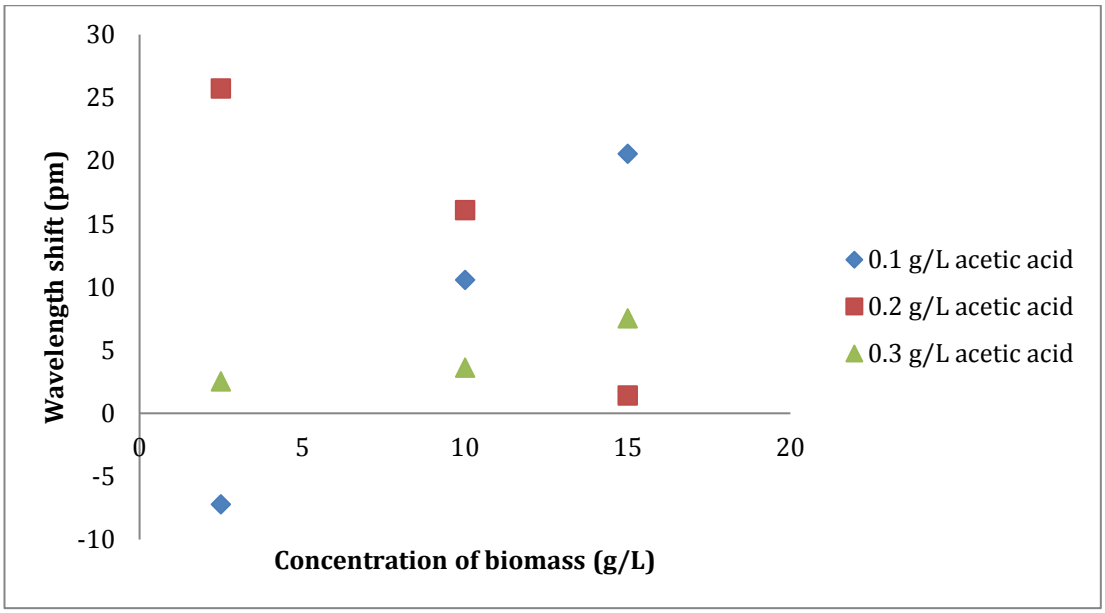

Figure 98 : Wavelength shift measurements of acetic acid/biomass solutions

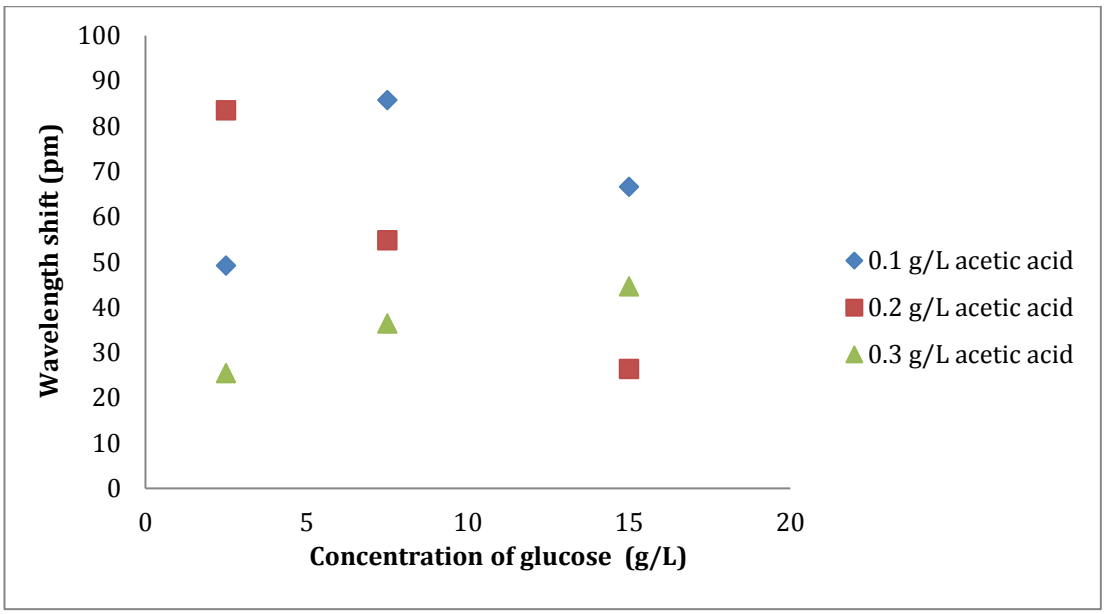

Figure 99 : Bragg wavelength measurements of glucose/acetic acid solutions

In Figure 99, the shift in Bragg wavelength does not follow the same trend for all three concentrations. When compared to Figure 100 the trend observed in the measured results of the 0.3 g/L are expected, albeit lower than the expected value. 0.1 g/L acetic acid with 10 g/L glucose is higher than the 15g/L solution and the 0.2 g/L acetic acid solution shows the opposite trend with a significant change as the concentration of glucose is increased.

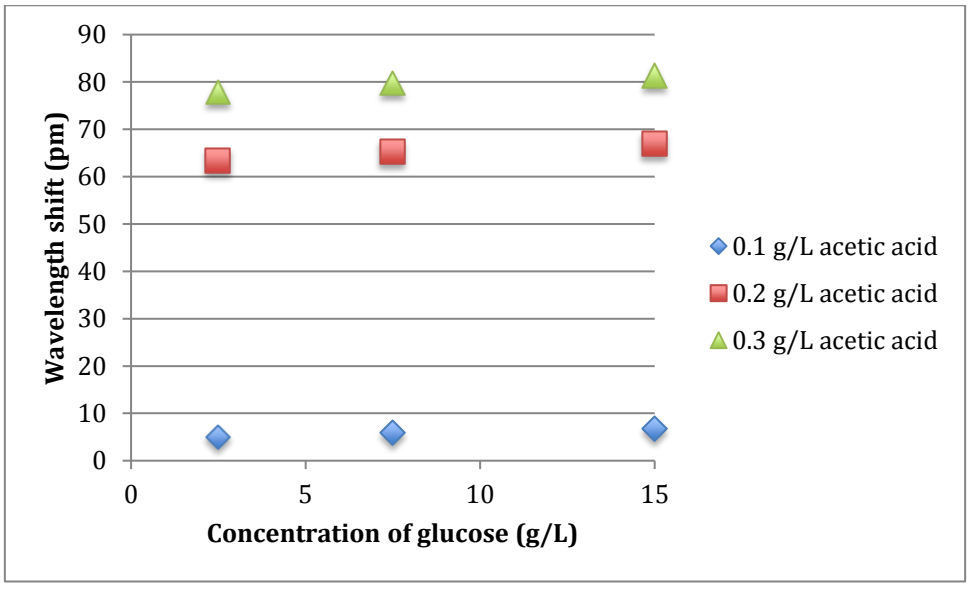

Figure 100 : Predicted change in Bragg wavelength shift of the glucose/acetic acid solutions

5.7.3 Off-line fermentation analysis

The first fermentation was carried out with refractive measurements taken off-line using the process described in 5.7.2. The probe design used for these measurements was design 1. The Bragg wavelength measurements show a decrease as the fermentation progresses (Figure 101) when this is compared to what would be expected – a decrease due to the decrease in glucose concentration, an increase due to the biomass concentration increasing and an increase in acetic acid concentration causing an increase in the wavelength shift. The decrease seen is due to the larger change seen in a decrease of the Bragg wavelength caused by the glucose which is larger than the increase caused by acetic acid and biomass. This is in correlation with the individual analyte measurements when the largest change in Bragg wavelength is found in the glucose measurements. The decrease in the wavelength shift for the fermentation is in agreement with the sugar consumption found by Campbell *et al.* (2013)[33]

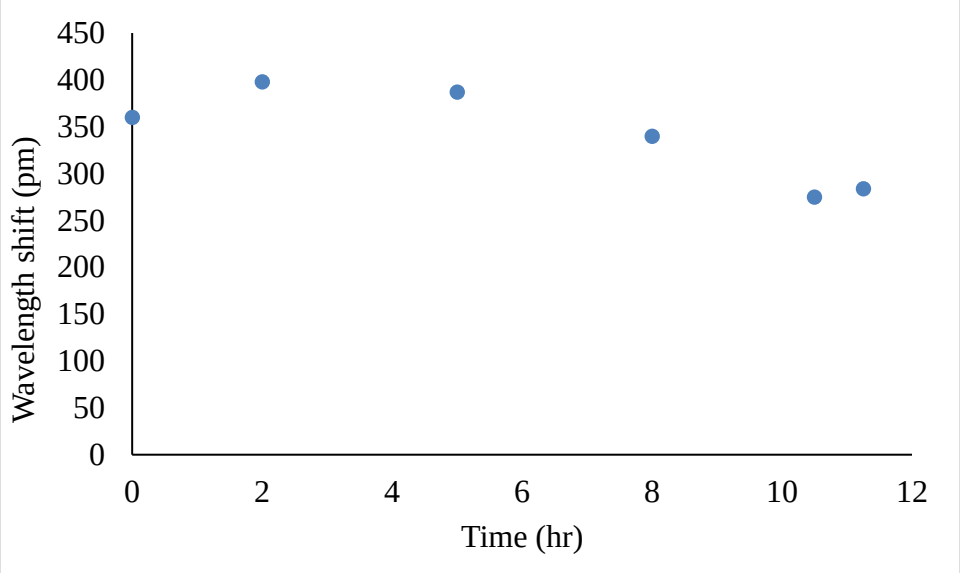

Figure 101 : *E. coli* fermentation 1 with off-line Bragg wavelength measurements

From the off-line analysis of the glucose and biomass concentrations (Figure 102), the glucose concentration becomes 0 at 9.5 hours and after this the shift in Bragg wavelength begins to level off. The biomass concentration increases throughout the

fermentation process but begins to stabilise as the same time as the glucose is consumed.

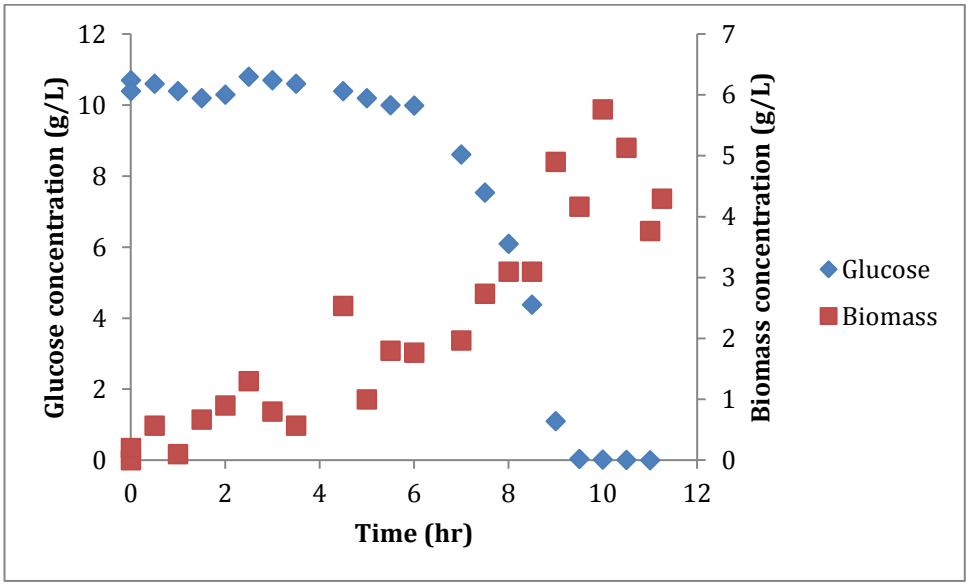

Figure 102 : *E. coli* fermentation 1 glucose and biomass concentrations

When two fermentations are compared the off-line wavelength shift are similar. Fermentation 1 produces a steep decrease in the wavelength shift at the start of the fermentation but then begins to decrease more slowly whereas fermentation 2 starts with a small change in wavelength shift with a decrease starting at 11.5 hours. (Figure 103)

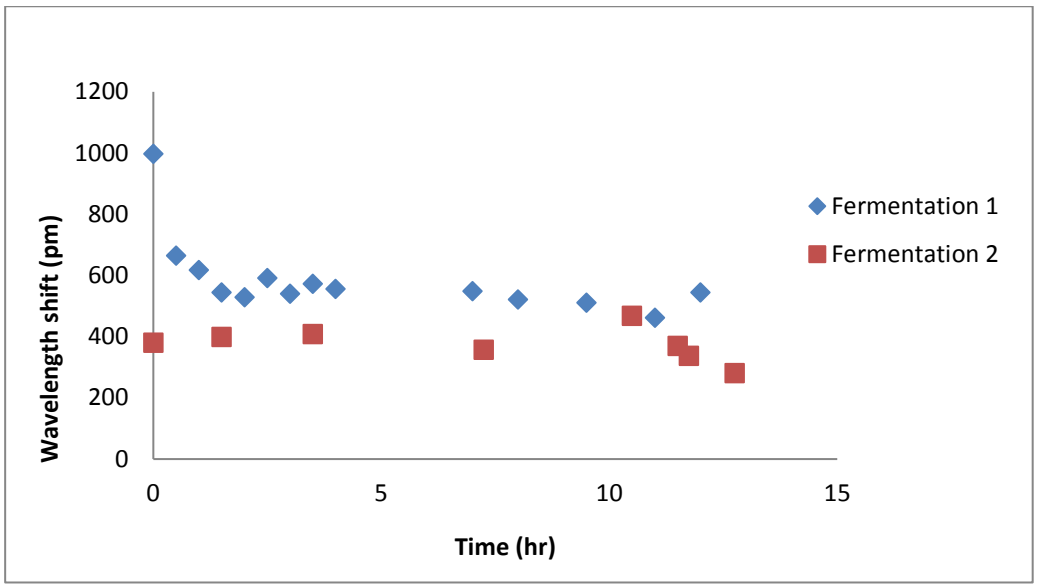

Figure 103 : Comparison of the refractive index trend of two fermentations

The wavelength shift can be related to the other off-line measurements taken. The optical density of fermentation 2 increases more rapidly than fermentation 1, this increase in optical density and therefore density would cause a steeper increase in the PTI contribution of biomass than fermentation 1. (Figure 104)

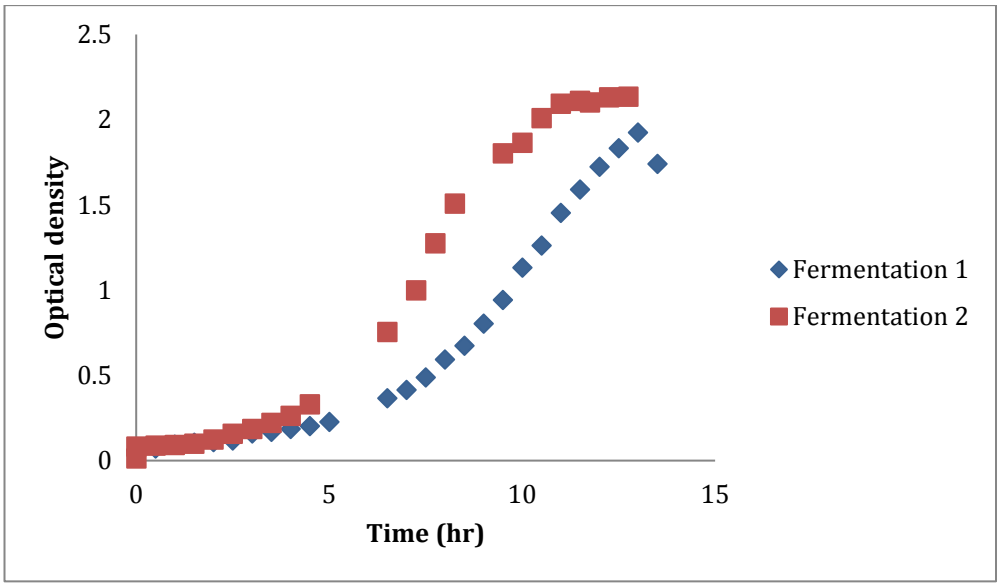

Figure 104 : Comparison of the optical density of two fermentations

When the glucose concentration is considered the glucose is consumed quicker in fermentation 2 than fermentation 1 when this is considered in terms of the wavelength shift the consumption of glucose would cause a larger decrease in the RI. (Figure 105)

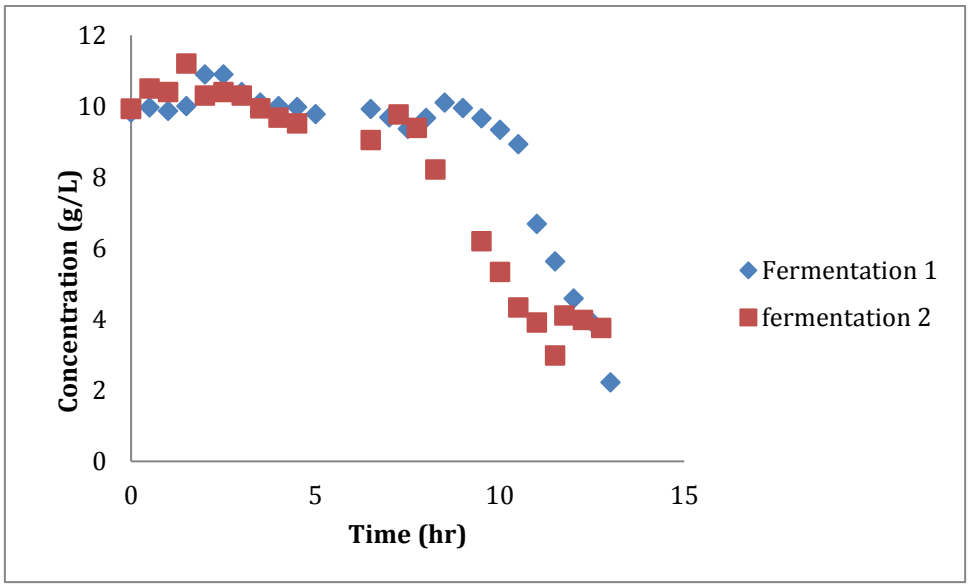

Figure 105 : Comparison of the glucose concentrations of two fermentations

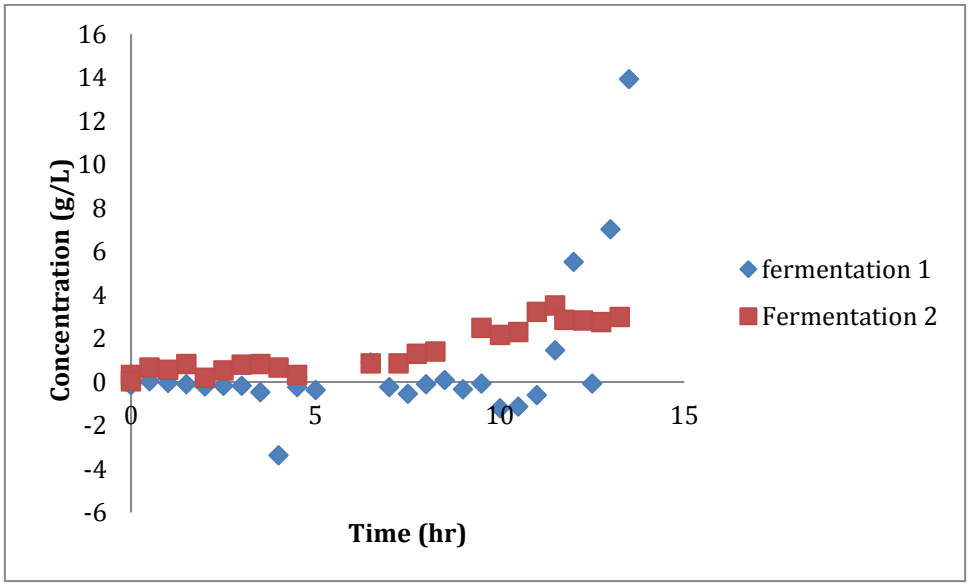

Figure 106 : Comparison of the biomass concentration of two fermentations

When the biomass is considered in fermentation 1 (Figure 106), the concentration of biomass remains low until 11.5 hours when the biomass concentration increases rapidly. Fermentation 2 has the expected steady increase over the course of the

fermentation. As an increase in biomass concentration causes an increase in the wavelength shift, fermentation 2 will have a steady increase in the shift of the Bragg wavelength and fermentation 1 will have little change in Bragg wavelength until the sharp increase. This could explain the steep decrease in the Bragg wavelength shift at the start of fermentation 1 as the biomass causes no increase in the wavelength shift so the contribution is from glucose or acetic acid.

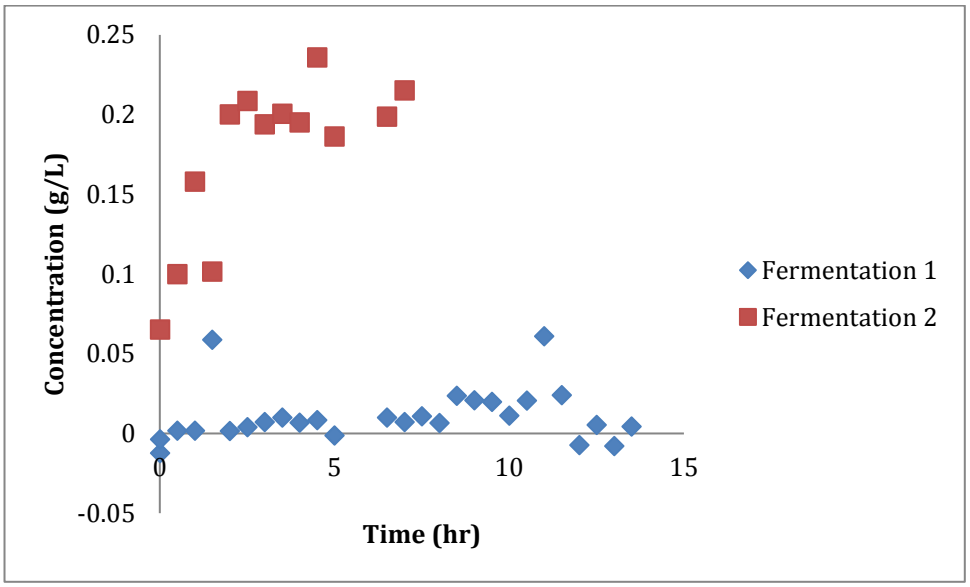

Figure 107 : Comparison of the acetic acid concentration of two fermentations

The acetic acid contribution to the wavelength shift for fermentation 2 is due to the increase in acetic acid concentration over the course of the fermentation (Figure 107) and so would cause an increased shift in the Bragg wavelength. When the increase caused by the biomass and the acetic acid are combined with the decrease caused by the change in glucose concentration would produce the trend as seen in Figure 103. In fermentation 1, the acetic acid concentration and biomass concentrations are low until later in the fermentation, therefore, the glucose concentration decrease will have a greater effect on the wavelength shift.

5.7.4 Glucose fed fermentation

To determine the ability of the probe to detect changes in the glucose level, a glucose fed fermentation was carried out. When the concentration of glucose within the fermenter had reached close to 0g/L (Figure 108) the fermenter was fed with a 10 g/L

glucose solution. The fermenter was fed at 11 hours; this caused a slight decrease in the optical density due to the cell mass being diluted by the increase in the media concentration. (Figure 109)

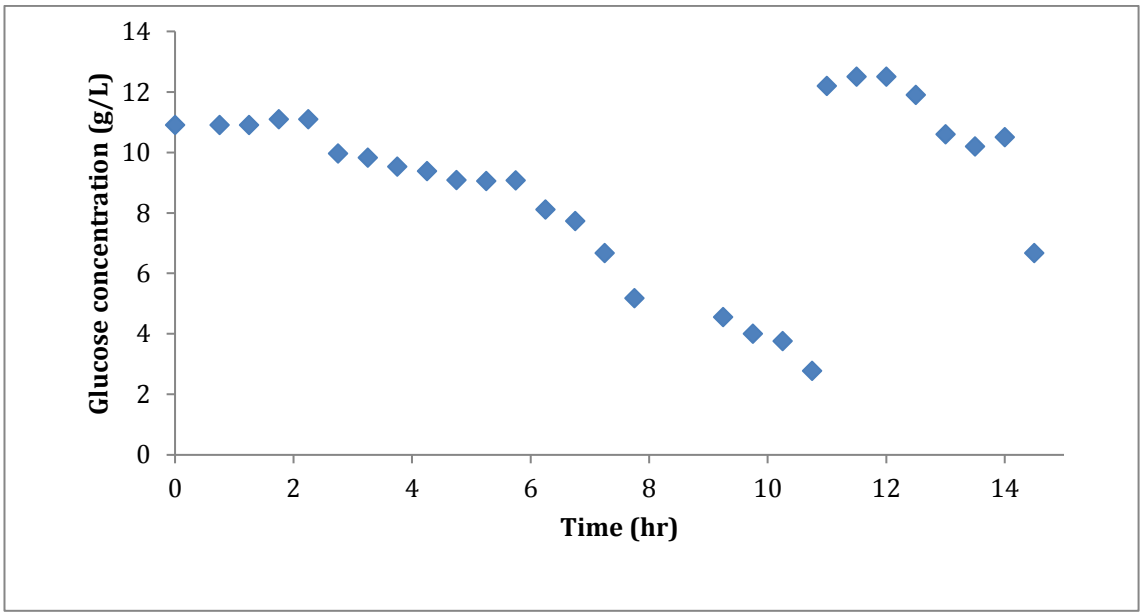

Figure 108 : Glucose concentration for *E. coli* glucose fed fermentation

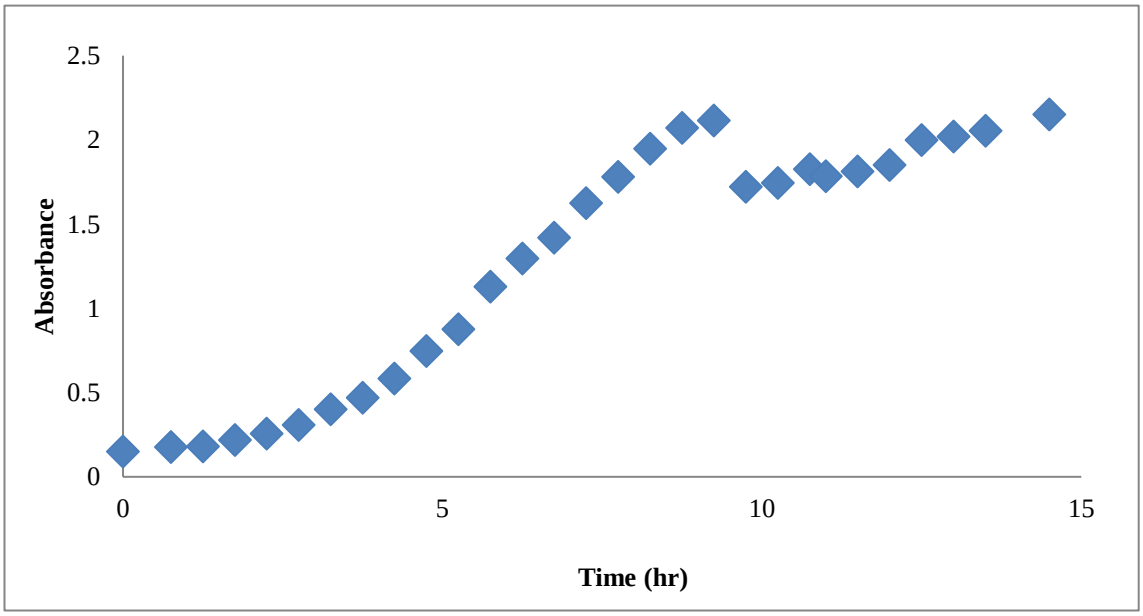

Figure 109 : Optical density measurements for *E. coli* glucose fed fermentation

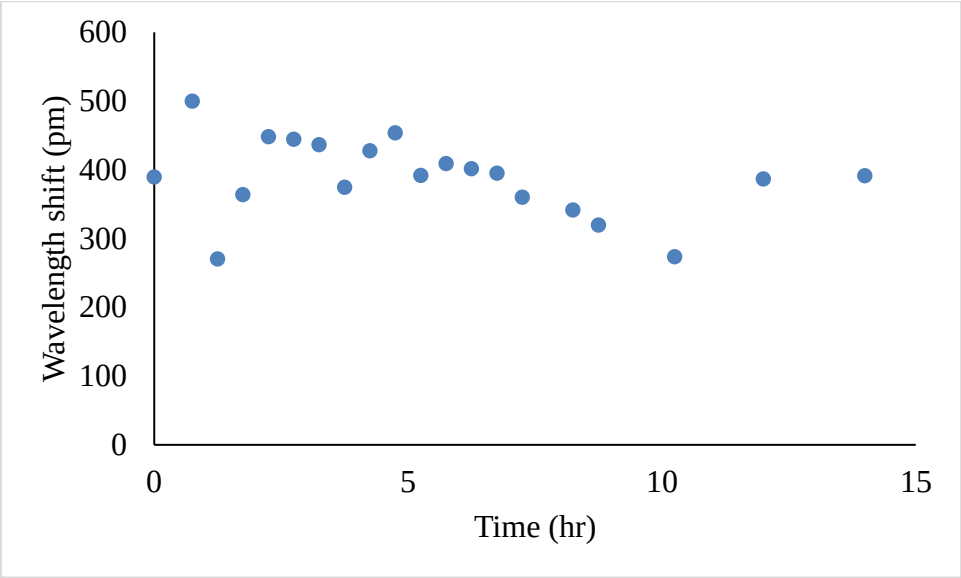

Figure 110 : *E. coli* glucose fed fermentation off-line Bragg wavelength shift measurements

When the wavelength shift is examined, (Figure 110) the trend shown is the same as in the previous fermentations until the glucose feed occurs. The shift in wavelength decreases at the start of the fermentation with the glucose contribution causing the Bragg wavelength to decrease in conjunction with the biomass concentration. (Figure 111) However, the glucose feed is detected as the wavelength shift shows an increase when the glucose feed is introduced.

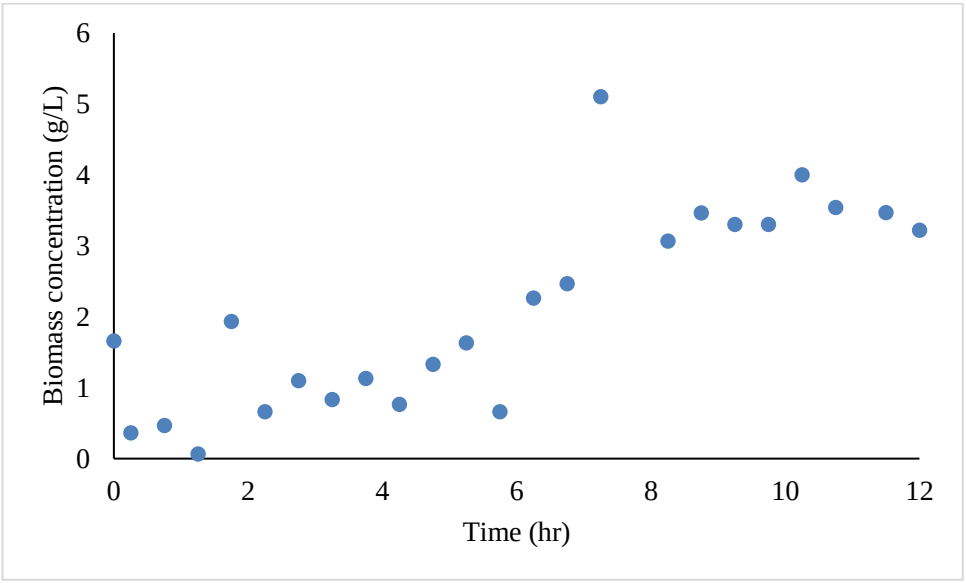

Figure 111 : Biomass concentration for *E. coli* glucose fermentation

5.7.5 On-line fermentation measurements

When the probe was used on-line (Figure 112), the fermentation proceeded as expected but the probe did not produce the same results. There was an increase in the wavelength shift with a sharp increase at ~ 11 hours. When the probe was removed from the fermenter, it was evident that the probe surface had become covered in cell material. Due to the nature of the fermentation broth it is not possible to see the probe surface during the fermentation and so it was not possible to identify the time when the surface of the probe had become contaminated. This fermentation was carried out using probe design 2 so there were no ridges for the cell material to become trapped so the cell material must have been attached to the surface of the sensor.

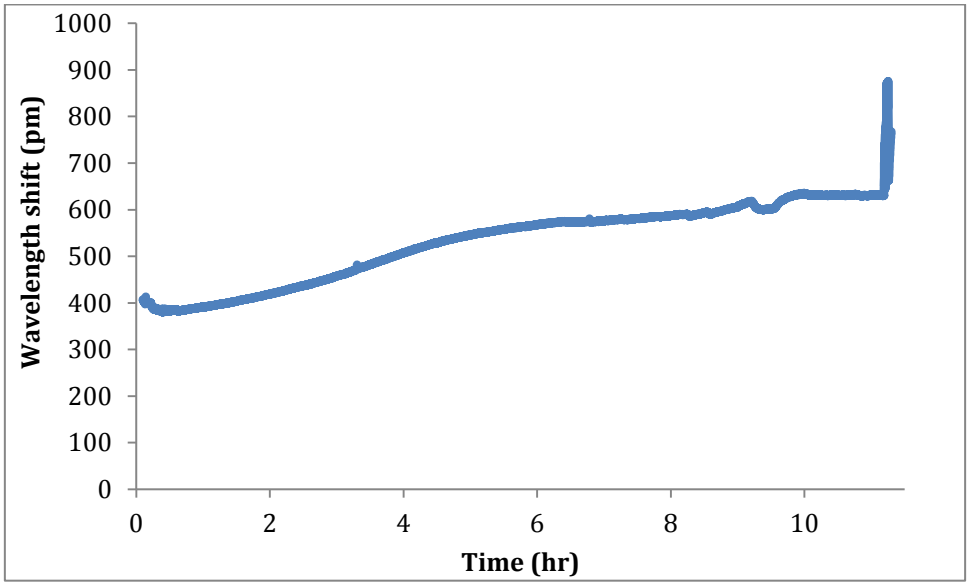

Figure 112 : On-line refractive index measurements of an *E. coli* fermentation

5.8 Conclusions from experimental work

The Stratophase probe is largely unaffected by changes in the fermentation conditions with the controlled parameters causing small changes in the refractive index. There is potential to monitor Bragg wavelength shifts using the Stratophase probe. From the work carried out on the effect of fermentation conditions on the Stratophase probe it can be seen that pH will affect the Bragg wavelength measurements but with the pH control in the fermenter keeping the pH level at 7 this should not be a factor. A small change in Bragg wavelength is found with increasing agitation which may have an

effect on the wavelength shift within the fermenter but this change is smaller than that seen with some of the key analytes so should not affect the overall Bragg wavelength profile. The aeration rate is maintained at a constant level therefore the changes seen in the Bragg wavelength with changing aeration will not be found. When the analytes are analysed individually glucose causes an increase in the wavelength shift as the concentration increases which has also been observed in the literature. The biomass caused issues with preparing samples but with an increase in concentration of the biomass there is an increase in the wavelength shift. The acetic acid changes differ from the changes reported in the literature this could be due to the low concentrations used which were chosen as they replicate the conditions within the fermenter. When the analytes are considered together the expected changes are not as large as the measured changes this could be due to a number of factors including poor mixing and the biomass samples not being representative. When a fermentation is monitored off-line changes in glucose and biomass concentration have an effect on the Bragg wavelength and the effect of glucose is also shown when the fermentation is fed with glucose. Off-line there is potential to monitor certain analytes within the fermentation broth which can be transferred between micro-organisms such as glucose and biomass. Further work would need to be done to allow the probe to be used on-line in fermentation solutions as the biomass fouls the probe and leads to difficulty modelling the process.

5.9 References

1. Gao, S.; Zhang, W.; Zhang, H.; Geng, P.; Lin, W.; Liu, B.; Bai, Z.; Xue, X., Fiber modal interferometer with embedded fiber Bragg grating for simultaneous measurements of refractive index and temperature. *Sensors and Actuators B: Chemical* **2013,** *188* (0), 931-936.

2. McClimans, M.; LaPlante, C.; Bonner, D.; Bali, S., Real-time differential refractometry without interferometry at a sensitivity level of 10(-6). *Appl. Opt.* **2006,** *45* (25), 6477-6486.

3. www.stratophase.com, www.stratophase.com. *2009* (07/11/09).

4. International Food Information, S., Dictionary of Food Science and Technology (2nd Edition). International Food Information Service (IFIS Publishing).

5. Wypych, G., Handbook of Solvents. ChemTec Publishing.

6. Mohammadi, M., colloidal refractometry - meaning and measurement of refractive-index for dispersions - the science that time forgot. *Adv. Colloid Interface Sci.* **1995,** *62* (1), 17-29.

7. Gerry, H. M., Refractive Index Measurement. In *Measurement, Instrumentation, and Sensors Handbook, Second Edition*, CRC Press: **2014;** pp 1-11.

8. Brandenburg, A., Differential refractometry by an integrated-optical Young interferometer. *Sensors and Actuators B: Chemical* **1997,** *39* (1–3), 266-271.

9. Kendrick, B. S.; Kerwin, B. A.; Chang, B. S.; Philo, J. S., Online size-exclusion high-performance liquid chromatography light scattering and differential refractometry methods to determine degree of polymer conjugation to proteins and protein-protein or protein-ligand association states. *Analytical Biochemistry* **2001,** *299* (2), 136-146.

10. Bali, L. M.; Shukla, R. K.; Srivastava, P.; Srivastava, A.; Srivastava, A.; Kulshreshtha, A., New approach to the measurement of refractive index. *OPTICE* **2005,** *44* (5), 058002-058002-6.

11. Leung, A. F.; Vandiver, J. J., Automatic refractometer. *OPTICE* **2003,** *42* (4), 1128-1131.

12. Xiong, B.; Hu, J., Laser-based refractive index detection for micro-channels. *Analyst* **2011,** *136* (4), 635-641.

13. White, I. M.; Fan, X., On the performance quantification of resonant refractive index sensors. *Opt. Express* **2008,** *16* (2), 1020-1028.

14. Loock, H.-P.; Wentzell, P. D., Detection limits of chemical sensors: Applications and misapplications. *Sensors and Actuators B: Chemical* **2012,** *173* (0), 157-163.

15. Bornhop, D. J.; Dovichi, N. J., Simple nanoliter refractive index detector. *Analytical Chemistry* **1986,** *58* (2), 504-505.

16. Bruno, A. E.; Krattiger, B.; Maystre, F.; Widmer, H. M., On-column laser-based refractive index detector for capillary electrophoresis. *Analytical Chemistry* **1991,** *63* (23), 2689-2697.

17. Krattiger, B.; Bruno, A. E.; Widmer, H. M.; Geiser, M.; Dändliker, R., Laser-based refractive-index detection for capillary electrophoresis: ray-tracing interference theory. *Appl. Opt.* **1993,** *32* (6), 956-965.

18. Tubino, M.; Junior, J. G. R.; Bauerfeldt, G. F., Biodiesel synthesis with alkaline catalysts: A new refractometric monitoring and kinetic study. *Fuel* **2014,** *125* (0), 164-172.

19. Zabala, S.; Arzamendi, G.; Reyero, I.; Gandía, L. M., Monitoring of the methanolysis reaction for biodiesel production by off-line and on-line refractive index and speed of sound measurements. *Fuel* **2014,** *121* (0), 157-164.

20. Wade, J. H.; Bailey, R. C., Refractive Index-Based Detection of Gradient Elution Liquid Chromatography using Chip-Integrated Microring Resonator Arrays. *Analytical Chemistry* **2013,** *86* (1), 913-919.

21. Plata, M. R.; Koch, C.; Wechselberger, P.; Herwig, C.; Lendl, B., Determination of carbohydrates present in *Saccharomyces cerevisiae* using mid-infrared spectroscopy and partial least squares regression. *Anal. Bioanal. Chem.* **2013,** *405* (25), 8241-8250.

22. Santos, R. C. R.; Vieira, R. B.; Valentini, A., Monitoring the conversion of soybean oil to methyl or ethyl esters using the refractive index with correlation gas chromatography. *Microchemical Journal* **2013,** *109* (0), 46-50.

23. Alamilla, F.; Calcerrada, M.; Garcia-Ruiz, C.; Torre, M., Validation of an analytical method for the refractive index measurement of glass fragments. Application to a hit-and-run incident. *Anal. Methods* **2013,** *5* (5), 1178-1184.

24. Yeh, C.-H.; Chow, C.-W.; Sung, J.-Y.; Wu, P.-C.; Whang, W.-T.; Tseng, F.-G., Measurement of Organic Chemical Refractive Indexes Using an Optical Time-Domain Reflectometer. *Sensors* **2012,** *12* (1), 481-488.

25. Zibaii, M. I.; Kazemi, A.; Latifi, H.; Azar, M. K.; Hosseini, S. M.; Ghezelaiagh, M. H., Measuring bacterial growth by refractive index tapered fiber optic biosensor. *J. Photochem. Photobiol. B-Biol.* **2010,** *101* (3), 313-320.

26. Sparrow, I. J. G.; Smith, P. G. R.; Emmerson, G. D.; Watts, S. P.; Riziotis, C., Planar Bragg Grating Sensors #8212;Fabrication and Applications: A Review. *Journal of Sensors* **2009.**

27. Belle, S.; Scheurich, S.; Hellman, R. In *Interrogating Water Content in Organic Solvents by Planar Bragg Grating Sensor*, SENSOR+TEST, Nurenberg, Germany, Nurenberg, Germany, **2009.**

28. Voulgaris, I. Production of novel amine oxidases from microorganisms. Thesis [Ph. D] -- University of Strathclyde, **2011.**

29. Stratophase Feed-on-Demand: The use of Metabolic Rate Index for closed loop control of feeding in upstream bioprocesses. (accessed 11/09/2017).

30. Washburn, E. R.; Olsen, A. L., The precision with which the concentrations of solutions of hydrochloric acid and sodium hydroxide may be determined with the immersion refractometer. *Journal of the American Chemical Society* **1932,** *54* (8), 3212-3218.

31. Yunus, W. M. b. M.; Rahman, A. b. A., Refractive index of solutions at high concentrations. *Appl. Opt.* **1988,** *27* (16), 3341-3343.

32. Yeh, Y.-L., Real-time measurement of glucose concentration and average refractive index using a laser interferometer. *Optics and Lasers in Engineering* **2008,** *46* (9), 666-670.

33. Campbell, B., A Novel Micro-optical Sensor Automates Control of Bioprocesses. *Sensors Online* **2013**.

34. Reyes-Coronado, A.; García-Valenzuela, A.; Sánchez-Pérez, C.; Barrera, R. G., Measurement of the effective refractive index of a turbid colloidal suspension using light refraction. *New Journal of Physics* **2005,** *7* (1), 89.

35. Agreda, V. H., *Acetic Acid and its Derivatives*. Taylor & Francis: **1992.**

36. Reis, J. C. R.; Lampreia, I. M. S.; Santos, Â. F. S.; Moita, M. L. C. J.; Douhéret, G., Refractive Index of Liquid Mixtures: Theory and Experiment. *ChemPhysChem* **2010,** *11* (17), 3722-3733.

6 Conclusions and future work

Fermentations are complex systems, which vary greatly between the microorganisms used. From the work conducted, it may be possible to monitor a *X. campestris* or *E. coli* fermentation with novel on-line measurements. Generally, some work would need to be done on optimising the probe design for each of the measurement techniques as the probes currently used have some problems when placed in a fermenter.

From the work completed investigating the use of infrared monitoring in a *X. campestris* fermentation it was shown to be possible to monitor the fermentation using a combination of off-line glucose and optical density measurements to produce a model that would allow prediction of the xanthan and biomass concentration within the fermenter. These models have a large error associated with them so to make the model more robust, future work would include investigation of a better reference technique to monitor the xanthan concentration within the fermentation samples for a UV-vis testing method. MIR off-line monitoring produced a PLS model which can monitor the glucose consumption within the fermenter and the xanthan production due to the decrease in the 5 peaks associated with glucose in the 980 -1200 cm^{-1} and the appearance of a new broad peak in the same region attributed to xanthan production (RMSEC of 2.78 g/L). Again the reference technique caused problems and a better reference method may improve the predictions of the model. Further fermentations would need to be carried out to determine the robustness of the models and also to obtain a larger calibration set. The NIR models were not as successful at modelling the *Xanthomonas* fermentation, the water peaks from the media masked areas of interest. However, further work could be done to look for other regions of interest. Future experiments that could be carried out would be running the *Xanthomonas* fermentations with the same media and procedure with the time extended to determine if more xanthan would be produced as well as running different reference methods for the off-line results. If these experiments were successful then a more robust calibration model could be built using MIR which would hopefully model the decrease in glucose and the increase in xanthan in the same wavelength region. If the off-line model was successful then work could be carried out to investigate the use of an on-line MIR probe to monitor the reactions to test the model in a 'real' environment. As there are currently IR probes that can be used within a fermenter, these designs should be

investigated first rather than designing a new probe. From the work contained in this thesis, this is the first stage in a longer strategy to monitor a *Xanthomonas* fermentation on-line with IR techniques.

From the acoustic monitoring experiments, the model solutions show that as the concentration increases there is an increase in the velocity. This certainly has potential for monitoring of fermentation reactions as the change in velocity by changing concentration could be used to monitor the progression of a fermentation. For example, a *Xanthomonas* fermentation could be monitored by correlating the change in velocity to the increase in xanthan production. From the results of the starch model solutions analysis, the parabolic relationship between the velocity and concentration when particles are present would need to be considered in any future work and analysis of actual fermentation samples off-line would help to produce a better understanding of this. With the changes in the rheological properties of xanthan solutions as the concentration increases the pseudo plastic behaviour and the other properties would allow measurement of the concentration of the xanthan in a sample. The acoustic measurements and the rheological measurements could be combined to form a model to predict the xanthan concentration however, further work would need to be done on other analyte concentrations and samples to take this further. Adaptations in the probe design will have to be made to allow the use of the probe in the fermenter for example; the probe must have appropriate fixtures to hold the transducers in place that will not be affected by the pressure of the autoclave or be sensitive to agitation. Future experiments could include measuring the velocity and attenuation coefficient of other fermentation analytes such as glucose and biomass and modeling how a change in concentration during the fermentation effects the acoustic measurements. Once this analysis had been carried out, fermentation samples could be analysed off-line to collect information on the changes in acoustics during a fermentation to better understand matrix effects within the fermenter. Using the fermentation sample results and off-line reference analysis it may be possible to model the changes within the fermenter If the probe could be redesigned then eventually this model could be transferred into monitoring the fermentation on-line. As there were few experiments carried out on the prototype probe, not enough data was collected to fully investigate the combination of rheology and acoustics but the change in velocity at higher xanthan

concentrations along with the increased velocity at these concentrations would suggest that there is potential to combine these analyses.

When a fermentation is monitored off-line using the RI probe changes in glucose and biomass concentration have an effect on the Bragg wavelength and the effect of glucose is also shown when the fermentation is fed with glucose. Off-line there is potential to monitor certain analytes within the fermentation broth which can be transferred between micro-organisms such as glucose and biomass. Further work would need to be conducted on using the probe for complex media to understand the interactions of the chemicals in the media. From the literature, it has been shown that glucose consumption can be monitored and from this calibration models should be able to be built. A much larger data set would be required than was obtained in these experiments. There is potential for the IR and RI measurements to be used in conjunction with each other to provide greater insight into the fermentation process. Both of these techniques involve the monitoring of the fermentation process using the interaction of the samples with light. NIR and MIR are established techniques which involve a range of wavelengths for measurement. The novel refractive index probe designed by Stratophase focuses on the region of 1510-1590 nm which is within the NIR region. The difficulties discussed in the IR chapter regarding the complexity of fermentation monitoring also apply to the refractive index measurements with the Stratophase probe. Glucose is the most promising analyte to monitor during the fermentation as it has been shown by this experimental work as a potential monitoring method as well as in the literature and it was shown that there is a possibility of monitoring the glucose consumption during a *Xanthomonas* fermentation using 980-1180 cm^{-1} region.

Probe design has been shown to be a vital part of the use of these techniques in the monitoring of fermentation reactions. The probe design must take into account the robustness of the probe and the ability to be sterilized and measure over a long period of time. The novel probe designed by Stratophase proved to potentially useful for the monitoring of an *E. coli* fermentation but again the design of the probe will need further work. As the biomass fouls the sensor window as material became trapped in the sensor window. Methods to prevent fouling would need investigated including any

potential anti-fouling coatings/membranes. The probe itself does not always survive the autoclaving process due to the high temperature and pressure conditions. The acoustic probe used in these experiments would also need changes to be made before it could be used on-line, the transducers would need to be more secure and be able to withstand the autoclave process. The placement of the transducers would also need further work as the current design of a circular holder may cause disruption in the mixing in the fermenter and potentially create dead zones. The probe would ideally have a design as in Figure 79, which has the same design as NIR probes already on the market.

While there no one technique has been successfully monitored on-line using the novel probes or the use of NIR for a novel organism, steps have been taken to understand the processes and the effects of the complex media and morphology on the measurements. All three measurement techniques look promising but would require much further investigation before applied to industrial processes.